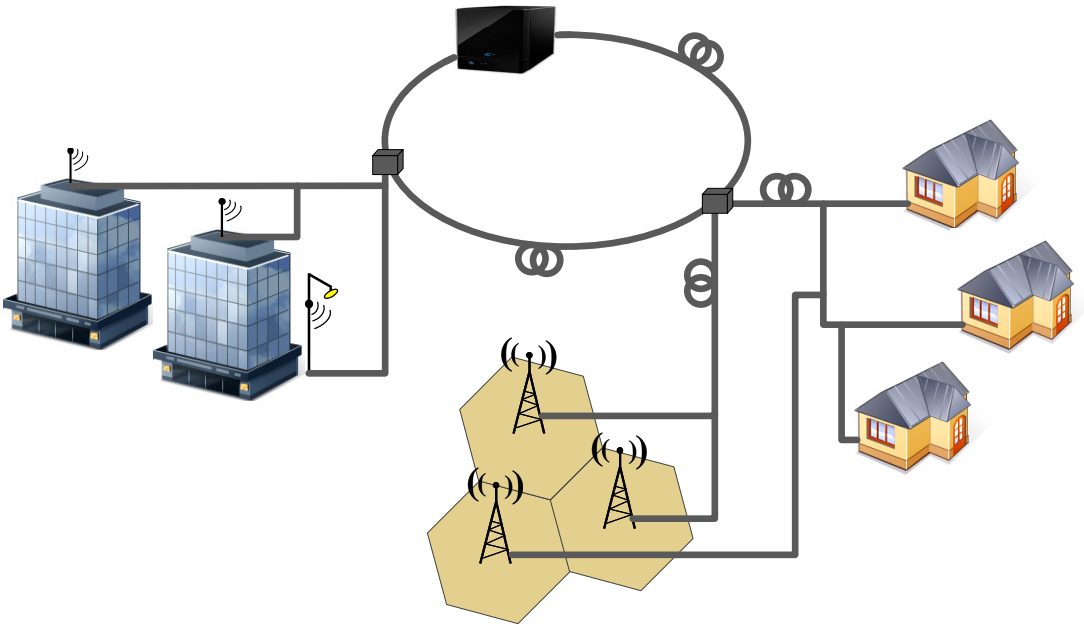

Sílvia Medeiros Vaz Pato

Next Generation Access Networks: Towards Higher Data Rates and Optical-Wireless Convergence

Thesis submitted in candidature for the degree of Doctor of Philosophy in Electrical and Computer Engineering

March 2012

· U C ·

UNIVERSIDADE DE COIMBRA

PhD thesis supervised by Professor Doutor Henrique José Almeida da Silva, Associate Professor in Electrical and Computer Engineering Department of Faculdade de Ciências e Tecnologia da Universidade de Coimbra.

Work partially supported by Nokia Siemens Networks Portugal S.A. and by Fundação para a Ciência e a Tecnologia, under the research grant SFRH/BDE/15627/2006.

Aos meus pais, Luis e Ana Maria

Resumo

A notável evolução das redes de acesso, tanto fixas como móveis, tem sido impulsionada pelos crescentes requisitos de largura de banda. Com o aumento contínuo de tráfego e estagnação das receitas dos operadores, a próxima geração de redes de acesso enfrenta o desafio de suportar elevadas capacidades a baixo custo, indo ao encontro das necessidades dos operadores e dos utilizadores. Esta tese identifica métodos e propostas para melhorar o desempenho destas redes.

A primeira parte desta tese é dedicada às redes ópticas de acesso de elevado débito. O impacto das limitações físicas destes sistemas, tais como os efeitos não-lineares da fibra e a largura espectral das fontes ópticas multi-modais, é avaliado, mostrando que é importante dimensionar correctamente os vários parâmetros do sistema para garantir um desempenho em conformidade com as especificações. O impacto destas limitações no desempenho do sistema é significativamente minorado com a introdução de códigos correctores de erros, e é confirmado que esquemas de igualização de potência, responsáveis por reduzir o efeito perto-longe característico de redes ópticas passivas, produzem melhorias substanciais. Com base neste facto, é desenvolvido um método de igualização de potência para aplicação em sistemas de transmissão em modo de rajada, totalmente óptico e com benefícios significativos.

A convergência de redes fixas e redes sem fios é o tópico investigado na segunda parte desta tese, onde é incluída uma análise técnica e económica de arquitecturas ópticas para suporte distribuído de antenas remotas. O dimensionamento de protocolos de transmissão digital de sinais de rádio em termos de capacidade requerida mostra que, actualmente, sistemas de baixo custo devem optar pelo uso de métodos de transmissão analógicos. Neste contexto, é modelado um sistema analógico com capacidade para suportar sinais de rádio com elevada largura de banda, mostrando que estes sistemas são adequados aos requisitos futuros.

Palavras chave

Redes ópticas passivas, correcção de erros à posteriori, igualização de potência em modo rajada, convergência de redes sem fios e redes ópticas, rádio sobre fibra.

Abstract

The remarkable evolution of access networks, both wired and wireless, has been mainly impelled by ever-growing bandwidth demands. In view of the continuous traffic growth and stagnating operator revenues, next generation access networks face the challenge of cost-effectively providing higher capacities to meet both customer and operator needs. The present thesis is focused on identifying methodologies and improvement approaches for such systems.

The first part of this work is devoted to optical access networks exploiting high data rates. The performance impact caused by the main physical layer limitations of these systems, which include the effect of fibre nonlinearities and the impact of the spectrum of multimode optical sources, is assessed, showing that design rules should be carefully derived to assure a compliant performance. The introduction of correction codes is proven to have a significant benefit on minimizing the influence of such limitations, and burst-mode power equalization is shown to be a fundamental feature to effectively overcome the near-far effect characteristic of typical passive optical access systems. This is the basis for a proposal of an all-optical burst-mode equalization scheme, which is shown to significantly improve the system performance.

The convergence of wired and wireless domains in the access landscape is the focus of the second part of this thesis, which comprises a technical and economical analysis of optical architectures adequate to support a distributed network of remote antennas. Digital radio transmission protocols are dimensioned in terms of required capacity, showing that nowadays the choice of analogue radio transmission allows the deployment of lower-cost systems. An analogue fibre link designed to carry high bandwidth radio systems is modelled, proving the suitability of such systems to support legacy and future wireless transmission protocols.

Keywords

Passive optical networks, forward error correction, burst-mode power equalization, wireless optical convergence, radio-over-fibre.

Agradecimentos

O trabalho descrito nesta dissertação contou com o apoio e colaboração de várias pessoas e entidades a quem pretendo endereçar o meu reconhecimento.

Inicio expressando o meu agradecimento ao meu orientador, Professor Henrique Silva, que, apesar de todas as contrariedades que surgiram, se manteve sempre certo da finalização deste projecto. Agradeço toda a confiança que demonstrou ter em mim, as suas críticas e comentários pertinentes e a cuidada supervisão científica do meu trabalho.

Agradeço à Nokia Siemens Networks (NSN) Portugal S.A. por me ter proporcionado a candidatura a uma Bolsa de Doutoramento em Empresa que me permitiu iniciar esta caminhada e estendo estes agradecimentos à Fundação para a Ciência e a Tecnologia, pela bolsa concedida. À NSN agradeço ainda a compreensão que foi mostrada durante a escrita desta dissertação, permitindo-me alocar parte do meu tempo à finalização deste projecto.

Ao longo destes anos tive o privilégio de trabalhar com vários colegas. Agradeço em particular ao Rui Meleiro pelas ideias que nunca lhe faltam, ao Daniel Fonseca pelas críticas certas na altura certa, ao Ruben Luís pela sua perseverança no desenrolar de qualquer assunto e ao João Santos pela sua disponibilidade para discutir e desenvolver novas ideias. No âmbito do projecto FUTON, agradeço ao Filipe Ferreira que demonstrou grande empenho nas nossas discussões e produção de resultados, o que resultou num produtivo trabalho conjunto. Por todos os momentos bem passados, obrigada também ao José Pina, Fernando Jesus, Rui Morais, Lara Pellegrino e Pedro Inácio. Aos parceiros do projecto FUTON, em particular à Universidade de Kent, Acorde e III-V Lab, agradeço a boa colaboração nas tarefas conjuntas que permitiu alcançar resultados muito positivos e manter contacto para futuras cooperações.

A todos os meus amigos e familiares agradeço a compreensão que tiveram durante o desenrolar deste doutoramento, percebendo e aceitando as minhas ausências e/ou falta de disponibilidade, em particular ao longo deste último ano.

Aos meus pais, o meu mais sincero bem-haja por estarem sempre presentes, por serem muito meus amigos, por me apoiarem e me darem valor. Agradeço todo o carinho e compreensão que sempre mostram. À minha irmã agradeço o sorriso e toda a amizade!

Finalmente, um agradecimento muito especial ao João, por todo o apoio, motivação, carinho, disponibilidade, por me ter feito acreditar nas minhas capacidades e me ter mostrado que não era impossível. Foste uma peça fundamental por todas as razões! Obrigada!

Table of Contents

List of Figures

List of Tables

List of Acronyms

ADC	Analogue-to-Digital Converter
ADSL	Asymmetric Digital Subscriber Line
APD	Avalanche PhotoDiode
APON	ATM Passive Optical Network
ASE	Amplified Spontaneous Emission
ATM	Asynchronous Transfer Mode
AWG	Arrayed Waveguide Grating
AxC	Antenna-Carrier
BER	Bit Error Rate
BPON	Broadband Passive Optical Network
BS	Base Station
BTS	Base Transceiver Station
CAGR	Compound Annual Growth Rate
CAPEX	Capital Expenditures
CATV	Community Antenna Television
CDD	Carrier Density Depletion
CDMA	Code Division Multiple Access
CDR	Clock and Data Recovery
CG	Coding Gain
CH	Carrier Heating
CM	Cable Modem
CO	Central Office
CPRI	Common Public Radio Interface
CRC	Cyclic Redundancy Check
CRRM	Common Radio Resource Management
CU	Central Unit
CW	Continuous Wave
CWDM	Coarse Wavelength Division Multiplexing

DAC	Digital-to-Analogue Converter
DAS	Distributed Antenna System
DBWS	Distributed Broadband Wireless System
Demux	Demultiplexer
DFB	Distributed FeedBack
DL	DownLink
DML	Direct Modulated Laser
DOCSIS	Data Over Cable Service Interface Specification
DSC	DownStream Channel
DSL	Digital Subscriber Line
DSP	Digital Signal Processing
DWC	Downstream Wavelength Converter
DWDM	Dense Wavelength Division Multiplexing
E/O	Electrical/Optical
EAM	Electro-Absorption Modulator
EC	European Commission
EDFA	Erbium-Doped Fibre Amplifier
EFM	Ethernet in the First Mile
EOP	Eye Opening Penalty
EPON	Ethernet Passive Optical Network
ER	Extinction Ratio
EVM	Error Vector Magnitude
FDD	Frequency Division Duplex
FDM	Frequency Division Multiplexing
FEC	Forward Error Correction
FP	Fabry-Perot
FSAN	Full Service Access Network
FTTB	Fibre-To-The-Building
FTTC	Fibre-To-The-Curb
FTTH	Fibre-To-The-Home
FUTON	Fibre Optic Networks for Distributed, Extendible Heterogeneous Radio Architectures and Service Provisioning
FWHM	Full Width at Half Maximum
FWM	Four-Wave Mixing
GEM	Generic Encapsulation Method
GFP	Generic Framing Procedure

GMSK	Gaussian Minimum Shift Keying
GPON	Gigabit-capable Passive Optical Network
GSM	Global System for Mobile communications
HDLC	High-level Data Link Control
HDTV	High Definition Television
HFC	Hybrid Fibre Coax
HSPA	High Speed Packet Access
IEEE	Institute of Electrical and Electronics Engineers
IF	Intermediate Frequency
IIP3	Third-order Input Intersect Point
IM3	Third-order InterModulation
IM-DD	Intensity Modulation and Direct-Detection
IMT-A	International Mobile Telecommunications-Advanced
IP	Internet Protocol
IP3	Third-order Intercept Point
IPTV	Internet Protocol Television
IQ	In-phase and Quadrature
ISDN	Integrated Services Digital Network
ISP	Internet Service Provider
ITU	International Telecommunication Union
ITU-T	ITU-Telecommunication standardization sector
LAN	Local Area Network
LC	Local Converter
LC-BTS	Local Converter located in the Base Transceiver Station
LC-RRH	Local Converter located in the Remote Radio Head
LE	Local Exchange
LO	Local Oscillator
LRE	Long-Reach EPON
LTE	Long Term Evolution
MAC	Medium Access Control
MC	Monte Carlo
MF	Master Frame
MG	Message Group
MIMO	Multiple-Input Multiple-Output
MPN	Mode-Partition Noise
MSR	Mode-Suppression Ratio

MT	Mobile Terminal
Mux	Multiplexer
MZI	Mach-Zehnder Interferometer
MZI-SOA	SOA-based Mach-Zehnder Interferometer
MZM	Mach-Zehnder Modulator
NCG	Net Coding Gain
NF	Noise Figure
NG PON	Next Generation Passive Optical Network
NGOA	Next Generation Optical Access
NRZ	Non-Return-to-Zero
O/E	Optical/Electrical
O/E/O	Optical/Electrical/Optical
OA	Optical Amplifier
OADM	Optical Add/Drop Multiplexer
OBSAI	Open Base Station Architecture Initiative
ODE	Ordinary Differential Equations
ODN	Optical Distribution Network
OFDM	Orthogonal Frequency-Division Multiplexing
OFDMA	Orthogonal Frequency-Division Multiple Access
OIP3	Third-order Output Intersect Point
OLT	Optical Line Terminal
ONU	Optical Network Unit
OPEX	Operational Expenditures
OSNR	Optical Signal-to-Noise Ratio
PLR	Packet Loss Ratio
PON	Passive Optical Network
POTS	Plain Old Telephone Service
PSC	Passive Splitter/Combiner
PtMP	Point-to-MultiPoint
PtP	Point-to-Point
QAM	Quadrature Amplitude Modulation
QoS	Quality-of-Service
QPSK	Quadrature Phase Shift Keying
RE	Radio Equipment
REC	Radio Equipment Control
RF	Radio Frequency

RIN	Relative Intensity Noise
RMS	Root Mean Square
RN	Remote Node
RoF	Radio-over-Fibre
R-ONU	Optical Network Unit with Reflective Semiconductor Optical Amplifier
RRC	Root-Raised Cosine
RRH	Remote Radio Head
RS	Reed-Solomon
RSOA	Reflective Semiconductor Optical Amplifier
Rx	Receiver
SBS	Stimulated Brillouin Scattering
SCM	Sub-Carrier Multiplexing
SDH	Synchronous Digital Hierarchy
SDM	Space Division Multiplexing
SFDR	Spurious-Free Dynamic Range
SHB	Spectral Hole Burning
SMF	Standard Monomode Fibre
SNR	Signal-to-Noise Ratio
SOA	Semiconductor Optical Amplifier
SPM	Self-Phase Modulation
SRS	Stimulated Raman Scattering
TC	Transient Control
TDD	Time Division Duplex
TDM	Time Division Multiplexing
TDMA	Time Division Multiple Access
TIA	TransImpedance Amplifier
TL	Tunable Laser
TL-ONU	Optical Network Unit with Tunable Laser
TPON	Telephony over Passive Optical Network
Tx	Transmitter
UDWDM	Ultra-Dense Wavelength Division Multiplexing
UL	UpLink
UMTS	Universal Mobile Telecommunications System
USC	Upstream Channel
UWC	Upstream Wavelength Converter
VDSL	Very high bit-rate Digital Subscriber Line

VoD	Video-on-Demand
VoIP	Voice over Internet Protocol
WC	Wavelength Converter
WC-RN	Remote Node with Wavelength Converter
WDM	Wavelength Division Multiplexing
WiMAX	Worldwide interoperability for Microwave Access
WLAN	Wireless Local Area Network
WWW	World Wide Web
XGM	Cross-Gain Modulation
XPM	Cross-Phase Modulation

List of Symbols

A_{eff}	effective area
A^{ao}	acousto-optic effective area
B	data rate
BER_{in}	Bit-Error Rate before Forward Error Correction
BER_{out}	Bit-Error Rate after Forward Error Correction
$B_{\text{n.av}}$	measurement bandwidth for $I_{\text{n.av}}$
D	fibre dispersion parameter
d	wireless propagation distance
F_{A}	excess noise factor of an avalanche photodiode
f	frequency
f_{c}	UMTS chip rate
f_{s}	sampling frequency
G_{comp}	gain of a single component
G_{cs}	cascaded gain
G_{link}	optical link gain
G_{FEC}	Forward Error Correction gain
g_0	unsaturated amplifier gain
g_{B}	Stimulated Brillouin Scattering gain
g_{R}	Stimulated Raman Scattering gain
h_{CH}	contribution to the overall SOA gain due to the Carrier Heating
h_{N}	contribution to the overall SOA gain due to the Carrier Density Depletion
h_{SHB}	contribution to the overall SOA gain due to the Spectral Hole Burning
I_{d}	dark current
$I_{\text{n.av}}$	average equivalent input noise current of the receiver
k	mode-partition coefficient
k_{A}	ionization-coefficient ratio
k_{B}	Boltzman constant
k_{SBS}	Stimulated Brillouin Scattering polarization factor
k_{SRS}	Stimulated Raman Scattering polarization factor
L	fibre length
L_{eff}	effective interaction length
IL_{link}	optical link insertion loss

M	avalanche gain
M_{IQ}	I and Q sample width
M_{opt}	optimum avalanche photodiode gain
N_{AxC}	size of an antenna-carrier container
NF_{comp}	noise figure of a single component
NF_{cs}	cascaded noise figure
N_{min}	individual FEC frame length, excluding redundancy bits
N_p	total packet length, excluding redundancy bits
n	refractive index
n_{DMUX}	number of encoders/decoders in the implementation of a Reed-Solomon code
n_{out}	noise power density at the output of the link
n_{PL}	path loss exponent
n_0	ordinary refractive index of the material
n_2	nonlinear index coefficient
q	electron charge
Q	Q-factor
Q_{penalty}	Q-factor penalty
P_{CW}	Continuous-wave power
P_{IF}	power of IF signal
P_{in}	input power
$P_{\mathrm{main\_avg}}$	average main mode power of a multimode signal
P_{N}	noise power
P_{out}	output power
P_{RF}	power of RF signal
P_{sat}	amplifier saturation power
P_{rx}	received power
P_{SBS}	Stimulated Brillouin Scattering threshold power
P_{side}	side mode power of a multimode signal
$P_{\mathrm{side\_avg}}$	average side mode power of a multimode signal
P_{S}	parameter to determine the saturation power of an optical amplifier
P_{SE}	probability of a symbol error
P_{SRS}	Stimulated Raman Scattering threshold power
P_{USE}	probability of an uncorrectable symbol error
P_{tx}	transmitted power
PL	path loss
$\Re$	receiver/photodiode responsivity
R_{L}	load resistor
R_{MSR}	MSR factor
s_{laser}	slope efficiency of a directly modulated laser
s_{md}	slope efficiency of the modulation device
s_{mzm}	slope efficiency of a MZM device

S_{rx}^2	average received signal power
T	absolute temperature
T_B	damping time of acoustic waves
T_{ff}	fibre-to-fibre transmission of the modulator
T_0	room temperature assumed to be 290K
t	maximum correcting capability of a Reed-Solomon code
V_π	on-off switching voltage of the modulator
w	mode field radius
X_σ	accepted log-normal variation in the channel path loss
Z_{src}	impedance of the optical source
α	fibre attenuation parameter
α_{MPN}	MPN-induced power penalty
α_{src}	parameter that accounts for laser frequency response variations
Δf	effective noise bandwidth of the receiver
$\Delta P_{critical}$	critical power budget
ΔT	relative delay between main mode and side modes
$\Delta\lambda_L$	space between modes of a multimode signal
$\Delta\nu_P$	pump light bandwidth
$\Delta\nu_{SBS}$	spontaneous Brillouin bandwidth
ε_{CH}	nonlinear gain suppression factors due to Carrier Heating
ε_{SHB}	nonlinear gain suppression factors due to Spectral Hole Burning
ϕ_{NL}	nonlinear phase shift
γ	nonlinear parameter
γ_n	f^2 noise coefficient characteristic of a transimpedance amplifier
λ	wavelength
ρ	material density fluctuation around a mean value ρ_0
σ_{MPN}^2	noise variance due to Mode Partition Noise
σ_{rx}^2	receiver noise variance
σ_s^2	shot noise variance
σ_T^2	thermal noise variance
σ_λ	root-mean square spectral width of the laser source
τ_1	carrier-carrier scattering time
τ_h	temperature relaxation time
τ_S	carrier lifetime
Ω	Stokes shift frequency
Ω_B	Brillouin frequency shift
Ω_R	Raman frequency shift
$\xi(r)$	acoustic wave mode

Chapter 1

INTRODUCTION

The emergence of digital telecommunications and, more recently, the appearance of new computer applications, has been the predominant impact factor for the latest social and economic worldwide development. The possibility of being connected anywhere and anytime, which is currently worldwide spread, opens the window for numerous service opportunities, typically requiring the provisioning of significantly high bandwidth.

In contrast with the earliest telecommunications services, such as telegraphy, telephony, radio and television, computer networks and the Internet have been experiencing a remarkable growth. Applications such as web browsing, electronic mail, file sharing, Voice over Internet Protocol (VoIP), IP Television (IPTV), High Definition TV (HDTV), online gaming, Video on Demand (VoD) and social networking have made Internet almost omnipresent in the current day-to-day lifestyle.

These new bandwidth-hungry applications are clearly highly dependent on the capacity provided by the telecommunications infrastructures. In fact, with a capacity growth doubling every year, the paradigm in telecommunications networks has rapidly changed from supporting local and low bandwidth traffic to providing worldwide connections with high bandwidth consuming traffic. This evolution has been verified in all segments of the telecommunications networks, ranging from the access to the metropolitan and backbone networks, which were forced to cope with the larger traffic volumes by upgrading their systems and technologies.

Currently, service providers, and generically the telecommunication industry as a whole, are facing an important challenge. Since the users expect high bandwidths, low loading times and reduced latency in real-time services, telecommunications networks need, besides providing a high transmission capacity, to be reliable, flexible, fault tolerant and low energy consuming, and all these characteristics should be achieved with ever decreasing cost per transported bit. As depicted in Figure 1.1, and referred by many different organizations, operators are now facing a growing gap between their revenues and the increasing bandwidth demands. This is verified because the increasing expenditures necessary to upgrade the network capacity are typically not supported by proportionally augmenting operator revenues. In reality, most operators experience a very slow, or even null, revenue increase. Therefore, the present challenge requires new network technologies and architectures, allowing to upgrade the capacity while simultaneously reducing the cost per transported bit.

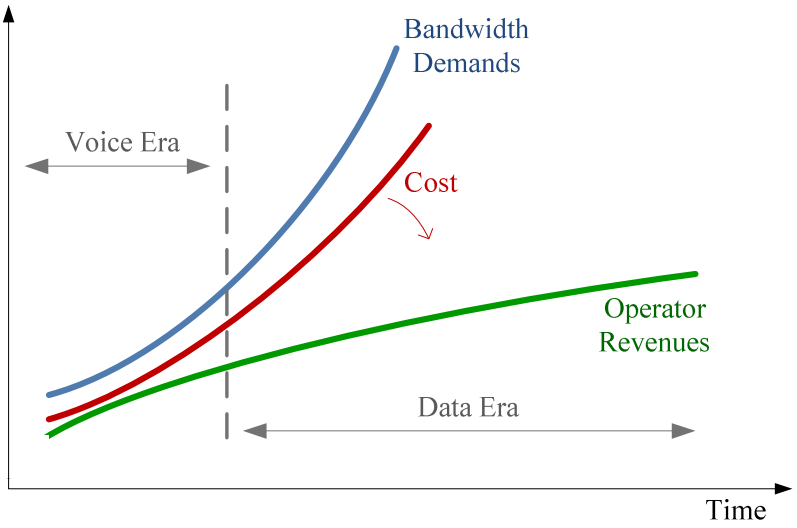

Figure 1.1 – Increasing gap between bandwidth demand and operator revenues.

The abovementioned requirements associated with increasing bandwidth demands have been fulfilled with different technologies in each network segment. The access has probably been the network segment where a more sweeping evolution took place. Fixed access networks have evolved from the Plain Old Telephone System (POTS), to Integrated Services Digital Network (ISDN), Asymmetric Digital Subscriber Line (ADSL) and Very high bit-rate Digital Subscriber Line (VDSL), all of which utilize twisted copper pair as the transmission medium. In parallel, the Data Over Cable Service Interface Specification (DOCSIS) has been developed to exploit the Hybrid Fibre Coax (HFC) network of traditional

Community Antenna TV (CATV) operators. More recently, the merits of optical fibre as the transmission medium for access networks have been exploited through Fibre-To-The-Home (FTTH) deployments, using Passive Optical Network (PON) approaches, with special emphasis on Gigabit-capable PON (GPON) and Ethernet PON (EPON). Simultaneously, wireless access networks have advanced from second generation (2G) technologies, such as the Global System for Mobile communications (GSM), to the third generation (3G) Universal Mobile Telecommunications System (UMTS) and its 3.5G upgrade High Speed Packet Access (HSPA), whereas the IEEE 802.11 protocol, known as Wi-Fi, has emerged to dominate the Wireless Local Area Network (WLAN) landscape.

In agreement with the foreseen bandwidth demand growth, future access networks will have higher capacity. In the wired side, advanced PON architectures, supporting higher data rates or different transmission paradigms, have been considered by operators, manufacturers and standardization bodies, addressing the potential requirement of 1 Gbit/s per subscriber. Moreover, the so-called fourth generation (4G) wireless systems, whose contenders are the Worldwide interoperability for Microwave Access (WiMAX) and the Long Term Evolution (LTE), are approaching commercial deployment, while more sophisticated wireless systems, such as LTE-Advanced, are being researched and standardized.

The importance of access networks coping with bandwidth increasing demands in a cost-effective manner is crucial to avoid this network segment from being a bottleneck between customers and backbone networks. In this context, the focus of the present work is the identification of methodologies to help fulfilling such objective. A brief introduction to the evolution of access networks, from copper to current systems, with special focus on optical access approaches, is presented in the next section. The following section discusses the envisioned progress trends for access networks, along with existing proposals to realize these networks. The objectives and organization of this thesis are summarized in section 1.3 and, finally, the contributions of this work in the context of next generation access networks and the associated scientific publications are highlighted in section 1.4.

1.1. Evolution of Optical Access Networks

The access network comprises the network infrastructure that connects the central hubs of the service providers with the end-users, which are either business or residential subscribers. The first technology developed for access was POTS, which evolved to ISDN, but soon the

telephone companies were pushed to react to the growing bandwidth demands, in order to satisfy the subscriber needs. This reaction came in the form of advanced Digital Subscriber Line (DSL) standards [Fos98]. All DSL flavours use the existing telephone copper line infrastructure, and require a DSL modem located at the end-user premises and a Digital Subscriber Line Access Multiplexer (DSLAM) located at a service provider hub. With the development of DSL standards, the bandwidth utilization has increased by two orders of magnitude, from under 100 kHz for narrow-band ISDN to over 20 MHz for VDSL, enabled through advanced Digital Signal Processing (DSP) technology combined with innovative algorithms and coding methods. In spite of the significant bandwidth improvements, DSL technology still presents some limitations to support high bandwidths at long transmission distances (the radius of the area serviced by a single hub is less than around 6 km).

Cable television companies did not fall behind and responded to the bandwidth demands by integrating data services into their coaxial cable networks, using Cable Modem (CM) technology [SA00]. A CM (or cable TV modem), the key component of a CATV network, has a connection speed of about 500 kbit/s to 1.5 Mbit/s, and is deployed in Point-to-Point (PtP) systems, covering distances over 100 km. Typically, CATV operators use HFC networks, which are characterized by fibre deployments connecting hubs to remote optical nodes, while coaxial cable is deployed to connect these remote nodes to the subscribers. The main drawback of such architecture is that the bandwidth of an optical node must be shared by all end-users connected to it, which results in low access rates when the traffic load is large.

Although being much faster than the analogue 56 kbit/s modem, DSL and CM are far from being true broadband solutions, since both are not capable of satisfying the stringent demands of the emergent bandwidth-hungry applications. The obvious evolution would be to bring optical fibre technology into the access landscape, in the form of Fibre-To-The-Building (FTTB), Fibre-To-The-Curb (FTTC) or FTTH deployments [Yam96], [LNL+05]. Since optical fibre is a transmission medium with a virtually infinite bandwidth capacity, it is suitable to support multiple-play services in a cost-effective manner, fitting the access networks characteristics and demands. In fact, FTTB, FTTC or FTTH architectures can support gigabit per second speeds at costs comparable to DSL and HFC networks, by deploying a passive system designated by PON.

PON emerged in the last decade as an attractive platform for meeting the access requirements. It only has active elements outside its Optical Distribution Network (ODN), offering low-cost, flexibility, scalability and simple infrastructure management. In a PON, the

integrated data services are digitally transmitted over a shared optical fibre infrastructure that connects a Central Office (CO), where an Optical Line Terminal (OLT) is located, to fibre-terminating nodes named Optical Network Units (ONUs). A passive Remote Node (RN), typically in the form of a power splitter/combiner, is deployed between the CO and the ONUs. The feeder network is the portion of the network that connects the OLT to the remote node, and the distribution network connects the remote node to the ONUs.

The forerunner PON architecture is the TPON, originally called PON for telephony [SHP+88]. Several enhancements have been proposed to the basic TPON architecture, but its development was accelerated with the establishment of the Full Service Access Network (FSAN) working group [FSA], in the 1990s, which was formed by an alliance of major telecommunications service providers and system vendors. The first PON standard specified by FSAN was based on the Asynchronous Transfer Mode (ATM), and has therefore been referred to as APON (ATM PON) [BRH90]. The International Telecommunications Union (ITU) has designated APON as ITU-T G.983 standard. Further improvements added to the original APON standard led to the final version of ITU-T G.983 standard, being more often referred to as Broadband PON (BPON) [ITU05].

In 2001, the FSAN working group started the development of the GPON standard [ITU08], initially ratified in January 2003, which represents a significant boost in both the total bandwidth and in bandwidth efficiency, when compared with the BPON standard [Cae04]. The main purpose of the FSAN working group when developing GPON was to support full service, including voice (Time Division Multiplexing (TDM) over SONET/SDH), Ethernet (10/100 BaseT), ATM, etc., by using a Generic Framing Procedure (GFP) in an evolutionary scenario from BPON, with enhanced management and security mechanisms [Cae04]. The FSAN began developing a new GPON version in 2007, and the standard was formally ratified by the ITU in September 2010 [ITU10]. Currently known as XG-PON1, its most important feature is its increased bandwidth, reaching 10 Gbit/s in the downstream direction and 2.5 Gbit/s in the upstream.

During the 1990s, when the FSAN working group started its activities, it was expected that ATM would become the most widespread data-link technology. However, Ethernet technology has become a universally accepted standard for Local Area Networks (LANs), allowing for remarkable cost savings. The deployment of Gigabit Ethernet in LANs was pursued very quickly, and 10 Gigabit Ethernet equipments were soon available in the market. Moreover, the low-cost Ethernet technology, very well adapted to IP traffic, was also

penetrating in metropolitan and backbone networks, thereby guaranteeing interoperability with a myriad of existing equipments, and showing that it would also be suitable for being deployed in access networks.

The Ethernet in the First Mile (EFM) work group [EFM] developed this idea and, in June 2004, the EPON standard, referred to as IEEE 802.3ah [IEEE04], was ratified by the Institute of Electrical and Electronics Engineers (IEEE). The purpose of the EFM group was to combine Ethernet and PON technologies in order to provide a cost-effective and high-performance access technology [KP02]. Using the Point-to-Multipoint (PtMP) architecture inherent to the original Ethernet, adaptation of Ethernet to the PON architecture was straightforward [Cae04]. More recently, in 2009, a new standard was ratified for EPON systems operating at data rates up to 10 Gbit/s [IEEE09]. These new systems, still without field deployments, represent a smooth evolution of the first generation EPON and will be further addressed in the next section.

According to Infonetics Research [Inf11], currently there are more than 35 million PON FTTH subscribers worldwide. This report, based on 2010 statistics, predicts that PON FTTH subscriptions will continue to grow driven by the global broadband phenomenon. A Compound Annual Growth Rate (CAGR) of 25% is estimated until 2015, when the number of subscriptions is predicted to reach 109 million, with 34% EPON subscribers, 61% GPON subscribers and 5% BPON subscribers. In 2010, Asia Pacific was the leading region for PON FTTH subscribers (75%), followed by North America (21%). The FTTH subscriptions in Europe-Africa are increasing, and the forecast indicates that they will grow to 18% of the global subscriptions by 2015. The current preference in Asia Pacific is for EPON systems, representing 98% EPON subscriptions in 2010, whereas 44% of GPON subscribers reside in North America. Although with a still reduced PON FTTH penetration, GPON leads in Europe-Africa with 85% of PON subscribers in 2010.

1.2. Next Generation Access Networks

In view of the perspectives and traffic forecasts for the next few years, network operators, manufacturers and standardization bodies are deeply committed to develop appropriate solutions for next generation access networks [BGH+11]. The current development progress regarding access networks is gaining a remarkable importance for deploying future systems that comply with customers and operators needs [LSK06], [EKM10].

In the current fixed access landscape, active PtP Ethernet continues to be an option in several regions, offering up to 1 Gbit/s links to the end-users. However, most key players are now convinced that FTTH solutions bring several benefits in terms of cost, upgradeability and also environmental impact. Therefore, in this context, Next Generation PON (NG PON) systems are being developed guaranteeing that new and legacy services, both analogue and digital, can be supported over a converged infrastructure.

As illustrated by the commonly used tendency curves shown in Figure 1.2, a clear differentiation exists nowadays between both wireline and wireless access. Wireless systems are typically connected through leased line services (such as E1/T1) transmitted over copper (most common solution) or fibre, or microwave-based PtP links, to provide bandwidth Internet services and mobility to the end-users. On the other side, wired systems, relying on copper plant, HFC network or optical fibre, guarantee the highest bandwidth needs, albeit without providing mobility. Anyway, a similar evolution track is registered for both systems. It is therefore clear that being able to benefit from the high capacities of next generation fixed access networks, while keeping the wireless autonomy, represents the most desirable scenario from an end user point of view.

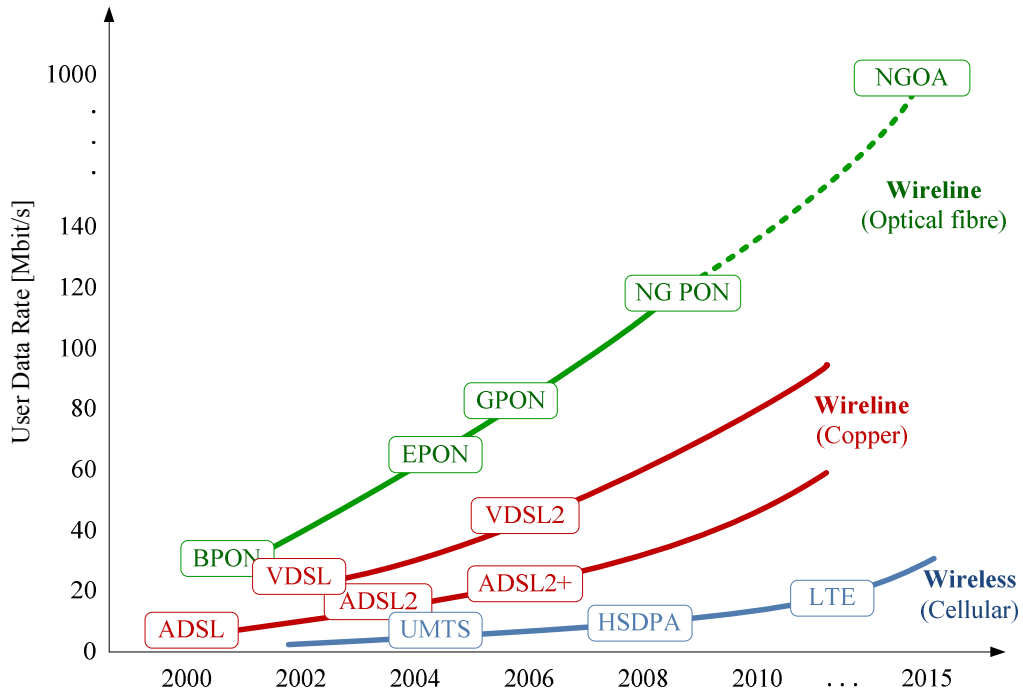

Figure 1.2 – Evolution of access technologies.

Coping with the abovementioned requirements, all next generation broadband access approaches should verify a number of key conditions to be presented as profitable solutions [EKM10], [BGH+11]. Amongst them, the maximum utilization of the already installed fibre plants, a flexible upgradeability, and the capability to provide higher bandwidth than current solutions may be selected as the most important, when combined with optimized technology in terms of cost, performance and energy savings. Another important aspect that should be considered is the mobile backhaul support. With the data rate increase of wireless systems, as shown in Figure 1.2, the bandwidth demands for backhauling cellular traffic are dramatically increasing. All these conditions have been the main drivers for the design, specification and development of next generation access solutions, which are expected to support mobile backhauling applications simultaneously with voice, data and video traffic for residential and business subscribers.

With their standardization process already ratified, the following NG PON systems were specified pursuing the data rate increase trend, reaching transmission rates of up to 10 Gbit/s [EKM10]. As referred in section 1.1, these systems are the next in the deployment stack, since they represent a straightforward evolution of first generation GPON and EPON systems. The XG-PON1 [ITU10] allows an increase of the downstream transmission rate from 2.5 Gbit/s to 10 Gbit/s and of the upstream transmission rate from 1.25 Gbit/s to 2.5 Gbit/s when compared to GPON. The lower data rate for the upstream is justified by the difficulty of providing higher speeds at a reasonable cost. With a work that started one year earlier, IEEE set up the 802.3av group to develop a 10 Gbit/s variant of EPON systems [IEEEav], completing the corresponding standard in 2009 [IEEE09]. Contrasting to ITU, IEEE opted for two upstream data transmission speeds, specifying a symmetric version, with 10 Gbit/s up- and downstream, and another version that maintains the 1 Gbit/s upstream speed of EPON systems, increasing only the downstream speed to 10 Gbit/s. A very important feature of both standards is that they can be deployed over an existing fibre infrastructure, guaranteeing compatibility with previous GPON/EPON systems, since a different wavelength allocation plan is used [EKM10]. These mixed deployments are especially relevant when different subscribers (residential, multi-dwelling units, business, etc.) need to be supported by the same network. Another important aspect of these standards is the supported extended link budgets [EKM10]. For instance, XG-PON1 was designed to support split ratios up to 1:256, which is a significant boost compared to GPON. Other enhancements of XG-PON1 include improved security and power saving features, enabling a more reliable and energy efficient system.

FSAN has already started to work towards solutions for NG PON2 systems [FSA]. This effort began in 2010 and it is expected that an agreement about the better approach will be reached in 2012-2013. Although initially NG PON2 was seen as an opportunity to re-design the evolution direction of FTTH approaches, it is now clear that most operators wish to maintain the existing physical infrastructures, as much as possible, and therefore the coexistence of all three PON generation systems must be assured.

Access networks based on Wavelength Division Multiplexing (WDM) technology have therefore a high probability of being selected for NG PON2 networks, beyond 10 Gbit/s systems [BGH+11]. WDM-PONs, and also WDM/TDM-PONs, were earlier proposed in the literature [IFR97], [FHJ+98], [PLJ+04], and a few field implementations took place [LCL+09], but without massive deployments. A WDM-PON is generally recognized as a PON in which each ONU has a dedicated wavelength channel for each transmission direction to/from the OLT, enabling virtual PtP connections. Under specific conditions, the WDM technology over a TDM-PON also enables an increased number of ONUs connected to the same trunk fibre, with the consequent increase of the number of subscribers, and a longer network reach. The use of WDM allows superimposing multiple types of signals over a TDM-PON, such as baseband signals, video or radio channels, and addressing them to ONUs with different characteristics. Furthermore, it enables the provisioning of different Quality-of-Service (QoS) specifications, in order to serve residential and enterprise customers over the same structure.

Typically, a PON has a tree or tree and branch topology and, therefore, when WDM is added the tendency is to maintain this topology. However, according to the technology chosen for the RN, different features will characterize the network architecture. If a passive coupler is employed, such as in a typical TDM-PON system, a “broadcast and select” network is obtained. On the other hand, a wavelength routing device may be used, selecting the specific wavelength to be delivered to each ONU [FHJ+98]. The deployment of WDM-PON systems requires the use of wavelength agnostic ONUs, usually referred to as colourless ONUs. The candidate schemes under research to realize such devices include injection locking methods [WIRF98], wavelength seeding [PCB06] and spectrum slicing [PJS+07] techniques, as well as wavelength tuning [ZA10], which represents a big challenge in the evolution towards low cost and high performance devices.

An alternative approach for future access is to devise a coherent PON system, making use of coherent transceivers, and designated by Next Generation Optical Access (NGOA) [Bil10], [RSG10]. As indicated in Figure 1.2, this option provides a very high bandwidth,

reaching 1 Gbit/s per end-user, and offers a high splitting factor of about 500-1000, in an extended reach network with up to 100 km. These characteristics are attained using Ultra-Dense WDM (UDWDM), with a wavelength grid of only a few GHz. NGOA is a wavelength agnostic system, where all UDWDM channels are distributed to all ONUs and a tuneable transceiver at the ONU selects its assigned channel [SGR+11], which clearly requires even more research progress on these optical components to reduce their cost. The use of coherent detection enables to overcome the high losses resulting from high splitting ratios and long reach, also enabling to relax the stringent optical requirements by means of electronic signal processing. Such solution offers smooth upgrade possibilities for individual channels towards higher data rates. Moreover, it provides high flexibility for different operators to access the same fibre infrastructure without interference, since at each ONU the operator can be freely selected, allowing for network reconfigurations on demand. In a system such as NGOA, an important advantage is the fact that different high bandwidth traffic flows may be easily supported over different channels. This may become particularly relevant in network scenarios where wired and wireless systems need to coexist over the same infrastructure, since they would be separated in the wavelength domain, thereby reducing expenditures, while avoiding complex adaptation layers between both systems.

1.3. Objectives and Organization of the Thesis

The evolution of access networks in the past few decades has created several areas of research, involving the development and improvement of the known architecture proposals as well as new disruptive approaches, such as those intending to integrate the two main telecommunications brands, optical and wireless. The present thesis addresses relevant physical layer issues in the development of high data rate PON systems, analysing their impact on network performance and proposing, whenever applicable, improved solutions. The support of wireless systems with an optical infrastructure is also addressed by this work, identifying and dimensioning the suitable architecture scenarios and evaluating the data transmission options. The main objectives orienting this thesis are the following:

- Investigation of physical layer impairments in high data rate PON systems; these impairments may be driven by any of the sub-systems that integrate the optical access network, namely the optical source, the transmission medium and the receiver;

- Analysis of error correction and detection methods to be applied in high data rate PON systems, and evaluation of the resulting benefits in the network performance;
- Investigation of the near-far problem typical of PON systems based on burst-mode transmission, and proposals for their mitigation in high data rate access networks;
- Research of optical architectures adequate to support the deployment of distributed antenna systems, balancing their capacity, power budget and cost;
- Investigation of radio transmission modes, analogue and digital, over a distributed antenna system, comparing the required capacity, components and cost;
- Assessment of analogue radio transmission performance in a distributed antenna system over a fibre optic infrastructure; this evaluation should comprise the analogue link design and modelling, its experimental validation and the predicted performance of the network applications under consideration.

This thesis comprises a total of seven chapters, divided in Part A and Part B, and complemented by 6 appendices. Part A, termed "Wired Optical Access Networks", is devoted to next generation wired access networks based on optical fibre technologies, and comprises Chapter 2, Chapter 3 and Chapter 4. Converged fixed-wireless access networks are the subject of Part B, designated "Integrated Fixed-Wireless Access Networks", which includes Chapter 5 and Chapter 6.

Chapter 2 is dedicated to the assessment of physical impairments in next generation PON systems that are operated with a data rate of 10 Gbit/s. Limitations driven by the optical source are addressed through modelling to verify how they affect the network performance. The effect of fibre nonlinearities is estimated aiming to determine the limits imposed in the power transmitted through the fibre. Focusing on the third sub-system of a typical access network, the optimum operating conditions of gain photodetectors are also investigated.

Chapter 3 concentrates on the use of error correction techniques to improve the performance of PON system operating at 10 Gbit/s. The fundamental concepts of the main types of correction codes are outlined and the most suitable code to be deployed in the considered scenario is identified. The benefits on the system performance attainable by using error correction are addressed and quantified.

Chapter 4 focuses on one of the main challenges of high data rate PON systems, which should be capable of dealing with burst-mode transmission. One approach to reduce the

impact of this operating mode on the performance is to take advantage of power equalization schemes to minimize the near-far effect characteristic of such systems. Therefore, a simple all-optical burst-mode power equalization scheme, based on cascaded optical amplifiers, is proposed, and its design rules and performance characteristics are reported. Two network applications for the proposed method are assessed, covering the use of PONs in access and metro-access networks.

Chapter 5 is the first chapter of part B and describes architecture scenarios for converged wired-wireless access networks. In this context, the compatibility of wireless transmission with PON systems is highlighted and a series of candidate fibre-optic architectures are proposed, compared and analyzed to support radio transmission in a scenario with distributed antennas. Analogue and digital transmission modes are assessed for the transport of these radio signals, with emphasis on the bandwidth requirements of digital transmission protocols and their use to map the radio information over PON systems. An economical comparison of analogue and digital approaches is also reported.

In the context of analogue fibre-optic architectures to support radio signals, Chapter 6 is dedicated mainly to the work carried out in the context of the European Commission (EC) project FUTON, and, therefore, presents an overview of the project concept and its main achievements. The work towards the analogue fibre link modelling is described, detailing the approach that makes use of externally modulated optical sources. This link modelling is based on an analytic approach that was used afterwards to create simulation models, validated by experimental tests. The second part of Chapter 6 describes the performance assessment of analogue radio transmission systems when operated with multiple technologies, representative of 2G, 3G and 4G wireless protocols.

Finally, Chapter 7 highlights the main conclusions and outcomes of the work developed along the progress of this thesis, pointing out some future research topics.

1.4. Contributions of the Thesis

This thesis reports the research work carried out by the author on next generation access networks. Proposals for optical access exploiting high data rates are the main research area of the first part of this work, whereas the convergence of wired and wireless domains, sharing the optical infrastructure to distribute radio signals, is the focus of the second part of the thesis.

The first part of the thesis, Part A, comprises the analysis of the main limitations of high data rate optical access networks, through assessment of their impact on network performance, and the evaluation of proposals that aim at minimizing such impact. Whenever applicable, the subjects covered in Part A are supported by a state-of-the-art description and an initial overview of previous works aiming at similar objectives.

Part B of this thesis details the work done focusing on the architectures to support the distribution of radio signals using an optical fibre infrastructure. The compatibility with the existent access networks is assessed and the available radio transmission protocols are analyzed. The final part of this thesis is dedicated to the work carried out in the framework of the FUTON project, mainly focusing on the link modelling analysis, with external modulators, and the evaluation of network performance when such links are deployed.

The majority of proposals and performance studies completed during the course of this research work are reported in scientific publications, presented at conferences and journals in the field of optical communications, in a book chapter, and also in contributions to standard bodies. In the following, the main contributions of the thesis are listed, along with the corresponding publications produced.

- Assessment of the performance limitations due to the use of multi-mode optical sources in high data rate PON systems, in terms of source spectral width, fibre dispersion and network reach [PMS07b];
- Evaluation of the impact of fibre nonlinear effects in 10 Gbit/s PON systems, identifying the constraints imposed on the transmitted power by the fibre nonlinearities [PT06], [PLMS07];
- Analysis of the optimum operating conditions of gain photodetectors to be used in 10 Gbit/s PON systems [PMS07a];
- Performance comparison of forward error correction codes and assessment of the requirements for exploiting block codes in burst-mode transmission systems [PSM09];
- Analysis of the performance enhancement attained with the use of forward error correction codes in burst-mode transmission systems, through analytic and simulation approaches [PSM09];
- Proposal and characterization of a novel all-optical burst-mode power equalization scheme, based on semiconductor optical amplifiers [PMF+08];

- Assessment of the performance merits attained by using the proposed burst-mode power equalization scheme in access networks [PMF+08] and in metro-access networks [PMS09];
- Proposal of an alternative paradigm for metro-access networks based on all-optical wavelength band conversion, with a detailed characterization of its functional elements and a comparative analysis of costs [PPS+09a];
- Analysis of converged wired-wireless access networks, assessing their compatibility with passive optical networks [PSP+08];
- Proposal of fibre-optic architectures for supporting distributed antenna systems, based on topological considerations [PPS+08], addressing their capacity in terms of the necessary elements and supported remote units, and performing a comparison based on the multiplexing techniques used while assessing their power budgets and economical viability [PPM09], [PP12];
- Evaluation of digital transmission options for distributed antenna systems, addressing the mapping of digital radio signals over passive optical networks [PPMS11];
- Comparative economical analysis of distributed antenna systems based on analogue and digital radio transmission approaches [WPP+09];
- Participation in the EC project FUTON, developing and disseminating its concept and main achievements [GPMG09], [PPS+09b], [MPP+09], [PMG+09], [MPL+10];
- Modelling and experimental validation of radio over fibre links employing externally modulated optical sources [WNA+10], [WNG+10], [WNA+11], used to predict the performance of a complete FUTON system;
- Characterization of analogue radio links, through simulation and experimental tests, using externally and directly modulated optical sources [PFMS10];
- Evaluation of the transmission of high bandwidth radio channels over an analogue fibre link, based on an externally modulated optical source, and assessment of the simultaneous transmission of radio signals from different wireless systems generations over the same physical infrastructure [FPSM11].

Part A

Wired Optical Access Networks

Chapter 2

PHYSICAL IMPAIRMENTS IN HIGHER DATA RATE PASSIVE OPTICAL NETWORKS

Nowadays, the solutions that offer fibre connections to the end-users, such as the different types of PON systems, enable a giant step forward when compared to other existing access architectures, in terms of reliability and offered bandwidth. However, as more bandwidth-intensive services become available to the users, the network capacity will start to get exhausted and new advanced paradigms will be needed in a near future.

The current PON technologies were developed ensuring that a smooth path for future upgrades was provided. Their development intended to allow for incremental upgrades, in order to profit from all installed equipment and matured technology. Amongst their possible upgrade scenarios, the most relevant are the wavelength upgrade, the spatial upgrade, and the data rate upgrade. While the former two scenarios were considered to be solutions for a longer timescale, the data rate upgrade attracted a large number of adepts at the time of the first generation PON systems releases, favouring the development of new standards considering data rates as high as 10 Gbit/s [IEEE09], [ITU10].

The rate upgrade to 10 Gbit/s is a very attractive solution, especially considering the EPON case, which may immediately profit from the maturity of the 10 Gbit/s Ethernet standard, applications and equipment. This upgrade scenario also allows for an incremental upgrade cost, in situations where only a subset of first generation users is migrated to higher

data rate. This possibility will call for a mixed rate PON system, requiring high speed electronics to be used at the OLT, which must be able to operate at both first generation and upgraded data rates. However, when operating a PON system at higher data rates, namely at 10 Gbit/s, several physical impairments arise at all sub-systems of the network, namely at the optical source, the optical transmission fibre and the receiver.

The acceptance of this new generation 10 Gbit/s PON systems by operators, service providers, and subscribers will depend largely on the system cost and complexity. For this reason, and in order to follow the principles inherent to the development of PONs, these systems should be kept as low cost and simple as possible. Since 80% of the network cost is due to the ONUs and their deployment expenditures, it is desirable to continue using low cost components to build these network elements. Thus, laser sources based on multimode lasers, such as Fabry-Perot (FP) lasers, are a common and natural option. However, these lasers may originate performance degradation due to the multimode operation over Standard Monomode Fibre (SMF), in the form of Mode-Partition Noise (MPN). Moreover, considering the use of a Directly Modulated Laser (DML), either a FP laser or a Distributed Feedback (DFB) laser, as optical source, which is the option currently employed in the first generation PON systems, severe fibre dispersion penalties will occur for high data rate transmission. As presented in [Pat06], this is especially significant for downstream transmission, because the upstream is operated in the 1300 nm window, near the zero-dispersion wavelength.

It is foreseen that optical access systems operated at 10 Gbit/s will support a higher number of subscribers than the current PON systems. Thus, the support of these higher splitting ratios, namely for 64 or 128 ONUs, may prove to be critical in keeping these systems competitive. However, high splitting ratios result in larger splitter losses, which demand launching higher powers into the fibre to attain similar performance. Consequently, such high powers may result in non-negligible performance degradation due to fibre nonlinear effects, such as Self-Phase Modulation (SPM), Stimulated Brillouin Scattering (SBS), and Stimulated Raman Scattering (SRS).

Another important difficulty to overcome when increasing the data rate is the decrease of receiver sensitivity. This impairment influences the network maximum reach, and the emitted and received power levels required to maintain a specified performance [Pat06]. In the upstream transmission this difficulty will be aggravated by the burst transmission operation mode. Also, in order to comply with higher capacity and/or reach, the optical power budget will become more critical. An obvious approach to minimize these difficulties is to

provide gain to the system, either by employing optical amplification in the terminal elements of the network [Pat06], [PMS06] or by using a photodiode with gain, such as an Avalanche Photodiode (APD), which would replace the usually employed PIN photodiode.

Table 2.1 summarizes the main optical impairments identified when upgrading to 10 Gbit/s the data rate of a currently deployed PON system, and their corresponding causes.

Table 2.1 Main physical impairments affecting the data rate upgrade of PON systems.

Impairment	Cause	Reference
Mode-partition noise	Multimode operation over SMF	[PMS07b]
Increased dispersion penalty	Use of 10 Gbit/s DML sources	[Pat06], [PMS06]
Fibre nonlinear effects	High power injected to the system	[PT06], [PLMS07]
Decreased receiver sensitivity	Increased data rate	[Pat06], [PMS06]
	Critical optical power budget	[PMS07a]

The development of PON systems operating at 10 Gbit/s, namely EPON systems [IEEE09], was influenced, amongst other factors, by the identification and analysis of these impairments. When designing a network system it is crucial to determine the main obstacles to overcome, thereby enabling the characterization and elimination of its weak points. Several solutions might be considered, but the more economical and less complex are always preferred, allowing to develop a simple and economically feasible system. Pursuing this objective, the limitations that arise from MPN are analyzed in section 2.1, the impact of the optical fibre nonlinear effects is investigated in section 2.2, and the replacement of the PIN photodiode by APD is addressed in section 2.3.

2.1. Limitations from Mode Partition Noise

The overall system cost and complexity are the driving factors for the success or failure of an access technology. Therefore, next generation systems should be kept as low cost and simple as possible, following the principles inherent to the first generation PON systems. One of the main cost-critical components is the optical source, especially at the ONU, where the cost is not shared among the users, as it happens with the OLT. It is therefore desirable to avoid the use of high-cost DFB lasers in the ONUs. The multimode FP lasers present a much lower cost,

for the same data rates, and thus their use should be considered for 10 Gbit/s systems, as it was for the first generation ONU optical sources. The use of FP lasers, or any other multimode laser type, originates performance degradations due to the transmission of multimode signals over a SMF. These degradations are patent in the form of MPN.

MPN is a phenomenon that occurs because of an anticorrelation between laser longitudinal modes. The different longitudinal modes fluctuate in such a way that individual modes exhibit large intensity fluctuations, although the total intensity remains relatively constant [Agr02]. This effect is only harmful when combined with the effect of fibre chromatic dispersion, which causes the modes to become unsynchronized. This is because each of the simultaneously emitted longitudinal modes suffers a different propagation delay, due to the chromatic dispersion of the fibre. As a result of such de-synchronization, the signal reaching the optical receiver exhibits additional fluctuations. Over a long distance and in a high bit rate transmission system, these additional fluctuations degrade the performance and translate into a noise floor which determines the minimum bit error rate achievable with increasing optical power received. In such cases, the overall system error rate cannot be improved beyond the limit set by this noise, because the Signal-to-Noise Ratio (SNR) due to MPN is independent of the signal power.

Ideally, when employing a laser designed to oscillate in a single longitudinal mode, the MPN should be completely avoided. However, this is not necessarily true, since the main mode is accompanied by several side modes of much smaller amplitudes. A parameter designated by Mode-Suppression Ratio (MSR) is introduced to quantify the single mode behaviour of the lasers [Agr02]. The MSR is defined as the ratio between the main mode power and the power of the most dominant side mode. The effect of MPN on the system performance is dependent of the MSR. A major difference between multimode and nearly single mode lasers is related to the statistics associated with mode-partition fluctuations. In a multimode laser, both main and side modes are above threshold and their fluctuations are well described by a Gaussian probability density function. On the other hand, side modes in a single mode laser are typically below threshold, and the optical power associated with them follows an exponential distribution [Agr02], [Oga82].

The influence of MPN on the performance of high data rate PON systems operating at 10 Gbit/s is assessed in the following. The MPN analysis is based on semi-analytic simulations.

2.1.1. Analytic Modelling of MPN

As previously referred, MPN can be the dominant limitation in single-mode fibre transmission systems. Since this noise is a function of the laser spectral distribution and of the fibre chromatic dispersion, the SNR due to MPN is independent of the signal power. Therefore, the overall system error rate cannot be improved beyond a specific limit.

A simple model that describes the power penalty due to MPN is presented in [Oga82], and the main formulation is replicated in the following. In this model it is assumed that the amplitudes of the longitudinal modes are different, but the total power carried by each pulse is constant. According to the analysis in [Oga82] and [AAS88], the MPN leads to an additional noise term at the receiver, with a variance given by:

$$\sigma_{\mathrm{MPN}}^2 = \left\{ \frac{k}{\sqrt{2}} \left(1 - \exp\left[-\left(\pi BDL\sigma_\lambda \right)^2 \right] \right) \right\}^2 , \tag{2.1}$$

where B is the system data rate, D is the fibre chromatic dispersion parameter, L is the fibre length, σ_λ is the root-mean square spectral width of the laser source, and k is the mode-partition coefficient defined in [Oga82]. Experimental measurements suggest that the values of k are in the range 0.5-0.8 [AAS88]. This additional noise component should be added to the receiver noise so that the effective SNR is determined according to [AAS88]:

$$\frac{1}{Q^2} = \left(\frac{\sigma_{\mathrm{rx}}}{S_{\mathrm{rx}}} \right)^2 + \sigma_{\mathrm{MPN}}^2 , \tag{2.2}$$

where σ_{rx}^2 represents the receiver noise variance (excluding the MPN), S_{rx}^2 represents the average signal power received, and Q is related to the Bit Error Rate (BER) using $BER = 1/2 \operatorname{erfc}\left(Q/\sqrt{2} \right)$, when only electrical receiver noise is considered. The penalty induced by MPN is determined by the increase in the received power that is necessary to maintain the same SNR, and is given by [AAS88]:

$$\alpha_{\mathrm{MPN}} = -5 \log\left(1 - Q^2 \sigma_{\mathrm{MPN}}^2 \right). \tag{2.3}$$

This formulation shows that the MPN-induced power penalty becomes infinite for $\sigma_{\mathrm{MPN}} \geq Q^{-1}$, demonstrating the importance of evaluating MPN in the design of a transmission system. A negligible MPN-induced penalty, $\alpha_{\mathrm{MPN}} < 0.5\,\mathrm{dB}$, can be guaranteed by designing the optical system such that $BDL\sigma_{\lambda} < 0.1$.

Since the impact of MPN on system performance is dependent on the MSR, it is important to quantify the effect of the side-mode fluctuations. This is accomplished by evaluating the system BER in the presence of MPN, considering the use of an ideal receiver (no thermal noise, no dark current, and 100% quantum efficiency). In this case, the relative delay between the main and the side modes, ΔT, is assumed to be large enough to make the side mode fall outside the bit slot, such as [Agr02], [HHL84]:

$$\Delta T = DL\Delta\lambda_{\mathrm{L}}\text{: } \Delta T > 1/\mathrm{B} \text{ or } BDL\Delta\lambda_{\mathrm{L}} > 1, \tag{2.4}$$

where $\Delta\lambda_{\mathrm{L}}$ is the wavelength separation between modes. Also, the main and the side modes are considered to be anticorrelated, such that if the power of the main mode drops below half of its average power, $P_{\mathrm{main\_avg}}/2$, the power of the side mode, P_{side}, exceeds $P_{\mathrm{main\_avg}}/2$, maintaining the total power nearly constant. In this scenario, and assuming that the probability of deciding 0 when 1 is received is equal to the probability of deciding 1 when 0 is received, the BER uniquely due to MPN is obtained by [Agr02]:

$$BER_{\mathrm{MPN}} \approx \exp\left(-\frac{P_{\mathrm{main\_avg}}}{2P_{\mathrm{side\_avg}}}\right) = \exp\left(-\frac{R_{\mathrm{MSR}}}{2}\right), \tag{2.5}$$

where $P_{\mathrm{side\_avg}}$ represents the average side mode power and R_{MSR} is the MSR factor. To estimate the total system BER, an additional noise term should be added to the receiver noise to account for side-mode fluctuations. Therefore, for a thermal-noise limited system, where the electrical noise variance for bits 1 may be assumed to be equal to the electrical noise variance for bits 0, which is typically the case of PIN receivers, the total BER is given by [LKB+85], [Agr02]:

$$BER = \frac{1}{2}\mathrm{erfc}\left(\frac{Q}{\sqrt{2}}\right) + \exp\left(-\frac{R_{\mathrm{MSR}}}{2} + \frac{R_{\mathrm{MSR}}^2}{8Q^2}\right)\left[1 - \frac{1}{2}\mathrm{erfc}\left(\frac{Q}{\sqrt{2}} - \frac{R_{\mathrm{MSR}}}{2\sqrt{2}Q}\right)\right]. \tag{2.6}$$

For a shot-noise limited system, as is the case when APD receivers are employed, the electrical noise variance for bits 0 is negligible in comparison to the electrical noise variance for bits 1, and equation (2.6) should be replaced by (the gain of the APD is not considered in this formulation, i.e. APD gain is assumed to be unitary):

$$BER = \frac{1}{2}\operatorname{erfc}\left(\frac{Q}{2\sqrt{2}}\right) + \exp\left(-\frac{R_{MSR}}{2} + \frac{R_{MSR}^2}{2Q^2}\right)\left[1 - \frac{1}{2}\operatorname{erfc}\left(\frac{Q}{2\sqrt{2}} - \frac{R_{MSR}}{Q\sqrt{2}}\right)\right]. \qquad (2.7)$$

Typically, at the OLT side of a PON system the cost is not as critical as for the ONUs. Therefore, the use of higher-cost single-mode DFB lasers is acceptable in the OLT. Apparently, this type of optical source should not be affected by MPN, but, as explained before, this is not completely true. Considering the downlink direction of a PON system (operating in the 1500 nm window) with a target BER of 10^{-12}, not accounting for MPN, Figure 2.1 depicts the total BER for several MSR values, assuming a PIN receiver at the ONU. Although not commonly used, if an APD receiver is employed in the ONU, the total BER obtained is shown in Figure 2.2, given by equation (2.7), also considering several MSR values.

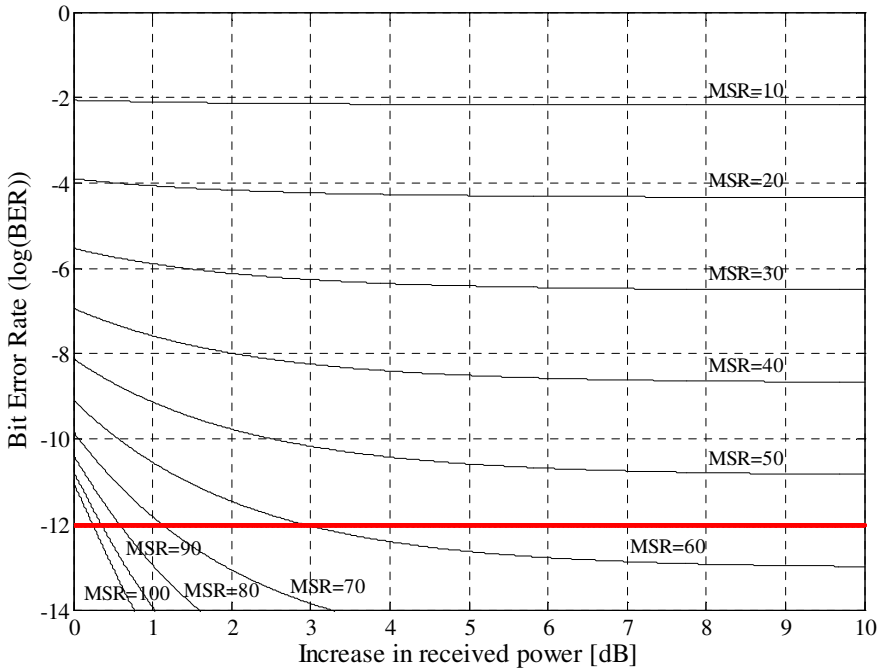

Figure 2.1 – Effect of MPN on the BER of DFB lasers for several values of MSR, considering a reference BER of 10^{-12} with no MPN and a PIN receiver.

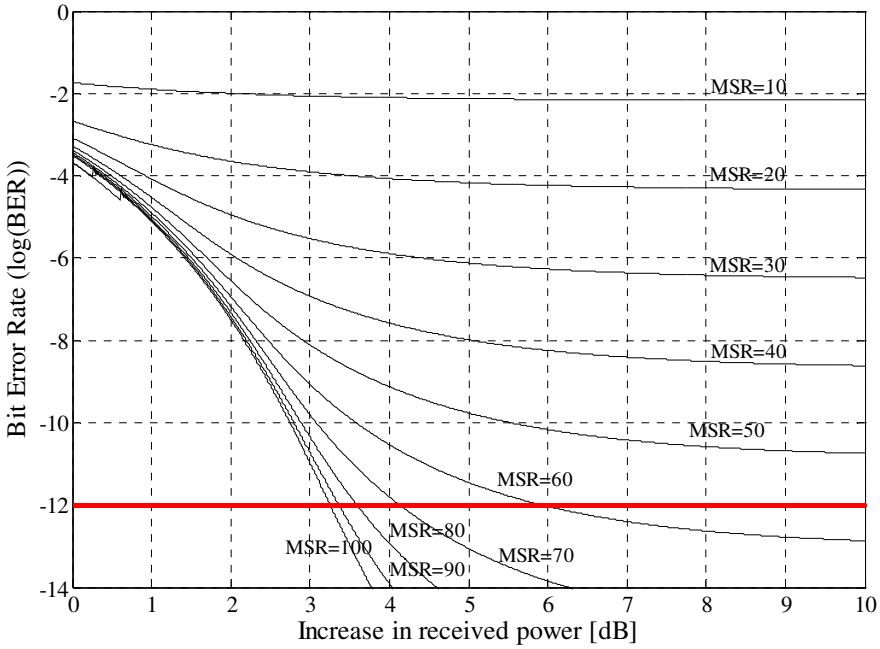

Figure 2.2 – Effect of MPN on the BER of DFB lasers for several values of MSR, considering a reference BER of 10^{-12} with no MPN and an APD receiver.

From these figures, the MPN induced power penalty is given by the intersection of the red line with the solid curves. As expected, the power penalty becomes infinite for MSR values below 56, since the 10^{-12} BER cannot be realized irrespective of the power that is received. The penalty can be reduced to the negligible level of 0.5 dB for MSR values in excess of around 85 (≈ 19 dB). Note that, in Figure 2.2, the APD receiver is considered to have an unitary gain, which justifies the higher power that is shown to be necessary in comparison with Figure 2.1 (for typical APD gains, the BER would present similar or better results than those obtained for the PIN receiver, resulting in a similar impact in terms of MPN).

Considering that the optical source in the ONUs is typically a multimode FP laser, the uplink transmission in a PON system will be likely affected by MPN. In spite of the uplink transmission window (1310 nm) being near the zero-dispersion wavelength, high data rate transmission will be degraded by the MPN. Figure 2.3 shows the distance-data rate product for such a scenario, considering a negligible MPN induced power penalty of 0.5 dB, for three different values of the mode partition coefficient, $k = 0.6$, 0.7 and 0.8. A fibre dispersion of 2 ps/nm/km and an optical source spectral window of 1 nm were assumed. This figure allows concluding that, for a 1 Gbit/s system, distances longer than 50 km are reachable for any value of k and with very low BER values. On the other hand, considering a transmission data rate of 10 Gbit/s, and assuming a target BER of 10^{-12}, distances between 5.5 km and 6.5 km are reachable, being impossible to reach 20 km (typical target distance in PON systems).

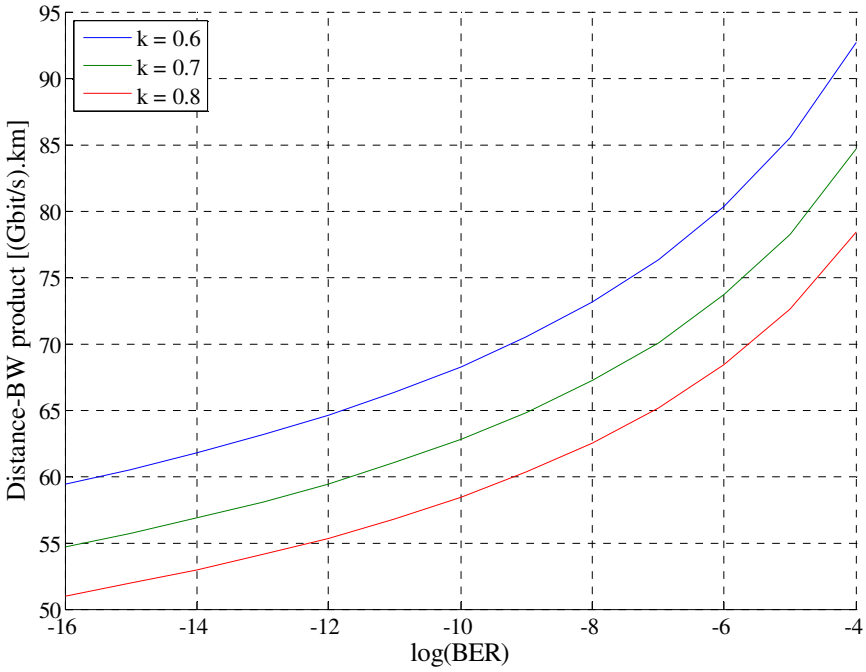

Figure 2.3 – Distance-data rate product as function of the bit error rate, considering a MPN penalty of 0.5 dB.

The conclusions drawn from Figure 2.3 are confirmed by the relative noise level of the received power in the presence of MPN (given by σ_{MPN}) and MPN induced power penalties presented in the following. Analytical results were obtained for transmissions at 1 Gbit/s and 10 Gbit/s for a Q-factor of 7, which corresponds to a BER of 10^{-12}, and considering a fibre dispersion of 2 ps/nm/km, and a laser Root Mean Square (RMS) spectral width of 1 nm, which is typical for commercially available 1 Gbit/s and 10 Gbit/s FP lasers. A maximum network reach of 20 km was assumed, and three different values for the mode partition noise parameter, *k*, were considered.

Figure 2.4 presents the relative noise level in presence of MPN for a transmission data rate of 1 Gbit/s, showing very low noise level values, even for 20 km reach. Moreover, Figure 2.5 depicts the MPN induced power penalty, also for 1 Gbit/s transmission, once again showing insignificant values. Confirming the results presented in Figure 2.3, these results obtained for a transmission data rate of 1 Gbit/s, show that the effect of MPN is negligible for any value of *k*.

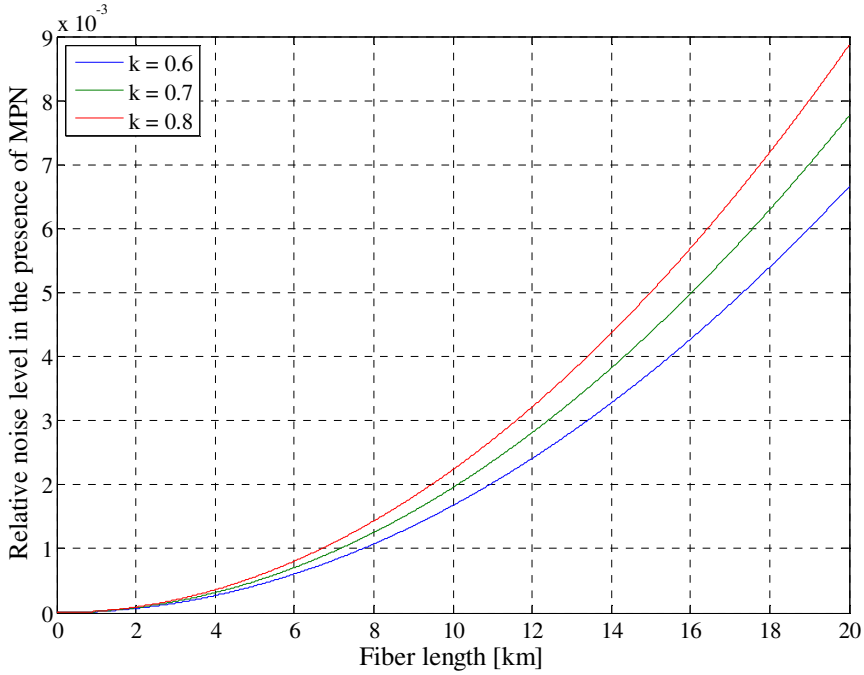

Figure 2.4 – Relative noise level in presence of MPN, considering a bit rate of 1 Gbit/s.

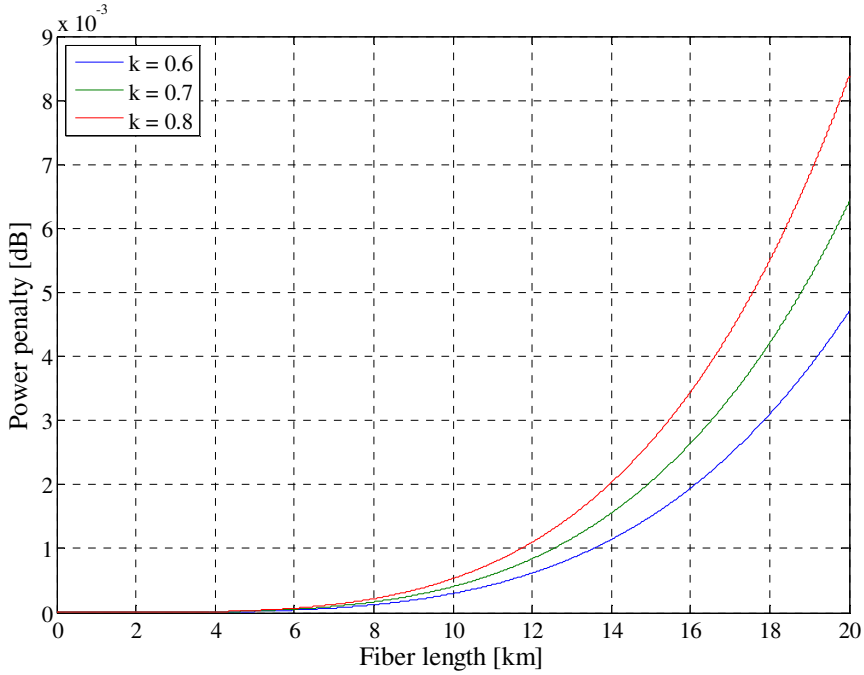

Figure 2.5 – MPN induced power penalty, considering a bit rate of 1 Gbit/s.

On the other hand, increasing the data rate up to 10 Gbit/s, the MPN induced penalty is shown to be very significant. The relative noise level in the presence of MPN, depicted in Figure 2.6, is shown to increase remarkably with the network reach. According to the previous formulations, the power penalty becomes infinite when the relative noise level is higher than Q^{-1}. Considering a 10 Gbit/s uplink PON system and a target BER of 10^{-12} (excluding the use of error correction techniques), this is verified for $\sigma_{MPN} = 0.143$, represented in Figure 2.6 by the black line. As observed here, the maximum network reach varies between 8 km and 10 km, for the three considered values of *k*.

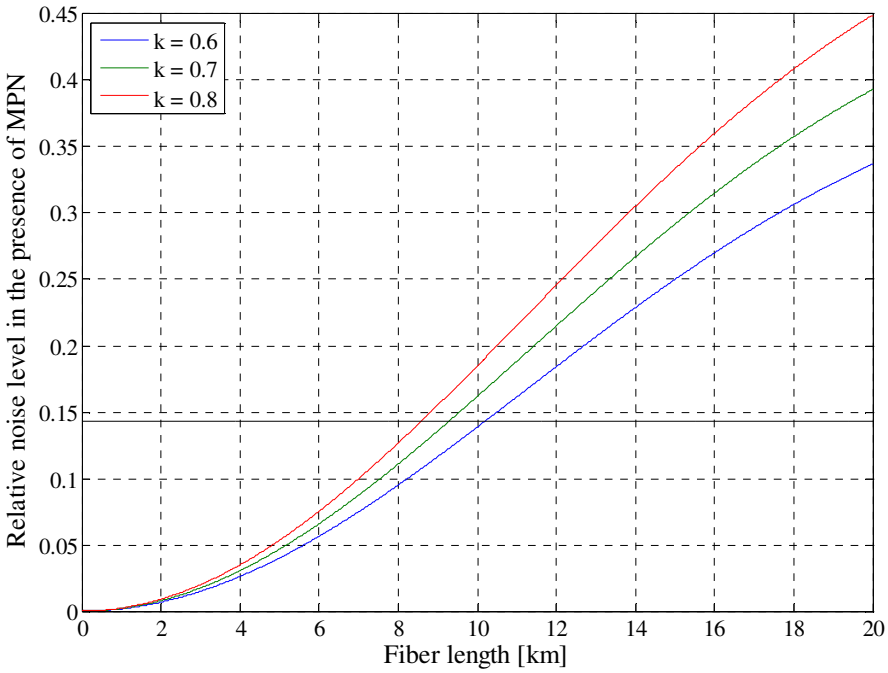

Figure 2.6 – Relative noise level in presence of MPN, considering a bit rate of 10 Gbit/s.

The power penalty due to the MPN in a 10 Gbit/s EPON uplink is depicted in Figure 2.7. The abrupt increase of the power penalty is evident for distances longer than 8 km to 10 km, where the power penalty becomes infinite, confirming the previous expectations. The critical points, for which the MPN induced power penalty is still negligible, equal to 0.5 dB, correspond to distances around only 6 km, for all values considered for *k*. For larger distances, the power penalty increases very sharply, invalidating the system for longer network reaches.

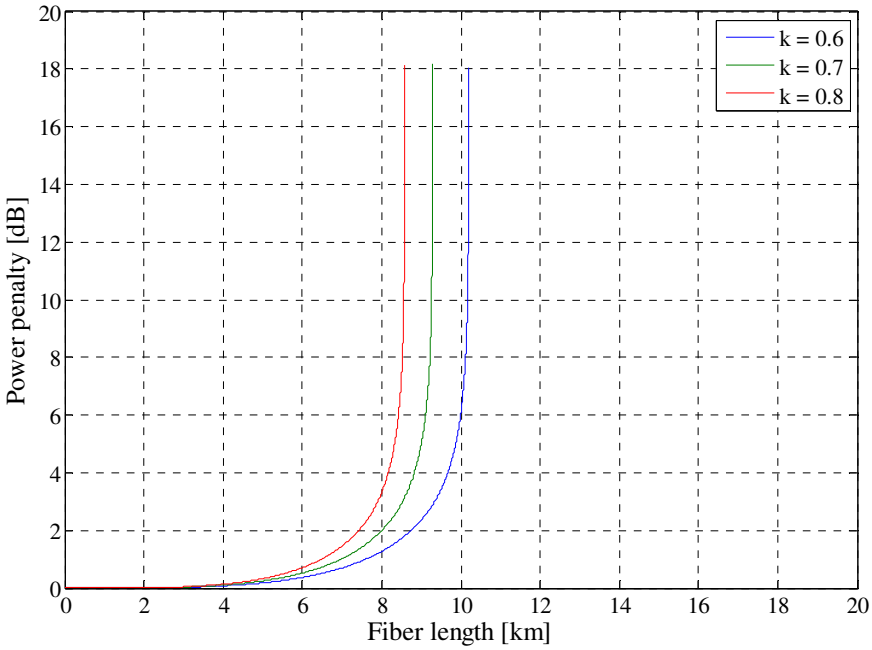

Figure 2.7 – MPN induced power penalty, considering a bit rate of 10 Gbit/s.

The viability of a 10 Gbit/s PON uplink system at a target distance of 20 km requires modifications of the laser parameters, namely of its spectral width. Figure 2.8 presents the MPN induced power penalty as a function of the source spectral width, considering a network reach of 20 km. Once again three different values are considered for the mode partition noise parameter.

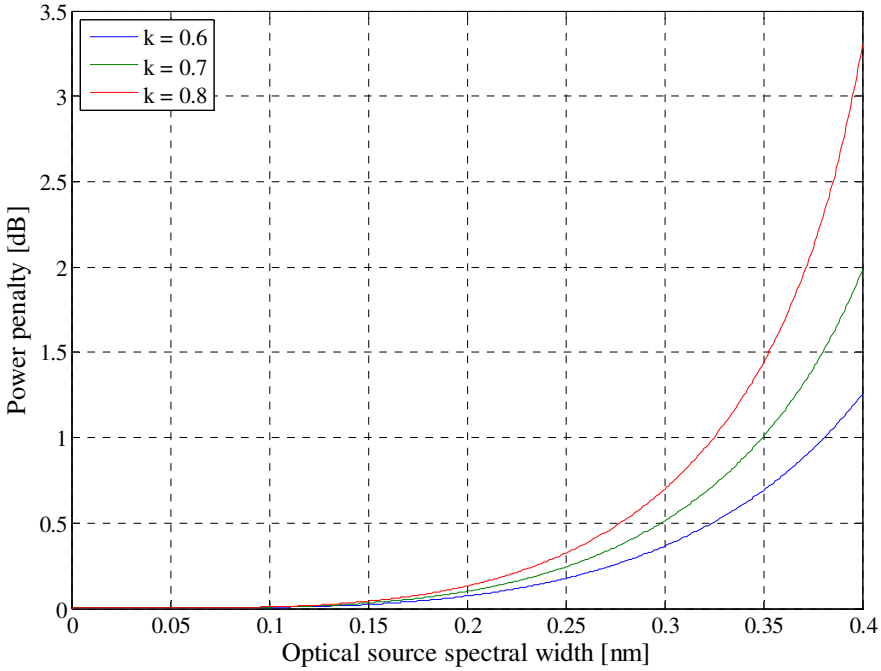

Figure 2.8 – MPN induced power penalty, for a data rate of 10 Gbit/s and a network reach of 20 km.

The curves presented in Figure 2.8 show that a negligible power penalty of 0.5 dB requires the use of a source with a spectral width around 0.3 nm. If a source with such spectral width is employed, the uplink system may be operated at 10 Gbit/s, and a distance of 20 km is reachable.

Several ways of reducing the MPN induced power penalty may be considered. The operation of the FP laser far from the threshold, thereby reducing the emission spectral width, is one possible solution. Employing this solution, a penalty due to the extinction ratio will occur, but is less harmful than the MPN penalty [Kei99]. Another solution is to employ Forward Error Correction (FEC), which would have the additional merit of protecting the system against other degradations. However, in a system with the characteristics of a PON uplink, the burst mode transmission may originate implementation difficulties, that must be considered. This subject will be further addressed in Chapter 3.

2.1.2. Influence of MPN in System Performance

The analysis presented in the previous sub-section shows that MPN will have a larger impact on the performance of the upstream transmission in a 10 Gbit/s PON system, as long as low-cost multimode optical sources are used at the ONUs and higher cost single mode lasers are shared as OLT optical sources. The influence of MPN is therefore assessed in this sub-section considering the upstream direction of a 10 Gbit/s PON system.

The upstream transmission is realized in the 1310 nm window, benefiting from being near the zero-dispersion wavelength of SMF, and enabling the use of a multimode semiconductor laser as optical source in the ONUs. This is not the case for the downstream direction, where the use of single mode lasers is allowed (in spite of high dispersion penalties due to chirp that may limit the transmission reach [Pat06]) not only because the cost is not so prohibitive but because the downstream direction is operated in the 1550 nm window, where the fibre dispersion is around 17 ps/nm/km, and the use of multimode lasers would result in severe dispersion penalties.

The influence of MPN may be translated into a severe degradation of the upstream system performance. This influence was assessed through simulation experiments, using a MATLAB-based simulation platform where the effect of MPN is considered by adding an additional noise variance to the receiver model, as explained in sub-section 2.1.1. The model used includes only the receiver electrical noise and the MPN, because no other optical noise affects the system (the eventual Relative Intensity Noise (RIN) from the laser is negligible and no optical amplification is considered).

To comply with the upstream PON system specifications, the simulation experiments were performed using an operation wavelength of 1310 nm, over a transmission fibre characterized by an attenuation of 0.4 dB/km. The optical signals are formatted according to the Non-Return-to-Zero (NRZ) line code, considering an extinction ratio of 6 dB and a data rate of 10 Gbit/s. The receiver is assumed to have a sensitivity of -18 dBm at a BER of 10^{-12} (typical value for commercially available 10 Gbit/s PIN receivers), determined for a perfect input signal with infinite extinction ratio, resulting in a sensitivity penalty of around 3 dB for signals with 6 dB extinction ratio.

The influence of the MPN coefficient on the system performance is assessed by the results presented in Figure 2.9, which shows the upstream system performance in terms of BER, as a function of the power received at the OLT for different MPN coefficients and for a scenario with only electrical noise. These results correspond to an uplink with 10 km length, considering a fibre dispersion of 1 ps/nm/km and a FP laser with a spectral width of 1.5 nm.

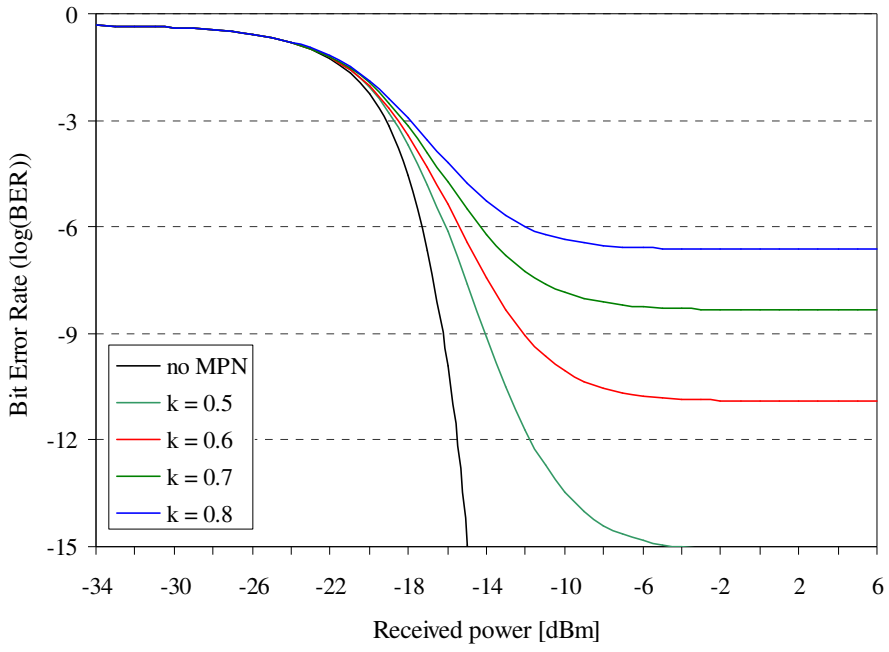

Figure 2.9 – Influence of the MPN coefficient, for L = 10 km, D = 1 ps/nm/km, and σ_λ = 1.5 nm.

Figure 2.9 shows that, independently of the MPN coefficient, the electrical noise is dominant for low received powers, whereas MPN becomes important for received powers around -18 dBm. A performance floor due to MPN is observed for all MPN coefficients that were considered. This agrees with the theoretical analysis presented in sub-section 2.1.1,

which showed that, beyond a certain level, the system performance cannot be improved by increasing the transmitted optical power, in the presence of MPN. The results presented in Figure 2.9 show that, for a moderate level of MPN with $k = 0.5$, a sensitivity penalty around 4 dB is obtained for a target BER of 10^{-12}. For this target BER, all other values of k considered produce an infinite penalty, again confirming the analysis presented in sub-section 2.1.1. These results clearly demonstrate the importance of including the MPN effect when evaluating the performance of a high data rate system employing multimode lasers.

In order to estimate the system specifications in presence of MPN, the use of $k = 0.5$ is assumed in the following, since it characterizes a moderate level of MPN. By fixing the fibre dispersion at 1 ps/nm/km, Figure 2.10 and Figure 2.11 depict the influence of the source spectral width on the system performance, as a function of the received power, for maximum network reaches of 10 km and 20 km, respectively. The system performance is evaluated in terms of BER, using a logarithmic scale, and the performance target is assumed to be BER = 10^{-12}. For this set of conditions, Figure 2.10 shows a compliant system (BER < 10^{-12}) for $\sigma_\lambda < 1.6$ nm, whereas Figure 2.11 shows that the system is viable only for $\sigma_\lambda < 0.4$ nm, both for received powers higher than around -18 dBm (receiver sensitivity considering only electrical noise). Above these values, MPN becomes the system limiting factor. While the threshold value obtained for the laser spectral width for a distance of 10 km is acceptable, the threshold value obtained for 20 km is a very stringent specification for the currently available commercial FP lasers.

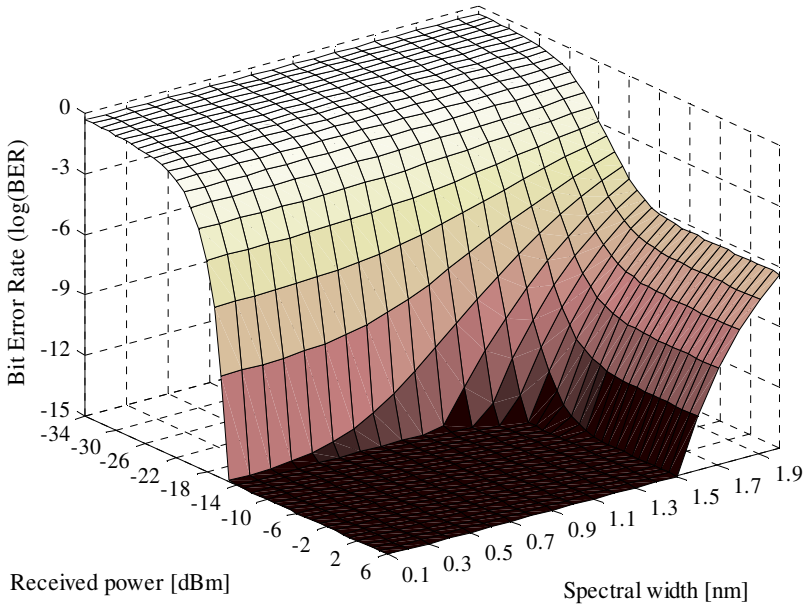

Figure 2.10 – Influence of σ_λ, for $k = 0.5$, $L = 10$ km, and $D = 1$ ps/nm/km.

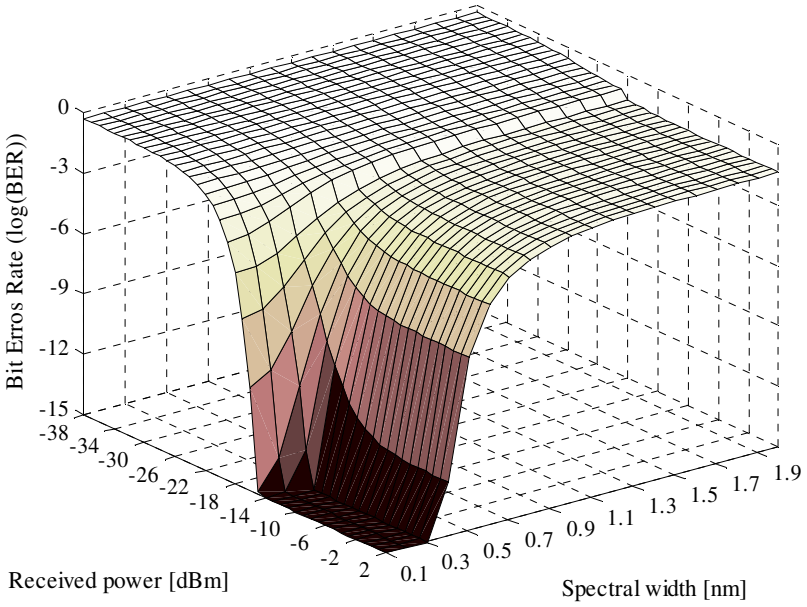

Figure 2.11 – Influence of σ_λ, for k = 0.5, L = 20 km, and D = 1 ps/nm/km.

Considering now two different values for the laser spectral width, namely $\sigma_\lambda = 1$ nm and $\sigma_\lambda = 2$ nm, which are realistic lower and upper bounds for commercially available FP lasers, Figure 2.12 and Figure 2.13 present the influence of the fibre dispersion, for a network reach of 20 km. It is shown that, for this distance, the fibre dispersion should be kept below 0.8 ps/m/km and below 0.4 ps/nm/km, for $\sigma_\lambda = 1$ nm and $\sigma_\lambda = 2$ nm, respectively, in order to enable compliant transmission.

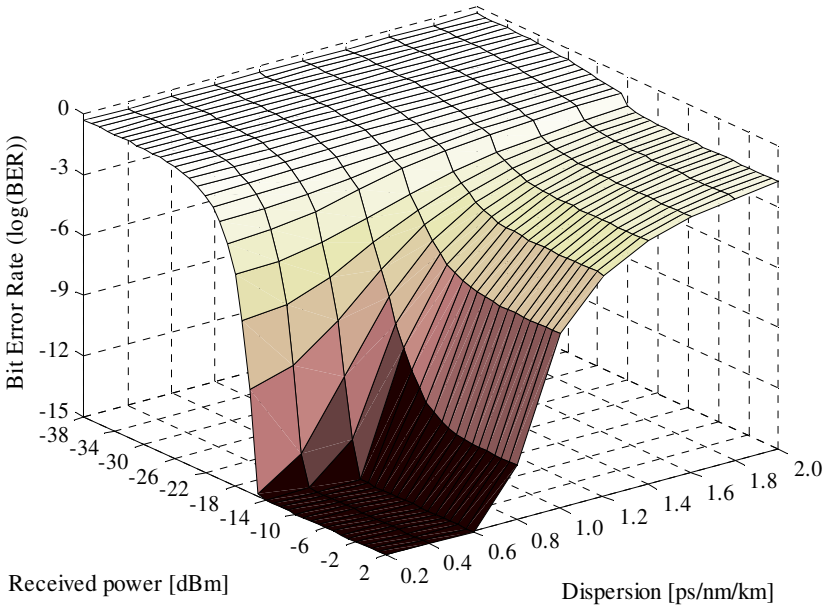

Figure 2.12 – Influence of D, for k = 0.5, L = 20 km, and σ_λ = 1 nm.

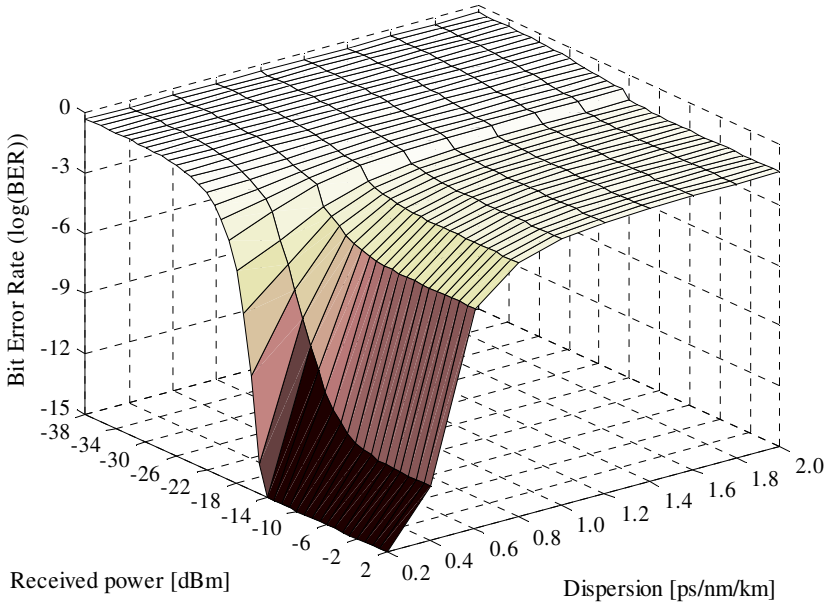

Figure 2.13 – Influence of D, for k = 0.5, L = 20 km, and σ_λ = 2 nm.

By fixing again the dispersion at 1 ps/nm/km, Figure 2.14 and Figure 2.15 present the reachable distances for realistic commercial values of σ_λ = 1 nm and σ_λ = 2 nm, respectively, as a function of the received power. In the scenario presented in Figure 2.14, the limiting effect of MPN prohibits transmission for distances above 16 km, whereas in Figure 2.15 it is shown that only shorter distances around 8 km are possible. Thus, if the use of commercially available FP lasers is assumed, the transmission is limited to the maximum of 16 km, for a reduced dispersion of 1 ps/nm/km.

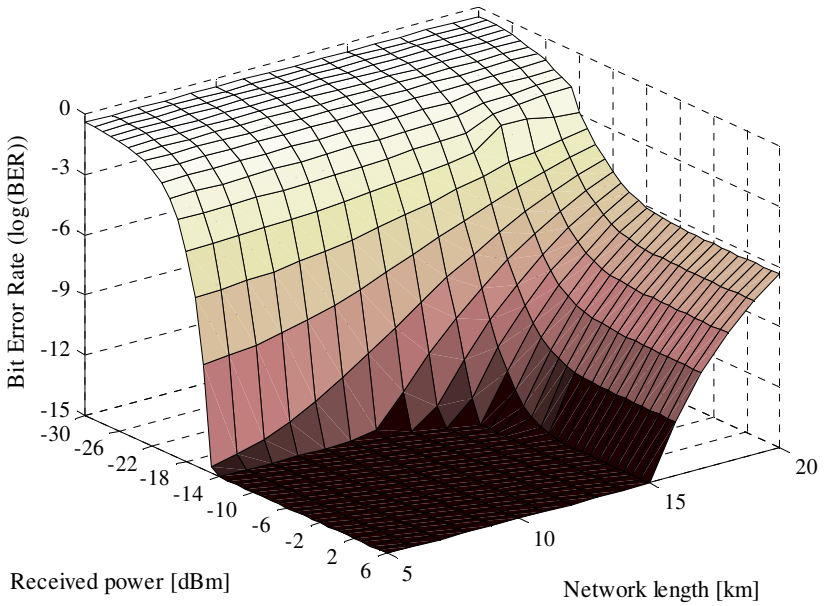

Figure 2.14 – Influence of L for k = 0.5, D = 1 ps/nm/km, and σ_λ = 1 nm.

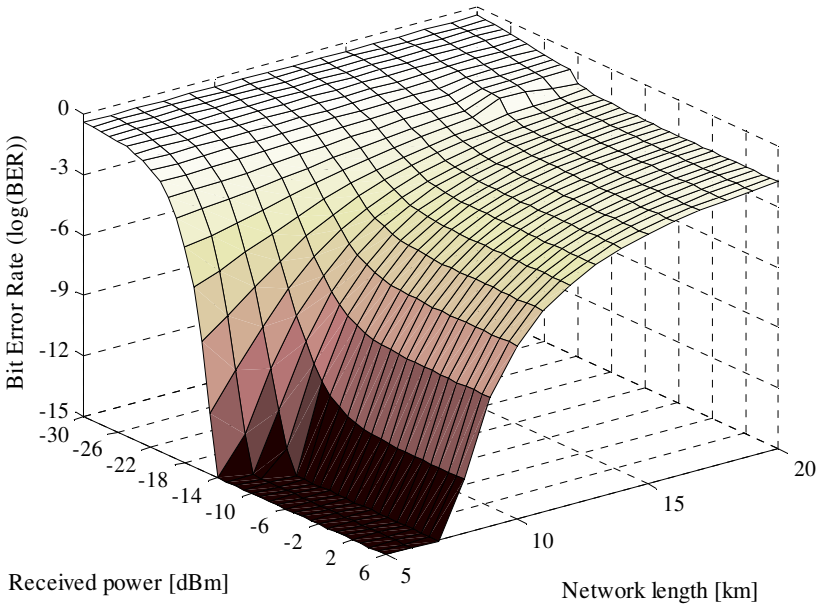

Figure 2.15 – Influence of L for k = 0.5, D = 1 ps/nm/km, and σ_λ = 2 nm.

The results presented above allow the specification of system requirements for a 10 Gbit/s PON upstream system employing multi-mode lasers, such as FP lasers. It has been shown that reduced values for the source spectral width should be used, in order to enable compliant transmission for a network reach of up to 20 km. If commercially available FP lasers are employed, one must guarantee very low fibre dispersion to reach the target distance of 20 km.

The low performance values obtained for lower received powers may be compensated by using optical pre-amplification at the OLT receiver, as proposed in [PMS06], since in this region the dominant noise is electrical, as opposite to the MPN dominance at higher powers. Moreover, FEC may be included in the system as a method for improving the network performance when MPN is present, as further detailed in Chapter 3.

2.2. Impact of Fibre Nonlinear Effects

During the standardization process of higher data rate PON systems, in particular the standardization process of 10 Gbit/s EPON systems, several physical layer issues were assessed in order to produce a compliant standard. Among them, the support of higher splitting ratios, namely 64 and 128, was analyzed. To mitigate these higher splitting losses, higher powers have to be launched into the fibre in order to attain similar system performance. Consequently, such high powers may result in non-negligible performance degradation due to fibre nonlinear effects.

High powers launched into the fibre may originate reflected powers due to light scattering effects, such as SBS and SRS. These effects are inelastic processes, which manifest themselves in different ways. SBS, an interaction between light and acoustic waves in fibre, causes frequency conversion and reversal of the propagation direction of the light [Agr02], [SHTT90], [FN93]. SRS, an interaction between light and vibrations of silica molecules, causes frequency conversion of light and transfers part of the energy to longer wavelengths [Agr02], [Chr90]. These nonlinear light scattering effects occur when the light launched into the fibre exceeds a threshold power level specific of each process [Agr02]. Besides the stimulated light scattering effects, the nonlinear self-phase modulation should also be considered. In reality, all materials behave nonlinearly at high intensities and their refractive index varies with intensity. The physical origin of this Kerr nonlinearity is the non-harmonic response of electrons to optical fields, which results in a nonlinear susceptibility of the transmission medium. Therefore, the refractive index of the fibre presents a nonlinear dependence on intensity, causing SPM [Agr02], [Chr90], [SHTT90]. The interaction between group velocity dispersion and SPM, which produces different effects on the temporal pulse profiles, will eventually degrade the performance of a system such as a 10 Gbit/s PON system.

This section presents an assessment of the nonlinear effects that may influence the system performance, by estimating the maximum power that can be launched into the fibre without inducing significant performance degradation. The three main effects listed above are considered, namely SPM, SBS, and SRS. Other nonlinear effects, such as Cross-Phase Modulation (XPM) and Four-Wave Mixing (FWM), are not relevant in PON systems, since only one downstream/upstream data channel is transmitted through the optical fibre, using two separate spectral windows. In the following, the influence of SPM is evaluated by simulation, where attenuation and fibre dispersion are taken into account, and the light scattering effects (SBS and SRS) are estimated analytically. Moreover, the interaction of the analogue video overlay channel with the downstream digital data channel is taken into account.

The work reported in this section was developed under the framework of the IEEE P802.3av Task Force [IEEEav], in collaboration with Corning, for the assessment of SBS.

2.2.1. Stimulated Brillouin Scattering

The tendency of materials to compress in the presence of an oscillating electric field, at a specific pump frequency, results in the generation of an acoustic wave, at a frequency Ω equal

to the Stokes shift, named Brillouin frequency shift, Ω_B. In the SBS process, the input light generates backscattered Stokes light through interaction with the acoustic wave [Agr02], [FN93]. The Stokes light is continuously amplified during propagation by the interaction with the pump light, which in turn increases the amplitude of the scattered wave, resulting in a positive feedback loop.

In standard monomode fibres, light can travel only in the forward and backward directions. As a result, SBS occurs mainly in the backward direction, with a specific Brillouin frequency shift Ω_B. The SBS gain g_B depends on this frequency shift, because of the damping time T_B of acoustic waves, and has a relatively narrow Lorentzian profile given by [Agr02]:

$$g_B(\Omega) = \frac{g_B(\Omega_B)}{1+(\Omega-\Omega_B)^2 T_B^2}. \tag{2.8}$$

The peak value of the gain occurs for the Brillouin frequency shift, $\Omega = \Omega_B$ (which is typically 10.7 GHz), and depends on several material parameters, such as the density and the elasto-optic coefficient.

One criterion for determining at what point SBS becomes a limiting factor consists in defining the SBS threshold power, P_{SBS}, as the input pump power for which the backscattered power equals the fibre input power [Agr02], [FN93], [ITU07a]. Based on this definition, the SBS threshold for Continuous Wave (CW) pump light, assuming a Lorentzian linewidth profile, was earlier approximated by [ATM88]:

$$P_{SBS}^{CW} \approx 21\frac{A_{eff}k_{SBS}}{g_B L_{eff}}\left(\frac{\Delta\nu_{SBS}+\Delta\nu_P}{\Delta\nu_{SBS}}\right), \tag{2.9}$$

where $L_{eff} = (1\text{-}e^{-\alpha L})/\alpha$ is the effective interaction length for a fibre of length L, which accounts for fibre losses through the fibre attenuation parameter α, $\Delta\nu_{SBS}$ is the spontaneous Brillouin bandwidth, $\Delta\nu_P$ is the pump light bandwidth, and A_{eff} is the effective area, defined by the transverse distribution of the electric field $f(r)$ for the optical mode in the fibre [Agr01]:

$$A_{eff} = 2\pi\frac{\left[\int_0^\infty f^2(r)\,r\,dr\right]^2}{\int_0^\infty f^4(r)\,r\,dr} \approx \pi w^2, \tag{2.10}$$

where $2w$ is the mode field diameter. k_{SBS} in equation (2.9) is a polarization factor, varying between 1 and 2 depending on the relative polarizations of the pump and Stokes waves. For complete polarization scrambling, as in conventional SMF, $k_{SBS} = 3/2$ [DB94].

Equation (2.9) implies that the SBS threshold is directly proportional to the effective area, A_{eff}. However, more recent studies of the SBS effect in optical fibres revealed that the relation between the SBS threshold and A_{eff} is more complex, involving the structure of the acoustic wave [KKC+05], which was ignored in previous studies, where plane acoustic waves were assumed. A detailed analysis of the acousto-optic interaction in single-mode optical fibres has shown that the SBS threshold is directly proportional to a parameter called acousto-optic effective area, A^{ao} [KKC+05]. In order to demonstrate this relation, consider the three different fibres listed in Table 2.2, all with 25 km, and the dependence of the reflected and transmitted powers on the launched power presented in Figure 2.16.

Table 2.2 Fibre types considered to demonstrate the relation between the SBS threshold and the acousto-optic effective area, A^{ao}.

Fibre	**Application**	**Compliant standard**	A_{eff}	P_{SBS} **(measured)**
Fibre A	Used in most FTTx networks	ITU-T G.652	85 μm^2	8.1 dBm
Fibre B	Non-zero-dispersion shifted fibre	ITU-T G.655	72 μm^2	10.4 dBm
Fibre C	Enhanced SBS threshold	ITU-T G.652	88 μm^2	11.4 dBm

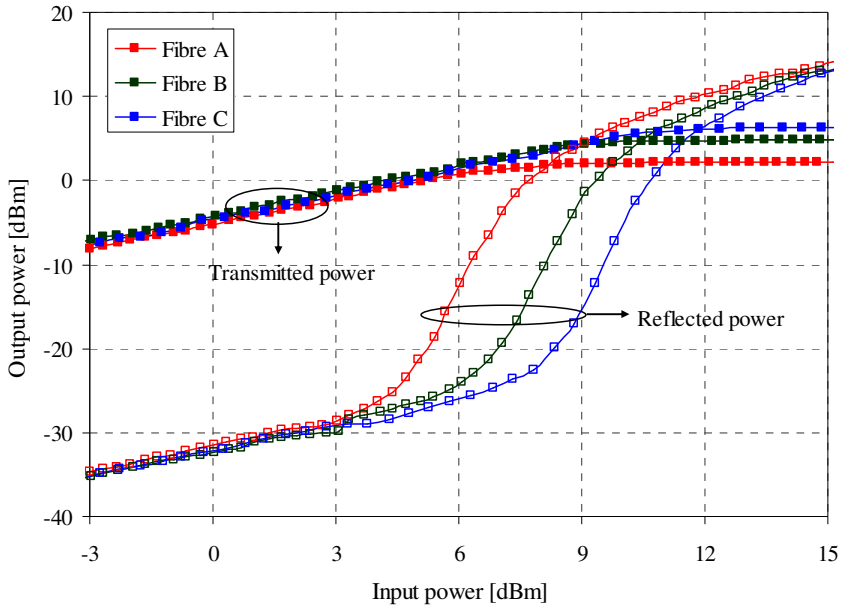

Figure 2.16 – Reflected and transmitted powers measured for fibres A, B and C (data from Corning, reported in [PT06]).

Considering the direct proportionality of the P_{SBS} on the effective area, A_{eff}, given by equation (2.9), Fibre B should have a SBS threshold lower than that of Fibre A, but the measured SBS threshold was found to be more than 2 dB higher. Moreover, since the effective areas of Fibre A and Fibre C are similar (and since they belong to the same ITU-T fibre type, SMF), according to equation (2.9) their SBS thresholds should be identical, but they differ by more than 3 dB.

Based on the previous facts, it is clear that the calculation of the SBS threshold based on the plane wave analysis [Smi72], [ATM88] is somewhat outdated and is not applicable to optical fibres where both optical and acoustic waves are guided. Therefore, the SBS effect is only properly described by solving the acousto-optic equation [KKC+05], [PT06], considering that the back-reflected (Stokes) power is described by a differential equation where the nonlinear term is inversely proportional to the acousto-optic effective area, A^{ao}, rather than the optical effective area A_{eff}. The acousto-optic effective area depends on the overlap between the acoustic $\xi(r)$ and optical $f(r)$ modes and is obtained through [KKC+05] (see also Appendix A for further insight on the calculation of A^{ao}):

$$A^{ao} = 2\pi \left[\frac{\int_0^\infty f^2(r)\, r dr}{\int_0^\infty \xi(r) f^2(r)\, r dr} \right] \int_0^\infty \xi^2(r)\, r dr \,. \tag{2.11}$$

Therefore, it may be concluded that, although Fibre B has a smaller optical effective area, its acousto-optic effective area is larger than that of Fibre A, which results in higher SBS threshold. The highest acousto-optic effective area was verified for Fibre C, resulting in a SBS threshold about 3 dB higher than for Fibre A, and leading to the designation of fibre with enhanced SBS threshold. Overall, the use of A_{eff} in the calculation of the SBS threshold with equation (2.9) should be replaced by A^{ao}.

Note that, $A^{ao} \approx A_{eff}$ for fibre profiles which are close to step-index, as conventional SMF. This explains why equation (2.9) was used over the years to describe the SBS threshold in optical fibres. Another modification in equation (2.9) is the replacement of the numerical coefficient 21 by 18, which was proven to produce better accuracy when low attenuation fibres ($\alpha < 2$ dB/km) are employed [KMV+02], [BR90], [EW96].

In digital systems employing intensity modulation, the SBS threshold increases. For the special case of the NRZ data format, typically used in PON systems, and considering the

average pump power of the modulated laser equal to the CW power when the laser is not modulated, the SBS threshold for a bit rate B is given by [FN93]:

$$P_{\mathrm{SBS}}^{\mathrm{NRZ}} = \frac{P_{\mathrm{SBS}}^{\mathrm{CW}}}{1 - \frac{B}{2\Delta\nu_{\mathrm{SBS}}}\left(1 - \mathrm{e}^{-\Delta\nu_{\mathrm{SBS}}/B}\right)}. \tag{2.12}$$

Once the power launched into the fibre surpasses the threshold level, the exceeding light is reflected backwards through SBS. Therefore, the SBS limits the launched power to a few mW, because of its low threshold.

Several schemes are available for minimizing the effect of SBS [FN93]. Benefiting from the narrowband properties of the SBS effect, a significant SBS suppression can be achieved by providing a low frequency dither to the laser [FN93]. In other words, SBS suppression can be achieved by directly modulating the laser with a sinusoidal current at a frequency much lower than the low-frequency cutoff of the receiver. Since the dither frequency is outside the receiver bandwidth, it will not introduce significant degradation in the presence of dispersion. Another option is to increase the source linewidth through direct modulation, causing the linewidth to broaden due to chirping [FN93]. However, this will cause higher dispersion penalties, degrading the system performance. The third option is to use SBS enhanced fibres [KKC+05] which, in the indicated reference, enable 3 dB higher launched power without SBS penalties, and can be used together with dithering.

2.2.2. Stimulated Raman Scattering

The spontaneous scattering caused by the parametric interaction of light with molecular vibrations of silica in an optical fibre is designated by spontaneous Raman scattering. Incident light scattered by the silica molecules experiences a Raman frequency shift, Ω_{R}, whose value is dictated by the vibration energy levels of silica. In this process, a lower frequency (Stokes) wave will experience optical gain generated by, and at the expense of, the higher frequency (pump) wave [Chr90]. As an acoustic process is not involved, spontaneous Raman scattering is an isotropic process that occurs in all directions. The spectrum of Raman gain depends on the decay time associated with the excited vibration state. In optical fibres, the maximum gain occurs when the Raman shift is about 13 THz [Agr02].

Similarly to the SBS case, Raman scattering becomes stimulated when the pump power exceeds a threshold value. The threshold power, P_{SRS}, is defined as the incident power at which half of the pump power is transferred to the Stokes field at the output end of a fibre of length L, causing performance degradation. It is given by [Chr90], [Bil99]:

$$P_{SRS} \approx 16 \frac{A_{eff} k_{SRS}}{g_R L_{eff}}, \tag{2.13}$$

where g_R is the peak Raman gain coefficient for co-polarized pump and Stokes waves, and k_{SRS} is a factor that depends on the relative polarizations of the two waves. The maximum value of the Raman gain is obtained when identical polarization along the fibre is verified for the pump and the Stokes waves. For conventional SMF, a degree of polarization scrambling should be considered and a value of $k_{SRS} = 2$ has been proposed elsewhere [FN93]. Note that equation (2.13) provides an order of magnitude estimate only, as many approximations are made in its derivation.

For most single-channel systems, SRS is not a limiting factor. However, when two high power wavelengths are present in the same fibre, detuned by less than 13 THz, they will interact through SRS, resulting in energy transfer from the short wavelength signal to the long wavelength signal. This situation may be verified in a PON downstream system, when a video overlay channel is deployed using the 1550 nm wavelength [CP06]. Thus, Raman-crosstalk may occur between the 1490 nm downstream data channel and the video overlay channel. Due to this nonlinearity, part of the 1490 nm information is copied to the 1550 nm wavelength, effectively degrading the video performance.

2.2.3. Self-Phase Modulation

The inclusion of nonlinear refraction in the system analysis is achieved by considering that the refractive index n has a weak dependence on optical intensity I [SHTT90]:

$$n = n_0 + n_2 I, \tag{2.14}$$

where n_0 is the ordinary refractive index of the material, and n_2 is the nonlinear index coefficient. The nonlinearity of the refractive index, known as Kerr nonlinearity, produces a carrier-induced phase modulation of the propagating signal, called Kerr effect. In single-

channel links, this gives rise to SPM, which converts optical power fluctuations into spurious phase fluctuations.

Due to SPM, and through the nonlinear parameter $\gamma = 2\pi n_2 / (A_{\text{eff}}\lambda)$, a nonlinear phase shift occurs [Agr02], given by:

$$\varphi_{\text{NL}} = \int_0^L (\beta' - \beta)\, dz = \int_0^L \gamma P(z)\, dz = \gamma P_{\text{in}} L_{\text{eff}} \,, \tag{2.15}$$

where $P(z) = P_{\text{in}}\exp(-\alpha z)$ accounts for fibre losses. In practice, since the signal power P_{in} is time dependent, this nonlinear phase shift varies with time. Actually, any changes in the optical power will produce corresponding changes in the nonlinear phase shift. Besides the attenuation, the influence of SPM depends also on the dispersion, which converts the SPM-induced phase fluctuations into intensity fluctuations, potentially degrading the system performance. The use of dispersion compensation techniques is the best way to minimize the effect of SPM.

2.2.4. Transmitted Power Constraints due to Nonlinear Effects

The limitations imposed by the nonlinear effects discussed above, namely concerning the maximum launched powers, should be considered in the design of 10 Gbit/s PON systems. Expectedly, these future systems will support a higher user density than current systems, which may require higher transmitted powers, and thus may have to operate near the zone affected by nonlinear effects. In the following, the influence of SPM is evaluated by simulation, whereas the limitations imposed by the inelastic scattering effects (SBS and SRS) are estimated analytically.

Aiming to assess the influence of SPM, the simulation model considers a 10 Gbit/s PON system with a single tree topology, supporting 64 or 128 ONUs. A specific set of parameters was assumed, and is justified in the following. The simulation results were obtained for operation in the 1550 nm window, which corresponds to the Downstream Channel (DSC) transmission. The 1310 nm window, used by the Upstream Channel (USC), was not considered because it is close to the zero-dispersion wavelength, and so the dispersive effects are negligible and the system is loss-limited. External modulation was assumed at the transmitter, as previous results [PMS06] demonstrated the poor performance of the 10 Gbit/s EPON DSC when direct modulation is employed. The NRZ modulation format and a fibre attenuation of 0.22 dB/km were assumed. The model used to characterize the fibre is based on the nonlinear Schrödinger equation, and includes the effects of attenuation, fibre dispersion and SPM.

Figure 2.17 depicts the simulation results obtained for the DSC of a 10 Gbit/s EPON with 128 ONUs. They represent the maximum launched power allowed into the fibre, in order to guarantee a normalized Eye Opening Penalty (EOP) not exceeding 1 dB. The EOP is defined as the ratio between the signal maximum eye opening and the eye opening of a reference signal, which was assumed to be a NRZ signal with infinite extinction ratio. The distance from the OLT to the optical Passive Splitter/Combiner (PSC), in the Y axis, is varied from 0 to 20 km, as well as the distance from the PSC to the ONU under analysis. Similar results, presented in Figure 2.18, were obtained for a network with 64 ONUs. Since the maximum allowed powers launched into the fibre were considered in the simulation, these results do not differ significantly from those in Figure 2.17.

The results presented in Figure 2.17 and Figure 2.18 show that, regarding SPM, the maximum allowed launched power may be considerably high, around 26 dBm for a feeder network with 20 km, with no significant degradation on system performance. Note that the transmission distance between the PSC and the ONU (distribution network) does not have the same influence in the final results as the distance between the OLT and the PSC (feeder network). This is justified by the large difference between the power levels of the signals in the feeder and in the distribution network.

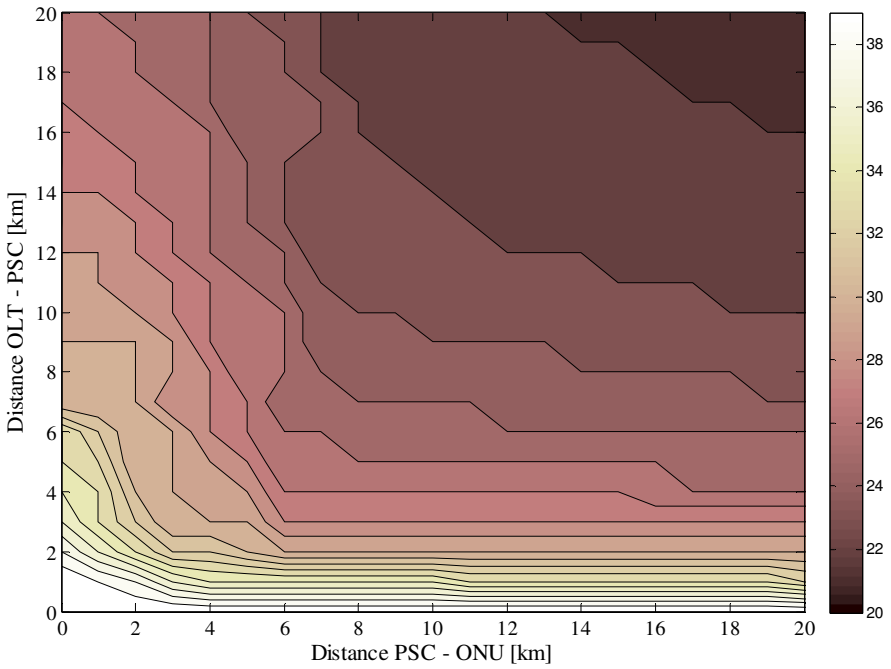

Figure 2.17 – Maximum power launched into the fibre, in dBm, to guarantee an EOP not exceeding 1 dB, in a network with 128 ONUs.

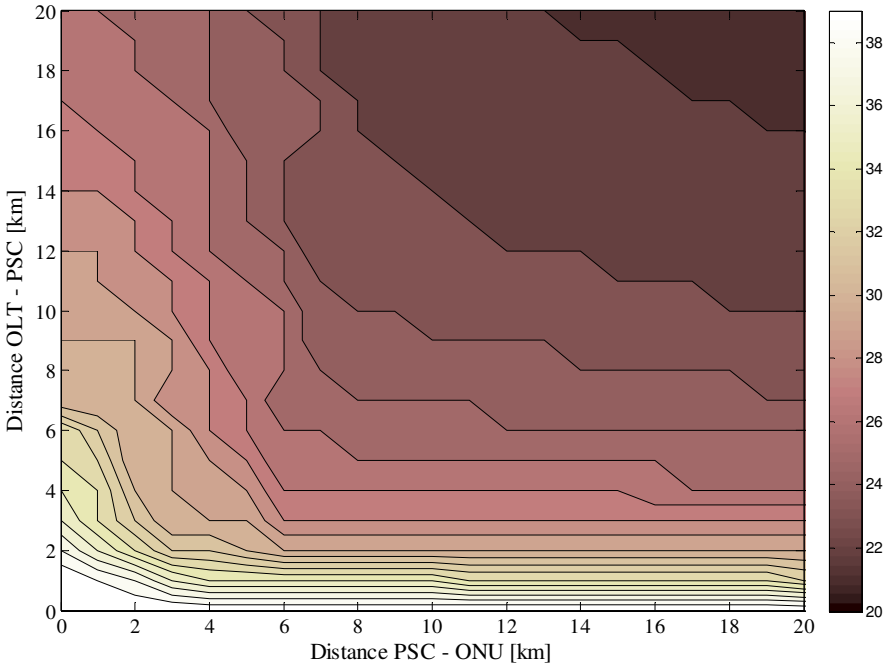

Figure 2.18 – Maximum power launched into the fibre, in dBm, to guarantee an EOP not exceeding 1 dB, in a network with 64 ONUs.

The large difference between the power levels in the feeder and in the distribution network suggests that in the distribution network, where the power level is much lower than in the feeder network, the nonlinear effects may be neglected. Therefore, simulation results were obtained considering linear transmission in the distribution network, and presented in Figure 2.19 and Figure 2.20, for networks with 128 ONUs and with 64 ONUs, respectively.

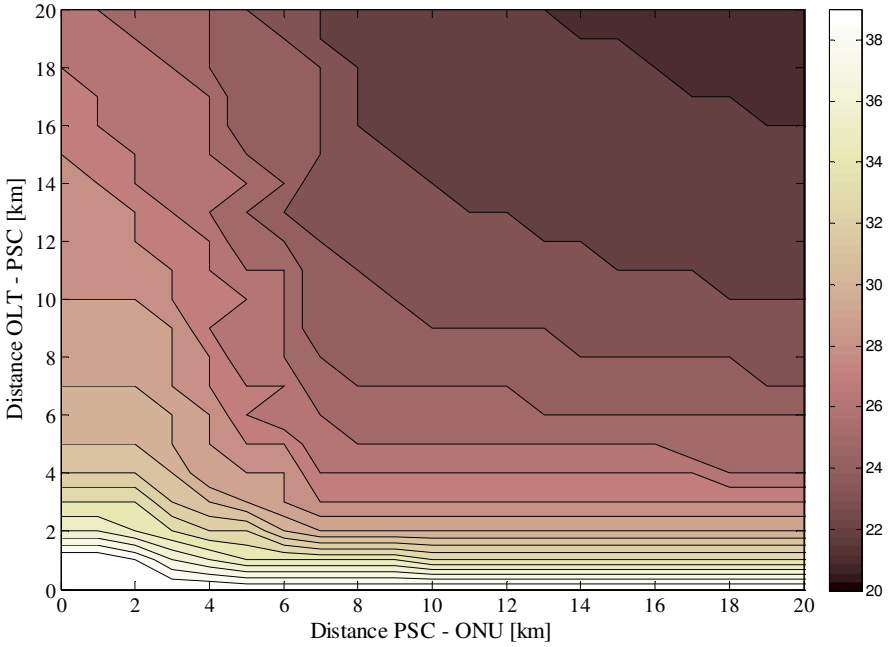

Figure 2.19 – Maximum power launched into the fibre, in dBm, to guarantee an EOP not exceeding 1 dB, with linear transmission between the PSC and the ONUs (128 ONUs)

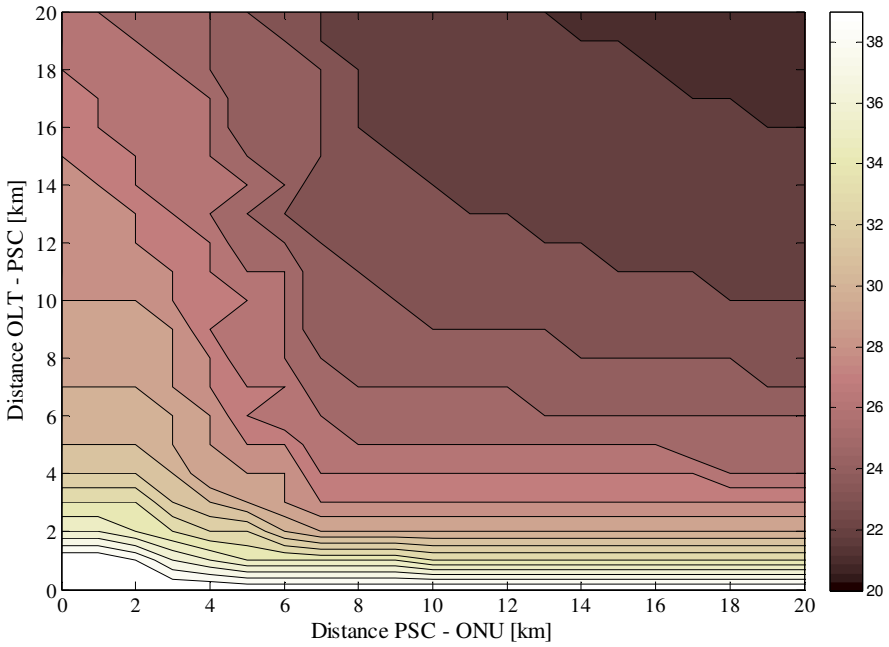

Figure 2.20 – Maximum power launched into the fibre, in dBm, to guarantee an EOP not exceeding 1 dB, with linear transmission between the PSC and the ONUs (64 ONUs).

Since the results in Figure 2.19 and Figure 2.20 do not significantly differ from those presented in Figure 2.17 and Figure 2.18, it can be concluded that the distribution network span may be treated as a linear medium, for both 64 and 128 splitting ratios.

Similarly to the simulation of the SPM effect, the analytic estimation of the influence of SBS and SRS was also performed only for the DSC, because the power launched in the USC will be lower than the power launched in the DSC, since weaker optical sources are used in the ONUs. These weaker signals should be compensated for by using, for example, optical pre-amplification in the OLT receiver [PMS06]. In the SRS case, the choice of analyzing only the DSC is also motivated by the existence of the downstream broadcast video signal.

For estimation of the SBS influence, two different network configurations were analyzed. The first corresponds to a worst case SBS scenario, where a single PSC is located near the ONUs. In this scenario, the feeder network, which is the network span with higher power level, and thus more susceptible to SBS effect, is 20 km long. The second network topology is a best case SBS scenario that considers the PSC located near the OLT, by reducing the feeder length to 0.5 km.

Therefore, in the worst case situation, the effective interaction length is $L_{\text{eff}} \approx 12.6$ km, for $\alpha = 0.22$ dB/km. Since conventional SMF (ITU-T G.652, Fiber A from Table 2.2) is typically used in EPON systems [Cor], the estimations of SBS threshold for CW transmission are based on modified equation (2.9), where numerical coefficient 21 is replaced by 18, and

consider $A_{eff} = 85\ \mu m^2$, $g_B = 5x10^{-11}$ m/W, $\Delta\nu_{SBS} = 50$ MHz, and $\Delta\nu_P = 50$ MHz. The SBS threshold for an intensity modulated NRZ signal at 10 Gbit/s is approximately 3 dB higher, given by (2.12). The analysis of the best case SBS scenario assumes the same set of parameters, except the interaction length, $L_{eff} \approx L = 0.5$ km. The estimated SBS thresholds are gathered in Table 2.3.

Table 2.3 SBS threshold powers.

	SBS (CW)		**SBS (10 Gbit/s NRZ)**	
	Worst case	Best case	Worst case	Best case
P_{th_SBS}	8.6 dBm	22.6 dBm	11.6 dBm	25.6 dBm

The values presented in Table 2.3 are in accordance with experimental data using SMF [KKC+05]. Note that these values are considerably low for deploying a network with high splitting ratios. However, if compliant enhanced SBS fibres are employed, an additional 3 dB improvement in the SBS threshold is obtained [KKC+05]. Thus, for the scenario considered above, the enhanced SBS threshold G.652 fibre (Fibre C in Table 2.2) will have a SBS threshold around 14.6 dBm, for NRZ modulated signals. Moreover, by applying one or several of the other available SBS suppressing methods, a significant improvement may also be achieved.

When SRS occurs in single-channel systems, part of the energy is transferred to a different wavelength. Typically, this effect only has significant influence for very high launched powers (around 500 mW) [SHTT90]. For the scenario of a PON system, the estimation of SRS verifies this fact. The analysis is based on (2.13), and assumes $g_R = 6x10^{-13}$ m/W. For the longer feeder network, with $L_{eff} \approx 12.6$ km, the SRS threshold power is found to be $P_{SRS} \approx 25.6$ dBm. The onset of SBS will prevent energy transfer from the signal wave to the Stokes wave and thus SRS will not result in a significant penalty, when only the transmission of the digital channel at 1490 nm is considered.

However, if an analogue video overlay at 1550 nm is deployed in the system together with digital data transmission at 1490 nm, then SRS results in energy transfer from the 1490 nm signal into the 1550 nm signal. For analogue powers ranging from 0 to 21 dBm, the additional loss of the digital signal could be 1.5 dB, as shown in Figure 2.21 [PT06]. In addition, due to propagation of both signals in the same direction, the intensity modulation of the shorter wavelength signal is transferred to the longer wavelength signal, causing additional penalties on the system performance [CP06].

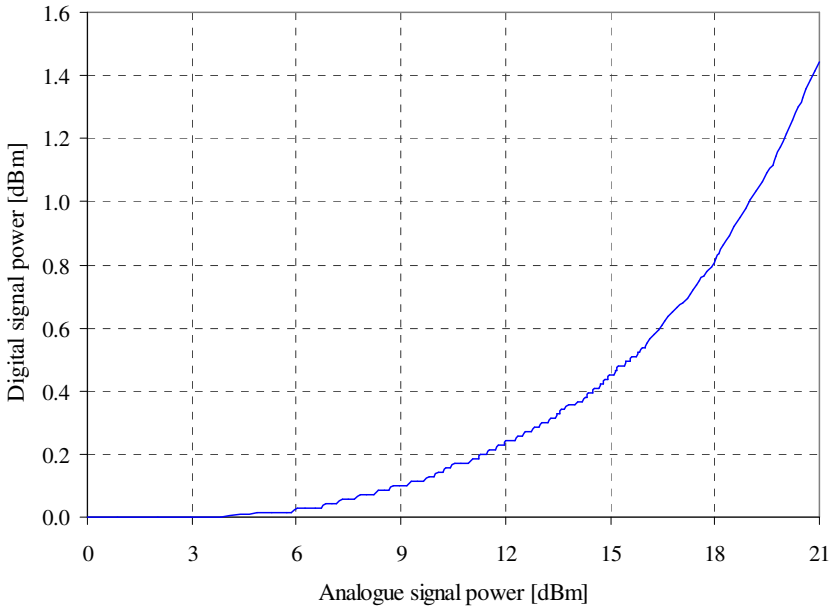

Figure 2.21 – Transfer of optical power between digital and analogue signal (data from Corning, reported in [PT06]).

An EPON operating at 10 Gbit/s with high splitting ratios was found to be a loss-limited system or a dispersion-limited system, when an external modulator or direct modulation is employed in the transmitter, respectively [PMS06]. The nonlinearities that are present in such system do not degrade the system performance, as long as launched powers are kept below 11.6 dBm, which corresponds to the limit imposed by the SBS effect in the worst case scenario analyzed. This limitation may be mitigated by increasing the source linewidth, or by providing a low frequency dither to the laser. The first option can be achieved through direct modulation of the source, since this causes the linewidth to broaden due to chirping. However, as referred above, the direct modulation will cause very high dispersion penalties, degrading the system performance. The second option seems to be the best active solution for minimizing the effect of SBS in a 10 Gbit/s PON system. The third (passive) option is to use SBS enhanced fibres, as referred above, that can enable a 3 dB higher launched power without SBS penalties and can be used together with dithering.

2.3. Optimum Gain of Avalanche Photodiodes

The new generation PON systems operating at 10 Gbit/s will be affected by a strong degradation of the receiver sensitivity [PMS06], as long as the 1 Gbit/s PON system conditions are maintained. Besides, in order to comply with higher capacity and/or reach, the

optical power budget will become more critical. The latter issue is also verified in several deployment scenarios of the first generation PON systems, when required to support higher number of users connected or longer network reaches.

An obvious approach to minimize these difficulties is to provide gain to the system, which may be achieved by employing optical amplification in the terminal elements of the network [PMS06] or by using a photodiode with gain, such as an APD, to replace the usually employed PIN photodiode. The gain elements should be located preferably in the OLT, since their cost would then be shared by all ONUs connected to the network. Therefore, the use of optical pre-amplification in the OLT was proposed in [PMS06], where the advantages of including this element were proven. However, the use of an APD in the OLT was shown in [PMS06] not to be a beneficial solution, if the APD is operated with fixed gain, which was found to be far from the optimum for ONUs at close range.

Therefore, it is important to analyse the conditions of the APD optimum gain, in order to provide a better perception of the low performance results obtained in [PMS06]. Those results show a better overall performance of the PIN configuration in the OLT receiver, due to the high APD excess noise that is generated for high received powers. When the APD is operated far from the optimum gain, this noise added to the system will cause performance degradation in the upstream system (from ONUs to OLT).

2.3.1. Theoretical Model for Optimum APD gain

In general, the use of APDs in broadband optical receivers will provide better SNR, when compared to receivers that employ PIN photodiodes, for the same received power. This improvement of the SNR results from the multiplication of the photodetected current by the avalanche gain, *M*. However, an additional contribution is added to the receiver shot noise, since the avalanche gain results from the random generation of electron-hole pairs through impact ionization. If the total shot noise is dominant over the thermal noise, the SNR in APD receivers will be worse than that in PIN receivers.

Based on the SNR analysis presented in [Agr02], the shot noise variance is given by:

$$\sigma_s^2 = 2qM^2F_A\left(\Re P_{rx} + I_d\right)\Delta f \ , \tag{2.16}$$

where q is the electron charge, $\Re$ is the receiver responsivity, P_{rx} is the power reaching the receiver, I_d is the dark current, Δf is the effective noise bandwidth of the receiver, which depends on its design, and F_A is the excess noise factor of the APD, given by:

$$F_A(M) = k_A M + (1 - k_A)\left(2 - \frac{1}{M}\right), \tag{2.17}$$

with k_A representing the ionization-coefficient ratio, in the range $0 < k_A < 1$.

In order to apply this analysis to more realistic receivers employing Transimpedance Amplifiers (TIAs), a modification of the approximation presented in [Agr02] for the thermal noise was obtained. This formulation is derived and presented in [Pat06]. In this case, the electrical noise contribution is accounted for by modifying the equation in [Agr02] for thermal noise variance, yielding:

$$\sigma_T^2 = \frac{4k_B T}{R_L}\Delta f + \frac{\gamma_n}{3}\Delta f^3, \tag{2.18}$$

where k_B represents the Boltzman constant, T is the absolute temperature, R_L is the load resistor, and γ_n is the f^2 noise coefficient characteristic of the TIA, given by [Pat06]:

$$\gamma_n = \frac{3\left(I_{n.av}^2 - G_{th}\right)}{B_{n.av}^2}, \text{ with } G_{th} = \frac{4k_B T}{R_L}. \tag{2.19}$$

Here, $I_{n.av}$ is the average equivalent input noise current of the receiver, and $B_{n.av}$ is the measurement bandwidth for $I_{n.av}$. For a given received power, the maximum value of SNR is obtained for an optimum value M_{opt} of the APD gain. Applying the above definitions for shot noise and thermal noise to the definition of SNR given in [Agr02], and after some analytic manipulation, the optimum gain is found to satisfy the following relation:

$$k_A M_{opt}^3 + (1 - k_A) M_{opt} = \frac{4k_B T}{q(\Re P_{rx} + I_d) R_L} + \frac{\gamma \Delta f^2}{3q(\Re P_{rx} + I_d)}. \tag{2.20}$$

Equation (2.20) shows that the optimum gain depends on several receiver parameters. Note, however, that the main difference between this formulation for the optimum gain and

the formulation presented in [Agr02] is the fact that here the optimum gain is dependent of the effective noise bandwidth of the receiver.

This analysis is valid for typical PON systems, where no optical amplification is employed and the laser source noise may be neglected. The influence of these other noise sources, as well as the influence of MPN, may, however, be considered by including their corresponding noise variances in the SNR assessment.

2.3.2. Results and Discussion

The importance of selecting the optimum APD gain, in order to achieve the maximum SNR value for the upstream PON system, is assessed in this sub-section by analyzing the results obtained employing the above formulation. The selection of the values used for the parameters was performed based on information provided by manufacturers. Therefore, an operating temperature of 300 K, a load resistance of 400 Ω, a dark current equal to 2 nA, a responsivity of 0.7 A/W, and an ionization-coefficient ratio of 0.4 were assumed, which closely characterize the less noisy APDs available in the market. The f^2 noise coefficient was determined considering an equivalent input noise current of 15×10^{-12} A/√Hz, measured in a bandwidth of 8 GHz.

Figure 2.22 depicts the values of the APD optimum gain as a function of the receiver effective noise bandwidth and of the received optical power.

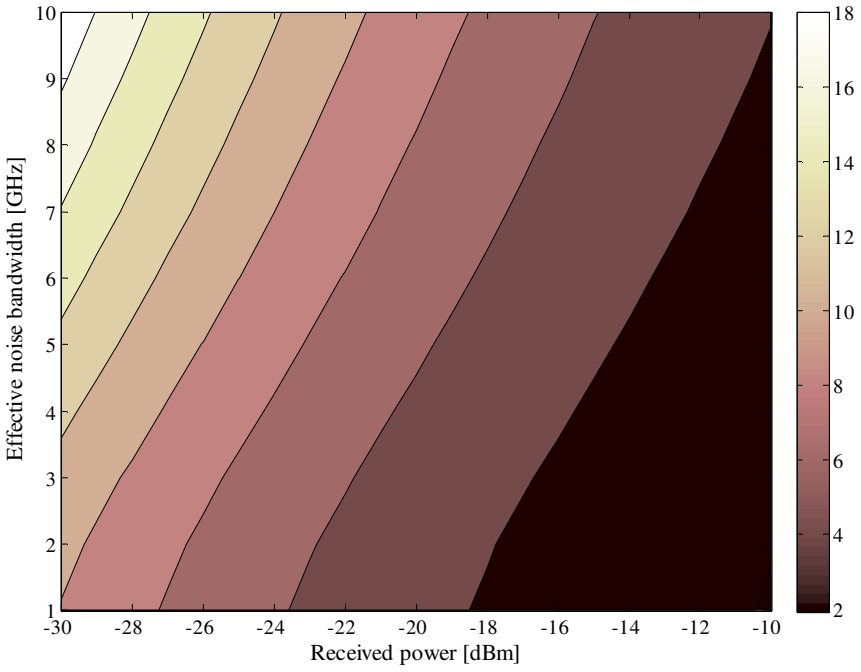

Figure 2.22 – Optimum APD gain, as a function of the effective noise bandwidth and of the received optical power.

The range selected for the received optical power in Figure 2.22 includes reasonable values, which comply with several PON system topologies, as well as different splitting ratios. The optimum APD gain is shown to vary from less than 2 to almost 20, in this range of received optical power. Moreover, the dependence of the optimum gain on the noise bandwidth is also evident.

The maximum achievable values for the SNR (in dB), obtained using the optimum APD gain, are plotted in Figure 2.23, also as a function of the effective noise bandwidth and of the received optical power. Considering a noise bandwidth around 7 GHz, which is suitable for 10 Gbit/s receivers, and a received optical power around -25 dBm, which is approximately the sensitivity for 10 Gbit/s APD receivers, the curves on Figure 2.23 show that the maximum achievable SNR value is less than 20 dB.

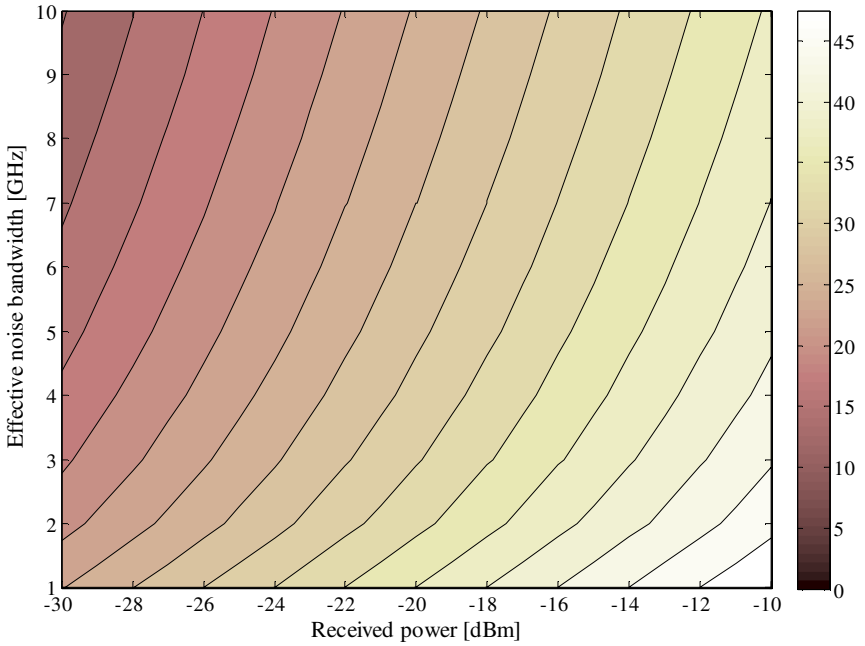

Figure 2.23 – Maximum achievable SNR values, for optimum APD gain.

The operation of an APD receiver near the optimum gain is very difficult to achieve in a PON upstream system. This is because a large range of optical powers reaches the receiver, due to the commonly uneven topology of PONs. Therefore, assuming that the APD operates with a fixed gain of 10, Figure 2.24 depicts the SNR penalty that occurs due to the operation far from optimum, which is justified by the excess noise that is generated in these situations. For instance, the curve corresponding to a noise bandwidth of 7 GHz shows a SNR penalty higher than 2 dB for the highest received powers and an optimum operation for received powers around -24 dBm. The network design should take into account this penalty and, if

possible, the APD operating gain should guarantee a SNR penalty not higher than 0.5 dB, in order to assure a satisfactory network performance.

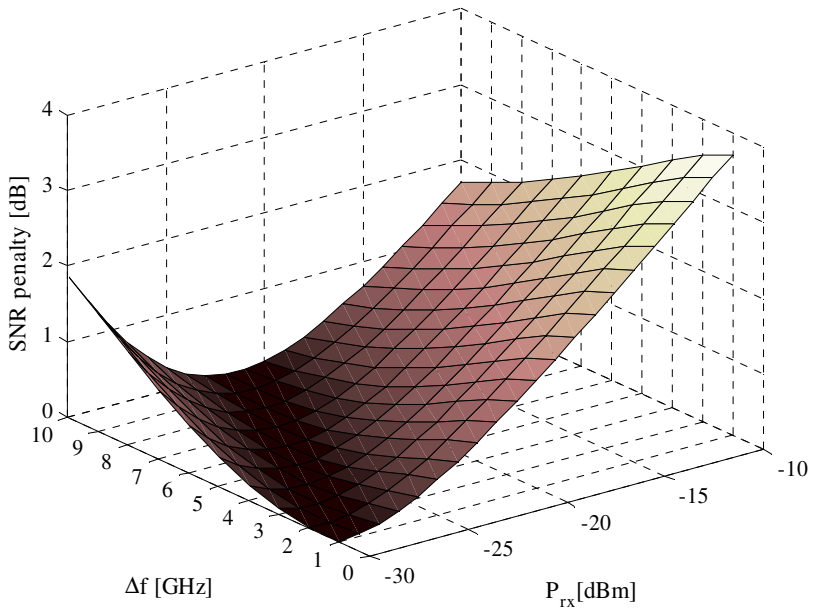

Figure 2.24 – SNR penalty, considering that the APD operates with $M = 10$.

The former results suggest that an APD gain lower than 10, for a noise bandwidth of 7 GHz, would result in a reduced maximum penalty, in the power range considered. Thus, the SNR penalty was determined fixing the noise bandwidth at 7 GHz and varying the APD gain, as shown in Figure 2.25. These results show that for an APD gain around 7, the penalty is always lower than 2 dB, increasing for low powers if the gain is reduced and for high powers if the gain is increased.

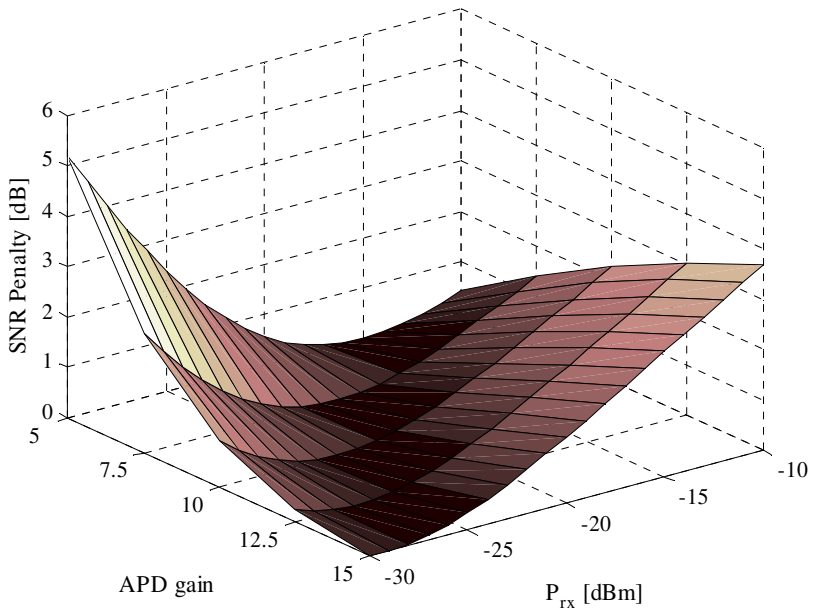

Figure 2.25 – SNR penalty, for $\Delta f = 7$ GHz, varying the APD gain.

2.4. Conclusions

Amongst the possible upgrades for PON systems, the data rate upgrade to 10 Gbit/s was the one that prevailed and attracted interest from a large number of operators and manufacturers. This upgrade scenario allowed to develop new systems with incremental upgrade costs, avoiding a very complex and disruptive process. However, in order to design and operate a PON system at higher data rates, namely at 10 Gbit/s, it was necessary to identify and overcome several physical impairments that might occur in all sub-systems of the network (optical source, optical transmission fibre and receiver). Such as for any other network system, for designing PONs it is fundamental to identify the main constraints, thereby enabling to overcome, or at least minimize, its weak points, through their characterization. In this process, several solutions should be weighted, but a simple and economically feasible system should always be the goal. With this in mind, along this chapter, some impairments were analyzed and characterized, and their impact in 10 Gbit/s PON systems was assessed.

Assuming that multimode FP lasers are employed as optical sources in the ONUs, the impact of MPN in the upstream sub-system of a 10 Gbit/s PON was evaluated. The system specifications regarding the maximum allowed values for source spectral width, fibre dispersion, and network reach were identified by simulation. It was shown that the MPN may have a severe impact on the system performance, whenever it becomes the limiting factor. Assuming a moderate MPN effect, compliant transmission of up to 20 km is possible only for reduced source spectral width, as well as small fibre dispersion. Since the SNR due to MPN is independent of the received power, alternative approaches are necessary to overcome this problem and FEC may have an important role in such task, as further discussed in Chapter 3.

The impact of fibre nonlinear effects on the performance of a PON system operating at 10 Gbit/s was also assessed. These nonlinear effects are caused by the high launched powers required to support higher splitting ratios. Three nonlinear effects were considered, namely SPM, SBS and SRS. The simulation results for SPM and the analytic estimates for SBS and SRS allow to conclude that the main nonlinear impairment in a 10 Gbit/s PON system is the SBS, limiting the power launched into the fibre and imposing restrictions on the network reach and/or splitting ratio, if no suppressing method is employed. In the worst case situation, with a feeder length of 20 km, the impact of SBS is meaningful for launched powers higher than 8.6 dBm, without modulation, and 11.6 dBm, for NRZ signals, whereas for SPM and SBS the threshold is achieved for launched powers around 26 dBm. Therefore, SBS is the

dominant nonlinear limitation for very high-speed, single-channel, intensity modulated systems, whereas SPM effect is not significant and SRS is important only when an overlay analogue signal is transmitted simultaneously with the downstream data signal.

Finally, the decrease of receiver sensitivity together with a critical power budget may require gain to be provided to the system. Therefore, the use of APD receivers may be proven to be essential, or at least beneficial, in next generation PON systems operating at 10 Gbit/s, due to the gain that they may provide. However, when operated far from an optimum value of the gain, they may instead cause performance degradation due to the added excess noise. An analytic study of the optimum APD gain was presented, taking into account the use of transimpedance amplifiers in the receivers. The results show penalties above 2 dB for APD operation far from the optimum gain, for the typical noise bandwidth of a 10 Gbit/s receiver, and a typical APD gain of 10. However, if the gain is decreased to around 7, the SNR penalty for the considered power range is less than 2 dB, assuring an acceptable network performance.

Chapter 3

CODING TECHNIQUES FOR PASSIVE OPTICAL NETWORKS

The use of forward error correction techniques in future deployments of access networks is quite foreseeable. It allows achieving higher capacity or longer network reaches, by providing extra gain to the system, thereby complying with the established demanding power budgets. Moreover, the inclusion of FEC codes allows the use of more cost-effective components and/or to improve the system performance, since a lower Optical Signal-to-Noise Ratio (OSNR) is necessary to attain the same error rate. This scenario is verified for high data rate PON systems, such as 10 Gbit/s EPONs. Effectively, one of the preliminary conclusions of the 802.3av Task Force [IEEEav] focused on the need of using some type of FEC in the system.

As referred previously, in a PON, and particularly in an EPON system [KP02], an OLT is typically connected to an optical PSC, delivering triple-play services to multiple ONUs, over a shared fibre optic infrastructure. The transmission of data in such a system, independently of the operation data rate, is conducted differently in both directions of the network. More precisely, in the downstream the traffic is broadcasted from the OLT to the ONUs, whereas the upstream traffic is managed through Time Division Multiple Access (TDMA), where transmission time slots are dynamically allocated to each ONU [KP02].

Therefore, in the downstream direction of a PON the transmission is performed in a continuous manner, which suggests the use of FEC codes already standardized for optical networks, such as the one described in ITU-T G.975 [ITU00]. However, in the upstream

direction the transmission resembles burst-mode operation, and a dedicated FEC technique may be necessary due to the specific characteristics of this type of traffic. Such scenario requires the identification of the most suitable code, through an analysis that should balance its correction capabilities, complexity and performance.

Bearing the above reasoning in mind, a brief overview of the most important classes of FEC codes is described in section 3.1, assessing the most suitable to be used in TDMA access networks. Concerning the traffic characteristics and the properties of such networks, the Reed-Solomon codes were found to be adequate, and the requirements for exploiting these codes in TDMA access systems are highlighted in section 3.2, followed by the analysis of the obtained performance improvement in section 3.3. The performance of the upstream transmission in a 10 Gbit/s PON system employing the selected FEC code is evaluated in section 3.4 and the benefits of introducing FEC are assessed aiming the minimization of characteristic impairments of such networks, such as the impact of MPN.

3.1. Overview of Forward Error Correction Codes

The transmission quality in communication systems is typically hampered by noise and distortion introduced by the transmission channel. A very effective manner to tackle this problem is by the introduction of channel coding techniques, such as FEC.

FEC differs from other standard error detection and correction methods, such as Cyclic Redundancy Check (CRC), since it is specifically designed to allow the receiver to correct errors in the currently received data. Using FEC techniques only the bits already received are used to correct the “current” bit, whereas using CRC, all bits in a frame need to be protected with a transmitted check sequence, in order to verify the integrity of the whole data frame received. In general, FEC codes tend to require greater bandwidth than other error-correcting codes, but have the advantage of correcting errors as data is received.

FEC is accomplished by adding redundancy to the transmitted information using a predetermined algorithm. Each redundant bit is invariably a complex function of many original information bits and the original information usually appears in the encoded output. The redundant information (codesymbols) is added to the data signal, producing codewords. It is ensured that the codewords differ by a minimum number of codesymbols, corresponding to the minimum code distance. The maximum fraction of errors that can be corrected is

determined in advance by the design of the code, so different FEC codes are suitable for different conditions. In the most commonly used FEC type, known as out of band FEC, the line rate information is increased in accordance with FEC rate [TKT06], and powerful error detection and error correction algorithms may be applied.

A wide diversity of FEC codes is currently employed in the global market of telecommunications [TKT06], [Miz06], [BPG+07]. These codes differ in several aspects, such as complexity, transmission overhead, coding gain, performance, and burst-error correction capability. However, due to the inherent low-cost and low-complexity characteristics of the access network, not all FEC codes are suitable to be deployed in this network segment. For instance, Turbo Codes [BPG+07], [Bur01], are not currently the best choice, due to their relative complexity, mainly related to the decoding process, which would increase the cost and the complexity of the terminal access network equipments. Turbo codes emerged in the early 1990s and consist on schemes that combine two or more relatively simple convolutional codes and an interleaver to produce a block code that can perform within a fraction of the Shannon limit. Due to this additional complexity of turbo codes, convolutional and block codes may be addressed as possible candidates for access networks, and a brief explanation of these two classes is given in the following, pointing out their advantages and disadvantages for deployment in this network segment.

3.1.1. Convolutional Codes

Convolutional codes [BPG+07] are a family of error correcting codes that present a good performance, for a relatively low decoding complexity. In the encoding process of these codes an output sequence is generated from the current and several preceding message input elements, using a continuous process responsible for creating redundancy in the encoded sequence. This redundancy is used by the decoder for error correction, in order to re-construct the original input message.

Linear convolutional codes are usually preferred, since they enable a structured decoding process. The input message is a sequence of k elements that origin a sequence with n elements ($n > k$) at the encoder output [BPG+07]. These n encoded elements do not depend only on the k elements that are input at a given instant i, but also on the preceding inputs at instants i-1, i-2,…, i-M, where M represents the memory of the encoder. The complexity of the decoder is directly related with the memory level, i.e., the higher is the memory level the

higher is the decoder complexity. However, higher memory levels enable stronger correction capabilities, and a trade-off between complexity and correcting capability may be necessary.

Regarding the decoding process, several algorithms have been proposed for convolutional codes [Vit71]. Among them, the Viterbi algorithm is one of the most used. It performs maximum likelihood decoding, but avoids taking into account all possible sequences, thereby decreasing the decoding complexity [Vit71].

The overhead increase with convolutional coding, especially for high data rates, is a strong limitation of this type of codes. Techniques such as puncturing allow reducing the redundancy, but at the expense of decreasing the code gain [AMB01]. Moreover, the encoder and decoder complexities make this code less appealing to be implemented in low cost access networks, both in the subscribers' terminals and in the central office.

3.1.2. Block Codes

The main characteristic of a block code is the fact that finite and constant length codewords are employed. Typically, a codeword of length n is formed by adding $(n - k)$ parity codesymbols to an input information block of k symbols. The parity symbols enable error detection and correction in the receiver, but a trade-off must be made between the code efficiency (information rate) and the correction capabilities of the code. Along the years, several decoding methods have been developed for block codes. The most used are algebraic, involving closed-form mathematical formulas with vectors and/or polynomials [Kam01], [JK95], [Lee05].

Block codes may be classified into binary and m-ary codes. One example of binary codes are Hamming codes, which have a correcting capability of one error per FEC frame, presenting a very small overhead, which results in a low coding gain. Other codes such as the binary BCH (Bose, Chaudhuri, Hocquenghem) codes [KT69], are usually designed for correction of random errors, with a coding/decoding process which is relatively easy to implement. Regarding m-ary codes, the Reed-Solomon (RS) [BDZ+04] is the most widely spread code. It is a subset of non-binary BCH codes that has a powerful random and burst correcting capability. The burst error correcting capability of RS codes is due to its symbol-based characteristics, and causes the decoder to be slightly more complex than that for binary BCH codes. Due to their efficiency regarding burst errors, RS codes originate very powerful codes when concatenated [KY03].

The RS codes have been considered very appealing for implementation in optical systems, due to their burst error correcting capability and relatively simple decoding process [TKT06], [BPG+07]. They present an optimum overhead, for a given error correcting capability, with a high coding gain. As for now, the RS code is the most attractive code to be implemented in the scenario under consideration, since its characteristics are well adapted to the requirements of access networks, particularly to the upstream direction of PON systems. Specifically, it is a block code, which is convenient for the TDMA traffic slots of the upstream direction, besides providing high gain to the system. Such gain is rather important for higher data rate systems (10 Gbit/s), enabling the use of lower cost laser sources (with lower output powers) and the use of typical receivers, which present low sensitivity values for high data rates.

3.2. Requirements for Exploiting Reed-Solomon Codes in TDMA Systems

The investigation of the physical impairments of a specific optical network is fundamental to select the suitable solution to overcome or minimize those impairments. If FEC is chosen to be employed, a correct selection of the code parameters should also be performed [AHK+02]. This selection should take into account the decisions made regarding the network components and specifications, in order for the chosen code to provide the necessary gain for each network scenario.

To avoid high development effort, it would be desirable to use the same code both for upstream and for downstream of a PON system. However, this situation may result in the selection of a non-optimum code for one of the directions. Several aspects should then be considered in the code selection process for a high data rate PON, as enunciated in the following:

- The upstream transmission is the most critical transmission direction, due to the typically weak laser sources and low cost equipment located in the ONUs. This leads to more stringent specifications in terms of emitted powers and sensitivities in the upstream than in the downstream, motivating the use of FEC encoding in order to comply with the specified power budgets.
- In the downstream direction, the complexity of the FEC decoder is an important aspect to be considered, since it will be located within the ONUs, and so a very complex or power consuming decoder is prohibitive.

- In the design of the optical system, different power budgets may be considered (depending on the infrastructure topology and on the supported density of end users). The specifications of a FEC code should be based on the most critical (higher) power budget, $\Delta P_{\text{critical}}$.
- Based on the equipment selected for ONUs and OLT transmitters and receivers, the emitted powers and receiver sensitivities are available to be used in the definition of the necessary FEC gain, by assuming a worst case scenario. Both for upstream and downstream, the worst case scenario is identified by assuming that the emitted power, P_{tx}, is equal to the lowest allowed value and the sensitivity, P_{rx}, is also equal to the minimum allowed. In this situation, a worst case power budget is obtained by the difference between these two values. The comparison of this power budget with the critical power budget will indicate the necessary FEC gain, as given by (using logarithmic units):

$$G_{\text{FEC}} = \Delta P_{\text{critical}} - \left(P_{\text{tx}} - P_{\text{rx}} \right). \tag{3.1}$$

After the establishment of the necessary FEC gain, the next step in the process of selecting the FEC code is the determination of the code overhead. In order to provide more bandwidth for data information, a relatively low overhead is desired. This may be accomplished using a sub-rating strategy, meaning that the FEC parity bandwidth will be accommodated by reducing the effective data rate in the Medium Access Control (MAC) layer [IEEE09]. A parallel question consists on selecting the FEC code based on its encoding/decoding complexity, instead of determining the overhead a priori. In this case, the code is selected and, based on the necessary FEC gain, the overhead is automatically determined, defining the maximum allowed MAC data rate.

This discussion should therefore be addressed for the upstream transmission of a high data rate PON system (TDMA-based), since its characteristics are more specific, when compared to the downstream direction. Moreover, these specific features should also be considered in the selection of appropriate RS code characteristics.

As previously mentioned, the allocation of upstream time slots may be performed dynamically. This implies that each ONU time slot may have different lengths from cycle to cycle. Thus, the FEC code should be able to perform equally for both long and extremely short packets. For simplicity reasons, a static allocation may be assumed, with equal time slots

for each ONU. Otherwise, one may consider the FEC frame length to be equal to the shortest packet length (excluding parity information), if dynamic allocation is employed. This should be verified due to FEC implementation complexity reasons, since low processing latency must be guaranteed at high data rates [PCA+02].

One important aspect of using out of band FEC is the amount of overhead that is added to the signal in the form of redundant information, which increases the transmission data rate. In an access network, the transmission rate increase may have a severe impact on the network performance, since it degrades the receiver sensitivity. Besides, as the transmission rate increases, the direct modulation of the laser sources will become even more critical [Pat06]. Therefore, the FEC overhead should be minimized.

Since the use of FEC encoding is motivated by the gain that it may add to the system, it is desirable to have a coding gain as high as possible, in order to overcome some system limitations, such as the low OSNR verified at the OLT receiver, or to allow for higher system capacity or longer distances. For PIN receivers, the coding gain is defined as the ratio between the OSNR without FEC and the OSNR with FEC, required to obtain the same BER. The correcting capability of the code increases when the coding gain increases, and it is also desirable to be as high as possible. The correcting capability is defined as the number of symbols that can be corrected in the FEC frame.

The ability of FEC coding to correct error bursts may prove to be critical in the upstream direction of a PON system. If, for instance, optical amplification is employed in either of the terminal equipments, transients may appear in the signal and eventually cause error bursts [FGW+03]. Moreover, if direct modulation is used in the transmitter, similar transients may degrade the signal and also cause error bursts.

3.3. Analysis of FEC performance with RS codes

RS codes are non-binary linear cyclic block codes, where the basic unit is an m-bit symbol, with m representing any positive integer higher than 2. Because of the systematic nature of RS codes, the redundancy information is added to the data in such a way that allows the decoder to detect and/or correct errors within a block of information. The linear property of RS codes guarantees that any linear combination of two codewords is also a codeword. Moreover, the cyclic property of RS codes indicates that another valid codeword is obtained by shifting the codeword.

RS codes are usually designated by RS(n,k) = RS(2^m-1, 2^m-1-2t), where n is the total number of symbols in a codeword and k is the number of data symbols in each block. The number of redundancy symbols (parity) is equal to 2t, where t represents the correcting capability of the code or, in other words, the maximum number of symbol errors in a block that is guaranteed to be corrected.

3.3.1. Analytic Model

A suitable criterion to evaluate the correcting performance of a RS code is the theoretical relationship between the BER after FEC (BER_{out}) and the BER before FEC (BER_{in}). The BER estimation for a system employing FEC is based on the simplified scheme presented in Figure 3.1. The data source generates the binary information at a rate of Rs bit/s and this information is then encoded and transmitted to the communication channel at a higher rate of Rc bit/s, since the encoder adds redundant information to the original signal. The communication channel introduces noise in the signal, and the degraded information reaches the receiver, being decoded afterwards.

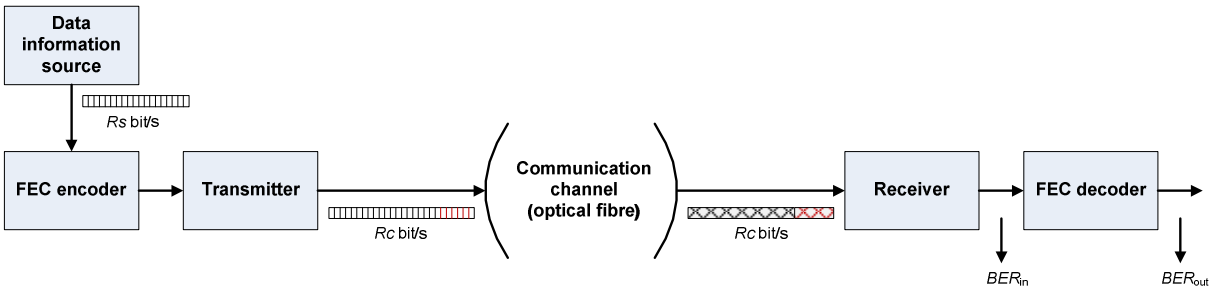

Figure 3.1 – Simplified diagram of a communication system employing FEC.

In this scenario, assuming that errors occur independently and that the probability of incorrect decoding is equal to zero, the relationship between BER_{out} and BER_{in} is given by [ITU00], [Tor84]:

$$P_{USE} = \frac{1}{2^m - 1} \sum_{i=t+1}^{2^m-1} i \binom{2^m - 1}{i} P_{SE}{}^{i} \left(1 - P_{SE}\right)^{2^m - 1 - i}, \qquad (3.2)$$

where P_{USE} is the probability of an uncorrectable symbol error and P_{SE} is the probability of a symbol error, which may be related respectively to BER_{out} and BER_{in} [ITU00], by:

$$P_{\mathrm{USE}} = 1-\left(1-BER_{\mathrm{out}}\right)^{m}, \tag{3.3}$$

$$P_{\mathrm{SE}} = 1-\left(1-BER_{\mathrm{in}}\right)^{m}, \tag{3.4}$$

Recalling the previous section, it should be guaranteed that the FEC processing speed is limited, but the latency must be reduced. Therefore, practical implementations of RS encoders/decoders operate in parallel, employing n_{DMUX} encoders/decoders, usually 16. In these implementations, the total packet length should be a multiple of n_{DMUX} times the individual FEC frame length, N_{min}, and excluding redundancy bits. This leads to the following relation [PCA+02]:

$$N \cdot N_{\mathrm{min}} = N \cdot n_{\mathrm{DMUX}} \cdot m\left(2^{m}-1-2t\right) \approx N_{\mathrm{p}}, \tag{3.5}$$

where N is an integer, representing a multiplicative factor for the basic packet size, and N_{p} is the total packet length, excluding redundancy bits.

Since this analysis is directed to a TDMA system, the most relevant performance parameter is the Packet Loss Ratio (PLR), instead of the BER. Assuming that a packet of length Nc is lost if one bit of the information it carries is erroneous, the PLR is given by [PCA+02]:

$$PLR = 1-\left(1-BER\right)^{Nc}. \tag{3.6}$$

Another important parameter in the RS code performance is its error correcting capability. As mentioned before, it is related with the amount of overhead, OH, that is added to the signal. A maximum correcting capability t is attained for a maximum overhead such that:

$$\frac{2t}{2^{m}-1-2t} \leq OH. \tag{3.7}$$

This overhead will be translated into an error rate penalty, or equivalently, a Q-factor penalty (Q_{penalty}), since the transmission rate is increased. It may be expressed as a relationship between the total transmission rate, including FEC, and the information rate B, as [Bol04]:

$$Q_{\mathrm{penalty}} = \sqrt{\frac{B+B\times OH}{B}} = \sqrt{1+OH}. \tag{3.8}$$

Expressing the BER as a function of the OSNR, and affecting it by the $Q_{penalty}$ defined by equation (3.8), yields:

$$BER = \frac{1}{2}\operatorname{erfc}\left(\frac{Q'}{\sqrt{2}}\right) = \frac{1}{2}\operatorname{erfc}\left(\sqrt{\frac{a \times OSNR}{2(1+OH)}}\right), \tag{3.9}$$

where $Q' = Q/Q_{penalty}$ and a is a constant approximately equal to 1.1236 for 10 Gbit/s NRZ signals [PCA+02], which is the format specified for EPON and GPON systems, considering an OSNR within 0.1 nm optical bandwidth. The Q-factor is expressed in equation (3.9) by the square root of OSNR affected by the constant a.

The performance of FEC can also be evaluated through the Coding Gain (CG), which is defined as the ratio of the OSNR required with and without FEC to obtain a given BER or a given PLR [ITU00]. Another performance metric that takes into account the data rata expansion factor is the Net Coding Gain (NCG), defined in dB as [ITU00]:

$$NCG = CG + 10\log_{10}(r), \tag{3.10}$$

where r represents the code rate, defined as $r = k/n$.

The capability to correct bursts of errors is a very well known characteristic of RS codes, besides being an important advantage of these codes over other available types. An upper bound on the error correction capability of RS codes is given by the Singleton bound. According to this bound, the maximum length of error bursts that can be corrected by a RS(n,k) code is (n-k)/2, where n and k are expressed as multiples of symbols. However, several publications show that when error location correlation within a burst is properly employed, the burst error correcting capability of RS codes can be increased beyond the Singleton bound, with relatively small probabilities of erroneous correction [DK95], [YLLW02]. Alternatively, the error burst correcting capability can be further increased using block interleaving [SZNA04], which is a process where code symbols are rearranged so as to spread bursts of errors over multiple codewords, eventually decreasing the actual number of errors in each codeword. The interleaving process is proposed by the ITU-T [ITU00], using a 16-way interleaved RS(255,239) code that can correct error bursts with up to 1024 bits.

3.3.2. Performance Assessment

The formulation presented in the previous sub-section enables the identification of the RS code parameters suitable for its deployment in a specific scenario. The performance of the chosen RS code may be evaluated by error rate measures or, alternatively, by using the coding gain metric. For instance, it is possible to define a maximum overhead and, from there, find the other optimum parameters, such as the code length and the achievable coding gain.

The first results, presented in Figure 3.2 and Figure 3.3, show the NCG and the amount of overhead achievable as a function of the error correcting capability of the code, by fixing the symbol size m in five different values, for a PLR of 10^{-6} and 10^{-12}, respectively.

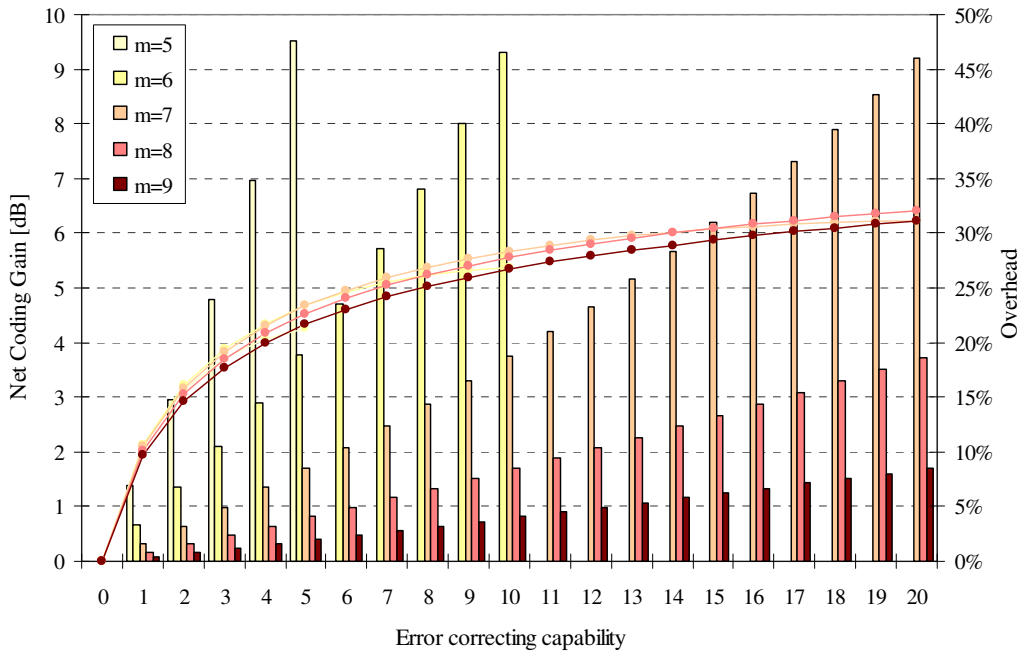

Figure 3.2 – NCG (lines) and overhead (bars), for PLR = 10^{-6}, as a function of the error correcting capability.

In Figure 3.2, the overhead is limited to 50%, which is already an unacceptable value for any transmission channel, and the correcting capability is also limited to 20, since this value corresponds to a code with very good correcting characteristics. In the same plot, the two lower m codes show very high overheads for low correcting capabilities, which make these codes not suitable. Considering an overhead of around 10%, correcting capabilities of 6, 12 or over 20 symbols are achievable for codes with $m = 7$, 8, and 9. The corresponding maximum NCG for these codes varies from around 5 dB for $m = 7$ to slightly above 6 dB for $m = 9$. A NCG higher than 5 dB is attained for codes with $m = 7$, but with prohibitive overheads, whereas for $m = 9$ the overhead is quite low and a very good correcting capability is obtained.

The conclusions drawn for Figure 3.2 are also valid for the results in Figure 3.3, except for the higher values obtained for NCG, as expected. In this situation the highest NCG is almost 8 dB, but with prohibitive overheads for both m = 7 and 8.

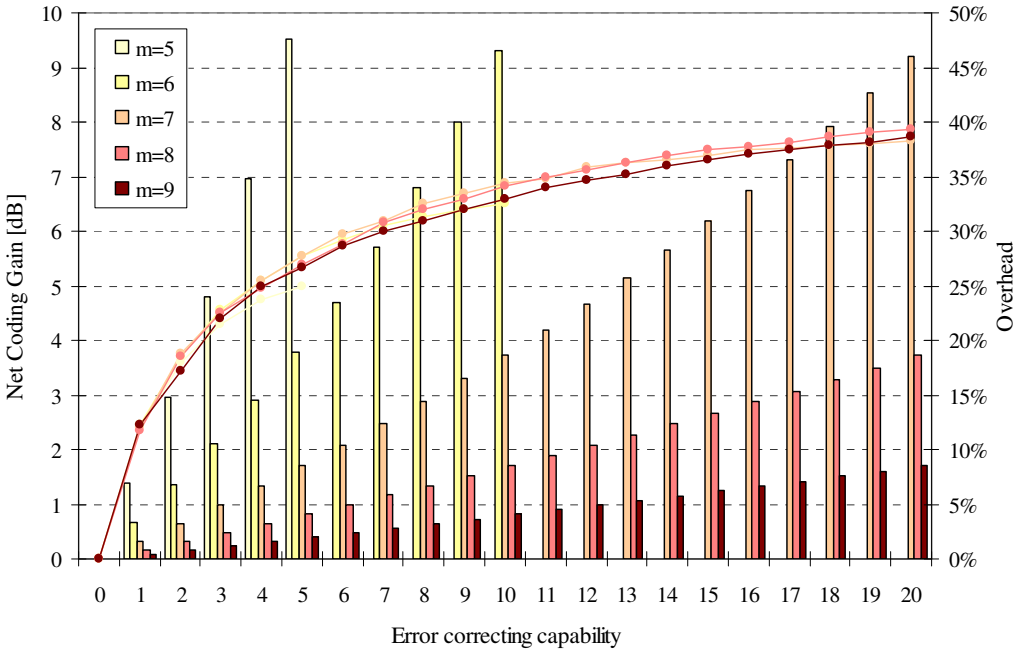

Figure 3.3 – NCG (lines) and overhead (bars), for PLR = 10^{-12}, as a function of the error correcting capability.

The previous results show that as higher is m, better correcting capabilities are attained with lower overheads. Note, however, that the NCG seems to be approaching an upper bound as the correcting capability is increased, and the encoding/decoding processes will become more and more complex for higher m values. Therefore, a trade-off should be made, considering the maximum overhead that is acceptable, and the desired NCG and correcting capability of the code.

The results depicted in Figure 3.4 show the performance also employing the NCG metric, but this time with the correcting capability fixed at 8, since this is characteristic of the standardized RS code [ITU00]. Three values for PLR are assumed, namely 10^{-6}, 10^{-9}, and 10^{-12}, and codes with m = 6, 7, 8, and 9 are used, since for m = 5 it has been shown in Figure 3.2 and Figure 3.3 that it is impossible to reach a correcting capability of 8, with an overhead below 50%. By analyzing the results of Figure 3.4 it may be concluded that, for any of the considered PLRs, the NCG is higher for the code with m = 7. For PLR = 10^{-6} the NCG ranges between 5 dB and 5.5 dB, for PLR = 10^{-9} it is around 6 dB, and slightly above 6 dB for PLR = 10^{-12}. The NCG differences observed for the different m values are quite small but show that, for this specific correcting capability, codes with m = 7 provide a better NCG.

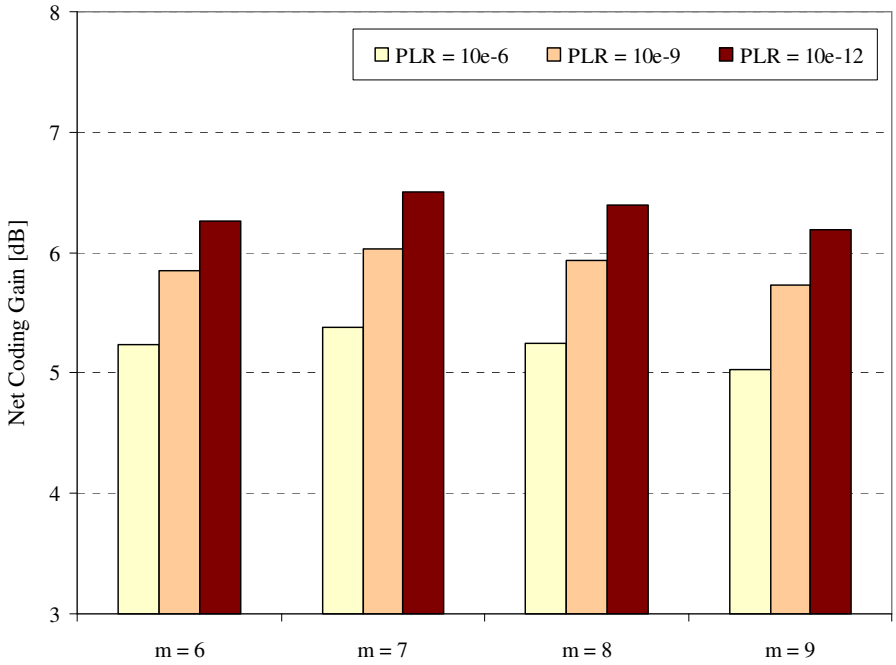

Figure 3.4 – NCG for a correcting capability of 8, for several values of PLR.

Previous calculations used PLR curves obtained considering the minimum frame length, recalling equation (3.6). The length of the information data with respect to the total FEC frame length (including redundancy bits) is depicted in Figure 3.5, as a function of the correction capability. Again, codes with m = 7, 8, and 9 are considered.

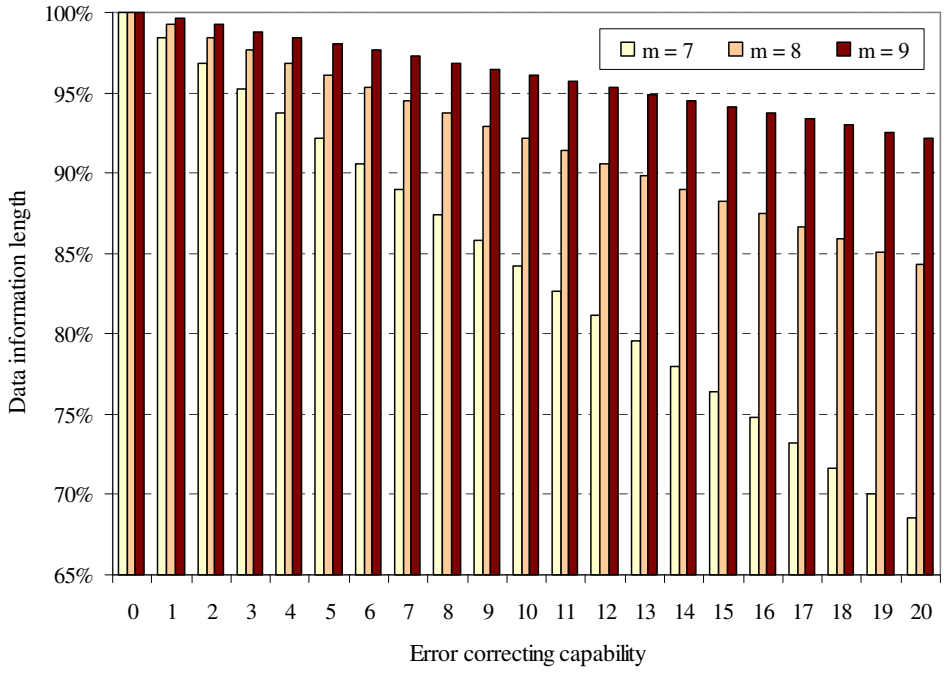

Figure 3.5 – Data information length with respect to the total FEC frame length.

Note that the results in Figure 3.5 do not represent the overhead as defined for previous results. Here, the percentage of information size is determined with relation to the encoded frame, whereas the overhead in earlier results is determined with relation to the frame size before encoding.

All previous calculations assumed that 16 encoders/decoders are working in parallel. By changing this parameter, the minimum frame size as defined by equation (3.5) will obviously vary. This variation will cause the PLR curves to change, since the PLR depends on the length of the packet that it refers to. By definition, PLR increases with the packet length simply because, for the same BER, the probability of occurring an error in the packet increases. The change of the PLR curves is also noted when a value for *N* in equation (3.5) is assumed different from unit, which was the value used to obtain all the previous results. Increasing this value will cause the frame length to increase, affecting the PLR curves. The variation of the frame size, by employing different multiplication factors to the minimum frame length, is not a severe issue on the performance of the codes, since the same multiplication factor is used for both encoded and decoded frames. The consequent result is a slight modification in the NCG value, which in most cases will not significantly affect the code performance. The influence of the number of encoders/decoders and of the frame multiplier *N* on the code performance was evaluated for two illustrative examples. Results are depicted in Figure 3.6 and Figure 3.7, for the RS(255,239) and RS(511,479) codes, respectively. Both have an overhead around 6.7%, corresponding to a correcting capability of 8 in the first case and of 16 in the second case.

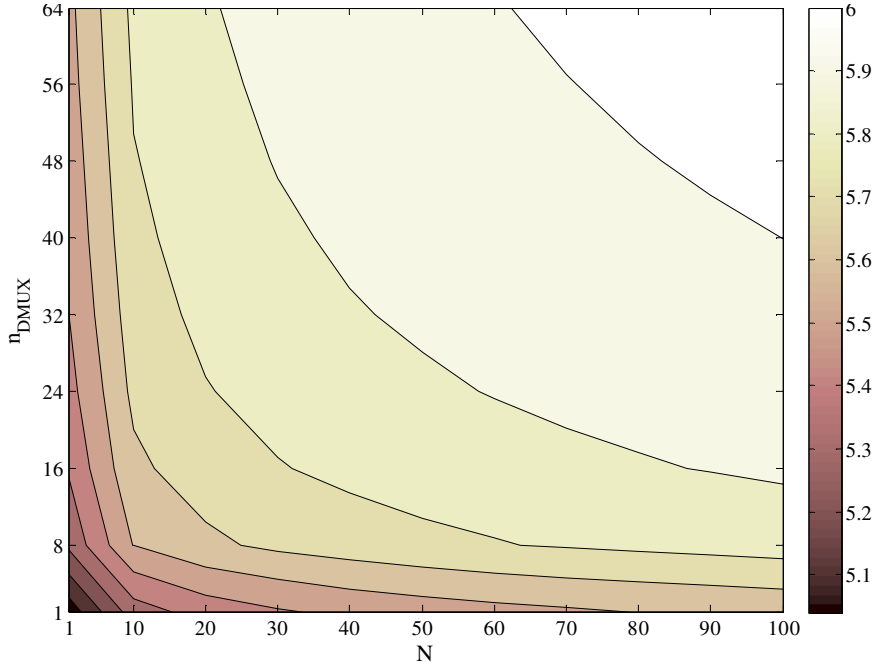

Figure 3.6 – NCG for RS(255,239), assuming PLR = 10^{-6}, and varying *N* and n_{DMUX}.

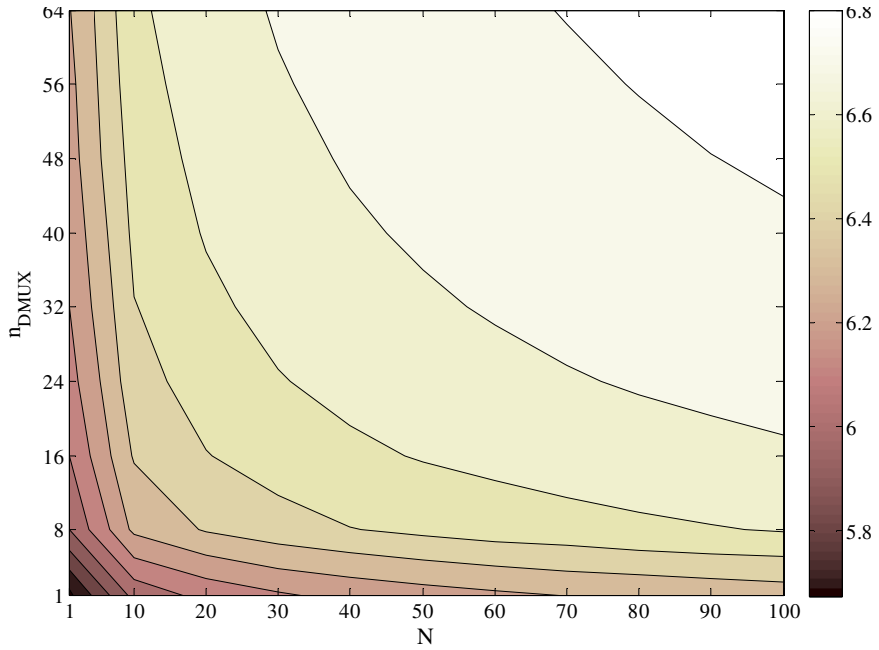

Figure 3.7 – NCG for RS(511,479), assuming PLR = 10^{-6}, and varying N and n_{DMUX}.

By observing the results in Figure 3.6 and Figure 3.7, one may conclude that the NCG has a variation of less than 1 dB, in both cases. Note that, in spite of slightly increasing the NCG, the increase of n_{DMUX} will result in more complexity of the FEC process. Moreover, for the maximum values considered for N and n_{DMUX}, frame durations of 1.2 ms and 2.8 ms are obtained for RS(255,239) and RS(511,479), respectively, assuming a data transmission rate of 10 Gbit/s. These values are noticeably high to be used in an access network that employs TDMA.

All the previous results have used mainly the NCG metric to evaluate the performance of FEC codes. Although NCG is an important quality metric, the behaviour of the system should also be assessed in terms of lost information. Therefore, the results depicted in Figure 3.8 – Figure 3.11 show the performance of the codes using the PLR curves, considering $n_{DMUX} = 16$ and $N = 1$. An error correcting capability of 8 was assumed, since it is enough to obtain good performance codes. In these figures, the red curves show the PLR for uncoded information, the green curves the PLR before decoding, and the blue curves the PLR after decoding. Four different codes were tested, using different values of m, namely RS(63,47), RS(127,111), RS(255,239), and RS(511,495). As expected, and as shown in Figure 3.2 – Figure 3.4, all tested codes have similar NCG, which may be visualized by the distance between red and blue curves. The main differentiating factor between these codes is their corresponding overhead. In fact, the overhead for RS(63,47) and RS(127,111) codes is prohibitive in this scenario, whereas the RS(255,239) code presents a lower overhead, near 7%, which may be acceptable. The coding loss due to the overhead is quite noticeable in the

plots of Figure 3.8 – Figure 3.11, by observing the distance between red and green curves. It is evident the very low overhead obtained for the RS(511,495) code, as shown by the almost superposition of these two curves in Figure 3.11.

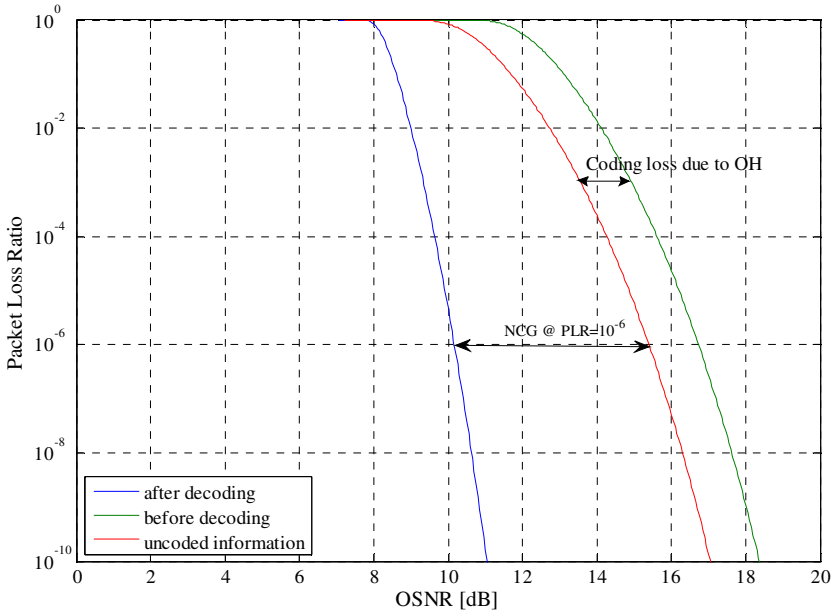

Figure 3.8 – PLR for RS(63,47), with correcting capability of 8.

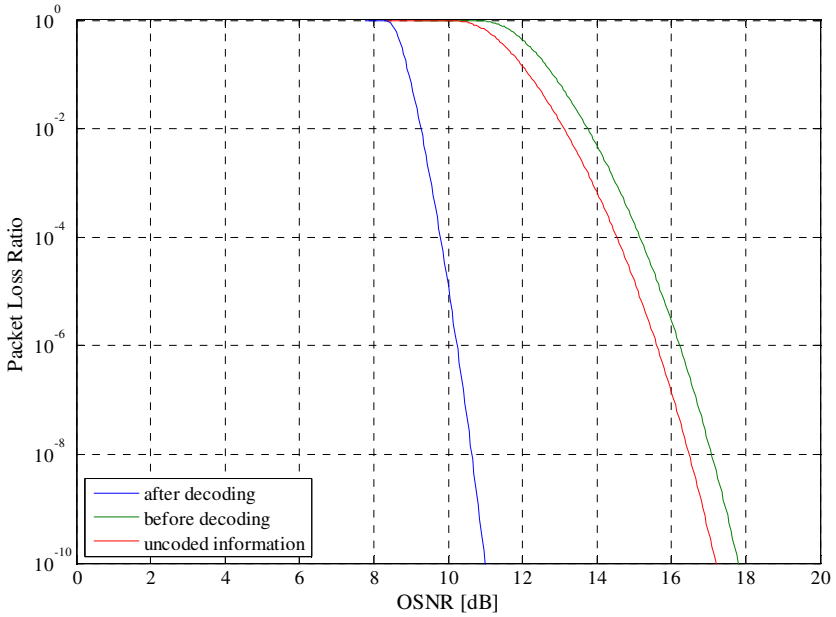

Figure 3.9 – PLR for RS(127,111), with correcting capability of 8.

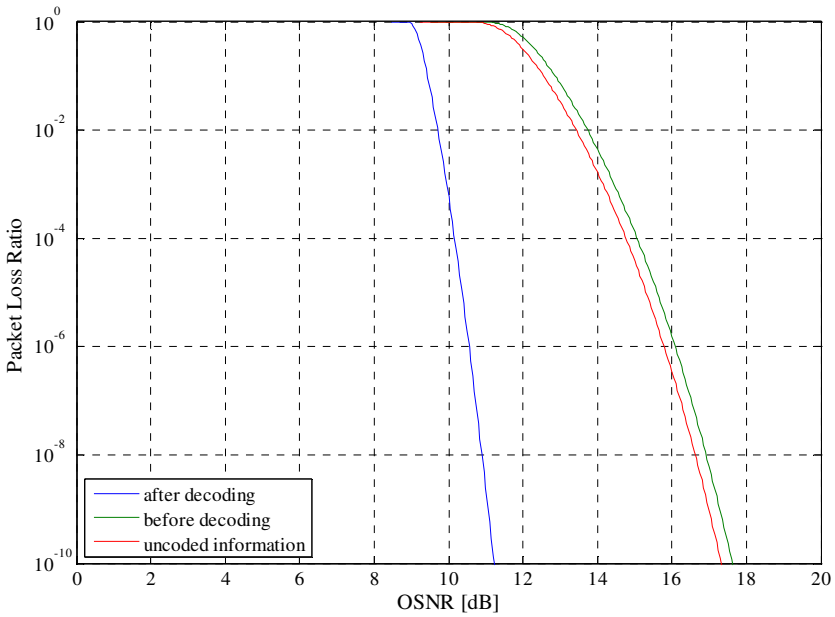

Figure 3.10 – PLR for RS(255,239), with correcting capability of 8.

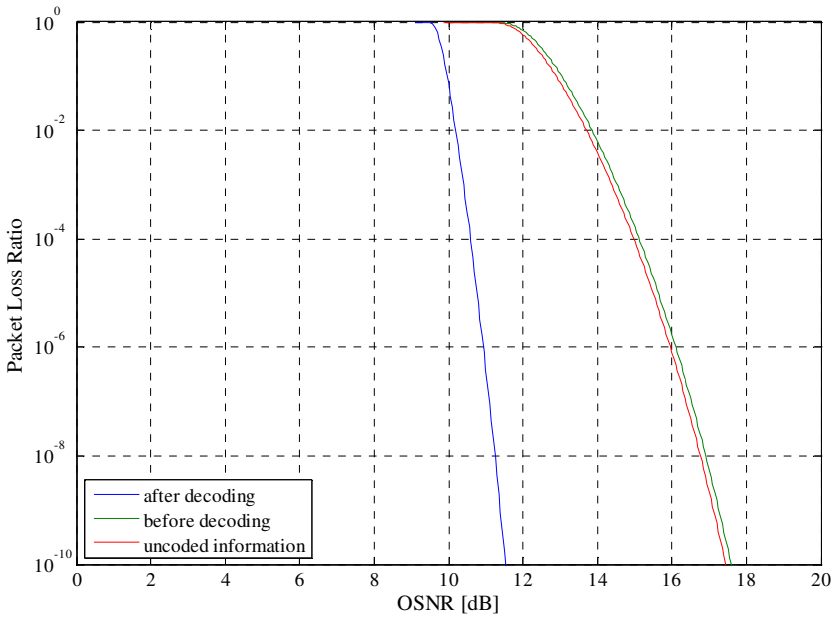

Figure 3.11 – PLR for RS(511,495), with correcting capability of 8.

After this analysis, and weighing all aspects that were addressed, the selection of a RS code with good correcting capabilities, both for random and burst errors, together with a relative low overhead, high NCG, and low encoder/decoder complexity, would be the most suitable choice. A good compromise between these aspects is achieved with the standardized RS(255,239). This code has an overhead around 6.7%, a NCG around 6 dB for PLR = 10^{-12}, and

a correcting capability of 8. Moreover, choosing an already standardized FEC code will augment the interoperability amongst different providers and will possibly result in lower cost encoders/decoders, since they will employ well developed and mature technologies. Also, it enables the use of the same code for upstream and downstream directions of the PON system.

3.4. Performance Enhancement in TDMA Systems using FEC Codes

The inclusion of FEC [Miz06] in the upstream direction of a PON operating at 10 Gbit/s will bring several benefits to the system, such as a less stringent OLT receiver sensitivity, despite the line rate increase due to FEC (if out of band FEC is employed). The validation of the selected code to be employed in the upstream of a 10 Gbit/s PON system is presented in this section. Simulations were performed, using a MATLAB-based tool specifically developed and validated for this work, to evaluate the upstream system performance for scenarios with and without FEC.

The following results were obtained considering the upstream transmission on a 10 Gbit/s EPON. The binary information signal was therefore generated according to the specifications for EPON frames [IEEE05], and coded using the RS(255,239), when applicable. The laser transmitter was modulated using the NRZ format at 10 Gbit/s and an extinction ratio of 6 dB was assumed. The frames emitted by each ONU were preceded by synchronization fields [IEEE05], intended to set the decision threshold and the sampling point at the burst-mode receiver in the OLT. All performance metrics were obtained for the frames payloads, which were composed by Pseudo-Random Binary Sequences (PRBS), with 2^9-1 bits.

Two different approaches were employed to verify the system performance: a semi-analytic approach that assumes a Gaussian approximation based on [RC01] and a Monte Carlo (MC) approach. Here, noise samples with a variance corresponding to the total system noise, namely the photodetector electrical noise and the laser noise, as presented in section 2.1 (when applicable), were added to the detected signal. The binary information is extracted from this resulting signal, and decoded afterwards. Error counting was performed for both sequences, before and after decoding. The OLT receiver was considered to have a sensitivity of -18 dBm at a BER of 10^{-12}, for an input signal with infinite extinction ratio, resulting in a power penalty of 3 dB for signals with an extinction ratio of 6 dB. Note that the propagated signals are residually affected by dispersion, since the spectral window specified for upstream operation (1310 nm) is near the zero-dispersion wavelength.

Figure 3.12 depicts the system performance in terms of PLR (logarithmic units), considering only the receiver electrical noise, since a typical PON system is not affected by optical noise, if the laser noise is neglected. The PLR calculation assumes the use of packets with a length of 255 bytes, to cope with the RS(255,239) code that is employed to perform FEC. Similarly to Figure 3.8 – Figure 3.11, the red curve represents the performance for an uncoded signal, the green curve the performance of a coded signal before decoding, and the blue curve represents the performance after decoding. Results obtained using semi-analytic and MC approaches show a general good agreement, validating both approaches. In the scenario illustrated in Figure 3.12, considering burst-mode operation and detection, and only electrical noise at the receiver, an improvement of more than 2.5 dB in the received power is achieved for a PLR = 10^{-6}. As expected, the coding loss due to the code overhead is very low, as confirmed by the small distance between red and green curves.

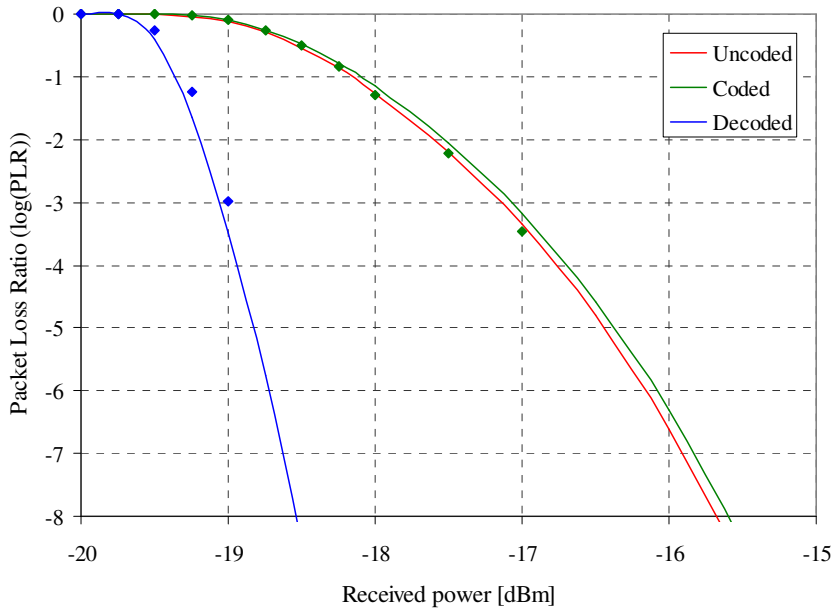

Figure 3.12 – 10 Gbit/s EPON upstream performance in terms of PLR, using semi-analytic (lines) and Monte Carlo (dots) approaches, and considering only the influence of electrical noise.

Besides the gain provided to the system when FEC is employed, another important benefit is the performance improvement achieved when MPN is present. This situation is verified when low-cost sources, typically multimode lasers, are used at the ONUs. In such scenario, the MPN characteristic of this type of lasers may affect the system performance strongly, and the use of FEC codes may be proven to be really important, since the SNR due

to MPN is independent of the signal power, as shown in section 2.1. Particularly, beyond the MPN floor, increasing the power will not increase the system performance. Therefore, upstream performance was evaluated once again using semi-analytic and MC approaches, and results for a 10 km network are depicted in Figure 3.13, considering, besides the receiver electrical noise, the influence of a moderate MPN with a coefficient of 0.5 (section 2.1), and the gain that is obtained by employing RS(255,239). A laser spectral width of 1 nm and a fibre dispersion of 1 ps/nm/km are assumed, since the PON upstream transmission uses the 1310 nm window, near the zero-dispersion wavelength of the fibre.

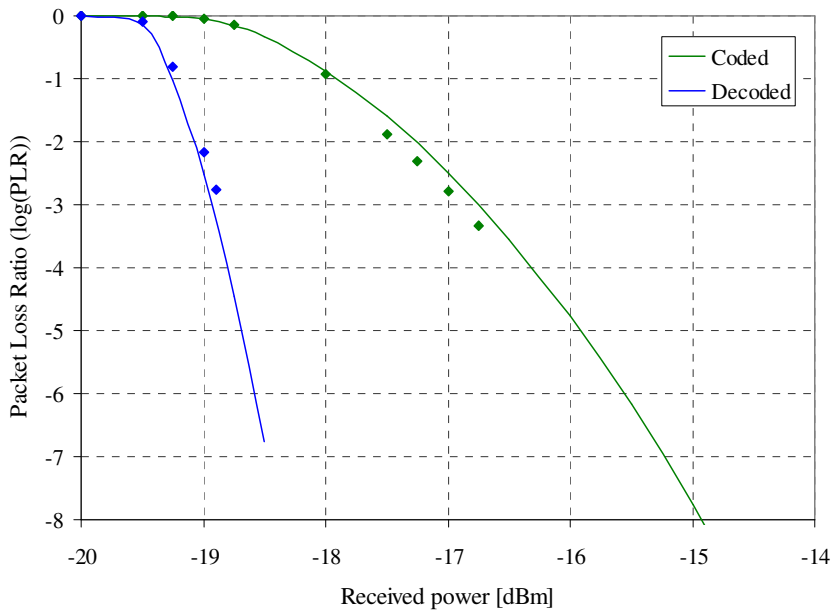

Figure 3.13 – 10 Gbit/s EPON upstream performance in terms of PLR, using semi-analytic (lines) and Monte Carlo (dots) approaches, and considering the influence of electrical noise and MPN (laser spectral width of 1 nm).

The results of Figure 3.13 show a gain in the received power of around 3 dB, for a PLR of 10^{-6}, which represents a significant improvement in terms of system performance. This may be translated in more users connected to the system or even larger network reaches. Moreover, it is an important achievement in MPN-limited systems, due to the MPN independence of the signal power level. In this type of systems, the use of FEC is the more effective solution to overcome the performance degradation due to the MPN.

Considering the same set of simulation parameters, but increasing the spectral width to 2 nm, which is a more typical value for commercial sources, the results of Figure 3.14 were obtained. Here, the results before decoding (green curve) show a very degraded system

performance, and an error floor due to the influence of MPN is visible. This error floor disappears with the inclusion of FEC, which improves significantly the performance of the system, as confirmed by the blue curve in Figure 3.14. Therefore, it may be concluded that the use of FEC in systems that are limited by MPN brings important benefits regarding those systems feasibility and performance.

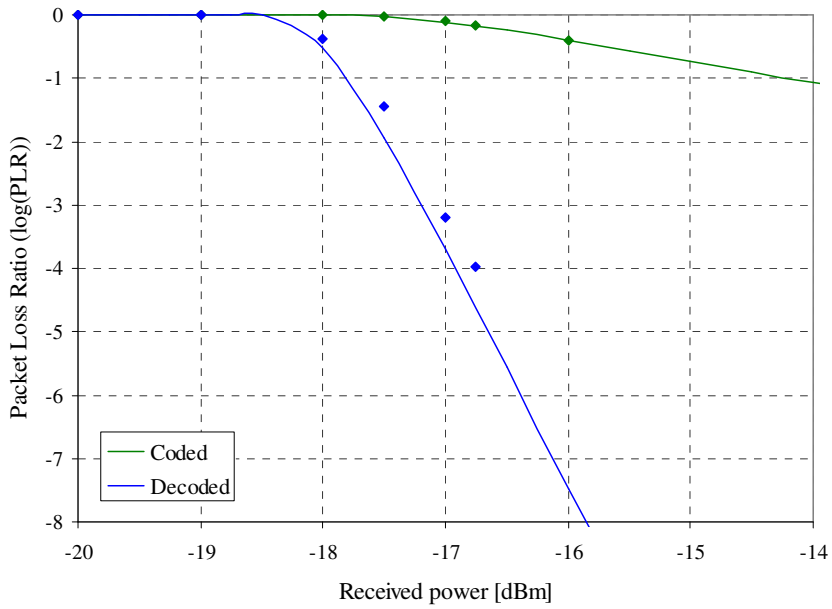

Figure 3.14 – 10 Gbit/s EPON upstream performance in terms of PLR, using semi-analytic (lines) and Monte Carlo (dots) approaches, and considering the influence of electrical noise and MPN (laser spectral width of 2 nm).

3.5. Conclusions

The inclusion of FEC codes in optical access network systems is becoming a real necessity, either for increasing the system capacity, regarding the number of online users, or for enabling network upgrades, especially those related with increased transmission rate.

Two classes of FEC codes were briefly addressed, and their advantages and disadvantages were identified, concerning their implementation in a 10 Gbit/s PON system. It was highlighted that RS block codes are the most suitable choice, due to their specific characteristics and maturity.

The performance of RS codes may be evaluated using several metrics. The most usual are the NCG, paying a special attention to the overhead that is added to the signal with FEC encoding,

and the error rate. When evaluating TDMA systems, the packet loss ratio should replace the simple bit error rate metric. Another important characteristic of a FEC code is its error burst correcting capability, which translates in a strong advantage of RS codes over other codes.

The described performance metrics of RS codes were used to obtain several comparative results that provide some guidelines about the characteristics and parameters that should be selected for a specific code to be employed in a given situation. These results show that, if the overhead is an important factor for the network, a code with longer codewords should be used, in order to obtain good results in terms of correcting capability. The NCG is an important metric, which does not depend directly on the overhead, and thus it is necessary to determine the overhead of a code to decide if it is suitable or not for the desired application. The length of the frames that are employed is important with respect to the complexity of the encoder and decoder. It is not crucial for the code performance, since the NCG does not suffer a significant change with the increase of the frame length. The error burst correcting capability is also an important characteristic of a code. The higher is the correcting capability of the code, the higher is the overhead, and therefore a trade-off between these two parameters should be found, based on the needs of each specific network scenario.

The upstream performance of a 10 Gbit/s PON was evaluated by simulation (semi-analytic and MC approaches), without FEC and employing the standardized RS(255,239) code. The inclusion of FEC was proven to be very advantageous in networks employing multimode laser sources, since it allows minimizing the penalty due to MPN. In these situations, since the SNR due to MPN is independent of the received power, FEC is proposed as a way to reduce the MPN-induced penalties. Significant improvements are attained using FEC, allowing for less stringent specifications for the most critical system parameters, which are the source spectral width and the fibre dispersion.

Chapter 4

BURST-MODE POWER EQUALIZATION

In all-optical WDM-based networks, a power level imbalance is commonly verified between signals travelling in different wavelengths. This occurs mainly due to different transmission paths and dynamic all-optical switching, with imperfect regeneration systems, which may introduce severe restrictions in the system, including instability and transparency limitations. Therefore, it is mandatory to introduce, in each network node, or at the receiver side, power management schemes that include the control of the amplifiers gain and the equalization of the power in each wavelength to a predefined level that should cope with the limited dynamic range of the receivers or the regenerators.

Power imbalance may also occur within the same wavelength in network systems that rely on optical packet- or optical burst-mode transmission. In a packet/burst switched scenario, the power level may vary from packet/burst to packet/burst, depending on the source of the packet/burst and on the transmission path. In these architectures, data are asynchronously transmitted from different locations and travel through different optical paths, resulting in significantly large optical power variations when reaching the receiver end. This fact increases the necessity for a fast equalization system in order to ensure the integrity of the receiving packet/burst, particularly the first incoming bits. Therefore, the burst-mode receivers used in these scenarios, both at intermediate or head-end nodes, need to handle asynchronous and unequal power level data streams accurately, ensuring an error free reception. This is accomplished by providing power equalization between the asynchronous

packets/bursts that reach the node, minimizing the input power variations and improving the dynamic range of the receiver.

The same considerations may be applied to access networks, namely to the upstream direction of PON systems, which uses TDMA, where transmission time slots are dynamically allocated to the ONUs, therefore resembling a burst-mode transmission. This was already a concern in the first generation of PON systems, but with the data rate increase this became a critical problem. Specifically, one of the main implementation issues of a 10 Gbit/s PON is the management of the burst-mode upstream transmission which demands, among other specific network elements, a fast and accurate burst-mode receiver to be placed at the OLT. This type of receiver differs from continuous-mode receivers mostly because they require an adaptive decision threshold for data regeneration, which depends on the power level of the received bursts. Besides, they must be able to perform dynamic clock recovery and phase alignment on a burst-by-burst basis [SCC97]. Overall, the cost of the OLT is increased due to the demanding specifications imposed on the high speed electronics required. This subsystem is essential to receive bursts from ONUs located at different distances from the OLT, since usually they reach the OLT receiver presenting different power levels. Typically, a PON system has an uneven network topology, i.e. a different power budget is obtained for each ONU, which forces the OLT burst-mode receiver to have a large input power dynamic range, in order to cope with all possible incoming power levels. In the first generation of PON systems, particularly EPON systems, this near-far problem has been solved using complex electronic circuits at the receiver side and/or transmitter side, as proposed in [PLJ04], where the possibility of informing the ONUs to adjust their output power was addressed, although not standardized under the 1 Gbit/s EPON standard [IEEE04], as was for GPON [ITU01].

As referred above, a burst-mode receiver may become less complex, featuring a reduced dynamic range, if optical power equalization is employed before the receiver. This chapter is therefore dedicated to burst-mode equalization schemes. A brief overview of different equalization schemes proposed in the literature is presented in section 4.1, emphasizing their advantages and disadvantages for optical access networks. Section 4.2 presents a proposal for a simple all-optical burst-mode power equalization scheme based on a cascade of two Semiconductor Optical Amplifiers (SOAs). The envisioned network applications for the proposed equalization scheme are addressed in section 4.3, where access and metro-access scenarios are considered, and the benefits brought by the use of this power equalizer are analyzed.

4.1. Overview of Power Equalization Schemes

The benefits of employing power equalization are clearly relevant in the network scenarios mentioned above, allowing to approach a burst-mode reception to that used in continuous mode transmission systems. For these different scenarios, several power equalization schemes were proposed in the literature along the years, using diverse technologies [Tom03].

A commonly used technology for optical power equalization is the Erbium-Doped Fibre Amplifier (EDFAs), proposed both for single channel systems [Zir92] and for WDM systems [NKL+99], [TF02]. Typically, in such systems, the power equalization is achieved by driving the amplifier into the gain saturation region, where lower input powers experience a larger gain and higher input powers experience a lower gain.

Alternatively, the use of SOAs as power equalizers was proposed for optical packet/burst switching systems [CSZE01], [TCT05], benefiting from the fast equalization that they provide, when compared to EDFAs. Moreover, SOAs were also used in power equalizing schemes for all-optical WDM networks [FZZ+99], integrating a power management solution for this type of networks. In metro-access networks, SOAs were proposed within an adaptive equalization scheme, where a fast control of the SOA driving current is employed [CYC+09]. Access networks may also benefit from using power equalization schemes, as shown in [Soe00]. When considering the use of SOAs for power equalization, different concepts were proposed, such as the use of polarization rotation [GPNL05], the use of controlled gain-clamped SOAs, or by employing electronics to control the gain of the SOAs [WSL+04].

Other applications for power equalization include optical buffering loops [LWF+07], wavelength conversion [DHS+98] and optical burst-mode regenerators [WSL+04], [SIS+05], [KPP+07]. The optical regenerator proposed in [KPP+07] is based on a single hybrid integrated SOA-based Mach-Zehnder Interferometer (MZI-SOA) with unequal splitting ratio couplers, configured to operate as a self-switch. This unbalanced MZI-SOA structure exploits the non-linear transfer function of the MZI to suppress the noise level of ‘0’ bits and also exploits the gain dynamics of the SOAs, which are placed in the upper and lower arms of the MZI, to achieve power equalization.

Although presenting some disadvantages to be employed in access networks, due to their excessive complexity and cost or due to the requirement of external controls, three of the

power equalization concepts proposed in the literature were selected as illustrative examples, and are briefly addressed in the following.

The first power equalization method, proposed in [Zir92], illustrates the use of EDFAs. This scheme was proposed earlier and is based on the exploitation of the saturation regime of the EDFA. The proposed concept consists of dividing the input signal and injecting it forward and backward into the EDFA. Both forward and backward signal parts cause the gain saturation in the amplifier, but only the forward signal part contributes to the output. The backward input signal is attenuated in a saturable loss, before entering the EDFA, leading to a non-proportional power increase when compared to the total input signal. On the other side, the forward signal power level is strictly proportional to the total input signal, and therefore, the EDFA gain saturation caused by the backward signal compensates for the forward signal, and consequently, the output signal power level will drop. Using this concept, the gain of the EDFA will be close to the small signal gain or close to unity, for weak or very strong input signals, respectively. In spite of its clear benefits in terms of power equalization and dynamic range improvement, the use of a scheme based on EDFAs is less suitable for being applied in access networks, mainly in the upstream direction where TDMA systems are operated using the 1310 nm spectral window, due to its relatively high cost and its characteristic operation on the 1550 nm window.

The second illustrative power equalization scheme exploits electronics to control the gain of SOAs [WSL+04]. This scheme is proposed as a fundamental component of a 3R regeneration device, where power equalization is mandatory, and it comprises a SOA in the saturation regime assisted by control electronics to increase the dynamic range. The incoming signal is split and a part is tapped to the control electronics, whereas the remaining is launched through a fibre delay line into the SOA in the saturation regime. The control electronic is responsible for tracking the power of the incoming optical packets, enabling to control the output power of a laser that is used as a probe signal for the SOA, which operates under Cross-Gain Modulation (XGM) regime, and thereby equalizing the incoming signal level. Besides operating steadily in the 1310 nm spectral window, SOAs are a more economical solution when compared to EDFAs, and therefore preferred to be used in access networks. However, the use of complex external circuits should be avoided in order to keep the end-nodes of an access network as simple as possible.

Since it is an important application for power equalizers, the third illustrative equalization method is also intended to be incorporated in all-optical burst mode

reception/regeneration [KPP+07]. This method comprises a SOA-based MZI switch configuration, consisting of an input and an output coupler, and of two optical branches, each one employing a SOA as the nonlinear active element. This configuration uses unbalanced coupling ratios and the two SOAs have different unsaturated gains. Since the MZI-SOA is also operated in saturation, the SOAs exhibit different gains for weak and strong bursts, thereby equalizing the incoming signals. Additionally, the different saturated gains of the SOAs also induce a differential phase shift between the signals travelling through the two arms of the MZI-SOA, leading to the interference between these signals at the MZI-SOA output. The combination of these features, together with the use of a CW counter-propagating beam for adjusting the gain level of the SOAs, results in a power equalized output burst, without increasing the noise level. This is an all-optical method, which does not require additional electronics, and therefore could be a good candidate for access networks. However, the high cost of MZI-SOAs may be prohibitive for such application.

4.2. All-Optical Burst-Mode Power Equalization

As previously referred, it is important to guarantee that a burst-mode receiver does not incur in high complexity. This can be attained by employing optical power equalization before the receiver, thereby balancing the power of the incoming bursts and consequently reducing the necessary dynamic range.

From the discussion above, the use of SOAs as power equalizers seems to be suitable for access networks, with special emphasis on high data rate systems operating at 10 Gbit/s. They are less expensive than other types of amplifiers and operate steadily in the spectral window typically specified for the upstream operation of a TDMA PON system (1310 nm), such as EPON or GPON, coping with the low cost and low complexity requirements of such networks. Besides providing equalization, the use of SOAs is also suited for high density networks, since gain is provided to the system, thereby compensating the high losses due to larger splitting ratios.

In this context, a simple all-optical power equalization scheme based on two SOAs was proposed, and it is described in the following. In this scheme, the first SOA acts as a gain stage and the second SOA operates in the saturation region.

4.2.1. Fundamentals of power equalization using SOAs

The main concept behind all-optical power equalization, employing optical amplifiers, is the Self Gain Modulation (SGM) effect, which causes higher input powers to experience lower gains due to amplifier saturation [FZZ+99], [Zir92]. The saturation occurs for relatively high input powers and, therefore, it is necessary to guarantee a power level at the amplifier input large enough to drive it into saturation.

Typical applications that exploit SGM in SOAs require the gain recovery time to be close to or smaller than the bit time [CSZE01], [TCT05]. In these applications, the zeros experience a larger gain than the ones and bit by bit equalization is obtained. However, a bit by bit power equalization results in signal distortion and degradation of the Extinction Ratio (ER), which is undesirable for the proposed equalizer. Since this scheme is intended to be applied for burst-mode power equalization, it should be guaranteed that the equalizer operates over the entire burst. This is achieved by designing the equalization stage to have a slow recovery time in order to respond to the average input power instead of the instantaneous signal power. In this way, bursts received from different locations, and therefore presenting different power levels, may be effectively equalized, which also leads to a smaller degradation of the output ER.

Further insight of the above mentioned feature is attained by analysing the equations that characterize the behaviour of a SOA. The selected model is based on [CSM00], which considers physical processes like Spectral Hole Burning (SHB), Carrier Heating (CH) and Carrier Density Depletion (CDD). The nonlinear processes slower than SHB, such as the Kerr effect and two photons absorption, are neglected in this model because their effect becomes significant only for few picosecond and sub-picosecond pulses. The dynamics of the intensity and phase of the propagating field within the amplifier waveguide depend on both time and distance along the propagation axis of the waveguide. An exact analytical integration [CSM00] along the longitudinal coordinate over the entire device length permits to reduce this two-dimensional problem to a set of Ordinary Differential Equations (ODE) in which time is the only independent variable. With this approach, the SOA is described by its impulse response, which is rigorously calculated including both the longitudinal variation and the temporal evolution of the field, yet avoiding the need to explicitly calculate the field inside the device. Therefore, the ODE set that describes the SOA behaviour by using its input-output relation is given by [CSM00]:

$$\frac{dh_N}{dt} = -\frac{h_N}{\tau_S} - \frac{1}{P_S \tau_S}\left[G(t)-1\right]P_{in}(t) + \frac{g_0}{\tau_S}; \tag{4.1}$$

$$\frac{dh_{SHB}}{dt} = -\frac{h_{SHB}}{\tau_1} - \frac{\varepsilon_{SHB}}{\tau_1}\left[G(t)-1\right]P_{in}(t) - \frac{dh_{CH}}{dt} - \frac{dh_N}{dt}; \tag{4.2}$$

$$\frac{dh_{CH}}{dt} = -\frac{h_{CH}}{\tau_H} - \frac{\varepsilon_{CH}}{\tau_H}\left[G(t)-1\right]P_{in}(t). \tag{4.3}$$

Here, h_N, h_{SHB} and h_{CH} represent the contributions to the overall gain of CDD, SHB and CH, respectively, whereas the nonlinear gain suppression factors due to CH and SHB are represented by ε_{CH} and ε_{SHB}. The optical power at the SOA input is represented by $P_{in}(t)$, and P_S is the saturation power for small-signals. g_0 represents the unsaturated gain of the device, which in linear units is given by $G_0 = \exp(g_0)$ and is also designated by gain for small-signals. The carrier lifetime is given by τ_S, τ_1 is the carrier-carrier scattering time, and τ_h is the temperature relaxation time. The overall gain is given by:

$$G(t) = \exp\left(h_N + h_{SHB} + h_{CH}\right). \tag{4.4}$$

The optical power at the output of the SOA is given by:

$$P_{out}(t) = G(t) \times P_{in}(t). \tag{4.5}$$

The solution obtained for this ODE set represents the field at the output of an ideal device. The description of a real device requires the inclusion of Amplified Spontaneous Emission (ASE), which is taken into account by adding an additional noise term at the receiver [RC01], [Agr02], and of the waveguide internal loss, which was assumed to be very low and therefore was neglected.

Considering the stationary state behaviour and manipulating the equations presented above, the SOA output saturation power is found to be given by [Pat06]:

$$P_{sat} = \frac{\ln 2}{\left(\frac{1}{P_S} + \varepsilon_{SHB} + \varepsilon_{CH}\right)\left(\frac{G_0}{2} - 1\right)}. \tag{4.6}$$

As verified by equation (4.6), the saturation power does not depend on the carrier lifetime, carrier-carrier scattering time or temperature relaxation time, depending uniquely on the intrinsic device gain and gain suppression factors.

The characterization of a single SOA is presented in the following. Using the parameters indicated in [CSM00], and considering an unsaturated gain of 22 dB, the curve presented in Figure 4.1 was obtained for the SOA gain dynamics, considering at the input of the SOA a CW signal and NRZ modulated signals with extinction ratios of 6 dB and 30 dB. As expected, the overlapping of the curves in Figure 4.1 shows that, using a modulated signal at the input of the SOA, the same gain values are attained, for an average input power of the modulated signal equal to the CW laser power. Moreover, by varying the SOA recovery time, through the increase of the carrier lifetime, no significant influence is verified in the device gain. The modulated signal consists on a PRBS, with 2^9-1 bits, modulated with NRZ format at 10 Gbit/s, with an extinction ration of 6 dB or 30 dB. The saturation power is also indicated in Figure 4.1, corresponding to a P_S parameter of around 0.015.

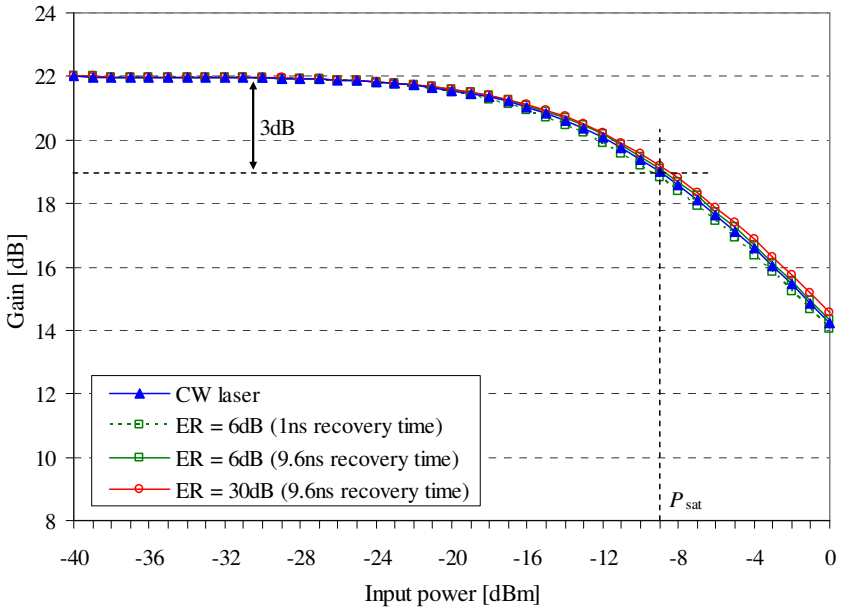

Figure 4.1 – SOA gain dynamics.

Considering now only 10 Gbit/s modulated signals, with input extinction ratio of 6 dB and 30 dB, the influence of the SOA recovery time on the signals extinction ratio at the output of the SOA was evaluated. Figure 4.2 presents the output extinction ratio penalty, as a function of the SOA recovery time, for different average powers at the input of the SOA. This penalty is presented as normalized by the maximum obtained for each recovery time. For both

input extinction ratio values, the power penalty decreases when increasing the SOA recovery time, always reaching a penalty floor. For an input extinction ratio of 30dB, this floor is reached for faster recovery times than for 6 dB input extinction ratio. This means that it is possible to improve the output ER by using SOA recovery times slower than 1 ns (time to transmit 10 bits at 10 Gbit/s), for signals with input ER of 30 dB, and slower than 2.4 ns (time to transmit 24 bits at 10 Gbit/s), for signals with input ER of 6 dB. Because it is a more realistic value for commercial optical sources, besides presenting a worst case condition when analysing the output ER, an input ER of 6 dB will be considered in the following.

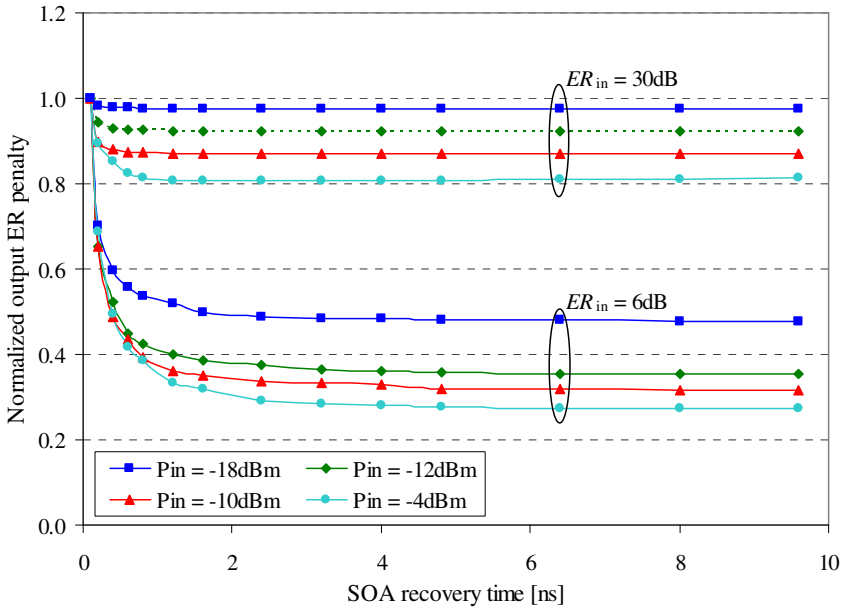

Figure 4.2 – Normalized extinction ratio at SOA output.

The results presented in Figure 4.3 show the output ER penalty, considering an input ER of 6 dB, as a function of the SOA recovery time and of the average power at the input of the SOA. As clearly visible, the ER penalty is more significant for higher input powers, where the SOA is operating near or already in the saturation regime. For these power levels, the penalty is much higher for faster SOA recovery times, which proves the benefits of using slower recovery times for SOAs that are intended to operate in the saturation regime, such as those used in burst-mode power equalizers.

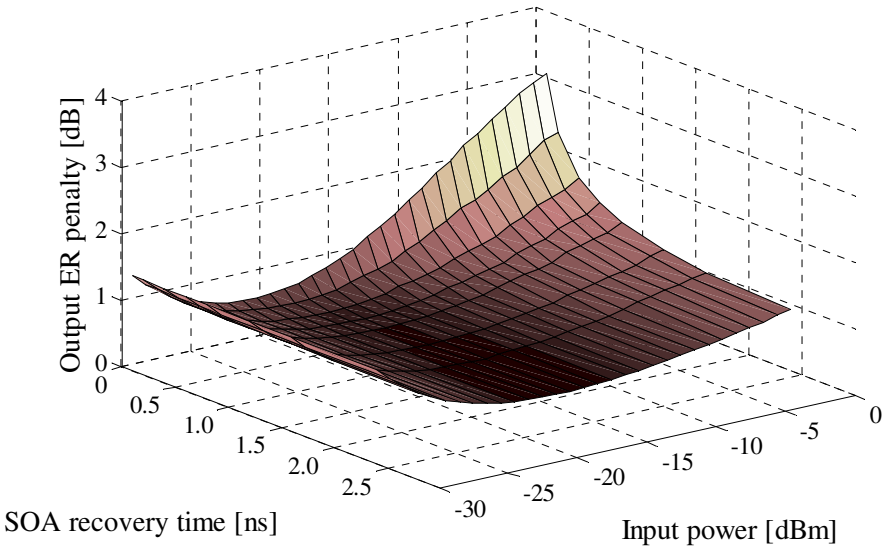

Figure 4.3 – Output ER penalty.

Just as an illustrative example, Figure 4.4 and Figure 4.5 present a signal with 6 dB extinction ratio, after passing through the SOA, for fast (1 ns) and slow (9.6 ns) recovery times, respectively. The average input power of this signal is -4 dBm (within the SOA saturation region). As shown in Figure 4.4 and Figure 4.5, the overshoots and undershoots verified in the SOA output signal when a fast recovery time (Figure 4.4) is considered are minimized (or even eliminated) when the recovery time becomes slower (Figure 4.5). In this situation, the signal is significantly equalized, presenting similar values for the zeros and ones levels, after the recovery time. This design issue is further discussed in the following sub-section.

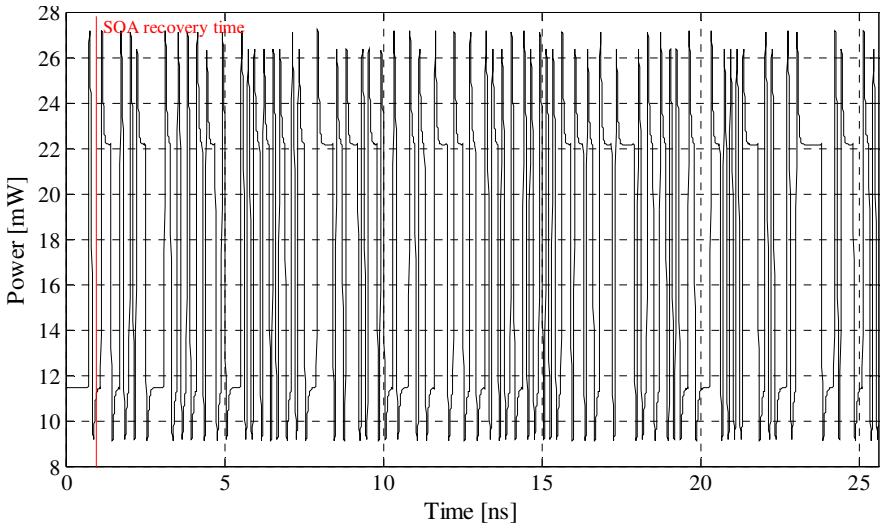

Figure 4.4 – SOA output signal for 1 ns recovery time.

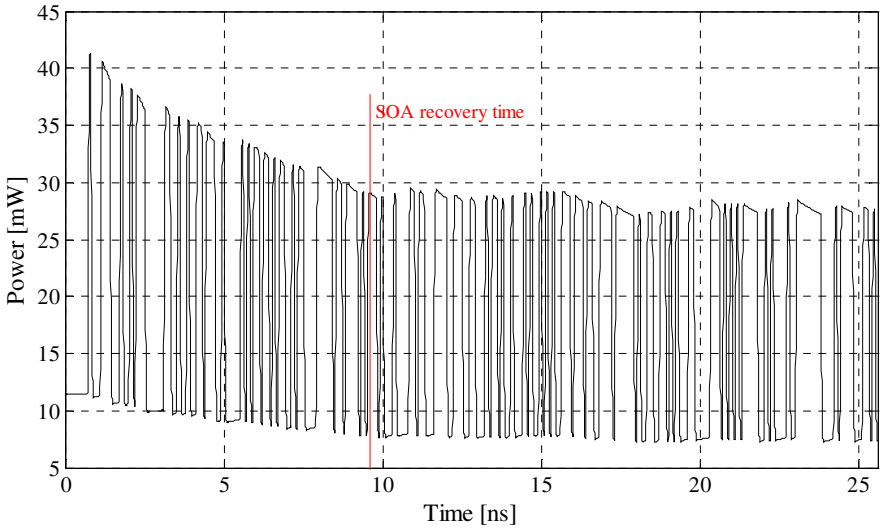

Figure 4.5 – SOA output signal for 9.6 ns recovery time.

4.2.2. Cascaded-SOAs Power Equalizer

As previously referred, the main concept behind all-optical power equalization is the exploitation of the amplifier saturation regime. However, in order to guarantee the operation of the amplifier in this regime, it is necessary that the input power level is large enough to drive the amplifier into the saturation. Because this occurs typically for a range of relatively high power levels, if the input signal has low power it will not be able to cause the saturation of the amplifier, and thus it will not be equalized.

In access or metro-access networks the power that reaches the receiver end or the interconnection nodes is commonly very low, due to the splitting losses experienced by the signals coming from different end-users. Therefore, in order to guarantee that the equalization scheme operates steadily in the saturation, another SOA is employed to increase the incoming power levels. Thus, the proposed cascaded-SOAs equalization scheme, depicted in Figure 4.6, is constituted by a first SOA, which acts uniquely as a gain stage, before a second SOA that acts as the equalization stage. In order to prevent damaging the photodetector due to the high output powers, an attenuator is placed after the equalizer. As presented in Figure 4.6, it is expected that the bursts at the input of the equalization scheme experience a gain g when passing through the gain-SOA and experience power equalization when passing through the saturated-SOA, thereby reaching the output of the equalizer with identical power levels.

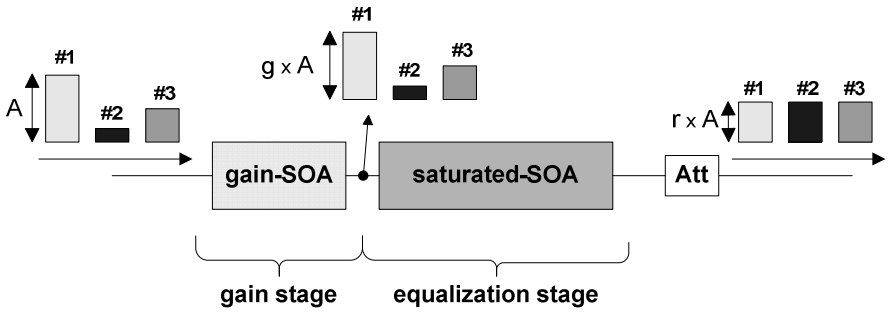

Figure 4.6 – Two-stage equalization scheme.

To guarantee that bursts received from different locations are effectively equalized, the SOA at the equalization stage should respond to the average input power of the received burst, instead of the instantaneous power, leading to a smaller degradation of the ER. Therefore, it is necessary to assess the rules that should be used when designing the equalization scheme. These rules only apply to the saturated-SOA, since the gain-SOA acts in the gain linear regime. Moreover, this design is tailored for burst-mode EPON upstream systems, where the bursts are formed by Ethernet frames preceded by idle fields that allow for laser turn-on time and stabilization [IEEE04], as presented in the schematic diagram of Figure 4.7. Here T_{on} represents the laser turn-on time, T_{rx} represents the time for receiver setting, T_{cdr} represents the time for clock locking and data recovery, T_{cga} represents the time for aligning the code gain and T_{off} represents the laser turn-off time. The design rules can be easily extrapolated for any other system, as long as overhead idle fields are considered.

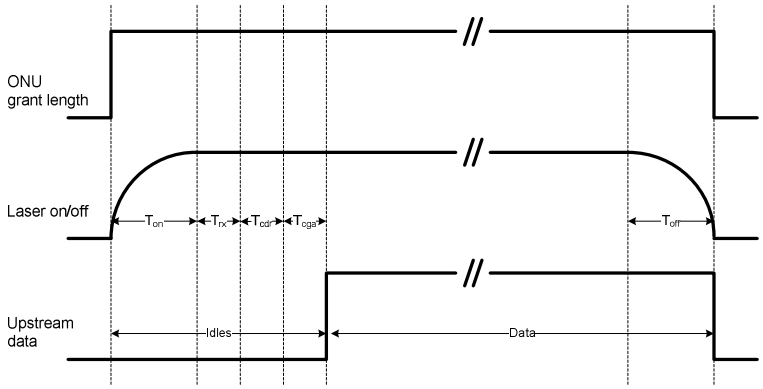

Figure 4.7 – ONU upstream time slot in an EPON system [IEEE04].

As explained before, the saturated-SOA should have a slow recovery time. The first rule must guarantee that this recovery time should be lower that the overhead field duration,

thereby allowing for the saturated-SOA to saturate before the synchronization fields. This situation is illustrated in Figure 4.8, where the transmission of a high power burst following a very low power burst is represented, with an extinction ratio of 6 dB. These bursts were generated in accordance with the fields specified for EPON frames, as shown in Figure 4.7, and a data rate of 10 Gbit/s was assumed for their transmission. The input signal powers represent the signals at the entrance of the power equalization scheme, and a recovery time of 9.6 ns, corresponding to 96 bits at 10 Gbit/s, was assumed for the saturated-SOA, whereas the gain-SOA was assumed to have a recovery time equal to the bit duration at 10 Gbit/s (0.1 ns). After experiencing the equalization effect (bottom plot in Figure 4.8) the power of both bursts is more balanced, and the stabilization of the gain occurs before the synchronization fields. As a consequence, the decision threshold and sampling point will not be affected by the SOA gain recovery. Furthermore, since the saturated-SOA must reach the steady state gain within the overhead field duration, the proposed equalization scheme does not impose a lower limit on the guard time between bursts coming from different ONUs.

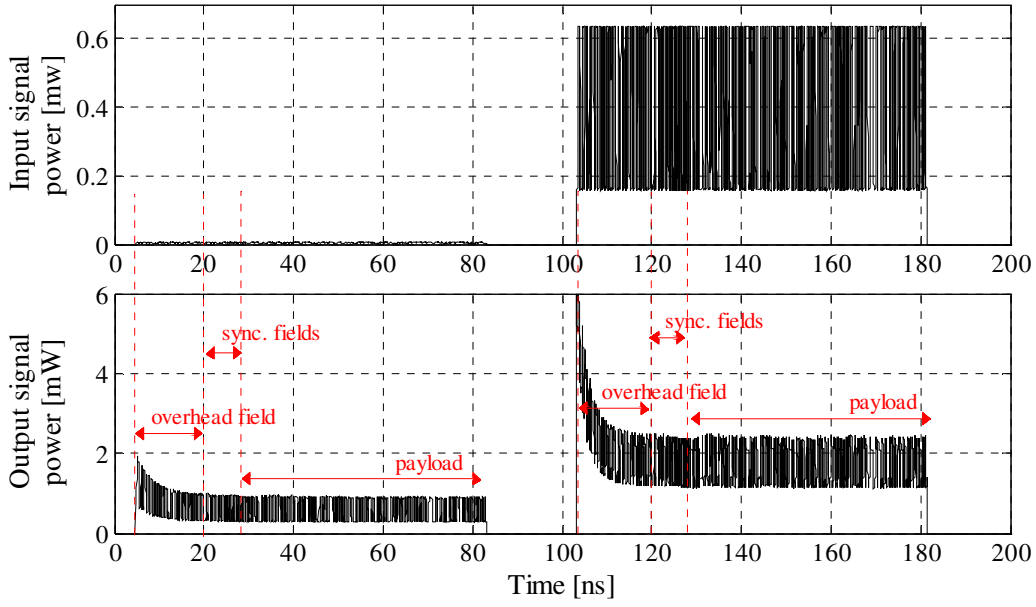

Figure 4.8 – Input (top) and equalized (bottom) bursts. The leftmost and rightmost bursts have average input powers of -23 and -4 dBm, respectively.

Secondly, in order to avoid the change of the saturated-SOA gain within the payload, which would deteriorate the data information bits, the recovery time should be higher than the duration of the longest sequence of consecutive zeros or ones being transmitted. To quantify this effect, simulations were performed assuming a saturated-SOA recovery time of 9.6 ns. It

was found that, when the payload of the frames was increased from 2^9-1 to 2^{13}-1 PRBS, lower additional Eye Opening Penalties (EOPs) were obtained. As an illustrative example, for bursts with average input signal powers of -23, -10 and -4 dBm, additional EOPs of 0.4, 0.3 and 0.2 dB were obtained, respectively. Due to the use of 64b/66b line coding in 10 Gbit/s EPON systems, a maximum number of 65 consecutive zeros or ones is foreseen to occur, in a worst case scenario. For such case, considering a payload carrying 65 zeros followed by 65 ones and comparing it to a 2^9-1 PRBS payload, additional EOP of 1.7, 1.2 and 0.7 dB were obtained for the same set of burst average input signal powers of -23, -10 and -4 dBm, respectively.

4.3. Network Applications

The power equalization benefits of the proposed scheme are accessed in this section, considering its use in practical implementation scenarios. Firstly, high data rate access networks based on PON systems are selected as the primary application. Secondly, the use of the proposed equalization scheme in metro access networks, that interconnect multiple PON segments, is evaluated.

4.3.1. Access Network

The use of the proposed equalization scheme in access networks is evaluated for the upstream direction of a 10 Gbit/s EPON systems, supporting 64 or 128 ONUs in an uneven topology, according to the prospects for these next generation systems.

An uneven topology is designated as such because it should support ONUs close to the OLT as well as distant ONUs, considered to be located at a maximum distance of 20 km. Therefore, to comply with these requirements, a first PSC should be located near the OLT, or even within the OLT, in a worst case scenario. This PSC connects directly (no fibre span) to at least one nearby ONU. The farthest ONU (at 20 km distance) is connected to the first PSC either directly or by using a cascade of PSCs. In a network with N ONUs, the first PSC is assumed to split the incoming power into N, $N/2$ or $N/4$.

As represented by the simplified diagrams in Figure 4.9, two different locations for the first PSC are considered: firstly, topology A, where the first PSC is located at 5 km from the OLT and secondly, topology B, where the PSC is located close to the OLT.

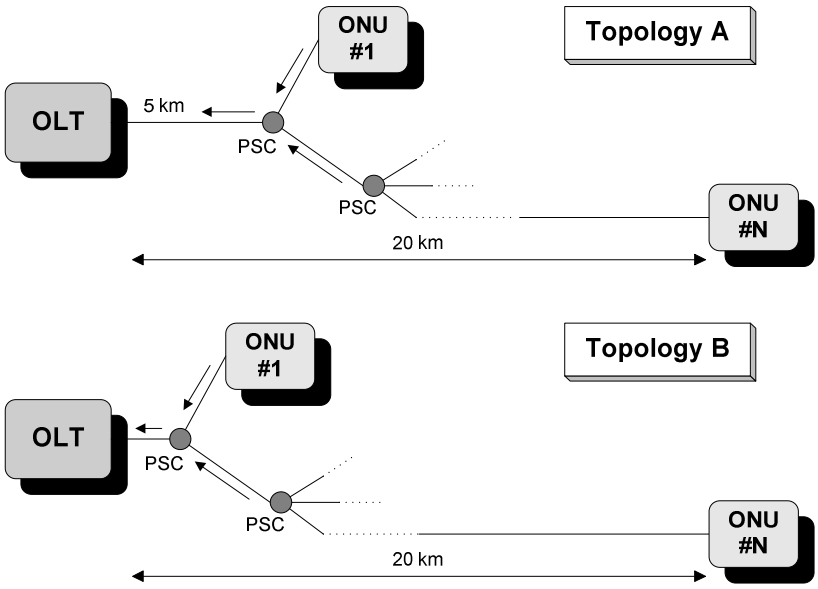

Figure 4.9 – Simplified diagrams of the uneven topologies under analysis.

Considering a fibre attenuation of 0.2 dB/km, and neglecting losses in splices and connectors, as well as the excess loss of the PSCs, the differences in the losses experienced by the signals emitted from the nearest and the farthest ONUs are presented in Table 4.1, for both topologies of Figure 4.9. It is shown that the equalization scheme should be able to equalize a maximum power range of 18 dB and 19 dB, for networks with 64 ONUs, in topology A and topology B, respectively, and 21 dB and 22 dB, for networks with 128 ONUs, in topology A and topology B, respectively. Based on these values, it is clear that topology B is the most stringent scenario for the dynamic range of the burst-mode receiver, when a first 1×2 PSC is employed. This worst case network configuration represents the basis for the following discussion.

Table 4.1 Loss differences experienced by nearest and farthest ONUs.

	Topology A		**Topology B**	
	$N = 64$	$N = 128$	$N = 64$	$N = 128$
1^{st} PSC $1 \times N$	3 dB	3 dB	4 dB	4 dB
1^{st} PSC 1×4	15 dB	18 dB	16 dB	19 dB
1^{st} PSC 1×2	18 dB	21 dB	19 dB	22 dB

In a high density 10 Gbit/s EPON with uneven topology, the lowest power reaching the OLT must be assessed, since it determines the system performance. Therefore, Table 4.2 summarizes the power loss experienced by the burst coming from the farthest ONUs, and the

corresponding received powers (P_{rx}), for low and high values of the ONU emitted power (P_{tx}), considered to be -1 dBm and 4 dBm, respectively.

Table 4.2 Power loss experienced by the bursts coming from farthest ONU.

	P_{tx} = -1 dBm		P_{tx} = 4 dBm	
	N = 64	N = 128	N = 64	N = 128
Power loss	22 dB	25 dB	22 dB	25 dB
P_{rx}	-23 dBm	-26 dBm	-18 dBm	-21 dBm

The simulation layout is based on the diagram presented in Figure 4.6. For simulation purposes, both SOAs in this equalization scheme were modeled using the approach presented in [CSM00]. The gain-SOA and the saturated-SOA were characterized by small signal gains of 25 dB and 22 dB and saturation output powers of 12 dBm and 10 dBm, respectively. A noise figure of 6 dB was assumed for both SOAs. The binary signal was formatted according to the specifications of EPON frames [IEEE04], and the laser transmitter was modulated using the NRZ format at 10 Gbit/s. An input extinction ratio of 6 dB was assumed. As explained in sub-section 4.2.2, the frames emitted by each ONU are preceded by an overhead field and by synchronization fields for receiver settling and clock recovery. The latter are used to set the decision threshold and the sampling point. All performance metrics were obtained for the frames payloads with 2^9-1 PRBS, except stated otherwise. A 30 nm simulation window was considered, and the ASE noise generated by the equalization scheme was modeled as additive white Gaussian noise. The BER was calculated using a semi-analytic method based in [RC01], where both ASE and receiver electrical noise are accounted for. For a BER of 10^{-12}, the photodetector sensitivity was assumed to be -18 dBm and -15 dBm, considering signals at its input with infinite and 6 dB ER, respectively. Hereafter all indicated input powers are measured at the input of the power equalization scheme.

Figure 4.10 shows the equalizer output signal power after the attenuator (refer to Figure 4.6), normalized by the lowest output signal power, as a function of the input power, illustrating its overall equalization capability. It is shown that the input power range of 19 dB is reduced to 4.7 dB at the equalizer output, in a network with 64 ONUs. Considering 128 ONUs, the 22 dB input power range is reduced to 5.8 dB at the output, enabling a reduction of 16.2 dB in the dynamic range of the OLT receiver.

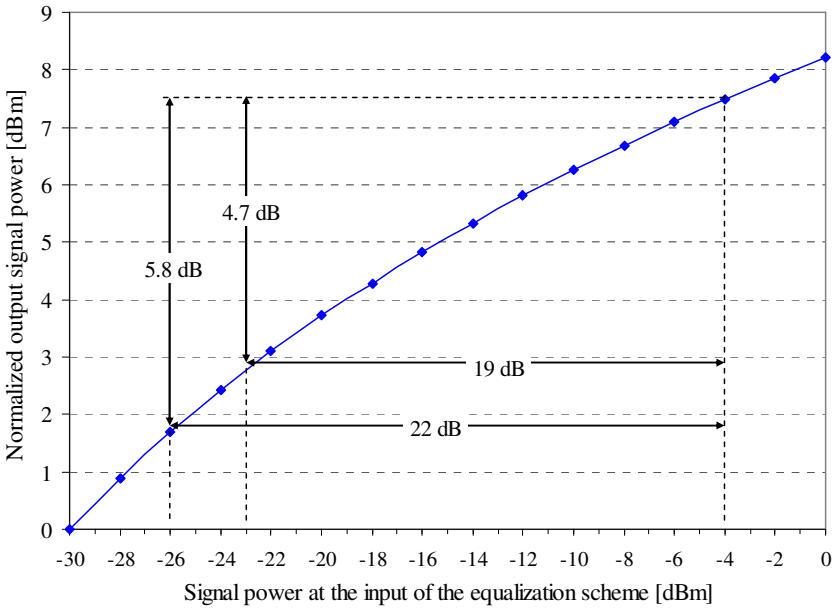

Figure 4.10 – Normalized output signal power, as a function of the signal power at the input of the equalizer scheme.

In spite of the significant equalization capabilities, this equalization scheme has some restrictions concerning the output ER, mainly when fast recovery times are considered, as previously explained. Figure 4.11 depicts the output extinction ratio penalty, as a function of the saturated-SOA recovery time, for different input signal power levels (P_{rx}). The gain-SOA is assumed to have a recovery time equal to the bit duration at 10 Gbit/s (0.1 ns).

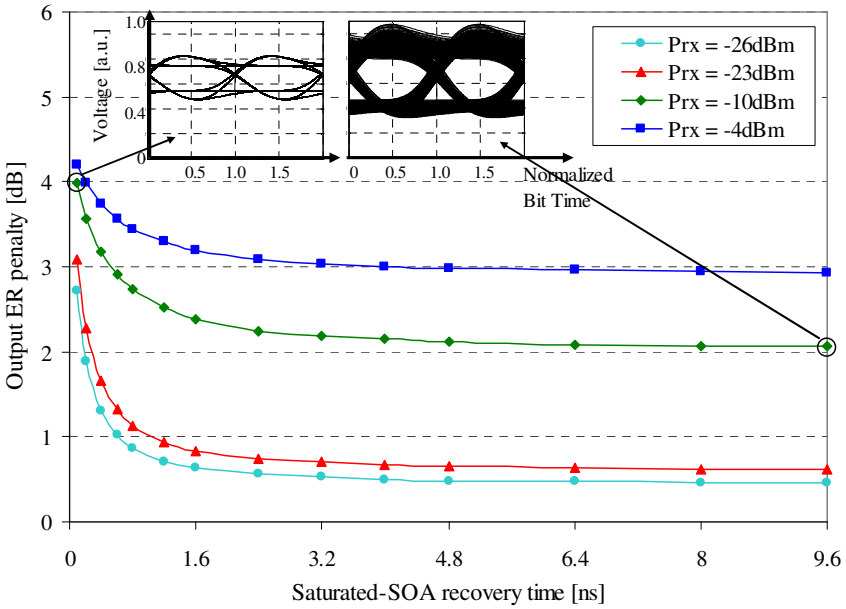

Figure 4.11 – Output ER penalty as a function of the saturated-SOA recovery time, for different signal powers at the input of the equalization scheme.

As expected, the results in Figure 4.11 show a higher ER penalty for smaller recovery times and a lower and nearly constant ER penalty for saturated-SOA recovery times above 1.6 ns. Identical results were also verified in Figure 4.2 for the case of a single SOA characterization. Moreover, higher ER penalties are obtained for higher input signal powers. Eye-diagrams for the payload information considering the faster (0.1 ns) and the slower (9.6 ns) recovery times of the saturated-SOA are depicted in the insets of Figure 4.11, for an input power of -10 dBm. These eye-diagrams confirm that a higher output ER is obtained for the slower recovery time, also clearly showing a larger eye-opening.

In spite of the extinction ratio degradation for fast recovery times, the system is able to show good overall performance mainly due to the gain provided by the proposed equalizer. Therefore, to evaluate the overall system performance, the BER as a function of the signal power at the input of the equalizer scheme is depicted in Figure 4.12, for different recovery times of the saturated-SOA. Once again, the gain-SOA is considered to have a fast recovery time, equal to 0.1 ns.

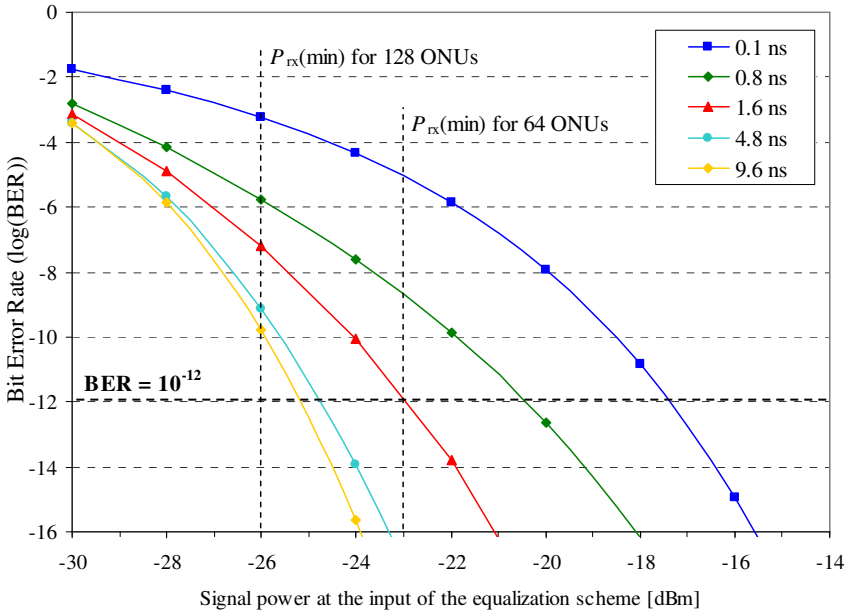

Figure 4.12 – System performance for several recovery times of the saturated-SOA.

Figure 4.12 shows that in a scenario where a fast recovery time (0.1 ns) is employed for the saturated-SOA, a target BER of 10^{-12} is not attained for input signal powers below -18 dBm, independently of the number of ONUs (64 or 128) supported by the network. Identical conclusion is obtained when a saturated-SOA recovery time of 0.8 ns is employed,

since a BER of 10^{-12} is only obtained for received signal powers higher than around -20 dBm. However, when a saturated-SOA with recovery time above 1.6 ns is used, the full power range reaching the receiver produces compliant BER for systems supporting 64 ONUs. For networks supporting 128 ONUs, the system performance (BER) for the received power range is quite below the FEC threshold, assumed to be at a BER = 10^{-4}, thereby validating the use of this equalization scheme. These results show that the proposed scheme enables a proper operation of the system supporting either 64 or 128 ONUs.

4.3.2. Metro-Access Network

The second application for the proposed burst-mode power equalization scheme is a scenario where metro and access network segments are interconnected to create the so called metro-access network. This envisioned scenario will need high capacity, especially in the metro part, which must carry the traffic to/from all of the subscribers. This is accomplished by employing WDM in the metro part, which avoids the deployment of more fibres as well as the increase of the system data rate, in a cost-effective and scalable way. Keeping TDM in the access part is essential in a near future, to avoid the higher costs of deploying a dedicated wavelength per end-user and, additionally, to allow backward compatibility with existing PON systems. Hence, in the metro part, each wavelength is operated using TDM techniques, both for upstream and downstream transmission directions. For further details on this network architecture and on the design of the node interconnecting metro and access parts see Appendix B.

These TDM/WDM metro-access networks will face some technical challenges. One is related to the higher network reach, up to 100 km, that should be accomplished, which may require to have amplification in the interface nodes between the WDM-TDM (metro) network and the TDM (access) networks, designated by remote nodes (RNs). A second challenge is the management of the burst-mode upstream transmission in the access network, due to the TDM operation in this network segment. This burst-mode transmission demands the use of a fast and accurate burst-mode receiver at the OLT, essential to receive bursts from ONUs located at different distances from the OLT. As verified for the access networks, in sub-section 4.3.1, this uneven network topology of each TDM access network incurs in different power budgets for each ONU, forcing the OLT burst-mode receiver to have a large input power dynamic range, in order to cope with all possible incoming power levels. These two upstream challenges of TDM/WDM metro-access networks may be addressed by employing the proposed power equalization scheme in the RNs, which allows minimizing the near-far

problem and enables the support of more users or even to increase the network reach, which is accomplished by the signal power amplification due to the use of SOAs.

In this architecture, depicted in Figure 4.13, the OLT is located in a WDM ring and handles all of the ingress and egress traffic of the network. The RN adds/drops the upstream/downstream wavelength carrying the traffic from/to the sub-set of subscribers that are attached to it. The main feature of the RN described in Appendix B is the wavelength conversion, required to enable a fully-transparent end-to-end transmission. Given the extended reach of the network, the RN should be able to amplify/regenerate the signals. This may be attained using SOAs that, when operated in the correct way, may also be used to minimize the near-far effect characteristic of TDM-PON systems before the traffic reaches the OLT. Any type of TDM-PON may be attached to these RNs, without compromising their specifications. However, in the following the use of 10 Gbit/s EPON will be assumed, which corresponds to a more demanding future system in terms of burst-mode operation, as previously demonstrated.

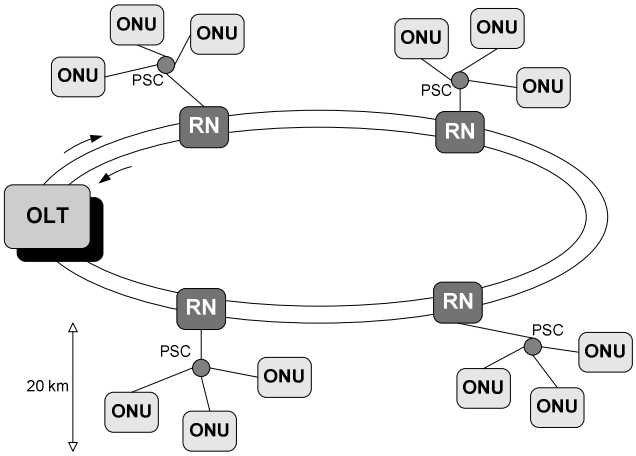

Figure 4.13 – Envisioned metro-access network configuration.

Typically, a TDM-PON has uneven topology, supporting ONUs close to the OLT as well as ONUs located at distances typically up to 20 km. As shown in sub-section 4.3.1, the worst case access topology configuration in terms of relative power budget, employs a first 1×2 PSC. Assuming this scenario and considering that each PON system attached to the RN supports 64 ONUs, Table 4.3 presents the upstream power budget values of the metro-access network. Here, $P_{\text{rx\_RN}}$ represents the power received at the RN, considering a first 1×2 PSC, and $P_{\text{rx\_OLT}}$ represents the power reaching the OLT, considering that no amplification occurs in the signal path, but assuming additional 4 dB losses in the WDM ring. A fibre attenuation

of 0.4 dB/km is assumed in the access segment, but a fibre attenuation of 0.2 dB/km is considered in the metro segment, because wavelength conversion between the 1310 nm and the 1500 nm windows is assumed in the RN. A maximum distance of 100 km is considered, and thus in the worst case, the signals emitted by the ONUs traverse 80 km of fibre in the WDM ring. The ONUs are assumed to be all equal, transmitting signals with the minimum power level considered in sub-section 4.3.1, namely P_{tx} = -1 dBm. The loss difference experienced by the signals transmitted from the nearest and the farthest ONUs is 23 dB, which corresponds to the maximum power range that the equalization scheme in the RN should be able to equalize. As presented in Table 4.3, the low power values reaching the OLT, P_{rx_OLT}, suggest that this configuration has probably a very low performance, requiring optical amplification to be used somewhere before the receiver.

Table 4.3 Envisioned metro-access network: upstream power budget.

	P_{tx}	Loss Difference	P_{rx_RN}	P_{rx_OLT}
Nearest ONU	-1 dBm	23 dB	-4 dBm	-24 dBm
Farthest ONU	-1 dBm		-27 dBm	-47 dBm

In the following, the use of power equalization in the RNs of the envisioned metro-access network is assumed. As referred above, the use of this scheme may bring benefits both in terms of network reach and dynamic range of the burst-mode upstream receivers, if well dimensioned for the scenario considered.

For simulation purposes, the power equalization scheme is characterized as in sub-section 4.3.1. Namely, the gain-SOA and the saturated-SOA have small signal gains of 25 and 22 dB and saturation output powers of 12 and 10 dBm, respectively, assuming a noise figure of 6 dB for both SOAs. The binary signal was formatted according to the specifications of EPON frames (see sub-section 4.2.2), and the laser transmitter was modulated using the NRZ format at 10 Gbit/s. An ER of 6 dB was assumed. For simplicity reasons, it is assumed that the remaining components of the RN have a negligible effect on the transmission.

In order to verify the overall equalization capability of the proposed scheme in the scenario described above, Figure 4.14 shows the signal power at the output of the equalizer, normalized by the lowest output signal power, as a function of the power reaching the RN. Moreover, the overall gain provided by the equalizer scheme is also depicted in Figure 4.14. It is shown that the input power range of 23 dB is reduced to around 6 dB at the output of the

equalizer scheme, which will result in a reduced dynamic range in the OLT receiver. Moreover, a similar reduction may be achieved for different input power ranges, which allows accommodating different topology configurations of the PON systems, or even to support higher splitting ratios.

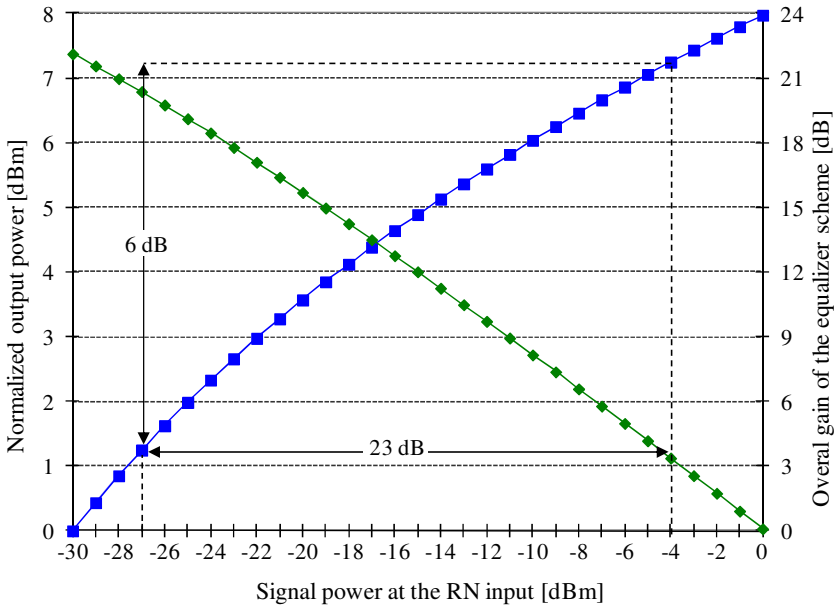

Figure 4.14 – Overall equalization capability when the equalizer is located at the RN: normalized power at the equalizer output (blue) and overall equalizer gain (green).

By analyzing the overall gain curve of the equalizer, presented in Figure 4.14, it can be concluded that the signals with power levels of -27 dBm and -4 dBm at the input of the RN will present output power levels around -7 dBm and -1 dBm, respectively, after the equalization process (output of the RN). Before reaching the OLT receiver, these average power levels will suffer losses in the WDM ring, including 16 dB from fibre attenuation plus 4 dB extra losses, to account for filters, splices or connectors in the signal path. Therefore, at the input of the OLT receiver, those signals will present an average power level of -27 dBm and -21 dBm, respectively, which are significantly higher than those presented in Table 4.3. This shows the importance of adding amplification in the system, which allows obtaining acceptable power levels at the OLT receiver input. This is confirmed with the following analysis of the overall system performance.

Figure 4.15 depicts the system performance, after the OLT receiver, for different power levels, as a function of the recovery time of the saturated-SOA used in the RN equalizer. The system BER was calculated using a semi-analytic method where both ASE and

receiver electrical noise are accounted for. A sensitivity of -15 dBm was considered for BER = 10^{-12} and input ER = 6dB. Figure 4.15 shows that transmission compliant with BER < 10^{-12} is attained for the two power levels considered. For signals with average power of -27 dBm, a recovery time longer that 4.8 ns is required, but for signals with average power of -21 dBm the recovery time may be as low as 0.8 ns. Although for the illustrative power level of -30 dBm the BER of 10^{-12} is never reached, the performance is still quite below the FEC threshold (BER = 10^{-4}). These results validate the use of this configuration, showing the feasibility of the extended metro-access network.

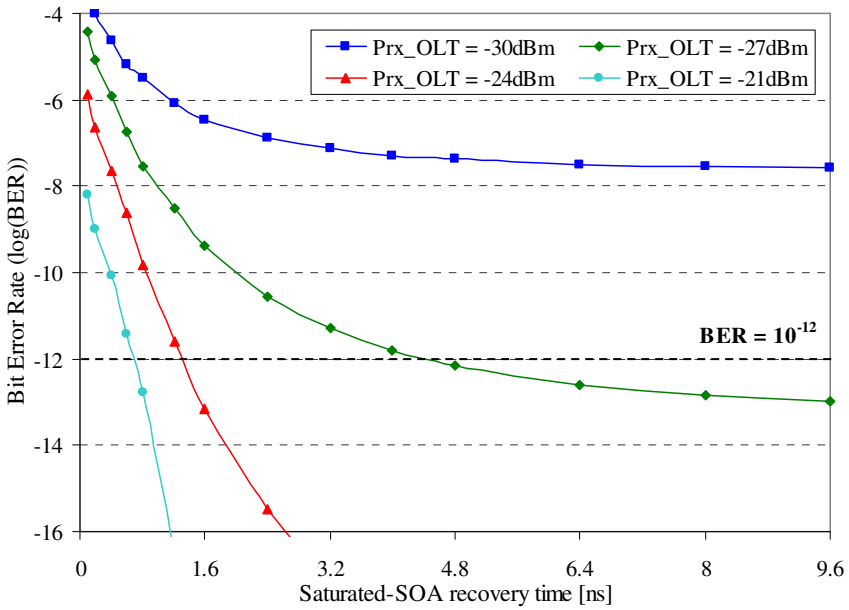

Figure 4.15 – System performance, for several input powers at the OLT receiver.

4.4. Conclusions

The use of burst-mode receivers is gaining increasing importance in all segments of optical networks, namely for core, metro and access applications. This element is necessary to handle burst transmission, typically characterized by the existence of asynchronous and unbalanced power level data streams, while ensuring an error free reception. The stringent requirements of burst-mode receivers, specially their sensitivity and input dynamic range, may be minimized by providing optical power equalization of the different data bursts reaching the

receiver, balancing their power levels. This fact is particularly important for high data rate access networks based on TDMA.

An overview of available power equalization schemes was presented, emphasizing their advantages/disadvantages to be employed in access networks. Moreover, the use of SOAs was considered to be appropriate for such scenarios, due to their suitable performance and associated low cost. The use of SOAs as power equalizers was characterized, in terms of gain and recovery time.

A 10 Gbit/s all-optical power equalization scheme based on two cascaded-SOAs to be applied in burst-mode applications was described. It includes a gain stage to pre-amplify the incoming signal in order to saturate a SOA located in a subsequent equalization stage. Design rules to optimize the recovery time of the saturated-SOA of the equalization stage have been discussed for EPON systems, based on the duration of the overhead fields and on the longest sequence of identical symbols. These rules may be easily extrapolated for other systems.

The performance of the proposed power equalization scheme was analyzed for different applications. Its use in 10 Gbit/s EPON systems was found to have a good equalization capability. Moreover, the use of different gain recovery times of the saturated-SOA proved that effective burst equalization may be attained, enabling also a compliant system performance, with significant benefits regarding the dynamic range of the OLT receiver.

A second application of the burst-mode power equalization was addressed. It involved the use of the proposed scheme based on the cascaded-SOAs to improve the performance of next-generation TDM/WDM metro-access networks. The power equalizer is placed in the remote node that interconnects the access and the metro segments, bringing advantages in terms of power gain and reduced dynamic range at the OLT receiver.

Part B

Integrated Fixed-Wireless Access Networks

Chapter 5

CONVERGED ACCESS NETWORK ARCHITECTURES

The main goal of the information society is to provide broadband services to everyone. As referred along this thesis, reaching such goal has been often promised through deploying optical fibre, in the form of FTTC and FTTH implementations. However, the impact of wireless telephony and wireless LANs in society has been of such magnitude that the liberation of a wired connection created in the end user a sense of autonomy that he/she is compelled to preserve. In fact, being able to benefit from the high capacities envisioned for next-generation fixed access networks, while keeping this autonomy, would represent the most desirable scenario from the end user perspective. This objective is addressed by International Mobile Telecommunications-Advanced (IMT-A) systems, which go beyond IMT-2000. In particular, IMT-A specifies ambitious data rates of up to 1 Gbit/s for low mobility users (e.g. pedestrians) and up to 100 Mbit/s for high mobility users (e.g. travelling by car or train) [ITU03].

Nowadays, the remarkable widespread adoption of broadband connectivity services, both fixed and wireless, is driving service providers and network operators to improve and modernize their physical infrastructures. On the fixed access side, the penetration of optical fibre deeper towards the customer premises is becoming very significant, with the worldwide deployment of multiple PON systems. Amongst all the possibilities for deploying fibre in the access segment, PONs are very attractive mainly due to their simplicity and due to the fact that they do not require active elements within the network plant. Moreover, leading

telecommunications carriers have concluded that the PON architecture provides the most cost-effective solution, in terms of both initial deployment and network operation costs, without sacrificing bandwidth. Turning to wireless access networks, the evolution has been mainly focused on innovative radio protocols and transmission techniques, such as Orthogonal Frequency-Division Multiplexing (OFDM), in order to augment the capacity available to individual users. Such techniques, exploited for instance by the recent LTE systems, require more radio resources. Since radio channels are one of the scarcest resources of network operators, the latter face the dilemma of being capable of supporting the upcoming bandwidth-hungry and sophisticated services without necessarily relying on additional radio resources. It is expected that realizing this objective in a cost-effective manner will require significant changes in the system architecture.

In this context, the convergence of wired and wireless systems over a common infrastructure is a foreseeable scenario. Particularly, the simultaneous support of both technologies over the same physical access infrastructure is expected to result in both Capital Expenditures (CAPEX) and Operational Expenditures (OPEX) savings, minimizing the number of parallel infrastructures that have to be installed and maintained. For wireless access networks, this coexistence, along with the need to efficiently accommodate increasingly smaller cells, can be attained by implementing an innovative wireless architecture based on a Distributed Antenna System (DAS). This approach is expected to be suitable for the support of future wireless systems [FUT], [CAY05], particularly those targeting the demanding IMT-A objectives. Typically, a DAS comprises multiple spatially separated antenna units, hereafter named Remote Radio Heads (RRHs), which are linked to a central location, hereafter designated by Central Unit (CU), via a transmission medium, like optical fibre. The immediate advantage of the DAS over a conventional single antenna system is that the same area can be covered with less power and improved reliability, because line-of-sight is present more often and power losses from penetration and shadowing can be more easily reduced.

It is therefore clear that joint efforts from wired and wireless telecommunication industry brands should be developed in order to efficiently exploit the bandwidth capabilities of the optical fibre. An example of such scenario is illustrated in Figure 5.1, where both wireless base stations and fixed end-users are served by a single fibre infrastructure. This also allows a common resource management to take place, enabling an optimized, or near optimized, resource allocation.

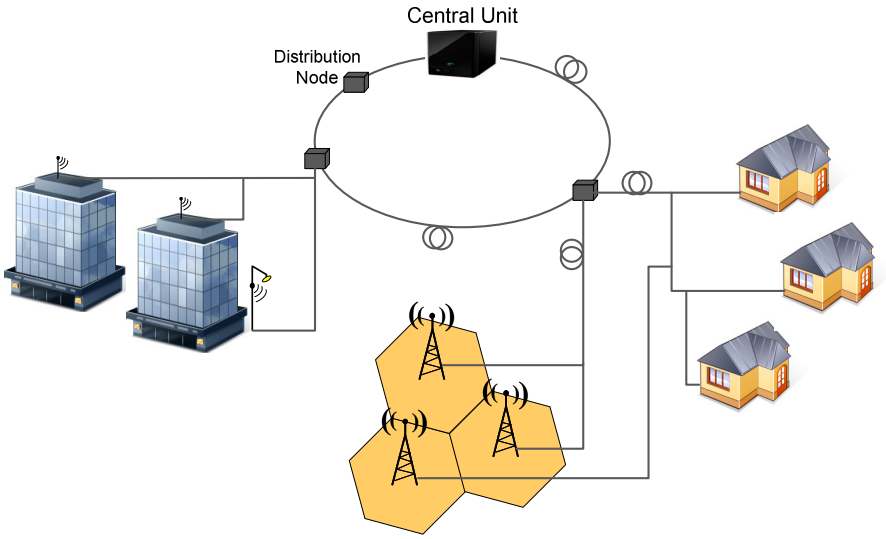

Figure 5.1 – Illustration of a fixed-wireless network convergence scenario.

This chapter is devoted to the analysis of converged wireless and fixed access architectures. The compatibility of wireless systems with the existent PON standards is addressed in section 5.1. A study focused on the possible fibre network topologies better suited for supporting a wireless distributed antenna system is presented in section 5.2, providing a power loss budget and an economical analysis. Section 5.3 addresses the use of digital or analogue transmission in DAS networks, focusing on the necessary transmission requirements and comparing both approaches in terms of cost.

5.1. Compatibility with Passive Optical Networks

The strong interest on PON systems in the global market of telecommunications should be considered in the analysis of the convergence of wired and wireless access networks. For all the reasons stated above, the use of a PON infrastructure to transport radio signals seems to be an appealing approach. Distributed radio networks require reliable and inexpensive networks to transmit, as transparently as possible, the radio signals between the RRHs and the CU. PONs are simple and economical when compared to other alternatives, therefore the transmission of radio signals over a PON infrastructure is expected to be a quite profitable approach, allowing for the deployment of a distributed network for the RRHs, benefiting from the fact that the PON is an inherently centralized system.

5.1.1. Wavelength Allocation Plans

The use of standardized, and deployed, PON systems to transport additional wireless services, must take into account the wavelength bands already allocated to wired services. Hence, the wavelength allocation plans specified for the most important PON standards are discussed in this sub-section, addressing the ITU-T allocation plan for GPON and the IEEE options for 1 Gbit/s EPON systems and also for the recently released 10 Gbit/s EPON standard. The use of WDM and/or Sub-Carrier Multiplexing (SCM) techniques is a possibility for significantly increasing the PON system capacity. Consequently, WDM-PON and SCM/WDM-PON systems may be envisioned as future upgrades of currently standardized PONs, in a scenario where the corresponding wavelength plans may be preserved.

The wavelength allocation in GPON systems is currently based on ITU-T G.983.3 [ITU01], and is schematically presented in Figure 5.2. When comparing it to the preceding ITU-T PON specifications, the downlink Basic-Band is a reduced portion of the original downlink band, from 1480 to 1500 nm, and an additional wavelength band (Enhancement Band), has been made available to provide video and WDM services, comprising two options. The first assigns the 1539-1565 nm band for additional digital services, and the second specifies the 1550-1560 nm band for analogue video distribution services. Note that the Enhancement Band may be used not only for downlink services, but also for additional uplink services, employing WDM schemes.

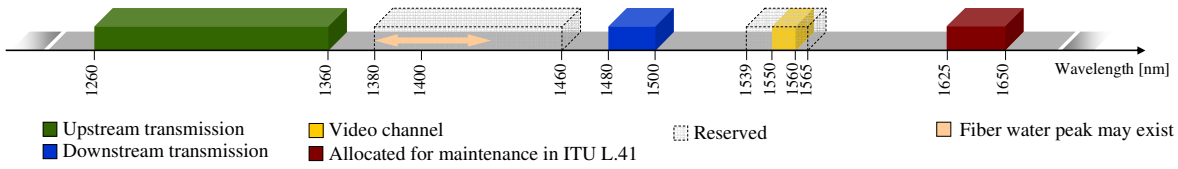

Figure 5.2 – ITU-T G.983.3 wavelength allocation plan.

In GPON systems, the uplink transmission uses the 1260-1360 nm band, just as in previous specifications, for operation data rates of 155 Mbit/s, 622 Mbit/s, 1244 Mbit/s and 2488 Mbit/s, when considering the use of a single fibre system. Between the uplink and the downlink bands, an Intermediate Band is specified from 1380 to 1460 nm, and is reserved for allocation by ITU-T. In case a band is necessary to perform maintenance tasks, GPON systems may use the 1625-1650 nm band, allocated by ITU for that specific purpose.

A more recent release of the GPON standard, ITU-T G.984.5 [ITU07b], specifies an improved wavelength allocation to enable the support of higher capacity systems. More precisely, this release specifies three options for the uplink band within the 1260-1360 nm spectral region, depending on the lasers that are used at the ONUs. The Intermediate Band is allocated for next generation access services, by defining two options which are related to the type of fibre that is deployed. The final difference concerns the Enhancement Band limits, which are slightly changed.

The EPON systems operated at 1 Gbit/s, specified by the IEEE 802.3ah standard [IEEE04], use a wavelength allocation plan based on the one defined by ITU-T 983.3. Although supported in an informal way, since the EPON official specifications do not mention video overlay, analogue video services are commonly deployed by the EPON providers. The wavelength channel used for these services follows the wavelength allocation plan specified for GPON systems (Figure 5.2).

The development of the new standard for EPON systems operating at 10 Gbit/s [IEEE09] aimed at a coexistence with the legacy IEEE 802.3ah compliant systems, operating at 1 Gbit/s. This objective imposed stringent requirements in terms of the wavelength plan for future systems. The spectral allocation presented in Figure 5.3 shows the overlay of what is specified for 1 Gbit/s and 10 Gbit/s EPON systems.

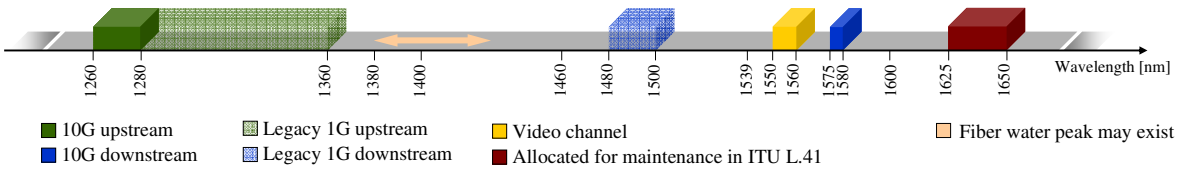

Figure 5.3 – EPON wavelength allocation plans (1 Gbit/s and 10 Gbit/s).

In the downlink direction, a WDM scheme must be employed to support the different data rates of legacy (1 Gbit/s) and future systems (10 Gbit/s), due to their incompatibility. Therefore, the 1 Gbit/s EPON downlink band is maintained, while a band spanning from 1575 to 1580 nm is allocated for the 10 Gbit/s EPON downlink. On the other hand, the use of a WDM scheme in the uplink is not a viable option since outside of the 1310 nm window, which is already reserved for 1 Gbit/s EPON, the optical fibre dispersion is considerably higher, causing larger signal distortion. In addition, changing the uplink band for 1 Gbit/s EPON systems is not a good option, because of the ongoing production and deployment of these systems. As a result, 10 Gbit/s EPON systems must employ a TDM approach in the

uplink to transport both data rates, thus sharing the same 20 nm wavelength band from 1260 to 1280 nm. This option leads to a potential compliance with the enhanced specifications for GPON systems, which will enable the massive production of low cost laser sources. Note that the use of a TDM approach in the uplink requires the design of an OLT receiver capable of receiving both data rates, which still requires significant development effort, though the initial results indicate its feasibility.

In 10 Gbit/s EPONs, the backward compatibility is maintained for video overlay services, which will use the same wavelength band specified by ITU-T G.983.3. However, the use of analogue video will be progressively abandoned, since the 10 Gbit/s EPON is expected to provide enough bandwidth to replace the analogue video by digital services, thereby allowing for significant cost savings.

The current allocation of wavelength bands for IEEE and ITU-T xPON compliant systems is presented in Figure 5.4, omitting the transmission direction for each band, and considering only GPON and EPON systems. Figure 5.4 clearly shows the allocated bands, represented in grey, and the free bands, represented in blue. These free bands may be used for deploying different services over the same underlying PON infrastructure, while maintaining the compatibility with the already deployed services. Note, however, that any additional service must not interfere with legacy ones, in order to preserve the quality of those services. Any additional service using these free bands will be compatible with GPON, 1 Gbit/s EPON and 10 Gbit/s EPON. If, for instance, the compatibility with 10 Gbit/s EPON systems is not necessary, the spectral band spanning from 1575 nm to 1580 nm may also be employed for the new services.

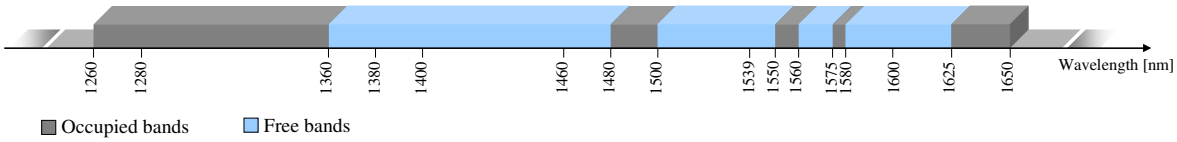

Figure 5.4 – Generalized xPON wavelength allocation plan.

The wavelength band allocated for analogue video transmission may be a suitable option to deliver additional radio services, since it is already used for analogue transmission, although currently only for downlink broadcast transmissions. Moreover, for systems such as 10 Gbit/s EPON, the use of this band for analogue video transmission will be gradually abandoned, leaving it available for other services, such as the support of wireless signals.

5.1.2. Multiplexing Schemes

As mentioned before, the convergence of wireless and wired access networks must assure fixed traffic and radio signals coexisting in the same infrastructure without interference. Considering the xPON wavelength allocation plans, two scenarios can be envisioned with respect to the transport of radio signals over a PON infrastructure. First, the radio signals may be transported using the wavelength bands already specified for PON standards, but employing some type of multiplexing technology, or, secondly, the bands that are left free by the PON standards may be allocated to these new services. The former scenario can be realized either by allocating the available video band, given its analogue nature and consequent suitability for carrying analogue radio signals, while the latter is realized by using the digital data channels to transmit the digital information or digitized versions of the original radio signals.

A very common way of increasing the transmission capacity of a single optical carrier is through SCM, which allows carrying several radio channels using Radio Frequencies (RFs), over a given optical carrier, as depicted in Figure 5.5. These sub-carriers may transport analogue or digitized versions of the radio signals, depending on the employed transmitters and receivers, and on the complexity that is acceptable for modulation and demodulation. This technique may be employed, allowing for the simultaneous transmission of wired and wireless services, using the baseband optical carrier and the sub-carriers, respectively.

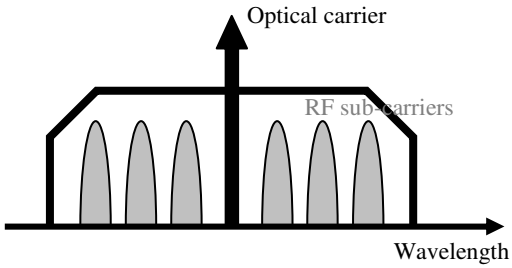

Figure 5.5 – Illustration of the SCM technique.

The wavelength band allocated in PON systems for analogue video distribution (1550-1560 nm), although currently used only for downlink broadcast transmissions, may be used by allocating one or more wavelengths within it, enabling the bidirectional transport of radio signals, as illustrated in Figure 5.6 a). In a case where only one wavelength is allocated for both uplink and downlink transmission directions, the RF bandwidth should be divided into two sub-bands, with each used only to transport uplink or downlink data. In spite of this being

a theoretical possibility, it may result in significant interference due to the partial overlapping of the modulated uplink and downlink optical carriers. As an alternative, the same wavelength (and respective modulated RF sub-carriers) could be fully used for both transmission directions during different time intervals, employing Time Division Duplex (TDD) techniques, as exemplified in Figure 5.6 b).

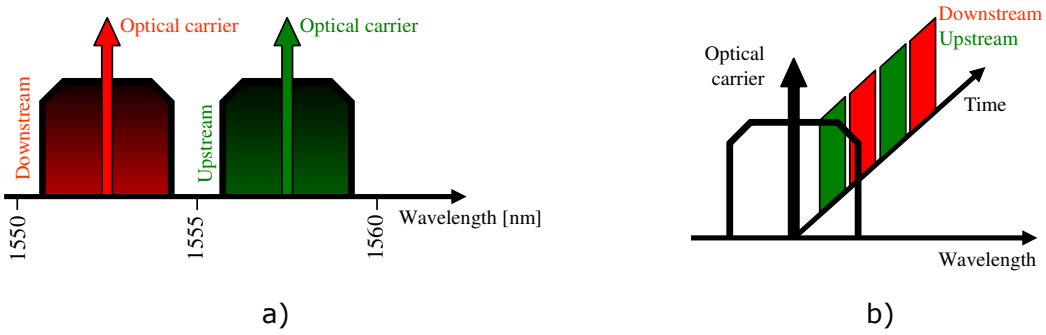

Figure 5.6 – Multiplexing techniques for transmission of radio signals.

The case illustrated in Figure 5.6 a) restricts the exploitation of the frequency spectrum for each transmission direction. In this approach, the differentiation between the terminals connected to the PON may be made with different RF carriers using SCM. However, this solution demands using stable light sources to assure a reduced drift of the central wavelength, in order to prevent any interference between both channels inside the available 10 nm band. This stringent requirement may be loosen by using the Enhancement Band reserved for digital services, in the 1539-1565 nm region [ITU01]. Furthermore, using SCM requires highly accurate filters to separate the RF sub-carriers supported by the optical carrier. The system performance may also be affected by the characteristics of both the laser and the photodetector, which can give rise to several intermodulation products originated by the beating of the RF sub-carriers with each other and with the optical carrier. This effect highly depends on the modulation frequency of the sub-carriers and on the number of simultaneous RF channels supported by the same optical carrier. Nevertheless, the SCM technique may also be applicable if down-conversion is used to bring the RF modulated carrier to Intermediate Frequency (IF) values, enabling the use of slower and less expensive electronic circuitries. The inclusion of additional wavelengths inside the allocated analogue video band, in the form of a WDM scheme, would enable the allocation of a unique wavelength pair for a given terminal (RRH), dramatically increasing the available bandwidth. However, if the number of analogue channels is excessive, the transmission performance of the PON digital data channels may be degraded, due to the fibre nonlinear properties [Cox04].

The alternative approach that uses a TDD scheme, as presented in Figure 5.6 b), is capable of allocating different time intervals for both directions, thereby preventing eventual wavelength collisions, since only one optical carrier is used. In this way, the frequency spectrum can be fully allocated to a given direction within its transmission window, but the available bandwidth must be (time) shared by all terminals, causing a limitation on the system scaling. Moreover, due to its half-duplex nature, the efficiency of the transmission channel can be severely degraded due to the fibre propagation delay on a typical PON infrastructure (typically extended to 20 km).

Alternatively to the use of the analogue video reserved band, the PON digital channels could serve as transparent tunnels to forward and receive radio data. By doing so, a flexible mixture of wireless services and legacy PON contents (data and video) can be supported. This alternative can be applied using two different methods. In the first, radio signals are transmitted in a digital baseband scheme, which in terms of transmission performance would be identical to that already confirmed for PON data services. However, a specific protocol must be defined to enable the multiplexing of information from different terminals, both in the uplink and in the downlink. The second method consists of digitizing the analogue radio signal before transmission. When compared to the digital baseband approach, this solution may require a simpler signal processing, since all information in the RF modulated carrier is maintained in the resulting bit flow. However, it relies on Analogue-to-Digital Converters (ADCs) and Digital-to-Analogue Converters (DACs), which must be able to deal with the high transmission frequencies of wireless protocols (such as 11 GHz for WiMAX), if no frequency down-conversion is used.

The bands that have not been defined for specific services in PON standards (see the non-allocated bands in Figure 5.2 and Figure 5.3) may be freely allocated to overlaid radio services, by assuring a minimal degree of interference with the legacy PON data. This option allows maximizing the fibre plant usage, since the same physical infrastructure can be easily shared by both technologies.

In WDM or WDM/SCM scenarios, the use of Coarse WDM (CWDM) or Dense WDM (DWDM) may be envisioned. CWDM provides the allocation of 18 different channels with 20 nm of width ranging from 1260 to 1625 nm. However, since bidirectional communication is required, this would limit the number of terminals using different wavelengths to only 9, assuming a single fibre for both directions. DWDM uses 50 GHz or 100 GHz channel spacing, comprising the wavelengths from 1490 to 1600 nm and neglecting

the 1260-1360 nm band. Both solutions use off-the-shelf components and may be deployed in a short time period, but the operational requirements are quite different. By using wider channels, the CWDM approach allows for the use of low-cost lasers (such as directly modulated light sources) without rigid wavelength stabilization. However, the 20 nm channel width results in a limited number of channels. On the other hand, DWDM systems can support several tens of channels, thereby providing far greater capacity, but at the expense of higher transmitter costs due to the need of very strict wavelength drift control.

The selection of a proper wavelength band for radio transmission depends on the fibre properties. Particularly, the variation of attenuation and chromatic dispersion with wavelength must be addressed. In a DWDM scenario, the 1500-1550 nm and 1600-1625 nm bands emerge as the most interesting options for radio transmission, considering the ITU-T G.983.3 wavelength allocation. If the wavelength allocation plan for 10 Gbit/s EPON systems is considered (see Figure 5.3), the 1575-1580 nm band is not available. For the CWDM approach, the 1380-1460 nm band could be considered only for short reaches, due to the high attenuation in this region. The 1360-1380 nm and 1460-1480 nm bands have better transmission conditions, but they only support two CWDM channels, the same number supported in the 1500-1550 nm band. Figure 5.7 illustrates these options.

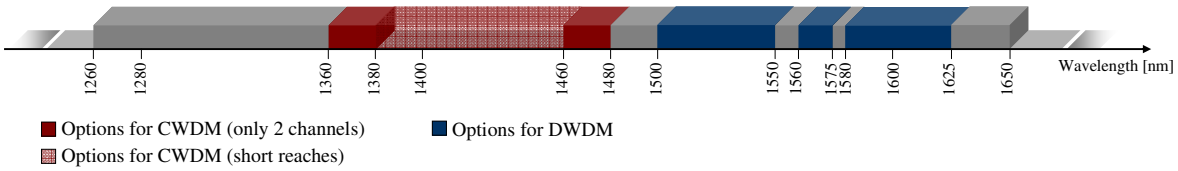

Figure 5.7 – Using the xPON free wavelength bands.

An important factor that can lead to the incompatibility between PON contents and radio information is related to the analogue nature of the video signal, often transmitted in PONs using the 1550-1560 nm band. Since this video signal requires a high transmission power to guarantee the SNR required for proper reception, it might significantly affect the signals transmitted in the wavelengths located in its proximity (see sub-section 2.2.4).

In case of no coexistence is required between wireless and wired services, the radio transmission over a passive optical fibre plant infrastructure which is not supporting any other type of services may be considered, representing a scenario where the wavelength bands providing the most advantageous transmission conditions can be freely selected without compatibility constraints.

5.2. Fibre-Optic Architectures

The use of a DAS for supporting future wireless systems presents several benefits over conventional wireless architectures, namely in terms of energy efficiency and improved reliability. In such a system, several RRHs are interconnected and served by a central station, allowing to concentrate here the processing functionalities, if suitable for decreasing the complexity of the remote units. The typical transmission medium between the RRHs and the CU is optical fibre, given its broadband and low loss features, creating the so-called Radio-over-Fibre (RoF) network [KLN+08]. This can also capitalize on the increasing penetration of fibre for fixed access services being verified worldwide with the multiple PON deployments, further emphasizing the importance of analyzing the fibre optic infrastructure more suitable to support a DAS system.

In general, a CU interconnects a set of RRHs serving a given geographical area, although multiple sets of RRHs may be connected to the same CU, benefiting from using the same rental space and thereby decreasing the OPEX. In this scenario, the CU must include an optical interface for each set of RRHs to transmit/receive the radio signals transmitted over the optical fibre. Alternatively, the same optical interface may be shared by different sets of RRHs, but a separate sub-system is necessary to split/combine the signals. This second approach will not be considered in the following, since it only represents an extension of the generic concept.

The architectures under discussion in this section, which addresses the requirements imposed by the DAS from the point of view of the underlying fibre-optic infrastructure, focus only on the physical connection between the CU and the RRHs. No considerations are made with respect to the network that interconnects the CUs, which should be based on digital transmission and probably requires a very large capacity.

5.2.1. Topological Considerations

The fibre-optic infrastructure to support a DAS network may be designed considering the typical physical topologies: chain/bus, star, tree-and-branch, and ring, which are represented by the simplified diagrams of Figure 5.8. The selection of the most suitable topology depends on several aspects, such as the deployment scenario and the number of terminals supported by the network. In order to maximize cost savings in the optical infrastructure, an important issue

is the minimization of the fibre layout. Clearly, the location of the CU and the RRHs determines what topologies require the smallest amount of fibre to provide the required connectivity. For instance, in a building requiring one antenna per floor, using the chain topology to connect all antennas will minimize the fibre layout. On the other hand, if the CU is located in the centre of the geographic area that is necessary to cover, the star is most likely the best choice, whereas in case the RRHs are distributed in a more irregular fashion, the tree-and-branch is probably a good option to connect these terminals to the CU.

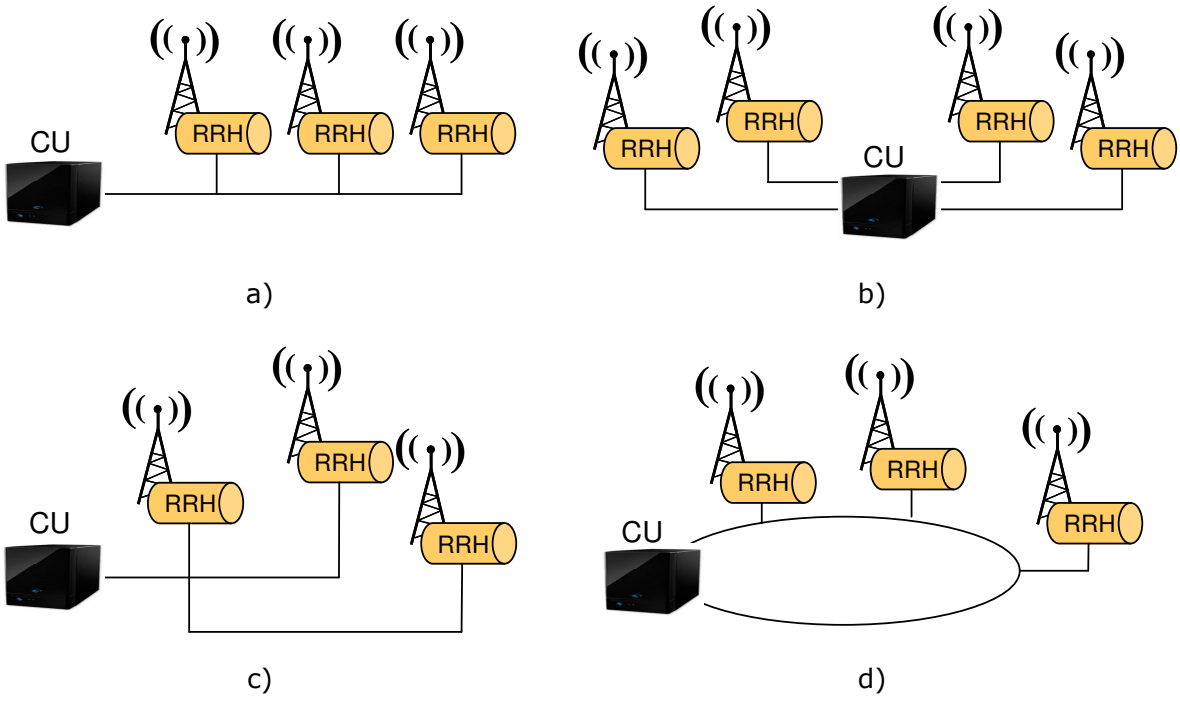

Figure 5.8 – Possible topologies for a DAS fibre plant. a) Chain/bus topology; b) Star topology; c) Tree-and-branch topology; d) Ring topology.

The topologies of Figure 5.8 may represent active or passive fibre plants. In active deployments, costly equipments like switches, routers, and/or add/drop multiplexers are placed within the distribution fibre network, requiring environmental enclosures and powering. On the other hand, passive fibre plants comprise elements such as passive splitters/combiners or passive wavelength routers (e.g. Arrayed Wavelength Grating, AWG), which require low maintenance and no powering. Although this latter option presents lower deployment costs, it may lack the flexibility provided by the active approach, which enables reconfiguration of the network to dynamically allocate resources where they are needed. Moreover, the active approach may eventually enable higher reach networks and/or connection of a larger numbers of subscribers, by employing amplification and/or regeneration. Security is commonly said to

be an advantage of active deployments, but passive deployments usually employ encryption mechanisms to minimize the security issues. The following analysis of the topologies depicted in Figure 5.8 firstly focuses on passive fibre plant infrastructures, operating using TDM or WDM schemes. Afterwards, the use of an active network is evaluated.

Table 5.1 compares the features of the different passive fibre plant topologies, when TDM is used over the topologies of Figure 5.8. The following considerations are assumed:

- A single CU supports *N* RRHs;
- The use of a single fibre implies using different wavelengths for downlink and uplink;
- The worst case loss factor is defined as the maximum power splitting that a signal going to/coming from a RRH experiences.

Table 5.1 Comparison of different passive topologies.

Topology	**Number of fibre ports per CU**	**Fraction of wavelength capacity per RRH**	**Additional duct usage for protection**	**Worst case loss factor**
Chain/bus	1	1/*N*	Yes	*N*
Star	*N*	1	Yes	1
Tree-and-branch	1	1/*N*	Yes	*N*
Ring	2	1/*N*	No	*N*

According to Table 5.1, the star topology requires a number of fibre ports equal to the number of RRHs being supported, but benefits from the lowest worst case loss factor. Conversely, the chain/bus, tree-and-branch and ring topologies have a worst case loss factor that grows with the number of RRHs, but are able to share the wavelength capacity among multiple RRHs. The ring inherently supports protection without additional duct usage, whereas the other topologies require using more ducts for this purpose.

When accounting for the countless possible spatial distributions of the RRHs, the star topology is the topology that requires more fibre to interconnect the CU and the RRHs. The ring requires an additional fibre link (from the last RRH to the CU) in order to enable survivability to single failures. The tree-and-branch, and to a lesser extent the bus, are the topologies that require the least amount of fibre in the majority of the spatial distributions of the RRHs. The star topology enables upgrading the capacity of a single RRH, since both the link and the port assigned to the RRH are not shared with the other RRHs. On the other hand,

a capacity upgrade on the remaining topologies requires upgrading the interfaces of both the CU and all the RRHs.

Independently of the fibre plant topology being considered, the WDM approach provides a virtual PtP connection between the RRHs and the CU, since each RRH is assigned a unique wavelength pair (for downlink and uplink transmission). The fibre length considerations presented for the TDM analysis are also valid for the WDM scenario. Moreover, the number of transceivers needed is the same in all of the topologies. However, additional WDM mux/demux stages are required, except for the star topology.

In networks that employ active components within the fibre plant, the considerations that have been made for the fibre length in passive approaches are also applicable. As discussed above, active networks are more expensive and require power in every/some of the splitting locations along the path between the CU and a RRH. Such a situation may hamper the cost-effectiveness prospects of a DAS network, which is intended to be low-cost and demanding low maintenance, as all access networks.

The star topology is equal for active and passive deployments, since only PtP connections are used between the CU and the RRHs, except for the case where in-line amplifiers or regenerators are necessary in the star arms, creating an active deployment (probably this situation will not be very common, due to the relative short reach of DAS networks, which enable the use of pre- or post-amplification). In all other topologies the passive elements located in splitting points of the topologies are replaced by active components, such as switches. This has the advantage of providing more dynamic networks, which can be an important feature for future DAS networks, but at the expense of increased CAPEX and OPEX.

In conclusion, the best topology in terms of fibre savings depends on the spatial distribution of the CU and RRHs. This requires having knowledge about the capacity of the systems, in terms of the number of terminals and respective bandwidth demands. Moreover, the selection of TDM or WDM will also depend on these aspects but, whenever convenient, hybrid topologies combining several multiplexing technologies may be addressed as a valid possibility.

Another important issue that must be considered is the cost of the network to be deployed, which is related to the number of network elements that are necessary to deploy within the fibre plant (low-priced passive elements or more costly active elements) and in the network terminals (number and type of required transceivers). Furthermore, it is also related to the deployment costs of the optical fibre, which depend on the implementation scenario (urban, suburban, rural, with or without reusable infrastructures).

In the cases where protection is required in the system, e.g. to serve a dense area of subscribers and where the consequences of a fibre cut, in terms of service disruption, can be disastrous for the network operator, the most suitable topology is the ring, which may be passive or active, depending on the degree of flexibility and dynamics that must be provided to the system in order to satisfy all the requirements. However, a balance should be made between the required flexibility and the resulting cost, in such a way that the envisioned network will be attractive for operators.

Finally, another aspect to consider is the type of networks that are currently used for the access segment. Most of the incumbent carriers worldwide are selecting FTTx deployments as their preferred option, employing, in most of the cases, PON systems, normally using tree-and-branches topologies. This strong interest for PON systems in the global market of telecommunications should be considered in the selection of the best topology for DAS networks, since the access arena is a very competitive market with very sensitive cost issues.

The combination of two or more different topologies may also be a suitable choice. For instance, a ring may be used to connect a set of RRHs, each connecting multiple antennas by using tree-and-branches or chain topologies. In this way, protection schemes may be easily employed in the ring to protect the network segment that carries more traffic, and lower-cost topologies may be used to connect the multiple antenna sites. In this situation, the ring topology should have active elements, enabling a flexible network, whereas the remaining parts may be passive to guarantee that no powering is necessary within these fibre plants, enabling to use less expensive components and to decrease the installation and maintenance costs.

5.2.2. Architectures for Distributed Antenna Systems

Bearing in mind all the considerations and trade-offs presented in the previous sub-section, it may be concluded that the connection between the CU and the RRHs should preferably use a tree or tree-and-branch topology. The main reasons for this selection are the fact that these topologies allow minimization of fibre layout and optimization of the resource sharing, whereas the advantages of the other topologies, such as the ring (easy support of protection schemes, mainly), were considered less important for this network segment. Moreover, passive architectures are preferred for DAS networks due to their lower cost when compared

to active deployments, both in terms of CAPEX and OPEX. These decisions are also supported by the standardised PON concepts and deployments.

Five candidate architectures, all based on tree-and-branches fibre plant topologies, are proposed in this sub-section for a DAS network. These architectures should be able to support future 4G wireless systems, which demand high bandwidth. Thus, preferably no wavelength sharing between RRHs is considered. The candidate architectures are classified according to the type of wavelength multiplexing used, as presented in Table 5.2.

Table 5.2 Candidate architectures for a DAS network.

Candidate architecture		**CWDM**	**DWDM**
(A)	CWDM mux/demux with two ports for each RRH	X	
(B)	CWDM mux/demux with downlink wavelengths shared by multiple RRHs	X	
(C)	CWDM mux/demux with uplink and downlink in single CWDM channel	X	
(D)	Broadcast and Select	X	X
(E)	DWDM mux/demux and Reflective RRHs		X

The capacity provided for each RRH is augmented by deploying a SCM scheme over each wavelength of the system, as explained in sub-section 5.1.2. This allows carrying multiple radio channels over a single wavelength to/from the same RRH, enabling the transmission of very high bandwidth wireless services, or even different wireless technologies, thereby optimizing the available bandwidth usage. By using SCM, the wavelength sharing between RRHs is possible in a scenario where each RRH selects its own sub-carriers. This is easily implemented in a broadcast-and-select architecture, since all wavelengths reach all RRHs, but may impose limitations in terms of eavesdropping. Although not presented, the following descriptions can be easily extended to consider a wavelength sharing scenario.

In order to manage the RoF infrastructure, a control/monitoring channel may be necessary. Since this channel does not require high data rates, it may be implemented as a low data rate digital channel, supported in the baseband, avoiding in this way the introduction of more sub-carriers, and the electronic devices required to generate and receive these sub-carriers. However, if the penalty of transporting baseband and radio sub-carriers on the same wavelength becomes prohibitively high, an additional sub-carrier must be used for the control/monitoring channel instead of carrying it in the baseband.

The candidate architecture A, presented in Table 5.2 and illustrated in Figure 5.9, is based on the most direct approach of using CWDM, where each RRH is served by a unique Uplink (UL) wavelength and a unique Downlink (DL) wavelength, and a single CWDM mux/demux is placed in a splitting point near the area comprising the set of RRHs connected to the CU. In this scenario, each CU may support at most 8 RRHs, since the CWDM grid specifies only 16 wavelengths (neglecting the two high loss wavelengths located near the fibre water peak). The wavelengths within the higher attenuation region (1271 mn, 1291 nm, 1311 nm, 1331 nm, 1351 nm, 1371 nm, 1431 nm, 1451 nm) are selected for DL transmission, since it is the less critical link direction, and the remaining 8 wavelengths (1471 nm, 1491 nm, 1511 nm, 1531 nm, 1551 nm, 1571 nm, 1591 nm, 1611 nm) are used in the UL.

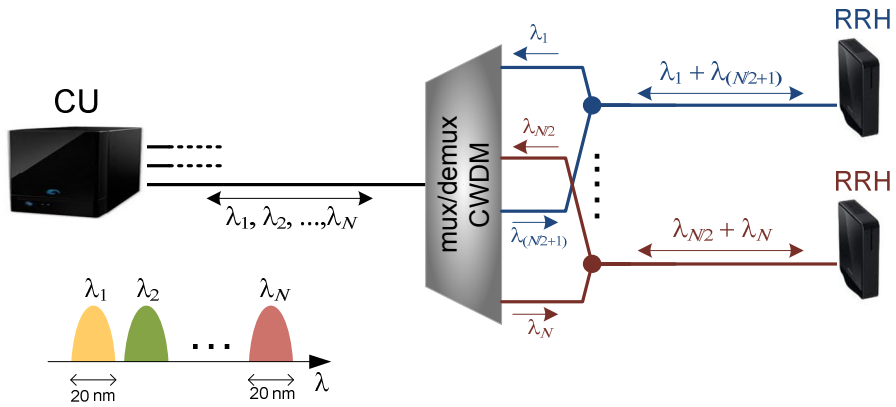

Figure 5.9 – CWDM mux/demux with two ports for each RRH and a single fibre between the mux/demux and each RRH.

Regarding the necessary amount of optical fibre for architecture A, a single fibre is required to connect the CU to the CWDM multiplexer/demultiplexer (mux/demux) at the splitting point (feeder section), and for the distribution section, from the splitting point to the RRHs, two options may be envisioned:

- Single fibre connecting the CWDM mux/demux to each RRH: this configuration is the one represented in Figure 5.9, and requires an additional coupler to connect the UL and DL ports of the CWDM mux/demux into the same fibre, for each RRH, which will incur in extra losses. In order to minimize interference and allow for low cost wideband filters in the RRHs receivers, the wavelength assignment should be carefully designed. Thus, assuming that the wavelength channels are numbered between 1 to 16 in increasing order of wavelength, the first RRH should use λ_1 (DL) and λ_9 (UL), the second RRH should use λ_2 (DL) and λ_{10} (UL), and so on. The last RRH should use λ_8 (DL) and λ_{16} (UL).

- Two fibres connecting the CWDM mux/demux to each RRH: this option avoids the use of filters in the RRHs to separate the UL and DL channels, while doubling the necessary amount of fibre in the distribution section. For this reason, it should be considered only if the additional losses of the single fibre case are not tolerable.

Architecture B is derived from architecture A and aims at alleviating some of its constraints, by allowing for instance the support of a larger number of RRHs with an equal sized CWDM mux/demux. As represented in Figure 5.10, each RRH uses a unique UL wavelength and one (or more) wavelengths are shared by all (or a set of) RRHs in the DL using SCM. The total number of RRHs supported by a single CU will therefore depend on the number of ports of the CWDM mux/demux and on the maximum number of sub-channels that a single wavelength is able to support.

Let us assume that using a specific laser source in the DL, the maximum number of radio channels that may be supported by a wavelength is $n_{sub} \times M_{max}$, where n_{sub} is the number of required sub-channels per RRH and M_{max} is the maximum number of RRHs in a set supported by the CU. In this case, the CWDM mux/demux should have at least M_{max}+1 ports, assuming that only one wavelength is used in the DL for all RRHs. For instance, assuming that each RRH requires 4 sub-channels per link direction, with a commercially available 9 channels CWDM mux/demux (1310 nm and 1471…1611 nm), a set of up to 8 RRHs may be supported by a single CU in this configuration, but only if the DL wavelength would be able to support 32 sub-channels.

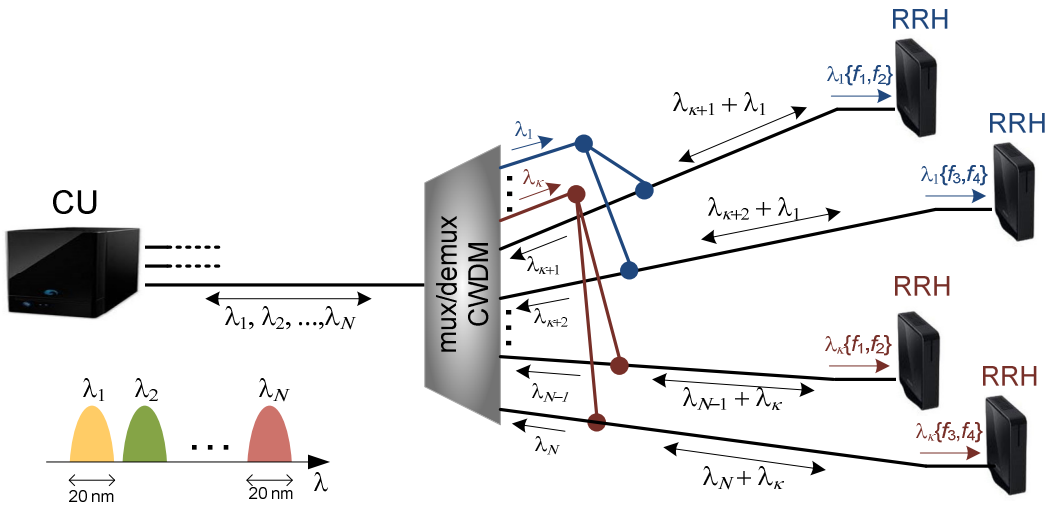

Figure 5.10 – CWDM mux/demux with downlink wavelengths shared by multiple RRHs.

For management purposes, if the baseband approach is selected to carry the control/monitoring channel in the DL, this channel must be shared (time shared, for instance) by the set of RRHs served by the same wavelength. Otherwise, an additional sub-carrier is required per RRH to support the control/monitoring channels, which can be a major disadvantage of this architecture.

The fibre layout in architecture B includes a single fibre from the CU to the CWDM mux/demux and a single fibre from the CWDM mux/demux to each RRH, although there is also the possibility of deploying two fibres in the distribution section, avoiding the coupling losses, as in the case presented for architecture A. The first option requires one power splitter and couplers near the CWDM mux/demux to broadcast each DL wavelength to the distribution fibres connected to the RRHs. These additional elements incur extra loss in the DL, which may be compensated by using an optical amplifier (per downlink wavelength) at the CU output. This is a valid possibility because the optical amplifier is intended to amplify a single wavelength channel only, and its cost is being mitigated through enabling more sub-carriers to be supported in a single wavelength.

The main goal of architecture C (refer to Appendix C for further details) is to support the maximum possible number of RRHs per set connected to the CU, while employing CWDM technology. Therefore, as depicted in Figure 5.11, the 20 nm bandwidth of each CWDM mux/demux port (less because of the typical Gaussian profile of the CWDM mux/demux filter response) is used to transport the UL and the DL wavelengths of the same RRH. In this way, the number of RRHs supported by a single CU set depends only on the number of CWDM mux/demux ports (16 at maximum).

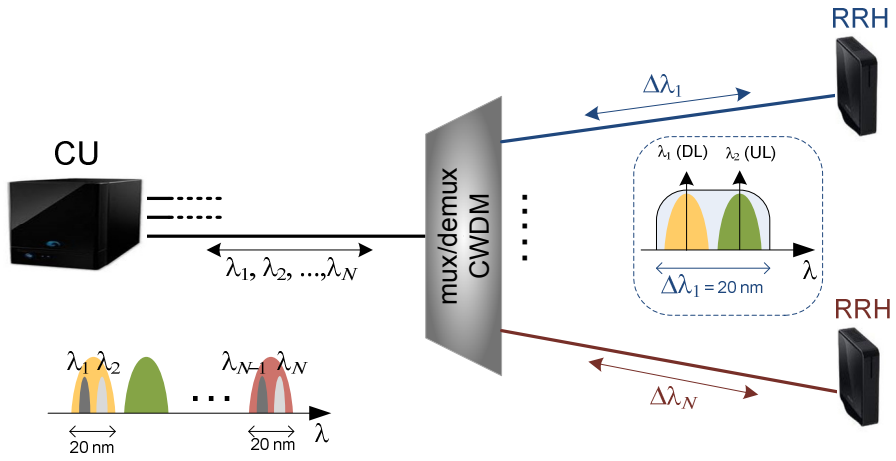

Figure 5.11 – CWDM mux/demux with both directions inside the same CWDM channel.

In order to guarantee the availability of as wide a spectral range as possible for each UL channel in architecture C, the corresponding DL wavelength should be placed in the proximity of the limit of the CWDM mux/demux port bandwidth. This would allow the use of low cost CWDM lasers (with large wavelength drifts) in the UL. The DL lasers must be tightly controlled in order to avoid large wavelength drifts, thereby minimizing interference with the UL wavelength. In this configuration the amount of fibre is minimized, since just one fibre is required to connect the CU to the CWDM mux/demux, as well as to connect the CWDM mux/demux to each RRH.

A conceptually different architecture is considered in option D. This architecture may be operated using CWDM or DWDM, depending on the number of RRHs to be supported and on the target cost for the system. This architecture, depicted in Figure 5.12, consists of a "broadcast-and-select" system that employs cascaded power splitters, with all DL wavelengths reaching all RRHs, where the corresponding wavelength is selected by using low cost filters (thin-film filters, for example). An alternative approach, but also more expensive, is to use an Optical Add/Drop Multiplexer (OADM) near each RRH (in a bus-like topology), to select the wavelength intended for that RRH and avoid that all channels reach all RRHs, thereby reducing power losses and enhancing protection against eavesdropping situations.

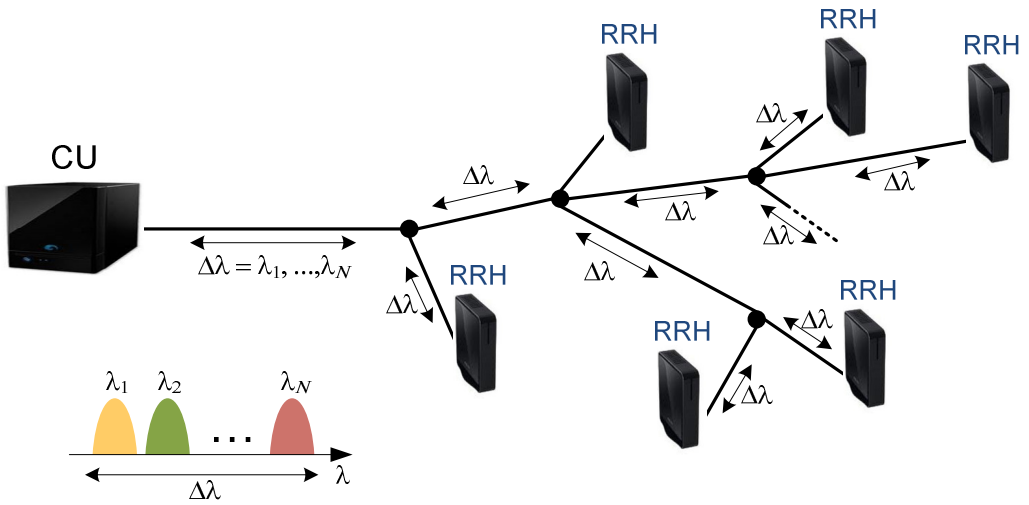

Figure 5.12 – Broadcast and select architecture.

If CWDM is used in architecture D, the number of supported RRHs is limited to 8, since it is assumed that each RRH requires an UL and a DL wavelength. On the other hand, if higher cost lasers and higher cost filters (DWDM) are employed, the maximum number of supported RRHs per CU is limited by the power loss budget, which is limited by the utilization of power

splitters. A possibility to increase the power loss budget is to use unbalanced power splitters, which would require a careful network design, but may eventually allow delivering higher powers to the RRHs that are connected to the CU via more power splitters.

Moving from CWDM to DWDM, the most advantageous architecture includes the use of a DWDM mux/demux placed in a splitting point near the area comprising the set of RRHs connected to the CU, and the use of a reflective device in each RRH, which receives a wavelength in the DL, remodulates it and sends it back in the UL. The reflective device proposed is a Reflective Semiconductor Optical Amplifier (RSOA), due to its relatively low cost and reasonable performance. This architecture, designated in Table 5.2 as architecture E, is illustrated in Figure 5.13.

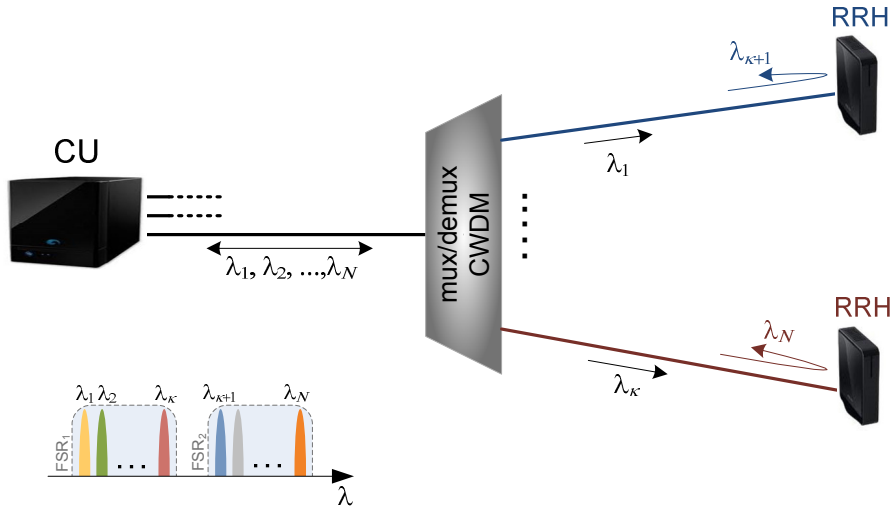

Figure 5.13 – DWDM mux/demux and reflective RRHs.

In this configuration a set of DWDM lasers is employed in the CU for DL transmission, with one wavelength per RRH. Another set of lasers (with different wavelengths) is used in the CU to generate the wavelengths for UL transmission. As an alternative to the second set, a broadband light source may be used, whose spectrum is sliced when passing through the DWDM mux/demux [HTF+01]. The DWDM mux/demux must be periodic, in order to allow for the DL and UL wavelengths to be transmitted by the same port (the DL and the UL wavelengths must be separated by a period of the mux/demux). A RSOA is placed in each RRH to modulate the CW wavelength sent from the CU and send it back uplink. The RSOA has also the advantage of providing some gain in the UL optical channel.

The five candidate architectures described above are compared in Table 5.3, taking into consideration aspects such as the number of supported RRHs, the fibre layout, and the

equipment necessary. The single and double fibre classification, used for architectures A and B, refers to the distribution section of the network, between the splitting point and the RRHs.

Table 5.3 Comparison of the candidate architectures.

	Architecture A		**Architecture B**		**Architecture C**	**Architecture D**	**Architecture E**
	Single fibre	Double fibre	Single fibre	Double fibre			
Maximum number of RRHs per CU set (M_{max})	$M_{max} \leq 8$		$M_{max} \leq 15$ (at most, requires $n_{sub\_tot} = 60$ ($15 \times n_{sub}$) sub-channels to be supported in a single wavelength!)		$M_{max} \leq 16$	CWDM: $M_{max} \leq 8$ DWDM: M_{max} is limited by the power loss budget	M_{max} depends on the DWDM grid and the number of ports in the mux/demux
Splitting point	$2 \times M_{max}$ channels CWDM mux/demux and M_{max} couplers	$2 \times M_{max}$ channels CWDM mux/demux	$M_{max}+n_{DL}$ channels CWDM mux/demux, n_{DL} power splitters, and M_{max} couplers (one per RRH)	$M_{max}+n_{DL}$ channels CWDM mux/demux and n_{DL} power splitters	M_{max} channels CWDM mux/demux	Low cost power splitters placed near the RRHs; a costly alternative is to use OADMs near each RRH in a bus-like topology	M_{max} channels DWDM (periodic and a-thermal, expensive)
Fibre layout	Single fibre in both the feeder and distribution sections	Amount of fibre doubles in the distribution section	Single fibre in both the feeder and distribution sections	Amount of fibre doubles in the distribution section	Single fibre in both the feeder and distribution sections	Single fibre connecting the CU to the RRHs (tree or bus topology)	Single fibre in both the feeder and distribution sections
DL transmitting equipment	M_{max} CWDM lasers (low cost)		n_{DL} CWDM laser (one per DL wavelength), low cost		M_{max} higher cost lasers, with wavelength drift control	M_{max} CWDM lasers (low cost) or M_{max} different DWDM lasers (higher cost)	M_{max} different DWDM lasers (higher cost)
UL transmitting equipment	M_{max} CWDM lasers (low cost)		M_{max} CWDM lasers (low cost)		M_{max} different CWDM lasers (low cost)	M_{max} CWDM lasers (low cost), or M_{max} DWDM lasers (higher cost)	M_{max} DWDM lasers or broadband light source (lower cost) in the CU, and a RSOA in each RRH
DL receiving equipment	M_{max} wideband optical filters (low cost)	No optical filters are required	M_{max} wideband optical filters (low cost) and $M_{max} \times n_{sub}$ electrical filters	$M_{max} \times n_{sub}$ electrical filters to select the sub-channels (n_{sub} different filters for each RRH)	M_{max} optical filters	M_{max} optical filters to select the proper wavelength (low cost for CWDM and higher cost for DWDM)	M_{max} optical filters
UL receiving equipment	M_{max} wideband optical filters in the CU (low cost)		M_{max} wideband optical filters in the CU (low cost)		M_{max} optical filters in the CU (higher cost)	M_{max} wideband optical filters (CWDM, low cost), or M_{max} narrow band (DWDM, higher cost), in the CU	M_{max} optical filters in the CU
Optical amplification	Difficult and expensive to implement, since a different amplifier would be necessary for each wavelength (up to M_{max} only for DL)		n_{DL} optical amplifiers at the CU output, to compensate the extra losses due to the DL power splitters		Difficult and expensive to implement, since a different amplifier would be necessary for each wavelength (up to M_{max} only for DL)	CWDM: difficult and expensive to implement (splitting losses are difficult to be minimized); DWDM: optical amplification in the DL is viable	May be used in the DL with a single device for all DWDM channels
Control/ monitoring channel	Digital baseband or additional sub-carrier in DL and UL wavelengths		In the DL, the digital baseband channel must be time-shared by the set of RRHs served by the same DL wavelength or an additional sub-carrier is required per RRH		Digital baseband or additional sub-carrier in DL and UL wavelengths	Digital baseband or additional sub-carrier in DL and UL wavelengths	Digital baseband or additional sub-carrier in DL and UL wavelengths

n_{sub}: number of sub-carriers to be supported per each wavelength
n_{DL}: number of downlink wavelengths in architecture B

5.2.3. Power Loss Budget Assessment

Assessing the power loss budget for the architectures described in sub-section 5.2.2 is important to determine their suitability for a specific scenario. The following assumptions are made:

- A mux/demux in the CU (equivalent to that used at the splitting point) is used for all configurations to multiplex the transmitting wavelengths and demultiplex the receiving wavelengths.
- Each CWDM/DWDM mux/demux has an insertion loss of $L_{mux/demux} = 3$ dB (based on several specifications for 8 channels CWDM mux/demux and for 8 channel DWDM mux/demux).
- The optical filters used in the RRHs have an insertion loss of $L_{RRH\_filter} = 1$ dB.

For architecture A, a higher attenuation is assumed for the DL than for the UL to cope with the proposed wavelength assignment (sub-section 5.2.2). It is considered that, on average, the DL attenuation is $\alpha_{DL} = 0.4$ dB/km and the UL attenuation is $\alpha_{UL} = 0.2$ dB/km. The power loss budgets for architecture A, for both single fibre and double fibre in the distribution network, are presented in Table 5.4.

Table 5.4 Power loss budget expressions for architecture A.

L_{TOTAL}	**Single fibre**	**Double fibre**
Downlink	$\alpha_{DL} F_{length} + 2\times L_{mux/demux} + L_{coupler} + L_{RRH\_filter}$	$\alpha_{DL} F_{length} + 2\times L_{mux/demux}$
Uplink	$\alpha_{UL} F_{length} + L_{RRH\_filter} + L_{coupler} + 2\times L_{mux/demux}$	$\alpha_{UL} F_{length} + 2\times L_{mux/demux}$

Here, F_{length} represents the length of the fibre between the CU and the RRH, and $L_{coupler}$ represents the insertion loss of a coupler. From Table 5.4 it can be concluded that, in both single and double fibre configurations, the limiting link direction is the DL, given the higher fibre attenuation for the wavelengths used in this direction.

For architecture B, the power loss budget expressions are given in Table 5.5. The same attenuation values as those for architecture A are assumed (sub-section 5.2.2). The splitter loss ($L_{splitter}$) depends on the number of splitting ports. Since the use of a 9 channels CWDM mux/demux is assumed, as well as the use of a single DL wavelength, the splitter should have 8 ports. As discussed in sub-section 5.2.2, optical amplification may be necessary. Therefore,

an optical amplifier with gain G_{amp_opt} = 10 dB is included to make this configuration viable (optical noise is assumed to be already accounted for in the amplifier gain). The losses of electrical filters are not included in these calculations because they are out of the scope of the optical power loss budget.

Table 5.5 Power loss budget expressions for architecture B.

L_{TOTAL}	**Single fibre**	**Double fibre**
Downlink	$\alpha_{DL} F_{length} - G_{amp\_opt} + 2\times L_{mux/demux} + L_{splitter} + L_{coupler} + L_{RRH\_filter}$	$\alpha_{DL} F_{length} - G_{amp\_opt} + 2\times L_{mux/demux} + L_{splitter}$
Uplink	$\alpha_{UL} F_{length} + L_{RRH\_filter} + L_{coupler} + 2\times L_{mux/demux}$	$\alpha_{UL} F_{length} + 2\times L_{mux/demux}$

For architecture C, besides the mux/demux in the CU, an extra optical filter is also required to separate the DL and UL wavelengths that are transmitted over the same mux/demux port. It is assumed that the filter has an insertion loss L_{CU_filter} = 1 dB. Moreover, since all CWDM wavelengths will suffer different fibre attenuations, a worst case α = 0.4 dB/km is assumed in both link directions. The corresponding power loss budget expressions are presented in Table 5.6, which show that the power loss budget is equal for the UL and DL because both UL and DL wavelengths use the same CWDM port and are assumed to experience the same attenuation. However, note that although the optical power loss budget is the same, different requirements may exist for the DL and the UL. In fact, the DL may need higher received power because of the SCM demultiplexing required.

Table 5.6 Power loss budget expressions for architecture C.

L_{TOTAL}	**Single fibre**
Downlink	$\alpha F_{length} + L_{CU\_filter} + 2\times L_{mux/demux} + L_{RRH\_filter}$
Uplink	$\alpha F_{length} + L_{RRH\_filter} + 2\times L_{mux/demux} + L_{CU\_filter}$

Concerning the power loss budget calculations for architecture D, the use of CWDM is assumed, using the entire grid of 16 wavelengths, such that in the worst case, the farthest RRH is reached after a splitting ratio of 1×8 (a set 8 RRHs may be supported by a single CU), while the cases of unbalanced splitting are neglected. In the following, the power loss budget values are obtained only for the worst case scenario, which is the farthest RRH. If it is further assumed that some careful network planning has been applied, and the farthest RRH is served

by the wavelengths that suffer less fibre attenuation, it can be assumed that, in this case $\alpha = 0.2$ dB/km, for both UL and DL. The expressions are presented in Table 5.7.

Table 5.7 Power loss budget expressions for architecture D.

L_{TOTAL}	**Single fibre**
Downlink	$\alpha F_{length} + L_{mux/demux} + L_{splitter} + L_{RRH\_filter}$
Uplink	$\alpha F_{length} + L_{RRH\_filter} + L_{splitter} + L_{mux/demux}$

In architecture E, since DWDM is used, the fibre attenuation is considered to be the same in the DL and the UL, and equal to $\alpha = 0.2$ dB/km. No amplification is considered in the DL, but an extra filter is required to separate the DL and UL wavelengths that are transmitted over the same mux/demux port (periodic), which is assumed to have an insertion loss of $L_{CU\_filter} = 1$ dB. For the UL power loss budget, the parameter G_{RSOA} represents the effective gain of the RSOA affected by the losses incurred in the DL transmission for the wavelength that is intended for UL transmission, and therefore depends on the fibre length. The effective RSOA gain is assumed to be 12 dB (independent of the optical power at its input), which is in accordance to low gain commercial devices. The power loss budget expressions for architecture E are presented in Table 5.8.

Table 5.8 Power loss budget expressions for architecture E.

L_{TOTAL}	**Single fibre**
Downlink	$\alpha F_{length} + L_{CU\_filter} + 2\times L_{mux/demux} + L_{RRH\_filter}$
Uplink	$\alpha F_{length} - G_{RSOA} + L_{RRH\_filter} + 2\times L_{mux/demux} + L_{CU\_filter}$

For a practical design it is necessary to find the relationship between the available power loss budget and the maximum network reach. Therefore, considering the assumptions described above for the different architectures, Figure 5.14 presents the power loss budget obtained for the downlink transmission direction, employing the described formulations, as a function of the fibre length. The solid curves correspond to architectures with a single fibre in the distribution network, whereas the dashed lines represent architectures A and B with double fibres in that segment. Similar results were obtained for the uplink transmission direction, and are presented in Figure 5.15.

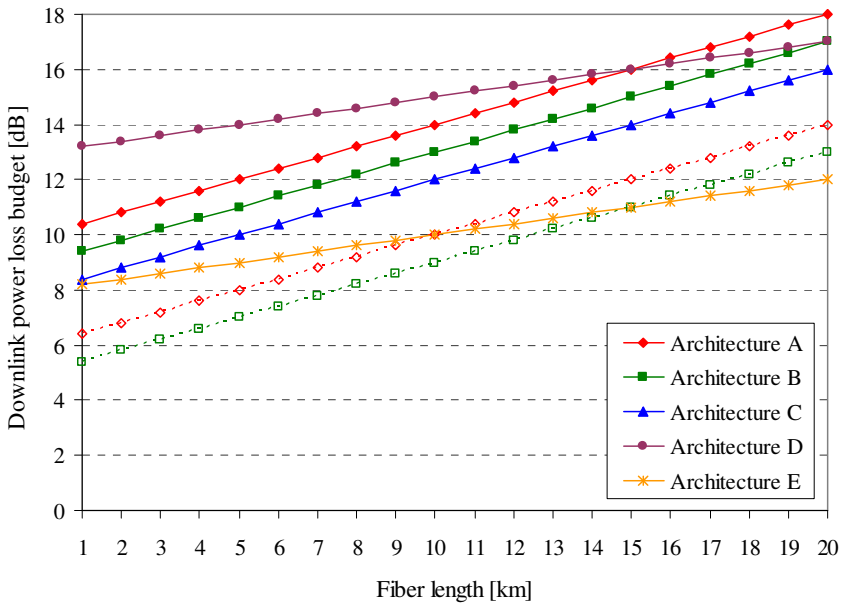

Figure 5.14 – Downlink power loss budget with varying fibre length.

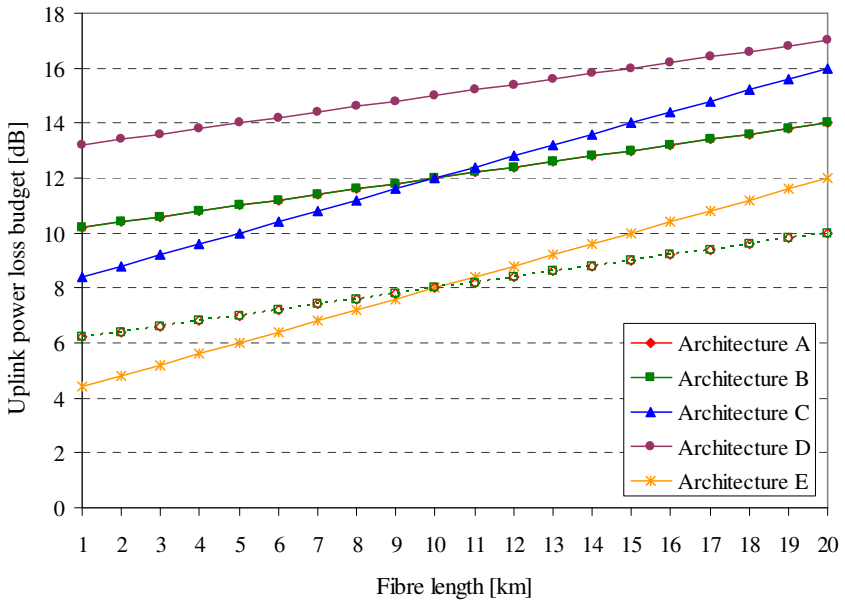

Figure 5.15 – Uplink power loss budget with varying fibre length.

The first conclusion drawn by comparison of Figure 5.14 and Figure 5.15 is that, for the fibre length range considered, the DL is the limiting direction in terms of the power loss budget for architectures A (both single fibre and double fibre configurations) and E, whereas for architectures C and D both directions result in equal power loss budgets. Architecture B, in both single fibre and double fibre configurations, is limited by the UL direction up to a fibre length of 5 km. For longer distances, architecture B becomes limited by the DL direction.

As expected, due to the higher splitting losses, architecture D is shown to be the one requiring a highest power loss budget for the same fibre length. For the UL direction this is the case over the entire range of fibre lengths considered, whereas for DL it is the case only up to 15 km, above which value architecture A (single fibre) becomes more demanding as a result of the higher fibre attenuation considered. Neglecting architectures A and B with double fibres, architecture E is the one demanding the least stringent power loss budget in the downlink. For the uplink direction, architectures A (single fibre) and B (single fibre) present equal power loss budget, as well as architectures A and B with double fibres, but with lower losses.

Note that for architecture B, 10 dB of optical amplification is considered in the downlink. Without optical amplification, this configuration would present a very stringent power loss budget that might even preclude its operability. If more wavelengths are used in the DL, the splitting ratio is reduced for the same number of RRHs, lowering the required optical amplification.

From the opposite perspective, Figure 5.16 and Figure 5.17 present the maximum attainable fibre length, by varying the power loss budget, for DL and UL, respectively. Once again, it is clear that architectures C and D present equal results for both DL and UL directions. Moreover, in the UL, architecture A (single fibre) and B (single fibre) result in equal network reach, as well as architectures A (double fibre) and B (double fibre), which is shown by the overlap of the corresponding curves in Figure 5.17.

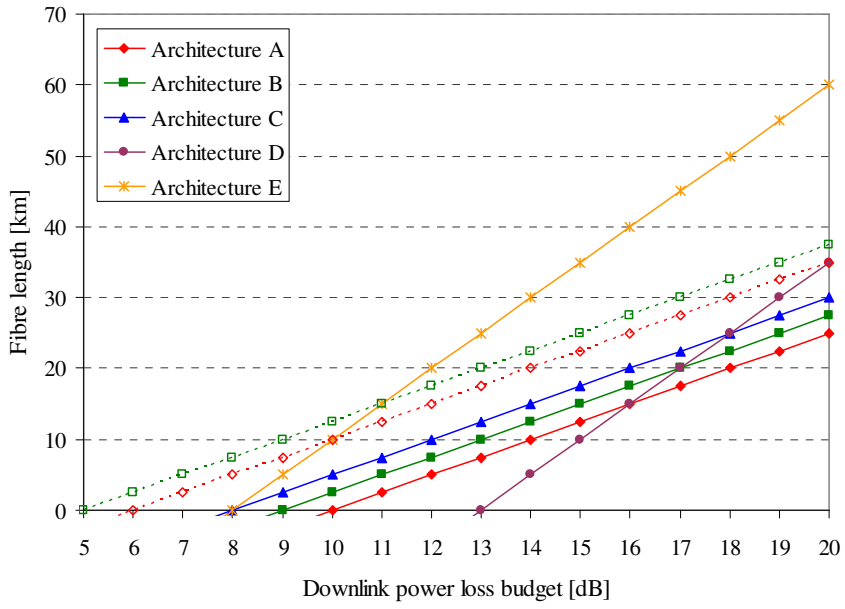

Figure 5.16 – Downlink network reach as a function of the power loss budget.

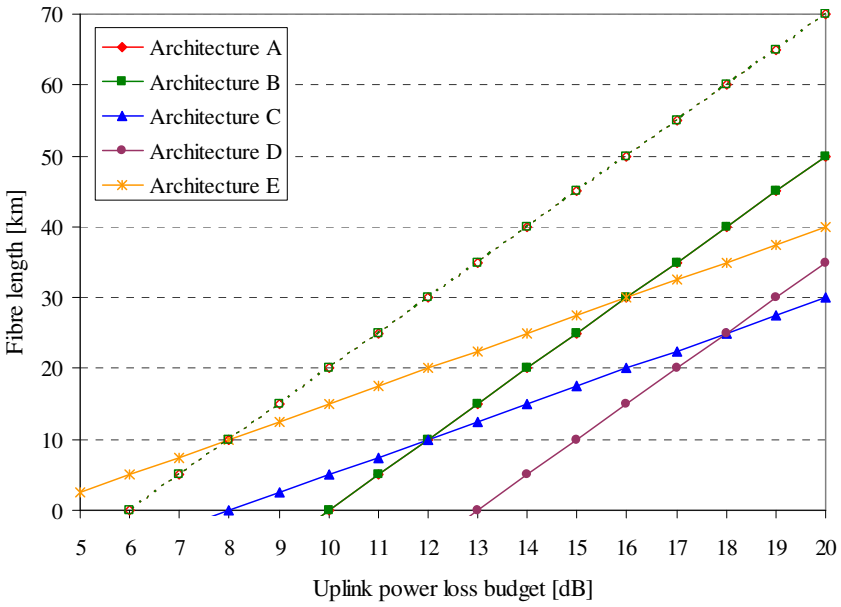

Figure 5.17 – Uplink network reach as a function of the power loss budget.

For an illustrative fibre length of 30 km, the less stringent architecture considering the downlink is option E, which requires a power loss budget of 14 dB. However, for such fibre length, this architecture is limited by the uplink, requiring a power loss budget of 16 dB for the same distance. The most stringent architecture for downlink for a reach of 30 km is architecture A (single fibre), requiring a power loss budget higher than 20 dB. Contrarily to the case of architecture E, for architecture A the downlink is the limiting direction, since the necessary power loss budget in the uplink for the same target distance is 16 dB. In the uplink, a network reach of 30 km requires 19 dB power loss budget for architecture D (most stringent case), 20 dB for architecture C, and around 16 dB for architectures A (single fibre), B (single fibre) and E. The double fibre architectures are less stringent requiring only around 12 dB power loss budget for a network reach of 30 km.

Note that, if an optical amplifier is used in the DL of architecture E, the network reach may be considerably increased and the cost of the system would probably not increase much. Moreover, more sub-channels may eventually be supported by each wavelength, justifying the cost increase. It is worth noting that with the UL being the limiting direction for this configuration, performance is dependent on the gain provided by the RSOA.

5.2.4. Comparative Economical Analysis

An economical comparison of the proposed candidate architectures is also important in determining which is most suitable, since the use of low-cost systems is one of the goals for all access networks. In the following analysis, architecture A is considered to be the reference scenario, and the definitions used in the following calculations are introduced in Table 5.9, considering that *M* represents the number of RRHs supported.

Table 5.9 Definitions used in the economical analysis.

Parameter	Definition
$C_{\text{CWDMlaser}}$	Cost of a CWDM laser
$C_{\text{DWDMlaser}}$	Cost of a DWDM laser (very low wavelength drift and temperature control)
C_{WBfilter}	Cost of a wide band filter
C_{NBfilter}	Cost of a narrow band filter
$C_{\text{mux/demux}(x)}$	Cost of a CWDM mux/demux with *x* ports
C_{PSC}	Cost of a splitter/coupler (considered independent of the number of ports)
$C_{\text{electFilter}}$	Cost of an electrical filter
C_{port}	Cost of a single mux/demux port
$C_{\text{amplifier}}$	Cost of an optical amplifier (to be used with CWDM wavelengths)
C_{OADM}	Cost of a OADM

The cost of fibre-optic architecture A is then given by:

$$C(\text{A}) = 2C_{\text{mux/demux}(2M)} + M \cdot C_{\text{PSC}} + 2M \cdot C_{\text{CWDMlaser}} + 2M \cdot C_{\text{WBfilter}} \,. \tag{5.1}$$

Since architecture A is assumed to be the reference, it is necessary to determine the relative cost of each of the remaining architectures to realize the comparison. The cost of architecture B is given by:

$$\begin{aligned} C(\text{B}) = {} & C_{\text{mux/demux}(M+n_{\text{DL}})} + n_{\text{DL}} \cdot C_{\text{PSC}} + M \cdot C_{\text{PSC}} + n_{\text{DL}} \cdot C_{\text{CWDMlaser}} + \\ & + M \cdot C_{\text{CWDMlaser}} + 2M \cdot C_{\text{WBfilter}} + (M \cdot n_{\text{DL}}) C_{\text{electFilter}} \end{aligned} \,. \tag{5.2}$$

After some manipulations, and assuming that the cost of the mux/demux is proportional to the number of ports x, that is $C_{\text{mux/demux(x)}} = x\, C_{\text{port}}$, it is found that architecture B is less expensive than architecture A (C(B) < C(A)) if the following is true:

$$\begin{aligned} & n_{\text{DL}} \cdot C_{\text{PSC}} + \left(M \cdot n_{\text{DL}}\right) C_{\text{electFilter}} < 2\left(M - n_{\text{DL}}\right) C_{\text{port}} + \left(M - n_{\text{DL}}\right) C_{\text{CWDMlaser}} \\ & \Rightarrow C_{\text{PSC}} + M \cdot C_{\text{electFilter}} < \frac{M - n_{\text{DL}}}{n_{\text{DL}}} \left(2C_{\text{port}} + C_{\text{CWDMlaser}}\right) \end{aligned} , \qquad (5.3)$$

showing that the economical viability of architecture B depends on the number of wavelengths it requires in the DL. That is, if a high number of sub-channels can be transported in a single DL wavelength, architecture B becomes more attractive than A.

Considering now architecture C and assuming that, for cost comparison purposes, equal sized mux/demux are used in both architectures A and C, despite the number of RRHs supported by architecture C, M_{max}, being twice that of architecture A, the cost of architecture C is given by:

$$C(\text{C}) = 2C_{\text{mux/demux}} + M \cdot C_{\text{CWDMlaser}} + M \cdot C_{\text{DWDMlaser}} + 2M \cdot C_{\text{NBfilter}} . \qquad (5.4)$$

After some manipulations, architecture C is found to be less expensive than architecture A, that is, C(C) < C(A), if:

$$C_{\text{DWDMlaser}} + 2C_{\text{NBfilter}} < C_{\text{DWDMlaser}} + 2C_{\text{WBfilter}} + C_{\text{PSC}} . \qquad (5.5)$$

It is unlikely that architecture C will be less expensive than architecture A, given the expected additional costs of narrowband filters and better lasers. However, architecture C has a longer reach without optical amplification and, more importantly, can support twice the number of RRHs. Consequently, for $9 \leq M \leq 16$, the cost of architecture C should be compared with that of the (expectedly) more expensive architecture E.

In order to determine the cost of architecture D, it is firstly assumed that it is deployed using power splitters with a CWDM scheme. As a result, its cost is given by:

$$C(\text{D}) = M \cdot C_{\text{PSC}} + 2M \cdot C_{\text{CWDMlaser}} + 2M_{\text{CWDfilter}} + M \cdot C_{\text{amplifier}} . \qquad (5.6)$$

Architecture D is less expensive than architecture A ($C(\mathrm{D}) < C(\mathrm{A})$), when:

$$M \cdot C_{\text{amplifier}} < 2C_{\text{mux/demux}} \,. \tag{5.7}$$

In the alternative where an OADM is used at the splitting points to reduce losses, the cost of architecture D becomes:

$$C(\mathrm{D}) = M \cdot C_{\text{OADM}} + M \cdot C_{\text{PSC}} + 2M \cdot C_{\text{CWDMlaser}} + 2M \cdot C_{\text{WBfilter}} \,. \tag{5.8}$$

In this second case, architecture D becomes less expensive than architecture A if:

$$M \cdot C_{\text{OADM}} < 2C_{\text{mux/demux}} \,. \tag{5.9}$$

The architecture D, when employing power splitters and CWDM, is expected to be more expensive than architecture A, since the cost of the required optical amplifiers is higher than the cost of the two mux/demux. The same conclusion may be extended to the case where DWDM is used, since higher cost lasers will be required, even using a single optical amplifier. The alternative with DWDM and OADMs is also expected to be more expensive than architecture A, for similar reasons.

Architecture E, which is based on DWDM equipment, is expected to be less economical than architecture A, since these components are more expensive than CWDM. On the other hand, architecture E supports a larger number of RRHs per CU than architecture A, increasing the sharing degree of the infrastructure costs.

From this analysis, and in view of the fact that CWDM technology requires less-expensive and uncooled electro-optical components, it is clear that the use of this technology will allow the deployment of a lower cost system. However, a trade-off is always necessary regarding the capacity provided by CWDM, which is considerably lower than that provided by DWDM, as previously referred.

5.2.5. Support of Legacy Systems

Together with the coexistence with wired services, the support of legacy wireless systems in addition to the 4G wireless systems over the same infrastructure may be of critical importance for the successful deployment of future DAS. Therefore, it is necessary to consider this

coexistence when designing the fibre-optic infrastructures, since additional resources may be necessary. There is strong motivation for the operators for future DAS networks to support legacy technologies, as their interest in deploying 4G systems may be conditioned by the possibility of maintaining current services, while using the same physical infrastructure for both. As a result, the fibre-optic infrastructure should provide the required resources to simultaneously support legacy and new technologies, thereby decreasing OPEX since the infrastructure is shared.

Typically, the legacy wireless systems do not demand as high capacity as 4G systems, since they use transmission channels with less bandwidth. Therefore providing an entire wavelength per RRH (per link direction) for legacy systems may represent a significant waste of resources. A more suitable approach would be to share the wavelengths per several RRHs, separating the services and the antennas using SCM. Several options may be addressed for the deployment of additional wavelengths needed for legacy systems, namely the use of WDM or Space Division Multiplexing (SDM), by deploying additional fibres. The selection of the most suitable option depends on the required legacy capacity per RRH and also on the percentage of RRHs that need to support legacy systems.

If SDM is selected as the multiplexing technology to support legacy systems over a future DAS network, a duplication of the entire fibre plant infrastructure is required, in the case where all RRHs support legacy systems. Since with this solution two completely independent networks will be necessary for 4G and for legacy systems, the considerations made for one of these networks do not affect the other. Consequently, the network for legacy systems will provide high capacity for all RRHs connected to the same CU (a dedicated wavelength per RRH is available), at the expense of increasing the necessary amount of fibre, and the number of transmitting/receiving equipment and network devices, when compared to a single 4G-dedicated network. This will obviously incur higher costs for the entire system.

When compared to SDM, using a multiplexing scheme based on wavelength division may be a less expensive alternative, since it does not require the duplication of the network fibre plant. Moreover, this option allows the optimization of the wavelength capacity. Two options may be envisioned:

- Support of legacy systems with two additional wavelengths (one UL and one DL), that are multiplexed with the 4G wavelengths, using CWDM or DWDM. Each of these additional wavelengths supports the legacy signals for all RRHs using SCM. If CWDM is used (in a configuration described by architecture A) the following relation

holds for the maximum number of RRHs (M_{max}) supported by the same processing unit within the CU:

$$2M_{max} + 2 \leq 16 \Rightarrow M_{max} \leq 7 . \quad (5.10)$$

- In a scenario where L RRHs ($L < M_{max}$) require the capacity of an entire wavelength for legacy systems, $2L$ additional wavelengths are necessary, and may be multiplexed with 4G wavelengths employing CWDM or DWDM. In the CWDM case, the following relation holds, showing that a very reduced number of RRHs may be supported with a single CU:

$$2M_{max} + 2L \leq 16 \Rightarrow M_{max} + L \leq 8 . \quad (5.11)$$

Among all the architectures previously discussed those that are proposed for the simultaneous support of 4G and legacy wireless systems are presented in Table 5.10, where a justification for each case is provided. Note that CWDM architectures are neglected because, following from (5.10) and (5.11), the number of available wavelengths is expected to be insufficient to support both next generation and legacy systems in a cost-effective manner.

Table 5.10 Selected configurations, considering simultaneous support of next generation and legacy wireless systems.

Multiplexing Scheme	**Selected Architecture**	**Justification**
SDM	-	The use of SDM does not limit the selection of any of the configurations, since two different networks will be deployed for 4G and for legacy systems.
WDM	D	Architecture D is a possible option, but only with OADMs (the larger losses of the power splitters prevent the support of a high number of RRHs); DWDM should also be selected, since it provides a larger number of optical channels (wavelengths).
	E	Architecture E, while also providing a large number of wavelengths, may be preferred over architecture D with OADMs and DWDM, assuming that the components maturity and cost enable this choice.

5.3. Signal Transmission over Distributed Antenna System

After the extensive study of the topologies and architectures for deploying a DAS network, presented in section 5.2, this section is devoted to the analysis of the different optical link types, focusing on the analogue and digital approaches. Nowadays, the large majority of deployed systems are digital, both in telecommunications and data networks. However, the number of applications based on analogue optical fibre links has been growing, such as the case of some future wireless services supported by a DAS network.

Currently, two protocols are specified for digital radio networks where the radio head is supported remotely, namely the Common Public Radio Interface (CPRI) [CPR] and the Open Base Station Architecture Initiative (OBSAI) [OBS]. These protocols, covering 3G and 4G technologies, specify a digitized and serial interface between a base station location, where the baseband processing functions are placed, and a RRH, which contains all the radio functions of a conventional base station. However, higher cell throughput in future wireless systems with channel bandwidths wider than 20 MHz (which is the maximum value specified for LTE) demands each RRH to support several sectors with Multiple-Input Multiple-Output (MIMO) channels, requiring the use of several antennas.

A promising alternative is to use analogue RoF [KLN+08], which allows for the use of less complex and more energy efficient RRHs. The implementation of a RoF network allows concentrating all switching, multiplexing, and processing functionalities at the CU, using the optical fibre to transparently transport the radio signals to/from multiple remote antennas. Therefore, and contrarily to the use of digital interfaces, this allows the remote antenna sites to perform only optical-electrical conversion, filtering and amplification of radio signals.

In the following, further insight will be provided on the use of analogue or digital approaches, pointing out their main characteristics, benefits and disadvantages.

5.3.1. Analogue Signal Transmission

Radio-over-Fibre emerged a few decades ago, but until now it did not have a widespread adoption [KLN+08]. Besides CATV transmissions using HFC systems, RoF was not the technology of choice. However, the new wireless architectures and required capacity will greatly benefit from using RoF, in terms of simplicity and cost [CLU+07]. The progress in the

development of optical components enables the design of a RoF system capable of transporting RF signals with advanced multilevel modulation formats over significant distances, thereby enabling its use in any next generation DAS network [MSL+09].

The definition and characterization of the optical link is very important in RoF systems. The simplest implementation of an optical link includes a modulator device, at the input end, responsible for modulating the optical carrier with the electrical signal, followed by an optical fibre that delivers the optical signal to a photodetector, which recovers the electrical signal. The analogue optical links are typically characterized by their transparency to the format of the signals, although limited by additional noise and distortion [Cox04].

Intensity modulation of the optical carrier used for signal transmission, followed by directed detection at the end side of the link, is the common choice for RoF applications. The simplest intensity modulation technique consists on directly modulating a laser with the electrical signal, to change its output power. Due to their narrow spectral linewidth, low noise and high linearity, DFB lasers are typically selected to act as DML for high-performance analogue optical links. The laser slope efficiency represents the efficiency with which the RF-modulation current is converted to modulated optical power. The gain of the analogue link is therefore dependent, among other parameters, on the laser slope efficiency. The RIN, typical of semiconductor lasers, is caused mainly by spontaneous emission.

An alternative to direct modulation is external modulation, where a laser operates in CW mode and an external device is responsible for intensity modulating the laser output power. This option is not limited by the modulation bandwidth of the laser, as with direct modulation, allowing it to be used in applications demanding higher bandwidth. Amongst the possible implementations of external modulation, the preferred one employs a Mach-Zehnder Modulator (MZM). The MZMs are based on the electro-optic effect, to change the phase of the input optical field, and use an interferometer to convert the phase change into an intensity variation.

Usually, in typical analogue optical fibre links, signal distortion is caused mainly by the modulating device, rather than the photodetector or the fibre. Signal distortion leads to the creation of new frequencies in the form of harmonics and intermodulation products [Cox04]. The transfer of RF signal power to these new frequencies not only reduces the efficiency of the optical link, but also causes interference with other RF signals, in multi-channel systems. Many linearization techniques were proposed to mitigate the effects of distortion [FS02], [SJ03], [LKH+08], which are particularly relevant for externally modulated links.

The concept of SCM, commonly used in RoF links, and already briefly introduced in previous sub-sections, is based on the transmission of multiple signals multiplexed in the frequency domain and transported by a single optical carrier. This multiplexing scheme allows increasing significantly the capacity of an optical fibre transmission system, benefiting from the fact that microwave devices are more mature than optical devices, which enables the use of very stable and highly selective filters. An electrical channel may be transmitted through the optical link at baseband, at an intermediate frequency, or at the radio frequency used in the wireless transmission. In a DAS RoF network with simplified remote antennas, the two first options require local oscillators to be placed in the remote sites, to perform electrical up-conversion of the signals, which may be considered necessary to support many wireless protocols. In this scenario, the relaxation oscillation of the light source (typically a DML) may be limitative, which can be mitigated by using an optical injection locking method of the light source [YB97]. In spite of the capacity increase, SCM may be limited by nonlinearities. In the case of simultaneous transmission of baseband and SCM, it may be required to shape the baseband pulses in order to decrease interference with the sub-carriers.

One of the main drawbacks of analogue transmission, when compared to digital, is its dynamic range, due to the relative immunity of the digital signal to noise and distortion, when compared to an analogue signal. In digital transmission, the dynamic range is unaffected by the losses incurred in the transport infrastructure (optical fibre, splitters, etc.) and, therefore, a digitized system can reach longer distances. On the other side, analogue transmission is shown to enable low-cost and low-maintenance high-performance links [ABB+08], [WNG09]. Moreover, for analogue optical links the propagation delay is simply given by the speed of light in the fibre and the fibre length, whereas in digital links additional delays are typically incurred in the digitization process.

A more detailed description of the design and characterization of an analogue optical link is provided in section 6.2, with special emphasis on externally modulated links.

5.3.2. Digital Signal Transmission

The digital transport of radio signals involves the use of digital interfaces in the base stations or central units, and in the RF modules, placed at the remote antenna sites. In order to minimize the cost of wireless systems, vendor-driven open standards for base stations were developed. This open standardization has several advantages, such as lower R&D costs,

shorter time-to-market, improved innovation and lower pressure on pricing, driven by the increased competition among component suppliers, and also a faster evolution of the enabling technologies. In response to the challenge of delivering open base stations, two industry initiatives have been formed to develop such specifications. Their aim was to create a wireless infrastructure in which RRHs can be deployed in a flexible and cost-effective manner, thereby enabling a widespread adoption.

OBSAI [OBS] was started in 2002, and aimed to define an open, standardized internal modular structure for wireless base stations. It defines a set of Base Transceiver Station (BTS) modules, as well as the digital interfaces between BTS modules, assuring in this way interoperability and compatibility between different vendors and manufacturers. This standardized BTS modular structure allows easy scalability for small to large capacity configurations. The second industry initiative, CPRI [CPR], was initiated as a response to OBSAI, in 2003. The goal of CPRI is to define a publicly available specification for the key internal interface of radio base stations, between the Radio Equipment Control (REC) and the Radio Equipment (RE) subsystems. Unlike OBSAI, CPRI does not specify mechanical or electrical interface requirements and has a much narrower focus. While OBSAI defines the three major interfaces in a BTS, namely RP1 for clock and synchronization information, RP2 for exchange of user data information to/from the baseband module, and RP3 to interchange formatted air interface user and signalling data, CPRI focuses solely on the link between the RF module and the baseband module in the BTS. Both these initiatives define a PtP interface between the baseband and the RF module. The use of this digital interface provides the necessary flexibility to either co-locate these two modules within a single enclosure or remotely locate the RF modules from the baseband module in a distributed topology. For more details see Appendix D.

The use of digital baseband signals requires high capacity channels, resulting in significant bandwidth consumption. This may be a weak point for DAS systems, since more ports, or higher capacity ports, will be required at the transmitting and receiving ends of the network. However, using digital transmission, the performance of the optical link will depend only on aspects such as the optical modulation formats employed, the transmission power, and the fibre nonlinear effects. Moreover, transceivers that are currently massively produced may be used for digital transmission of RF signals, eventually decreasing the cost and increasing the interoperability between manufacturers.

The digital optical links do not impair the RF performance of the overlaying radio system, and therefore the characterization of this link type should be based on the parameters typically employed to characterize a digital transmission system (transmission data rate, BER, etc.). In the following, the analysis will be based on the transmission data rate required to carry next generation wireless channels, which enables, when necessary, to determine how many standard transmission links (e.g. 10 GbE, 40 GbE) are necessary in a specific scenario.

Different operating line rates are currently specified for both OBSAI and CPRI links, as shown in Table 5.11, indicating that the maximum line rate for OBSAI is 6144 Mbit/s, whereas for CPRI is 9830.4 Mbit/s, which is considered to be adequate for WiMAX and LTE systems with channel bandwidth up to 20 MHz. The CPRI line rates have been selected in such a way that the basic UMTS chip rate, $f_c = 3.84$ Mbit/s, can be easily recovered, considering the 8b/10b line coding.

Table 5.11 Specified line rates for OBSAI and CPRI links.

Protocol	Specified line rates
OBSAI	768 Mbit/s, 1536 Mbit/s, 3072 Mbit/s, 6144 Mbit/s
CPRI	614.4 Mbit/s, 1228.8 Mbit/s, 2457.6 Mbit/s, 3072 Mbit/s, 4915.2 Mbit/s, 6144 Mbit/s, 9830.4 Mbit/s

In the following, the capacity of OBSAI and CPRI links in terms of antenna-carriers (AxC) is derived. One AxC is defined as the amount of digital baseband IQ (In-phase and Quadrature) data necessary for either reception or transmission of only one carrier at or from one independent antenna element. This derivation considers 3072 Mbit/s and 6144 Mbit/s line rates for both protocols, and 9830.4 Mbit/s data rate for CPRI. The first two are selected in order to enable a comparison between the capacity of both protocols, and the late one is included because it is the most interesting case in terms of supported capacity. Moreover, this analysis focuses on the use of WiMAX (assuming the use of Orthogonal Frequency-Division Multiple Access, OFDMA) and LTE. Channel bandwidths of 5 MHz, 10 MHz and 20 MHz are considered for both wireless technologies.

For OBSAI line rates, the maximum number of AxC that are supported by each link is presented in Table 5.12, for WiMAX and LTE protocols. These values were obtained directly from the OBSAI specification, version 4.2 [OBS].

Table 5.12 Number of Antenna-Carriers (AxC) supported by an OBSAI link.

OBSAI line rate	802.16 OFDMA (WiMAX)		LTE	
	Channel Bandwidth	Maximum Number of AxC	Channel Bandwidth	Maximum Number of AxC
3072.0 Mbit/s	5 MHz	10	5 MHz	8
	10 MHz	5	10 MHz	4
	20 MHz	2	20 MHz	2
6144.0 Mbit/s	5 MHz	21	5 MHz	16
	10 MHz	10	10 MHz	8
	20 MHz	5	20 MHz	4

For CPRI, and according to its specification version 4.2 [CPR], identical parameters may be obtained, since they are not directly available. Starting by the identification of the size of each digital baseband IQ data block [CPR], the values presented in Table 5.13 are determined.

Table 5.13 Size of CPRI IQ data blocks for each line rate.

CPRI line rate	3072 Mbit/s	6144 Mbit/s	9830.4 Mbit/s
IQ data block size	600 bits	1200 bits	1920 bits

With CPRI, the I and Q sample width (M_{IQ}) depends on the application layer and ranges between 8 to 20 bits in the downlink and between 4 to 20 bits in the uplink. Since OBSAI uses $M_{IQ} = 16$ bits (32 bits for one IQ sample), for both uplink and downlink, the same value is used here to determine the number of AxC supported with CPRI. Moreover, CPRI also specifies the use of AxC containers, which are mapped into the IQ data block of the CPRI basic frame. Each AxC container has exactly n IQ samples from the same AxC, where n represents the oversampling ratio with respect to the chip rate. Therefore, for LTE the size of each AxC container (N_{AxC}) is given in Table 5.14, for the different channel bandwidths.

Table 5.14 Size of the CPRI AxC container for LTE protocol, with M_{IQ} = 16 bits.

LTE channel bandwidth	**5 MHz**	**10 MHz**	**20 MHz**
Oversampling ratio (n)	2	4	8
AxC container size (N_{AxC})	64 bits	128 bits	256 bits

Contrarily to LTE, the case of WiMAX involves the selection of a mapping method. CPRI specifies three different methods for mapping WiMAX, namely the IQ sample method, the WiMAX symbol based method and the backward compatible method [CPR]. Hereafter the first method is assumed, where the size of the AxC container is given by:

$$N_{\mathrm{AxC}} = 2 \cdot \mathrm{ceil}\left(\frac{M_{\mathrm{IQ}} f_{\mathrm{s}}}{f_{\mathrm{c}}} \right), \tag{5.12}$$

where f_{s} represents the sampling frequency, which is equal to 5.6 MHz, 11.2 MHz and 22.4 MHz for channel bandwidths of 5 MHz, 10 MHz and 20 MHz, respectively [WiM08].

Based on the preceding assumptions, Table 5.15 summarizes the maximum number of AxC supported by each CPRI link, for both WiMAX and LTE protocols. This is obtained by finding how many AxC containers can be mapped into an IQ data block.

Table 5.15 Number of Antenna-Carriers (AxC) supported by a CPRI link.

CPRI line rate	**802.16 OFDMA (WiMAX)**		**LTE**	
	Channel Bandwidth	Maximum Number of AxC	Channel Bandwidth	Maximum Number of AxC
3072.0 Mbit/s	5 MHz	12	5 MHz	9
	10 MHz	6	10 MHz	4
	20 MHz	3	20 MHz	2
6144.0 Mbit/s	5 MHz	25	5 MHz	18
	10 MHz	12	10 MHz	9
	20 MHz	6	20 MHz	4
9830.4 Mbit/s	5 MHz	40	5 MHz	30
	10 MHz	20	10 MHz	15
	20 MHz	10	20 MHz	7

An interesting figure in the dimensioning of a digital system is the number of links that is necessary to deploy. Consequently, considering the capacity of the OBSAI and CPRI links presented above in Table 5.12 and Table 5.15, respectively, it is possible to determine how many of these links are necessary per each RRH, in a scenario where several antennas are placed within the same RRH, to benefit from covering a larger area or to employ MIMO techniques in order to improve the system performance.

Assuming that each antenna is served by a single AxC, the number of OBSAI and CPRI links necessary to serve a RRH with multiple antennas is presented in Figure 5.18 and Figure 5.19, for WiMAX and LTE systems, respectively. For both cases, a channel bandwidth of 20 MHz is considered, since it is the most demanding. Similar conclusions are retrieved for 5 MHz and 10 MHz, and the corresponding graphics are presented in Appendix E. Note that each OBSAI or CPRI link is defined as unidirectional, and therefore this analysis is focused only on one transmission direction. To consider both, the necessary capacity needs to be doubled. Furthermore, some links may be underutilized, whenever the link capacity is not a sub-multiple of the number of required antennas per RRH, which is also represented in Figure 5.18 and Figure 5.19, enabling a visual representation of the efficiency in each case.

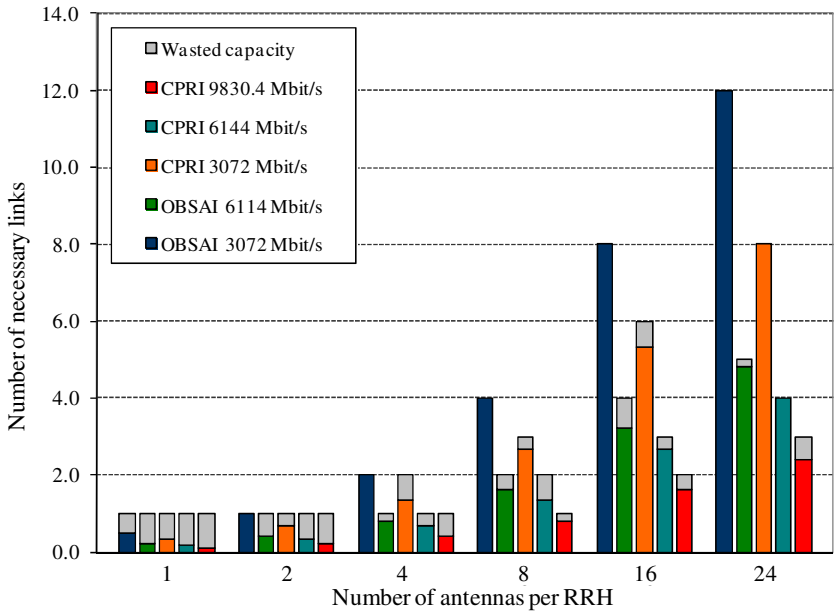

Figure 5.18 – Number of necessary OBSAI and CPRI links to support multiple antennas per RRH, for a WiMAX system with channel bandwidth of 20 MHz.

As expected, for both WiMAX and LTE systems, the use of high line rates, as those considered (above 3072 Mbit/s), results in a very low resource utilization, when only a single antenna is to be served. This conclusion is even more significant for lower channel bandwidths, where the wasted link capacity is equal or larger than 50%, not justifying the use of these line rates. In this particular case, it is therefore recommended to use a lower line rate, specified for both OBSAI and CPRI, as presented in Table 5.11.

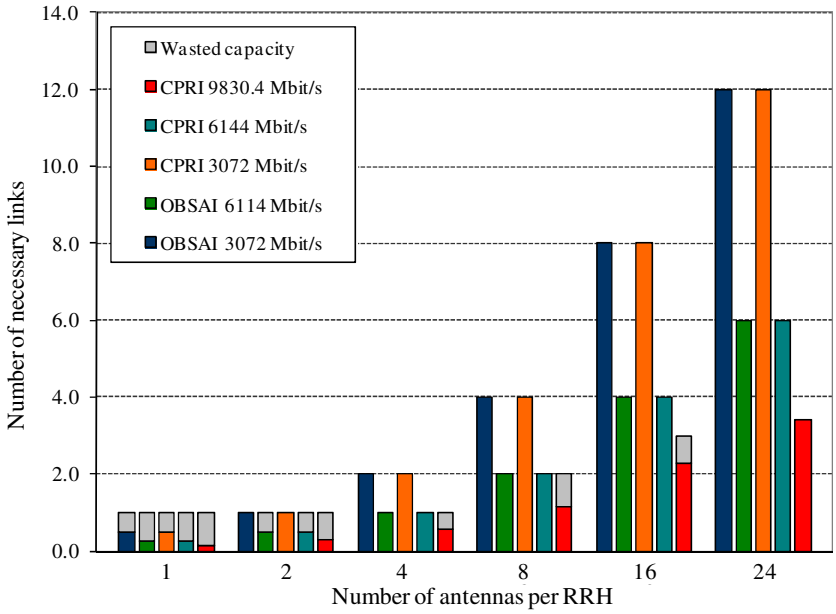

Figure 5.19 – Number of necessary OBSAI and CPRI links to support multiple antennas per RRH, for a LTE system with channel bandwidth of 20 MHz.

In general, for the same line rate, CPRI requires less capacity than OBSAI to serve the same number of antennas per RRH. This is patent in the results for 20 MHz channel bandwidth, particularly for the WiMAX case. Here, it is shown that a low number of links may be employed to serve RRHs with 8, 16 and 24 antennas, for both 3072 Mbit/s and 6114 Mbit/s line rates. As a consequence, in some situations, the use of CPRI results in higher wasted capacity than that for OBSAI, in spite of requiring less links. Similar conclusions may be drawn from the results for 5 MHz and 10 MHz channel bandwidths.

When comparing the support of WiMAX and LTE, it is shown that the LTE mapping is better adapted to the link capacities, resulting in lower wasted capacities. This is more evident if the number of antennas to be supported is larger. Note that the support of 24 antennas per RRH in the case of LTE results in an optimum resource utilization, since there is no wasted capacity, using either OBSAI or CPRI protocols.

This analysis should be extended to address the possible requirements of future wireless systems. It is expected that the channel bandwidths will keep increasing, reaching 100 MHz in a near future. Therefore, the known sample rate values for WiMAX and LTE were extrapolated, and Table 5.16 presents the approximate bit rate (unidirectional) for channel bandwidths of 100 MHz, obtained using the assumptions described above.

Table 5.16 Bit rate for WiMAX and LTE for channel bandwidths up to 100 MHz.

Channel Bandwidth	**802.16 OFDMA (WiMAX)**		**LTE**	
	Sample rate [Msample/s]	Bit rate, with M_{IQ} = 16 [Mbit/s]	Sample rate [Msample/s]	Bit rate, with M_{IQ} = 16 [Mbit/s]
5 MHz	5.6	179.2	7.68	245.76
10 MHz	11.2	358.4	15.36	491.52
20 MHz	22.4	716.8	30.72	983.04
100 MHz	112.0	3584.0	153.60	4915.20

The bit rate values for LTE and WiMAX show that LTE requires 33% more capacity than WiMAX. Therefore, for a channel bandwidth of 100 MHz, a bit rate of 4915.20 Mbit/s is obtained for LTE and a bit rate of 3686.40 Mbit/s is obtained for WiMAX. These differences are justified by the higher sample rate necessary for LTE. This protocol specifies a sample rate multiple of the UMTS basic sampling frequency (3.84 MHz), while WiMAX requires a lower sampling frequency. As can be seen by the large difference between the bit rate obtained in both cases for the same channel bandwidth of 100 MHz, a very important factor to predict the future necessary capacity is the expected sampling frequency for the technologies being developed, since it significantly impacts the bit rate. If OBSAI or CPRI is intended to be used for a channel bandwidth of 100 MHz, the lower line rate that is suitable is 6144 Mbit/s. OBSAI or CPRI links with this capacity may eventually carry a single channel with 100 MHz bandwidth, whereas a CPRI link with 9830.4 Mbit/s may carry up to two channels (note that the values in Table 5.16 indicate the information bit rate, and do not consider any type of protocol overheads).

The analysis presented above allows concluding that the transport of digital baseband signals requires high capacity channels. This significant bandwidth consumption may impair the deployment of digital baseband in low cost DAS networks, since more ports, or higher capacity ports, are required in both transmitting ends of the system. On the other side, the transceivers that are massively produced for all digital transmission systems may be used for digital transmission of RF signals, eventually decreasing the cost and increasing the interoperability between manufacturers, also benefiting from the development of compliant base stations employing either OBSAI or CPRI. Moreover, the performance of these optical links has been thoroughly studied in terms of optical modulation formats and fibre nonlinearities, which is advantageous for their design and deployment.

5.3.3. Mapping Radio Signals over Passive Optical Networks

The use of a PON infrastructure to interconnect the RRHs seems to be a very appealing approach. The wireless systems require reliable and inexpensive networks to transmit the information between the RRHs and the baseband module located in a central station, and the PONs are simple and economical when compared to other alternatives. Hence, the transmission of wireless information over a PON infrastructure is expected to be a very profitable approach, allowing the deployment of a distributed network of RRHs, benefiting from the fact that the PON is an inherently centralized system. In this way, one baseband module supporting multiple RRHs matches the hierarchical structure of PONs, with one OLT serving multiple ONUs. Moreover, using the deployed PON systems, the same fibre infrastructure may be shared between wireless and fixed networks, optimizing fibre deployment and consequently enabling additional cost savings.

When comparing the standards for PON systems, several differences are evident, including the data rate, the transmission protocols and the bandwidth efficiency [LSK06]. GPON systems operate at data rates up to 1244 Mbit/s in the uplink and 2488 Mbit/s in the downlink, using a Generic Encapsulation Method (GEM) for layer 2 framing, where each frame supports a maximum payload size of 4095 bytes [ITU05]. These characteristics result in a bandwidth efficiency around 94%, for both uplink and downlink. On the other hand, the 1G EPON standard released in 2004 [IEEE04] supports symmetric line rates of 1.25 Gbit/s and employs 8b/10b line coding. The use of Ethernet framing is specified for 1G EPON, with a maximum payload size of 1500 bytes. The use of line coding and a higher control message overhead result in lower bandwidth efficiencies for 1G EPON, namely ~73% for the downlink and ~69% for the uplink. More recently, IEEE released the 10G EPON standard [IEEE09] which specifies new systems operating at 10.3125 Gbit/s line rates, using 64b/66b line coding, and also employing Ethernet framing. In this case, since 64b/66b is more efficient than 8b/10b, a bandwidth efficiency around 96% is obtained for 10G EPON.

In order to evaluate the suitability of PON standards for the transport of digital radio data, it is necessary to determine how OBSAI/CPRI bit streams can be mapped over PON protocols. Therefore, Table 5.17 presents the number of OBSAI/CPRI bit streams that may be transported by each type of PON system. The PON effective bandwidth usage in each case, considering the bandwidth efficiency, is also indicated.

Table 5.17 OBSAI/CPRI bit streams over PON systems.

PON Systems		OBSAI		CPRI	
Type	**Bandwidth efficiency**	**# bit streams**	**PON effective bandwidth usage**	**# bit streams**	**PON effective bandwidth usage**
1G EPON 1.25 Gbit/s	~69% (worst case)	1 x 768 Mbit/s	89.04 %	1 x 614.4 Mbit/s	71.23 %
GPON 2.488 Gbit/s	~94 %	3 x 768 Mbit/s	98.52 %	3 x 614.4 Mbit/s	78.81 %
		1 x 1536 Mbit/s	65.68 %	1 x 1228.8 Mbit/s	52.54 %
10G EPON 10.3125 Gbit/s	~96 %	12 x 768 Mbit/s	93.09 %	16 x 614.4 Mbit/s	99.30 %
		6 x 1536 Mbit/s	93.09 %	8 x 1228.8 Mbit/s	99.30 %
		3 x 3072 Mbit/s	93.09 %	4 x 2457.6 Mbit/s	99.30 %
		1 x 6144 Mbit/s	62.06 %	3 x 3072.0 Mbit/s	93.09 %
		–	–	1 x 6144.0 Mbit/s	62.06 %
		–	–	1 x 9830.4 Mbit/s	93.09 %

From the values presented in Table 5.17, the potential data rate mismatch with the rates supported by standard PON systems is clear. In fact, GPON will only support the two lower OBSAI/CRPI line rates, with a low bandwidth usage, whereas 1G EPON will only support the lowest OBSAI/CPRI line rate. Only next generation EPON systems, operating at 10 Gbit/s, will have the capacity required to support all line rates defined for OBSAI/CPRI. Importantly, both GPON and EPON frames are not large enough to carry a single OBSAI/CPRI master frame [OBS], [CPR]. This will require the segmentation of every master frame on the transmitter side, in order to fit GPON or EPON frames, and the reassembly of the master frame at the receiver side, which must be performed without compromising the integrity of the master frame. This segmentation is also necessary to serve multiple antenna units with a single bit stream, in order to benefit from the shared infrastructure of a PON system (in this case, each antenna site should have an appropriate method to select the information directed to it and a procedure to label the information that is sent uplink).

The abovementioned discrepancies in terms of line rate and framing lengths suggest that an adaptation layer between OBSAI/CPRI and GPON/EPON system is required. This adaptation layer would be responsible to map the OBSAI/CPRI information into GPON/EPON frames for transmitting data over the PON and to perform the reverse operation when receiving data from the PON infrastructure.

When compared to PtP links, PON systems become more cost-effective by increasing the number of subscribers (or RRHs, in the case of a DAS network). Amongst the two types of PONs widely deployed (1G EPON and GPON), GPON offers higher capacity. However, the maximum numbers of supported AxC for WiMAX or LTE (even for channel bandwidths lower than 10 MHz) result in a too small number of RRHs, especially if MIMO and diversity reception (2 AxC are required per each RRH) are employed, which does not justify a cost-effective GPON deployment.

A more advantageous scenario is attained when 10G EPON is considered. Focusing only on OBSAI/CPRI line rates above 3072 Mbit/s, since they are the most interesting cases in terms of supported capacity, Table 5.18 presents the maximum number of AxC carried over a 10G EPON system, considering WiMAX and LTE with channel bandwidths of 10 MHz and 20 MHz. These values are based on those presented in Table 5.12 and Table 5.15.

Table 5.18 Maximum number of AxC supported over a 10G EPON system.

Protocol	**Bit streams**	**Channel bandwidth 10 MHz**		**Channel bandwidth 20 MHz**	
		WiMAX	LTE	WiMAX	LTE
OBSAI	3 x 3072.0 Mbit/s	15	12	6	6
	1 x 6144.0 Mbit/s	10	8	5	4
CPRI	3 x 3072.0 Mbit/s	18	12	9	6
	1 x 6144.0 Mbit/s	12	9	6	4
	1 x 9830.4 Mbit/s	20	15	10	7

Although 10G EPON is more attractive than 1G EPON or GPON for the deployment of high capacity DAS, some limitations still exist for a cost-effective 10G EPON deployment. For instance, when using MIMO and considering CPRI the following applies:

- With a single sector per cell (RRH), a maximum of 7 LTE RRHs at 10 MHz and 3 LTE RRHs at 20 MHz can be supported.
- With three sectors per cell (RRH), a maximum of 2 LTE RRHs at 10 MHz and 1 LTE RRHs at 20 MHz can be supported.

The solution to overcome these limitations may be the use of the new paradigms that are emerging for PON systems, such as those applying coherent transmission techniques [SGR+11]. These approaches enable the deployment of virtual PtP links for each RRH

(1 Gbit/s per subscriber has already been demonstrated), since given wavelength channels are dedicated to specific RRH, which also allows avoiding eavesdropping issues inherent to shared infrastructures. Moreover, a large number of RRHs can be supported with these new systems, even for the most demanding scenario (high channel bandwidth, MIMO, and 3 sectors per cell) where several channels may be allocated for each RRH in order to provide more capacity. The final benefit is the fact that wired and wireless services may be easily supported over the same infrastructure, since they will be separated in the wavelength domain, avoiding complex adaptation layers.

5.3.4. Comparative Economical Analysis

After evaluating the capacity provided by the digital links, it is also important to assess their economical viability, when compared to analogue links.

As referred in sub-section 5.3.1, SCM is typically used in analogue links to carry all radio and control channels between the central unit and the remote antenna sites (RRHs) in a DAS network. When compared to alternative transmission techniques or multiplexing technologies, SCM is expected to lead to lower cost system implementations, providing an efficient method to optimize the optical resources. Therefore, a typical SCM analogue link, using a directly modulated laser source, is considered in the following cost comparison with the digital approach.

The digital and analogue implementation schemes are represented by the simplified system layouts depicted in Figure 5.20 and Figure 5.21, respectively. Note that these representations aim only at the economical comparison of the two approaches. For a more specific design of the analogue links see Chapter 6. The grey blocks in Figure 5.20 and Figure 5.21 represent functionalities that are common to both implementations, although they may be placed at a different location within the system. The blocks represented in green (Figure 5.20) are specific of the digital approach and those in blue (Figure 5.21) are specific of the analogue approach. Since the grey blocks are common, the cost comparison should be based on the coloured ones. Moreover, in order to focus on future systems, the most interesting case is the transmission of 100 MHz radio channels, which, according to Table 5.16, will have a bit rate of 4915.20 Mbit/s (LTE-like system) per each radio channel, which can be mapped into a single 6114 Mbit/s CPRI/OBSAI link.

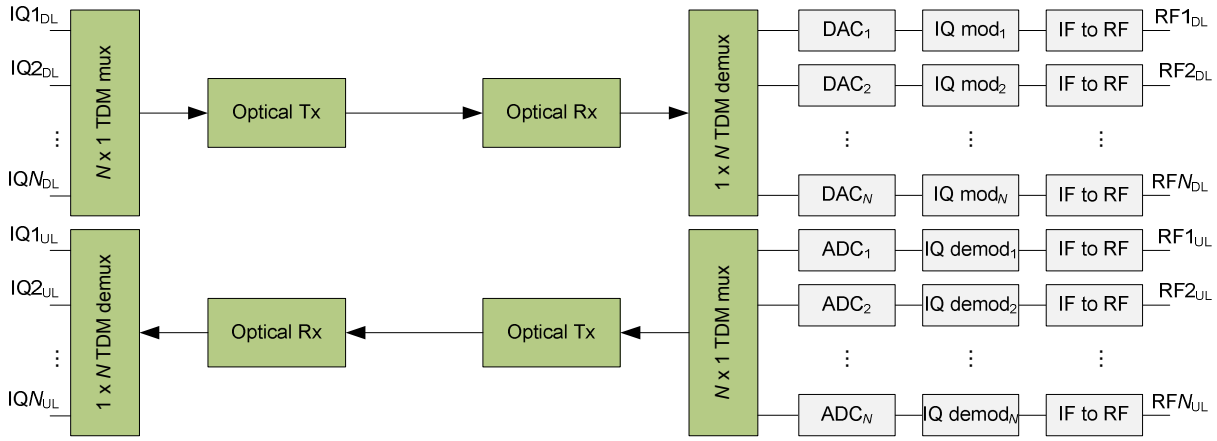

Figure 5.20 – Simplified system layout for digital link implementation.

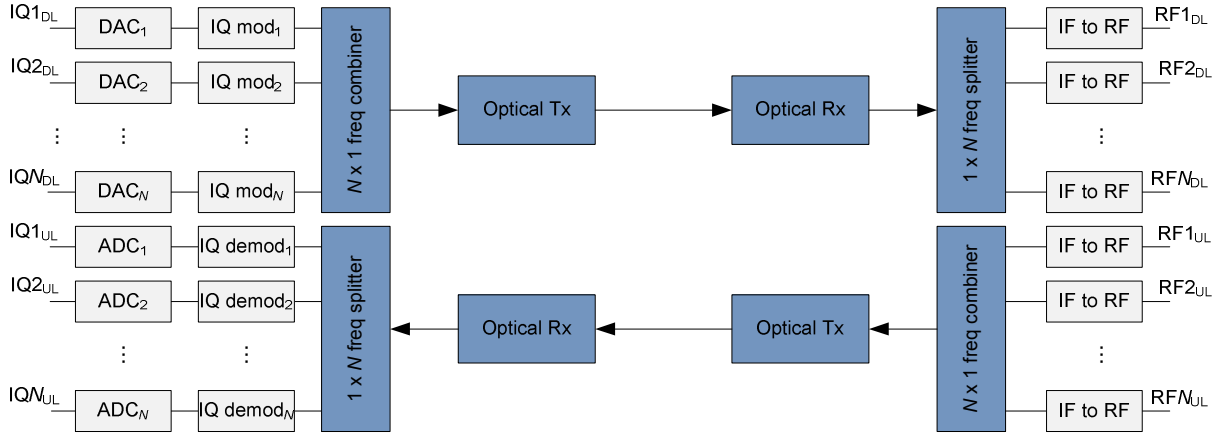

Figure 5.21 – Simplified system layout for analogue link implementation.

In the digital implementation, a digital output (IQ data) is connected to one or more RRHs, each requiring N radio channels per link direction. Such architecture would require up to N times the number of fibres/wavelengths, when compared to the analogue design supporting the same number of radio channels, due to the use of SCM is the latter case. Since the cost of this increase in the number of fibres is quite difficult to quantify and varies greatly from area to area, a less complex and possibly more relevant approach consists on basing the comparison on a scenario where the same fibre infrastructure is used for both systems. In such case, a serial digital link where all channels are time division multiplexed must be considered. The total line rate would then be dependent on the number of supported 100 GHz channels, but the cost of these digital serial links can be minimized by using standardised systems (10GbE, 40GbE, etc.). Therefore, assuming that each 6144 Mbit/s CPRI/OBSAI link supports a single 100 MHz radio channel, the cost of the bidirectional digital link as represented in Figure 5.20, is given by:

$$C_{\text{Digital}}^{100\text{MHz}}(N)=\begin{cases}2C_{\text{TxRx}}^{10\text{GbE}}+2N\cdot C_{\text{mux port}}^{10\text{GbE}}, N=1\\ 2C_{\text{TxRx}}^{40\text{GbE}}+2N\cdot C_{\text{mux port}}^{40\text{GbE}}, 2\le N\le 6\\ 2C_{\text{TxRx}}^{100\text{GbE}}+2N\cdot C_{\text{mux port}}^{100\text{GbE}}, 7\le N\le 16\end{cases}, \tag{5.13}$$

where C_{TxRx} represents the cost of a transmitter/receiver pair, $C_{\text{mux port}}$ represents the cost of the TDM multiplexer (which is considered to scale with N), and the indexes 10GbE, 40GbE and 100GbE represent the 10 Gbit/s, 40 Gbit/s and 100 Gbit/s Ethernet standardized links. This formulation shows that a maximum of 16 radio channels with 100 MHz bandwidth may be carried by a serial 100GbE link.

For the analogue link design, and considering the downlink, the digital IQ data generated at the base station are converted to analogue signals using DACs, and then frequency translated to intermediate frequencies. These IF signals are then power combined and transmitted through the optical link. The opposite operations are realized in the uplink. The multiplexing and demultiplexing of radio channels in the analogue system is accomplished using power combiners and splitters. Note that DACs are also used in the digital transmission system but placed at the RRHs, and therefore their cost does not need to be considered in the comparison.

The use of frequency translation and SCM in the analogue approach allows several radio channels to be transported using a single and relatively low frequency laser/photodiode pair per link direction. Lasers with bandwidths up to 10 GHz [DED+09] are capable of transmitting a much higher number of radio channels (considering a suitable frequency plan) than using the digital approach. These lasers must have a good analogue performance, with low distortion and low noise, which may increase their expected cost. However, commercially available lasers with good analogue performance can be currently found at a relatively low cost.

After the above discussion, it can be concluded that the cost difference between the two implementations may be reduced to the comparison of the cost of the optical transceiver modules and the comparison of the cost of the multiplexing technique, since all other functions are common to both systems. Regarding the transceiver modules, they will be clearly more expensive for the digital implementation, for the same number of radio channels being transported. For instance, using a laser with a bandwidth around 10 GHz, only one 100 MHz radio channel may be supported by the digital implementation, whereas with the analogue approach multiple channels may be carried [FUT]. When comparing the cost of the

multiplexing technique, a similar conclusion may be derived. For the analogue system this function is performed by simple power combiners/splitters, which are low cost components. On the contrary, the TDM multiplexers and demultiplexers necessary for the digital approach are very expensive components, especially if data rates of 40 Gbit/s or higher are required. The general conclusion is that the digital approach results in a cost that may be several orders of magnitude higher than the cost of the analogue implementation, and becomes even more critical in case a high number of RRHs is served by the optical link, mainly when the number of radio channels per RRH increases. For an example where the prices of each component are considered in the cost analysis, refer to [WPP+09].

5.4. Conclusions

The convergence of wireless and wired access networks is currently foreseen as a very promising approach to provide high bandwidth services at low cost to the end-users. A hybrid radio-optical infrastructure should therefore be designed and implemented, considering the current optical fibre deployments and future trends.

In view of this, the support of radio signals over optical networks has been assessed, focusing on the compatibility of radio systems with standard PON systems, in such a way that the coexistence of both technologies is guaranteed. After this analysis it is important to decide on the most suitable optical infrastructure to support the radio systems. Therefore, the characteristics and the advantages/disadvantages of possible topologies were briefly addressed and a comparison in terms of power loss budget and cost was presented for different types of fibre-optic architectures, based on tree-and-branches and bus topologies. It has been concluded that a CWDM approach should be selected for a low cost deployment, at the expense of supporting a much lower number of RRHs. On the other hand, if the cost is not prohibitive, a DWDM-based architecture would allow supporting a much higher user density.

This paradigm of DAS is gaining relevance for the deployment of future wireless systems, demanding the provision of very high bandwidths. The joint collaboration of wireless and optical players, deploying DAS and PON systems, respectively, may bring significant benefits in terms of CAPEX and OPEX, when merging both networks over the same optical fibre infrastructure. However, when considering the radio channels transmission using digital protocols, the first generation PON systems (EPON and GPON) do not have sufficient capacity to support a cost-effective deployment of multiple RRHs, serving WiMAX

or LTE end-users. In such situations, it is therefore important to rely on the next generation PON systems, operating at higher data rates, or even on the new proposals where high capacity PtP connections are emulated between the central unit and the RRHs.

Alternatively to the use of digital radio transmission protocols, an analogue approach may be used, based on SCM techniques. When comparing the cost of this approach with the digital one, it was found that analogue transmission links may be more than one order of magnitude less expensive, for next generation wireless signals. The high cost of the digital approach results from the large data rates that are required for wideband systems. Moreover, analogue transmission allows having less complex RRHs, with lower power consumption, which is a strong reason to select this approach for next generation DAS.

Chapter 6

DISTRIBUTED ANTENNA SYSTEM BASED ON ANALOGUE RADIO-OVER-FIBRE

The proliferation of wireless communication services has been quite remarkable. Allied to the inherent mobility feature, wireless services are now capable of providing larger bandwidths per end-user, a trend that is expected to be intensified given future bandwidth-hungry and sophisticated services. Considerable research and development is currently being verified in the wireless arena aiming at what is commonly called 4G systems, which are spurred by interdependent technical and economical deployment trends. Such 4G systems should fulfil several goals, among which is the provision of true broadband wireless access, requiring the development of new air interfaces, and an enhanced system capacity, when compared with current 3G networks.

In the evolution towards 4G, several modifications of the wireless systems are required. For instance, the support of more users at higher data rates requires the use of higher radio carrier frequencies, resulting in smaller radio cells (in a typical cellular system), due to increased propagation losses and line-of-sight restrictions. However, because interference does not undergo the same scaling effect as the cell size, the system capacity does not increase linearly with cell size reduction. Due to the radio cells reduction at higher frequencies, more and more antenna sites are needed to cover a certain area. Therefore, the consequent need for wireless networks to cope with these capacity issues together with the increasing bandwidth

demands, in a cost-effective manner, requires changes in the system architecture. As emphasized in the previous chapter, the use of a network paradigm based on distributed antennas allows coping with the stringent demands specified by the IMT-A objectives. Due to the use of multiple remotely located antennas, a DAS network is a less power consuming solution, when compared with a conventional single antenna architecture, also granting improved reliability since line-of-sight with the end-users is more often verified.

As for the wired access, one of the main concerns when designing or developing a wireless access system is obviously its cost, which should be low, while keeping the required system features. As shown in Chapter 5, the use of an analogue approach for transmitting radio signals over a DAS network has proven to be more cost-effective than its digital counterpart, which makes it the preferred option for a near future. In this case, the central unit is connected to the remote locations, where simple and low-power consumption antenna units are located. This simplicity arises from the fact that these units are composed only by one or more low power antenna elements, radio frequency converters and amplifiers, if necessary, and an optical transmitter/receiver pair. These elements enable to transmit/receive transparently the radio signals to/from the CU, avoiding complex processing electronics in the RRHs, and creating a typical radio-over-fibre network.

The use of this RoF infrastructure to interconnect simplified RRHs in microcellular environments has been considered since the early 90's [Coo91], but at that time the cost and maturity of the optical technology prevented a generalized deployment to occur. Other target applications have been considered, such as the simple fibre backhaul of base stations, to eliminate dead spots, or broadband wireless access networks for road vehicle communication networks, for intelligent transportation system [CG91], [KERW05]. However, the RoF infrastructure has never been considered part of the wireless system architecture, neither viewed as an enabler for the development of new architecture concepts nor processing options, until recently. In the past few years, this concept started again attracting more interest from researchers, manufacturers, telecommunication operators and standardization bodies [Mit09].

The work reported in this chapter was realized mainly in the framework of the EC project FUTON [FUT]. For this reason, a brief overview of the project objectives and main achievements is presented in section 6.1. Section 6.2 is then devoted to the description of the analogue modelling of FUTON radio links, with emphasis on externally modulated links using MZM devices, whereas section 6.3 focuses on the performance evaluation of a system transmitting analogue radio over fibre signals.

6.1. FUTON Overview

The project FUTON, which stands for "Fibre Optic Networks for Distributed, Extendible Heterogeneous Radio Architectures and Service Provisioning", is an FP7 project that started in January 2008 and ended in September 2010, and integrated 17 partners from industry (manufacturers, service providers and operators), universities and research institutes.

In the context of new architectures for wireless systems, the FUTON project proposed the development and prototyping of a hybrid fibre-radio DAS-based infrastructure, that allowed to transparently interconnect multiple RRHs (the designation "Remote Access Unit", RAU, was used throughout the project lifetime and in all project documents) to a central unit. This architecture enabled to consolidate all signal processing functions at the central location, where a CU was responsible for the joint processing of the radio signals being received from all the RRHs. This centralized processing allowed the development of virtual MIMO concepts to achieve broadband wireless transmission, as well as inter-cell interference cancellation, fulfilling the objectives specified for 4G systems. With FUTON, the use of RoF changed from the backhaul system to an aggregator system, where the infrastructure acts as a key enabler for the simultaneous transport of several wireless technologies.

The FUTON infrastructure should be capable of collecting/distributing the radio signals from/to the different antennas transparently, enabling their centralized processing. Based on this infrastructure, algorithms and protocols for a Distributed Broadband Wireless System (DBWS) were developed, enabling the delivery of the high bit rates sought in 4G. Furthermore, with multiband RRHs, the availability of the radio signals from heterogeneous systems at the same point opens new doors at both technical and business levels in terms of, for instance, the development of efficient Common Radio Resource Management (CRRM). Summarizing, the main goals of the project were:

- Specify, design, implement and provide proof of concept for a hybrid optical-radio infrastructure enabling the high bit rates envisioned for 4G.
- Exploit the potentialities offered by the optical infrastructure to develop mechanisms for inter-system coordination and optimum usage of the radio resources.
- Evaluate the implications of the FUTON concept on current wireless architecture models.

In the following, a brief overview of the core concept that was handled within the project is presented, followed by the description of the main achievements, with special emphasis on the architectures and sub-systems for the RoF network.

6.1.1. Concept

The generic architecture of the FUTON concept intends to cover a geographical area that is divided into several serving areas, where multi-frequency and multi-system RRHs are located, and linked to a CU by optical fibre. The wireless systems to be supported cover:

- Single attachment, where the user terminals communicate with a single RRH; for such systems, the fibre infrastructure provides a simple backhaul for radio signals.
- Multiple attachment, or distributed wireless systems, for which the user terminals can communicate with several RRHs; for such a case the fibre infrastructure provides a transparent transport network towards the CU.

The processing tasks related to all communications within a serving area are performed at the correspondent CU. For distributed wireless systems, the availability of the radio signals at a common location allows the joint processing of the signals to/from different RRHs, enabling the development of virtual MIMO links and efficient cross-layer algorithms to optimize the usage of the radio resources. This concept may be generalized to a cross-system model, since radio signals from heterogeneous systems will be available at the same point, enabling the development of efficient CRRM algorithms. A detailed representation for a single area, where the planes illustrate possible systems that can coexist in a serving area and are connected to the same CU, is depicted in Figure 6.1.

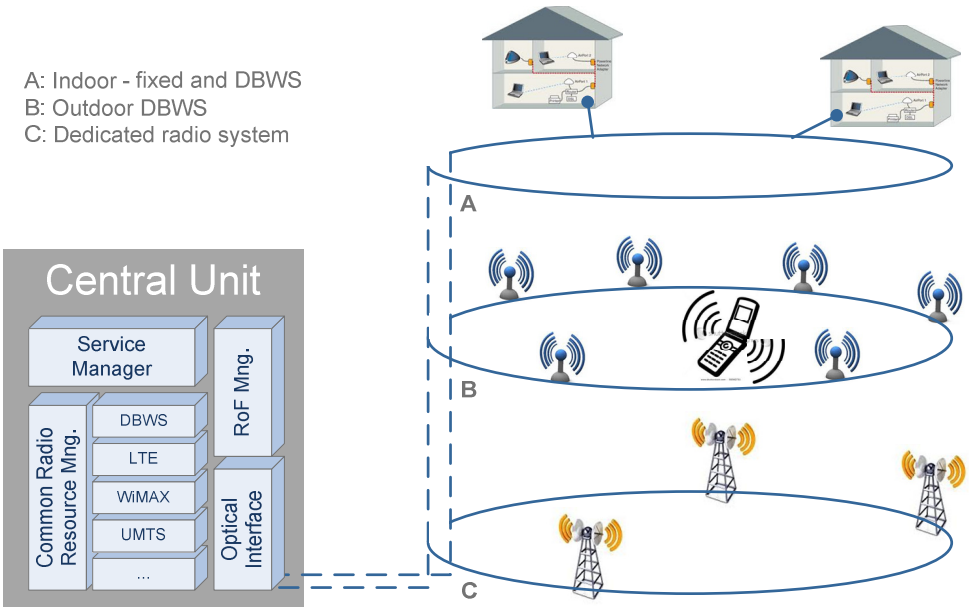

Figure 6.1 – FUTON generic architecture.

The FUTON architecture consists of a fixed infrastructure that provides enough flexibility to share its resources among a wide range of wireless systems and by fixed optical connections, instead of being allocated to a single system. The supported systems should include, among others, outdoor DBWS, where the infrastructure acts as a virtual MIMO enabler to achieve the target high bit rates, indoor DBWS, and dedicated radio systems.

The key aspects of the FUTON hybrid infrastructure are reliability and flexibility. To achieve these goals, FUTON uses a combination of RF translation with SCM and low-cost forms of WDM, maximizing the transparency and future-proof capability of the optical-radio infrastructure. The use of WDM should be limited to the coarse form (CWDM) and, most likely, only for the addressing of individual RRHs (not for the transport of multiple signals to/from each individual RRH). As shown in Chapter 5, CWDM will enable the use of less-expensive and cooler-less components. Basically, a bi-dimensional space consisting of optical wavelengths and electrical subcarriers can be defined. The RRHs are addressed by wavelength and the signals for the different antenna elements of the same RRH or associated with different wireless systems are separated in the electrical domain by SCM. By defining the appropriate granularity, both new RRHs and new wireless systems can be easily added.

From the viewpoint of the DBWS or other legacy wireless systems to be integrated, the optical infrastructure should be a transparent medium, providing flexibility for future radio systems, with reduced degradation of the radio signal quality. In this context, several objectives were identified and pursued. Amongst them, the following may be highlighted. After the definition of a suitable architecture, in terms of physical topology and multiplexing strategy, the specification of the optical, optoelectronic and RF components should take place, allowing the definition of performance requirements for the components that meet the system specification. The next step involves the design, fabrication and testing of new components, according to the previous specifications. These new components should then be applied in the construction and testing of the system units, namely the CU and the RRHs, leading to the complete prototyping, which should be available for testing and demonstration.

6.1.2. Project Achievements

The activities developed along the FUTON project were focused on the system modelling and evaluation. The main project outcomes were the definition and validation of the theoretical concepts, the development and testing of the key devices for the optical-radio

infrastructure/transmission, and the final demonstrations, which were intended to verify the operation of the developed sub-systems when integrated in the global FUTON concept.

The theoretical concepts developed within the project were directed to the definition of the DBWS concept, concerning its PHY and MAC layers and the compatibility that should be guaranteed with other wireless standards, both at the transmission level and at the infrastructure level. Moreover, novel algorithms addressing the optical-system related nonlinearities and corresponding compensation strategies were also developed [HLH+10]. The use of the proposed hybrid fibre-radio architecture, which was modelled and validated against experimental measurements, allowed to develop novel RRM, CRRM [SSG+10] and vertical hand-off algorithms, by taking advantage of the centralized topology and increased number of RRHs that can be deployed. Besides, the resource management of the RoF infrastructure was another focus of the project, where a planning tool was designed and a management unit was prototyped and tested. The final outcome of FUTON was the integrated demonstration of the project concept. This demonstration was based on prototype units for the CU and the RRHs, developed within the project consortium, that communicate between themselves through optical fibre, and through an air interface with Mobile Terminals (MTs) also developed within the project. The DBWS signals, generated and processed at the CU according to the developed algorithms, were transmitted over this physical infrastructure.

The optical modules, antennas and RF components of both CU and RRHs were fabricated, integrated and tested with Quadrature Amplitude Modulation (QAM) signals (64-QAM and 40 MHz bandwidth), according to the specifications in the 802.11n standard. Initially, commercial optical components were used, but specific devices were developed later. Amongst them, RSOAs with world-leading performance, in terms of bandwidth and modulation efficiency, were demonstrated [VPP+10], and semiconductor DMLs operating over a temperature range of 25ºC-70ºC were fabricated [DED+09]. Additionally, low-cost antennas with broadband performance were developed for the MTs and antennas with beam profiles suitable for illuminating street corridors were demonstrated for the RRHs [ZBEG10], and both were integrated with the developed RF hardware and optical links.

In the demonstration scenario, applying the developed devices and algorithms, a successful transmission was achieved in both uplink and downlink directions, for a single channel scenario or using SCM to simultaneously transmit several channels. For illustrative purposes, Figure 6.2 depicts some modules and setups used in the final project demonstration. For further details on the project and reported results, see [FUT].

a)  b) 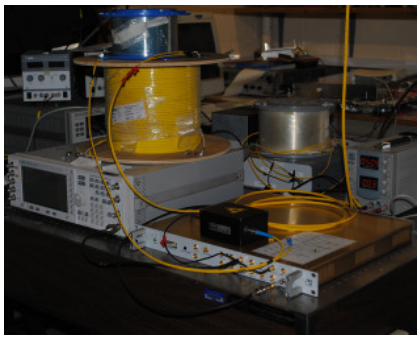

c)  d) 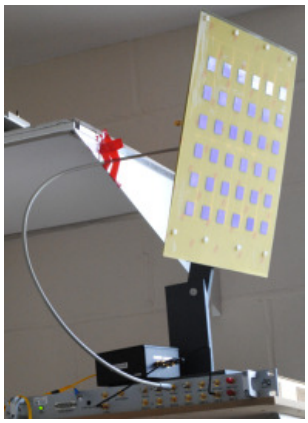

Figure 6.2 – FUTON final demonstration [FUT]: a) CU transmission module; b) setup at the CU; c) RRH complete unit; d) setup at the RRH.

6.2. Analogue Fibre Link Modelling

The computer aided design and characterization of a communication system for a specific environment is very important, enabling a prediction of the system performance prior to fabrication and deployment. This was also the principle followed within FUTON project regarding the fibre links that are the basis of the project concept.

In terms of characterization, an optical link may be compared to an active RF component, such as a RF amplifier, typically requiring parameters such as loss, bandwidth, noise figure and dynamic range. All these parameters are primarily determined by the modulation device and by the photodetector. The optical fibre may have a significant contribution for the loss, especially when long fibre lengths are considered, which consequently affects the noise figure. An indirect influence on the bandwidth may occur due to fibre dispersion, but the effects of the optical fibre on the dynamic range are negligible [Cox04].

A generic RoF link based on SCM, the multiplexing technology selected for FUTON systems, may be represented by the diagram presented in Figure 6.3. As previously referred, the use of SCM allows to increase the capacity of the optical fibre, since individual data signals are carried by separate electrical sub-carriers. In the transmission direction, these sub-carriers are combined using a RF power combiner and the resulting signal drives the modulation of an optical source. Because the sub-carriers are multiplexed in the frequency domain, the signal that is carried over the optical fibre is considered a Frequency Division Multiplexed (FDM) signal. In the receiving direction, a photodiode is used to detect the optical signal, which is afterwards divided into the corresponding sub-carriers by using a RF power splitter.

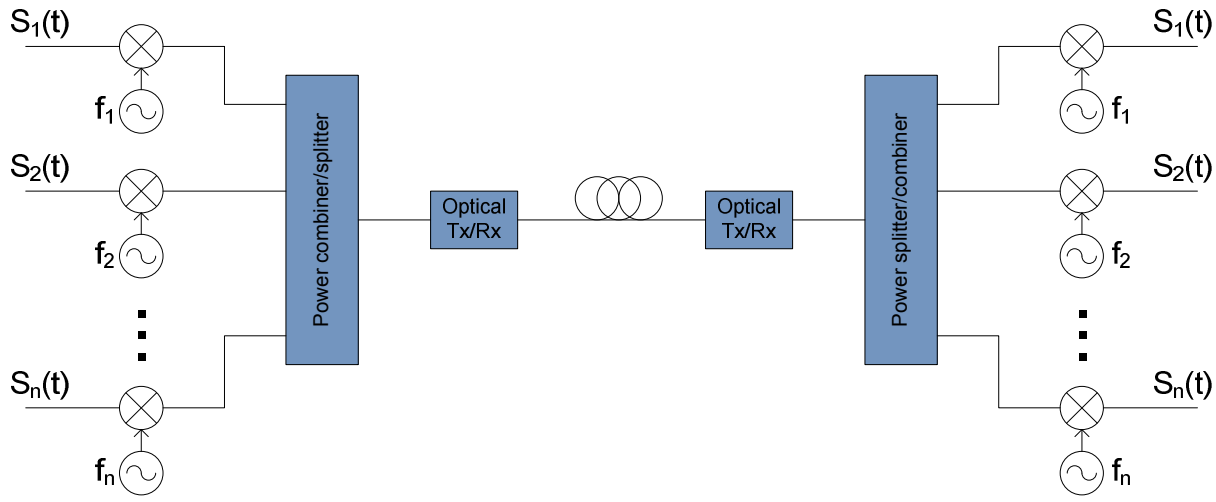

Figure 6.3 – Generic RoF link based on SCM.

For systems that follow the layout of Figure 6.3, which represents a link with Intensity Modulation and Direct-Detection (IM-DD), the optical link gain is given by [CABP06]:

$$G_{\text{link}} = s_{\text{md}}{}^2 \Re^2 , \tag{6.1}$$

where s_{md} represents the slope efficiency of the modulation device, in W/A, and $\Re$ is the responsivity of the detection device, in A/W. Through this relation, it is shown that a practical limit on link gain is set by the limits of slope efficiency and responsivity. For links using directly modulated lasers and PIN photodiodes, the link gain is limited to less or equal to 1, considering the laser input resistance and detector load resistance to be equal, performing like attenuators, due to RF losses that always occur. For these cases, the optical link gain may be expressed by [DNG+06]:

$$G_{\text{link}} = \left(\frac{s_{\text{laser}} \alpha_{\text{src}} \Re}{IL_{\text{link}}} \right)^2, \tag{6.2}$$

where η represents the laser slope efficiency and α_{src} takes into account laser frequency response variations, which are not modelled using the static slope efficiency. IL_{link} is defined as the optical link insertion loss, given by the ratio between the output power and the input power launched into the optical fibre.

As referred in Chapter 5, the analogue links may also be based on external modulation, instead of DML. In such case, the slope efficiency is not a native parameter and should be derived. For a MZM biased at quadrature, it is given by [CABP06]:

$$s_{\text{mzm}} = \frac{\pi P_{\text{CW}} T_{\text{ff}} Z_{\text{src}}}{2V_{\pi}}, \tag{6.3}$$

where P_{CW} represents the CW laser power driving the modulator, T_{ff} is the transmitivity of the modulator, Z_{src} is the impedance of the source, and V_{π} is the on-off switching voltage of the modulator. This relation clearly shows that the slope efficiency of MZM devices may be improved, and thereby the link gain, by increasing the CW optical power or by reducing the switching voltage of the modulator. Theoretically, by doing this, higher link gains may be attained for MZM-based links when compared to DML-based links.

Another important parameter for the characterization of optical links is the Noise Figure (NF), which is defined as the degradation of the SNR as a result of the noise added by the system. It is given by [CABP06]:

$$NF = 10 \log_{10} \left(\frac{n_{\text{out}}}{kT_0 G_{\text{link}}} \right), \tag{6.4}$$

where n_{out} is the noise power density at the output of the link, k is the Boltzmann constant and T_0 is the room temperature, assumed to be 290 K. The noise at the output of the link is mainly affected by the thermal noise of the link. This can be due to the input thermal noise or to the thermal noise generated by the modulation device and its interface circuit, which are not dominant, and due to the thermal noise generated in the photodetector circuit, which will typically dominate the total thermal noise at the output of the link.

One of the major limitations in analogue fibre-optic links is the signal distortion caused by device nonlinearities. This distortion leads to the creation of new frequency harmonics and intermodulation products [Cox04]. The efficiency of the fibre-optic link is hampered by the transfer of RF signal power to these new frequencies, which may also cause interference with other RF signals in a multi-channel system.

The most important form of distortion is the third-order Intermodulation (IM3) [Cox04], which is originated if two or more signals at different frequencies are used to modulate the optical source, such as in the case of SCM systems. Figure 6.4 a) depicts a representation of the generated harmonics when two tones, at frequencies f_1 and f_2, are used as input signals. In this case, the IM3 products generated at $2f_1$-f_2 and $2f_2$-f_1 lie very near the input frequencies, and therefore are more difficult to eliminate. Apart from these products, all other (both second- and third-order harmonics) can be easily filtered.

A typical test is usually performed in fibre-optic links using two tones, combined at the input of the optical fibre using a RF power combiner, and a representation of the typical results is depicted in Figure 6.4 b) [Cox04]. Here, the RF signal power (P_{out}) at the output of the fibre is plotted against the input RF signal power (P_{in}) for one of the fundamental tones and one of the third-order intermodulation products.

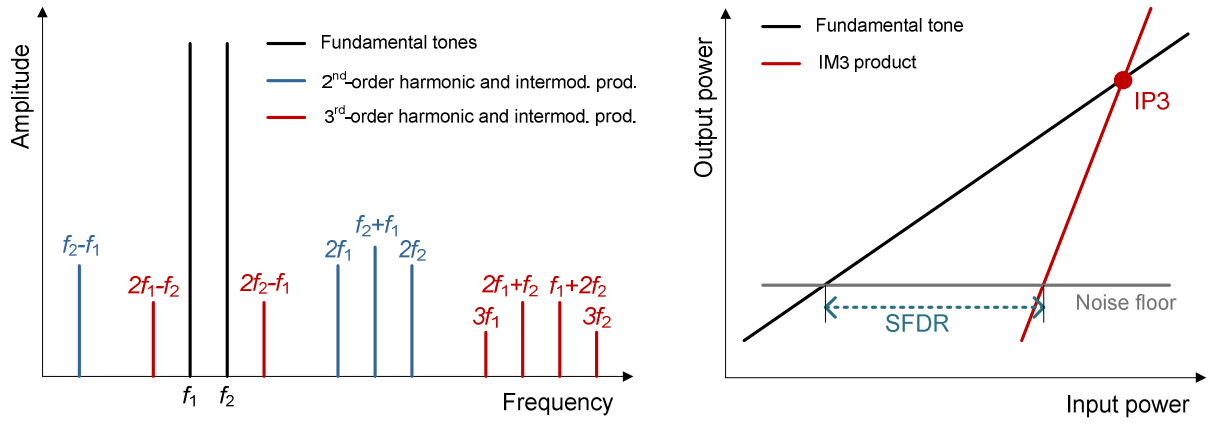

a) Intermodulation products b) Two tone measurements

Figure 6.4 – Intermodulation distortion.

From the type of measurement presented in Figure 6.4 b), two important measures can be derived. The first is obtained from the point of intersection of the lines for the fundamental tone and for the IM3 products. This measure is called third-order Intercept Point (IP3) and can be given either by the input or the output intercept powers, designated by third-order Input

Intersect Point (IIP3) or third-order Output Intersect Point (OIP3), respectively. The second measure is called Spur-Free Dynamic Range (SFDR) and is defined as the range of values between the input power value at which the fundamental tone output power crosses the noise floor, and the input power value for which the output power of the intermodulation products crosses the noise floor. In this range, the output is considered free of distortion. The SFDR measured from the output power axis would result in an equal value, contrarily to the IP3 case, where the IIP3 differs from the OIP3 by an amount equal to the gain of the link. Moreover, note that the SFDR is dependent on the noise floor of the link, which makes it also bandwidth dependent, similarly to the link noise.

The characterization of optical links is based also on a parameter named P1dB compression point, which represents the link input power for which the output power falls by 1 dB from a linear relationship [Cox04]. P1dB usually defines the maximum power that is acceptable at the input of the link, and depends on the transfer function of the optical source.

After characterizing the optical link, it is important to address the wireless system behaviour. The propagation in free space is typically characterized by the Friis formula, which is used to predict the received signal strength in a line-of-sight situation [Rap02]. Several path loss models are available to describe the difference (in dB) between the transmitted and the received powers. A typical representation of the path loss, *PL*, as a function of the wireless distance, *d*, is given by:

$$PL = 10n_{\mathrm{PL}} \log_{10}\left(\frac{d}{d_0}\right) + 20\log_{10}\left(\frac{4\pi f}{c} d_0\right) + X_\sigma, \tag{6.5}$$

where d_0 is a reference distance, f is the radio frequency, c is the speed of light, n_{PL} is the path loss exponent, and X_σ represents the accepted log-normal variation in the channel path loss. The path loss exponent allows site-specific variations to be included in the distance dependent model and is one of the most important parameters of all distance dependent models.

In the following sub-sections, the FUTON analogue link design is presented and characterized using the measures described above. A special attention will be given to external modulated links, using MZMs, after presenting a brief comparison with DML-based links. The characterization of FUTON link types other than MZM-based was a responsibility of other partners within the project consortium.

6.2.1. Comparative Analysis of DML- and MZM-Based Links

The most common RoF links are based on DML sources, but the external modulation alternative may also be appealing in some specific scenarios [CBJ90]. Several differences exist between both approaches, but the most significant is probably related to the signal distortion. In general, similar levels of IM3 can be achieved in DML- and MZM-based links, but the level of 2nd order distortion is much higher in DMLs than in quadrature biased MZMs [Cox04]. Since usually the signal distortion is caused mainly by the modulation device, rather than the photodetector or the fibre, many linearization techniques were proposed to mitigate the effects of distortion, especially in externally modulated links [URK+06].

The performance assessment of a typical RoF link is then presented here for DML- and MZM-based links, in terms of IIP3 and SFDR. The use of two tones with frequencies 3.50 GHz and 3.51 GHz was considered at the input of the optical source, in a link with 20 km of optical fibre characterized by an attenuation of 0.2 dB/km and a dispersion of 16 ps/nm/km. A 10 GHz PIN photoreceiver, characterized by a responsivity of 0.8 A/W, a transimpedance of 500 Ω and an equivalent input noise current of 1.16 μA, was also considered. The optical power at the input of the fibre is assumed to be 4 dBm, for both links.

The DFB laser used in the DML-based link was parameterized according to [CS97], with a bias current of 50 mA. This laser is characterized by a slope efficiency of 0.079 W/A and a threshold current of 18 mA. For the MZM-based link, a 10 Gbit/s commercial MZM was selected, characterized by an insertion loss of 4.1 dB and a V_π of 5.5 V. In order to obtain 4 dBm of optical power at the fibre input, a CW laser with output power of 11.1 dBm is considered, in order to compensate for the extra 3 dB losses due to the quadrature bias.

Figure 6.5 and Figure 6.6 present the results obtained for the output power of the fundamental tone and of the 2nd and 3rd order intermodulation products, as a function of the input power, for DML- and MZM-based links, respectively. As expected, the output power of the fundamental tone is almost the same for both links, since the same power was considered at the input of the fibre. However, a much lower 2nd order distortion is obtained for the MZM-based link, because the MZM is biased at quadrature, in order to minimize the effect of this type of distortion, as explained in [Cox04]. This is a clear advantage of MZM over DML, because, as expected, both show a similar level of 3rd order distortion.

The intersection between the linear approximations for the fundamental and the IM3 curve results in an IIP3 of 21.7 dBm for the DML-based link. This link is characterized by a

noise floor of -151.14 dBm/Hz and its SFDR was found to be around 106.3 dB·Hz$^{2/3}$. For the MZM-based link, an IIP3 of 24 dBm was obtained, and the SFDR was found to be around 107.3 dB·Hz$^{2/3}$. Both links present a SFDR which is in agreement with that specified for 4G systems, validating the use of these links for next-generation systems.

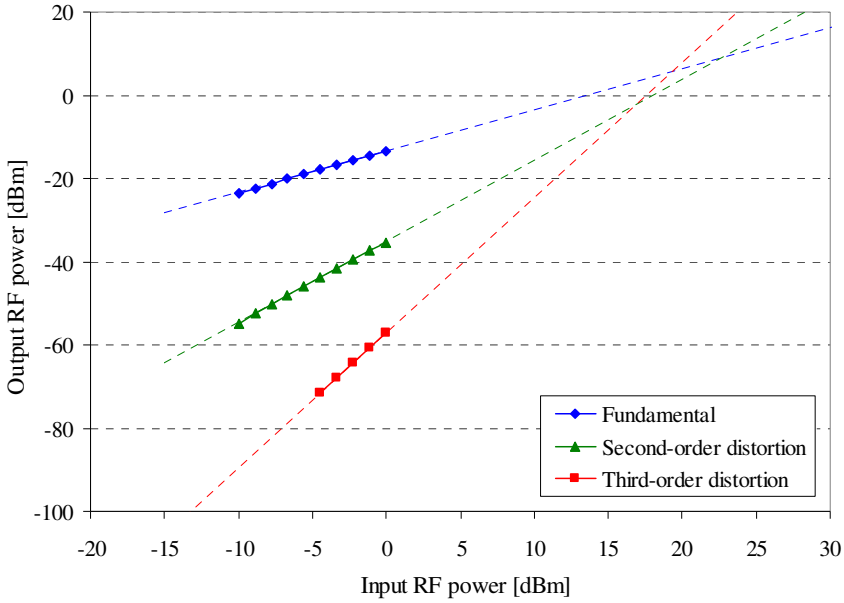

Figure 6.5 – Characterization of DML-based link.

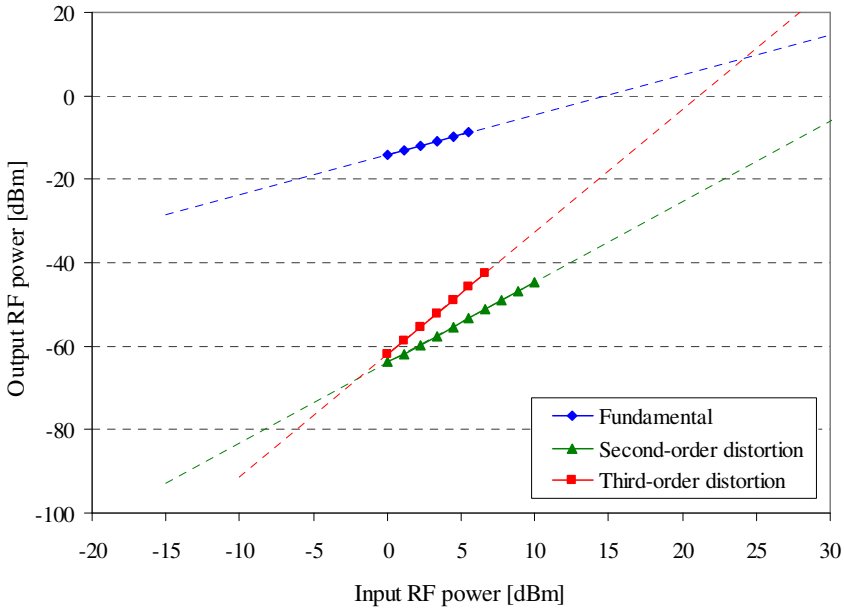

Figure 6.6 – Characterization of MZM-based link.

From Figure 6.5 and Figure 6.6, it is concluded that the performance of DML- and MZM-based links is similar for the sub-octave transmission bandwidth systems considered [WDK+09]. In spite of the advantages presented by the use of a MZM, from an economical perspective the DML should be the preferred choice for such scenario.

6.2.2. General FUTON Link Design

The FUTON system may be realized by employing different analogue optical link types, depending on selecting the use of a DML, a RSOA or a MZM as the electrical/optical (E/O) converter. Characterization measurements of these link types, which only differ due to the E/O device, have been conducted, and modelling work has been carried out to match the experimental results as closely as possible, using commercial software.

The FUTON system was designed to carry DBWS signals with bandwidths up to 100 MHz, and to be applied in dense urban areas which may be described by a Manhattan scenario, characterized by parallel and perpendicular blocks and streets. Therefore, each RRH was designed to support two sectors for outdoor street coverage, and each sector was designed to support 2x2 MIMO, enabling interference cancellation by using two transmitting antennas and two receiving antennas per sector. Consequently, each RRH supports a total of four 100 MHz bandwidth radio channels per link direction. An additional low-bandwidth channel for control, monitoring, and synchronization (CMS) was also provided.

The general RoF link design for FUTON is presented in Figure 6.7, considering the Frequency Division Duplex (FDD) transmission mode. The CU module comprises a DBWS 2-sector Base Station (BS), processing modules for electrical IF signals and CMS signal and optical/electrical (O/E) and E/O devices. The DBWS 2-sector BS handles the digital data signal processing and its output/input signals are digital IQ data. In the downstream direction, the DBWS data streams are converted from IQ to IF by electrical IF signal processing, according to the IF plan shown in Figure 6.7. A frequency translator is used to up-convert the CMS baseband signal to IF. The four IF data signals, the CMS signal and a reference signal for Local Oscillator (LO) locking are combined together, using SCM, and transported towards the RRH through the optical network.

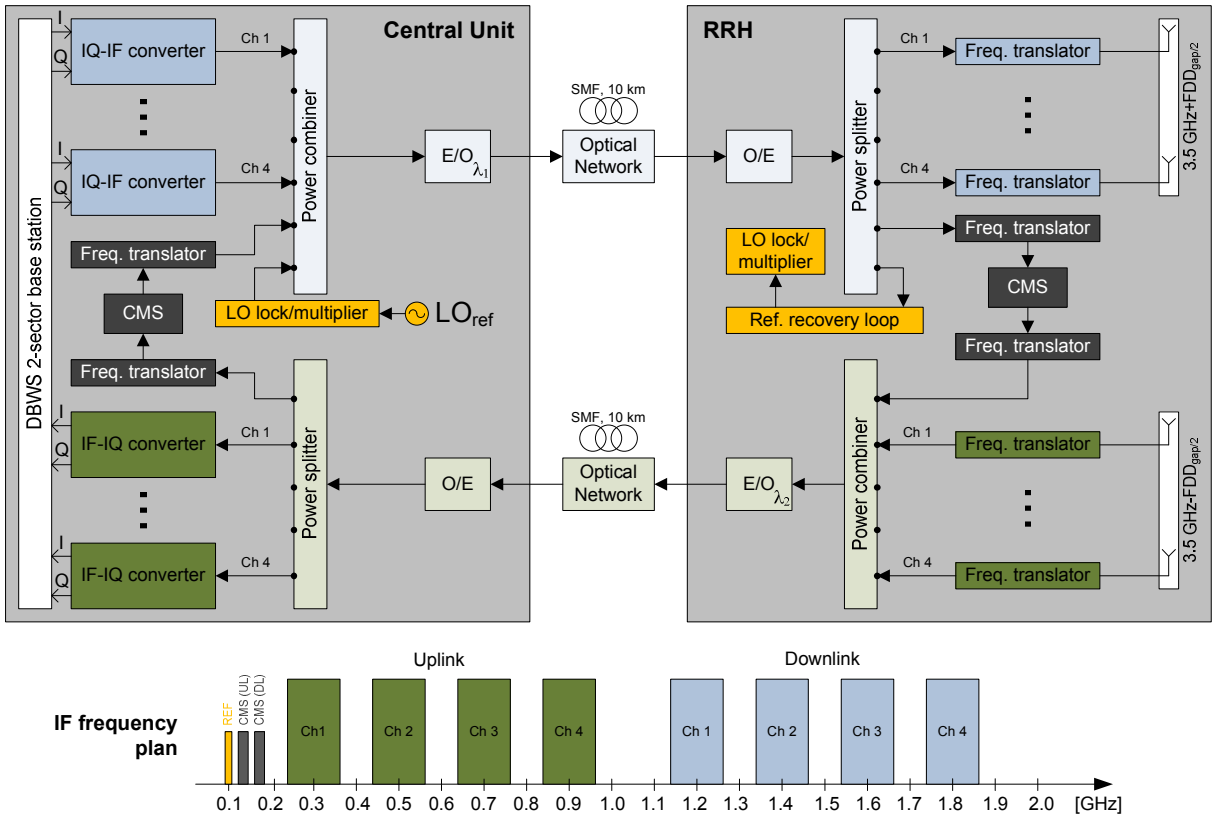

Figure 6.7 – General RoF link layout.

The main function of the RRH is to transmit information to/from the MT from/to the CU, via the optical link. Similarly to the CU, the RRH comprises an electrical IF signal processing module, E/O and O/E converters, and a CMS processing module. Besides these components, the RRH includes the antennas for transmitting/receiving signals to/from the MT, as shown in Figure 6.7. Similarly to the receiver part of the CU, in the downlink direction, the RRH comprises an O/E converter followed by a power splitter for terminating the optical network and retrieving the individual IF signals transmitted by the CU. The four DBWS IQ data modulated IF signals are frequency up-converted to 3.5 GHz, and then sent to the antennas for wireless transmission towards the MTs. A "reference recovery loop" module is included in the RRH to enable synchronization and to generate the reference signal (a 100 MHz low frequency signal identical to what is used in the CU) to be used for locking the LOs. With this method, the possible degradation of the phase noise of the "REF" signal reaching the RRH does not affect the frequency recovery process.

In the uplink direction, the functions in both the CU and the RRH are basically identical to those described for the downlink, but located in opposite positions.

The frequency plan defined for transmitting the DBWS signals within FUTON is also depicted in Figure 6.7. The uplink and the downlink channels occupy separate spectral bands, with the uplink band below 1 GHz, enabling the use of a RSOA as uplink optical source. With this plan the downlink components must operate up to 2 GHz, which is a very acceptable bandwidth, even for low-cost commercial components.

6.2.3. Externally Modulated Link Modelling

The general link design described in the previous sub-section was characterized depending on the type of optical source. In this sub-section, the MZM-based link will be described, but a detailed comparison between the three considered link types, namely DML-, RSOA- and MZM-based is presented in [WNG+10], [WNA+10].

The analogue links employing MZMs are typically more expensive than DML-based links, since they require an additional component, the optical modulator. An advantage of using a MZM is its high modulation bandwidth, which is not of fundamental importance in FUTON systems, since the use of IFs below 2 GHz is expected. MZMs introduce higher insertion losses than DMLs, and also suffer from non-linear distortion and bias drifting. Bias drifting is an issue because the gain is dependent on the MZM bias point, as previously pointed out.

The FUTON link type employing MZMs was analyzed through a link budget approach. The detailed MZM link diagrams, and the result of the power budget calculations, are depicted in Figure 6.8 and Figure 6.9, for downlink and uplink, respectively. In these diagrams the link functional elements are depicted and the values of their characteristic parameters are indicated. P_{RF} and P_{IF} represent the power of the RF and IF signals, respectively, and are given in dBm/100 MHz, whereas the noise power is represented by P_N, in dBm/Hz. Each component is represented by its gain, given by G_{comp}, and its noise figure, given by NF_{comp}. The accumulated cascaded gain, G_{cs}, and noise figure, NF_{cs}, is also presented in each step of the power budget calculation.

The electrical components of the system were assumed to have values matching commercial devices, which also allowed for a fair comparison with the other link types. The photodiodes and MZMs were characterized with values acceptable for available components, and equal devices were assumed for uplink and downlink in order to facilitate their eventual mass production/purchase.

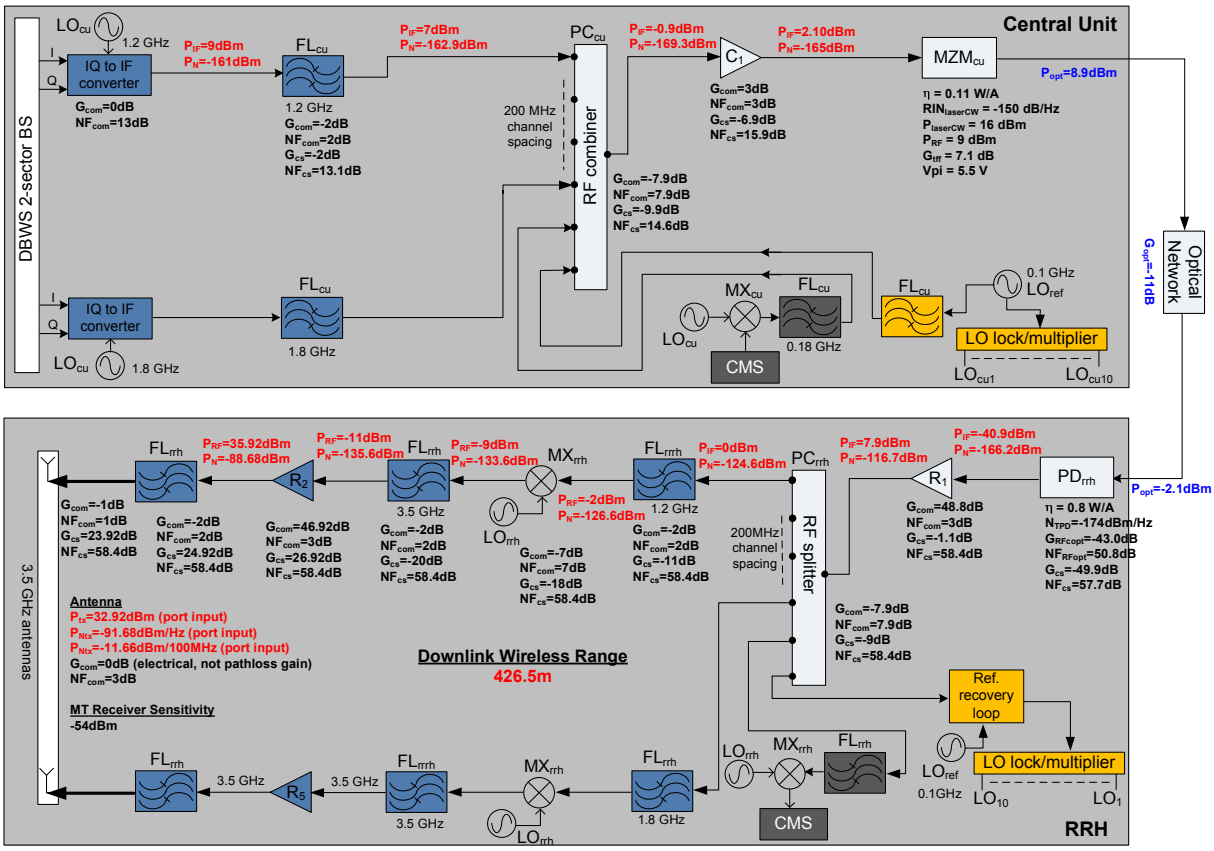

Figure 6.8 – Detailed downlink power budget for MZM-based FUTON links.

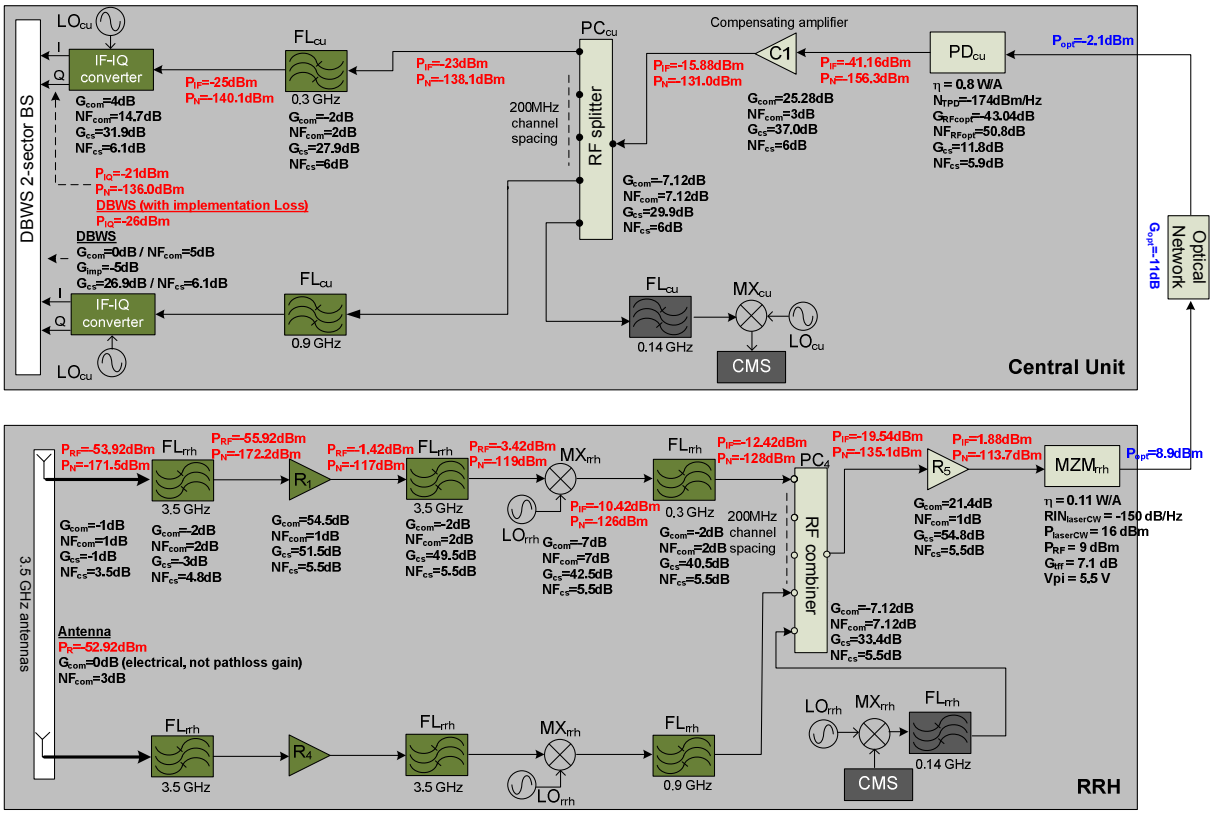

Figure 6.9 – Detailed uplink power budget for MZM-based FUTON links.

The link budget was optimized by adjusting the compensating amplifiers to guarantee an optimum performance, for a SNR of 30 dB when a DBWS signal formatted with 256-QAM was transmitted. The optical network was considered to have an attenuation of 11 dB, corresponding to the losses of 10 km of fibre plus the losses introduced by CWDM multiplexing/demultiplexing devices. It was considered that the MT has a receiver sensitivity of -54 dBm, a typical value for mobile units being commercialized nowadays. The formulations presented at the introduction of section 6.2 were used to determine the gain and noise figure of the link components.

In order to attain an optimum performance, the CW optical power should be set to 16 dBm (both for UL and DL), in order to guarantee that the high losses introduced by the MZM do not hamper the link. This is considered to be a high CW optical power and therefore an optical amplifier may be required to boost the optical power in a real scenario (in the case the CW laser is not capable of emitting 16 dBm). The noise introduced by this amplifier will probably have a negligible impact on the link budget since it will be much lower than the electrical noise of the rest of the link.

A relatively high power at the RF input of the MZM (for UL and DL), 9 dBm, was considered. This high RF power, considered to be an acceptable value for the MZM operation, is necessary to guarantee that the link is working properly, avoiding loop gain oscillations in the RRH [DNG+06].

The gain of the RF amplifiers was found to be very high, which is a design drawback since RF amplifiers tend to be more expensive than IF amplifiers. A possibility to alleviate this constraint is to have more gain at IF and lower gain at RF, in the RRH. This may be achieved considering, in the downlink, mixers which have IF/RF drive power higher than -3 dBm, which will enable the gain of the DL power amplifiers (R2-R5) to be reduced, with a corresponding increase in the gain of the DL compensating IF amplifier (R1). For the uplink, it is possible to drive the RF port of the mixers 10 dB below its current maximum power of -3 dBm, assuming that the mixers will not have additional conversion losses under these situations. A balance should be performed between the cost of the RF amplifiers and the cost of the mixers to determine what is the most cost-effective approach.

The gain of the uplink compensating amplifier C1 was determined in order to have an IF power of -25 dBm at the input of the IF to IQ converter, guaranteeing an optimum radio performance. A gain of 25.28 dB was therefore obtained for C1. The gain of the downlink R2

power amplifier was set in order to obtain the same wireless range obtained for the uplink, since the uplink is the most limiting direction.

The link budget calculations predicted a wireless range of up to 426.5 m between the antenna at the RRH and the mobile unit, which is considered to be suitable for the FUTON requirements, which specify a separation between neighbour RRHs of 500 m. This wireless range is similar to the one obtained for DML links. A path loss exponent of 2 was assumed.

The MZM-based FUTON link was also modelled by simulation, using the VPISystems^{TM} platform. The selected MZM model was a typical upper and lower arms configuration with dual electrode. This dual electrode configuration enabled the separate control of the DC and RF electrical signals, whereas the upper and lower arms enabled a separate electro-optic control. This model was selected because it is suitable to be configured in such a way that a number of different types of MZM devices (determined by the electrode configuration and crystal properties) can be represented. The remaining components of the link were modelled by their gain and noise figure, following the characterization determined by the power budget analysis.

6.2.4. Experimental Validation

In order to verify the analytic and simulation modelling of the link, an experimental validation of the downlink transmission was performed. Although not being a perfect reproduction of the layout presented in Figure 6.8, due to limitations of the material available, this validation was considered to be important to assess the reliability of the simulation modelling results.

The experimental setup is presented in Figure 6.10. Two MZM modules were used in the experiment. The first was a 10 Gbit/s modulator from SDL, model 10AP-Mod9204, and the second was a 40 Gbit/s modulator from Sumitomo, model DEH1.5-40PD. They are characterized by an insertion loss of 4.1 dB and 5 dB, respectively. For the first tests, using the SDL MZM, a CW laser (ECL-1520) with output power of 6 dBm was used, and an attenuation of 3 dB was included to emulate the link loss. These values were modified in the second experiment, with the Sumitomo MZM, where the same CW laser, with 3 dBm output power and an attenuation of 6 dB were used. In order to match the modelling presented in sub-section 6.2.3, the CW laser should have a higher output power, but due to limitations in the laboratory equipment, a lower output power laser was used. Therefore, the link attenuation was also set to lower values, namely 3 dB and 6 dB, to compensate the lower optical power

from the laser. The photodetector (Agere R2860D) had a responsivity of 0.8 A/W. In the following results, the input power indicates the power at the RF input of the MZM and the output power indicates the power at the input of the QAM demodulator, as represented in Figure 6.10.

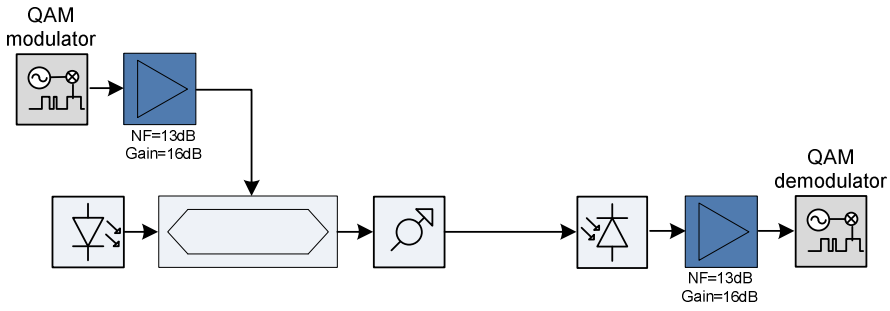

Figure 6.10 – Schematic diagram of the experimental setup for MZM link validation.

The QAM modulator and demodulator functionalities represented in Figure 6.10 were implemented using an Arbitrary Waveform Generator (Tektronix AWG7122B), with a 10 bit DAC of 12 Gsamples/s, and a digital oscilloscope (Tektronix DPO70804B), with a 10 bit ADC of 25 Gsamples/s and a bandwidth of 8 GHz, respectively. The signals used in the experiments were generated and processed offline using Matlab/VPISystems^{TM}.

The results for the SDL MZM link, depicted in Figure 6.11, were obtained for two tones with frequencies 2.468 GHz and 2.508 GHz, which were fed to the MZM. The points in Figure 6.11 represent the experimental results and the lines represent the linear approximations for the power of the fundamental tone and that of the IM3 product. The intersection between the linear approximations for the fundamental and the IM3 curve retrieves an IIP3 of 15.8 dBm for this MZM link. This link is characterized by a noise floor around -130 dBm/Hz, and its noise figure was found to be 12.7 dB. The SFDR of this link is around 94.8 dB·Hz$^{2/3}$ and the link gain is -4 dB.

The characterization of the link with the Sumitomo modulator was performed using two tones at 2 GHz and 2.030 GHz. The results obtained for this characterization are presented in Figure 6.12, where the points represent the experimental results and the lines are the linear approximations, both for the fundamental power and for the IM3 product. This link is characterized by a noise floor of around -135 dBm/Hz, a SFDR of 90.3 dB·Hz$^{2/3}$, a link gain of 22.3 dB, and an IIP3 of 16.3 dBm.

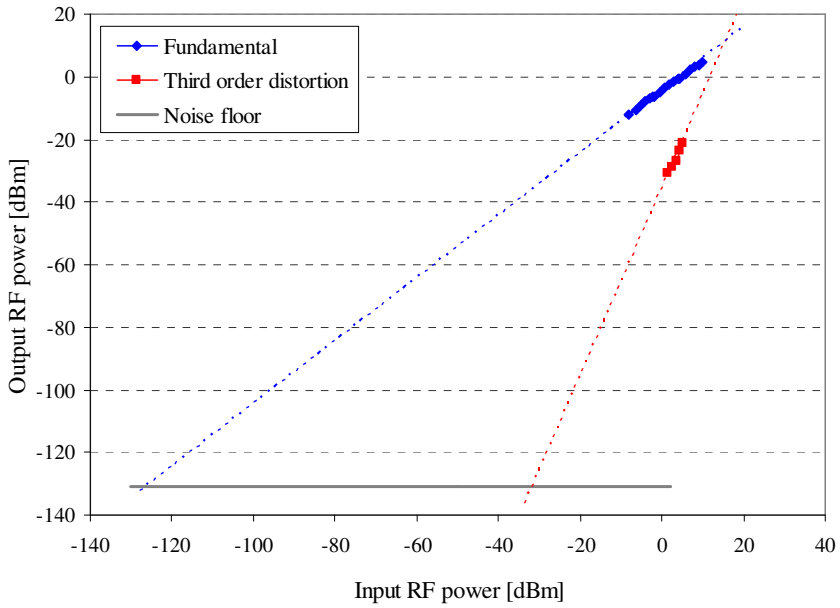

Figure 6.11 – Experimental characterization of the MZM link (SDL modulator).

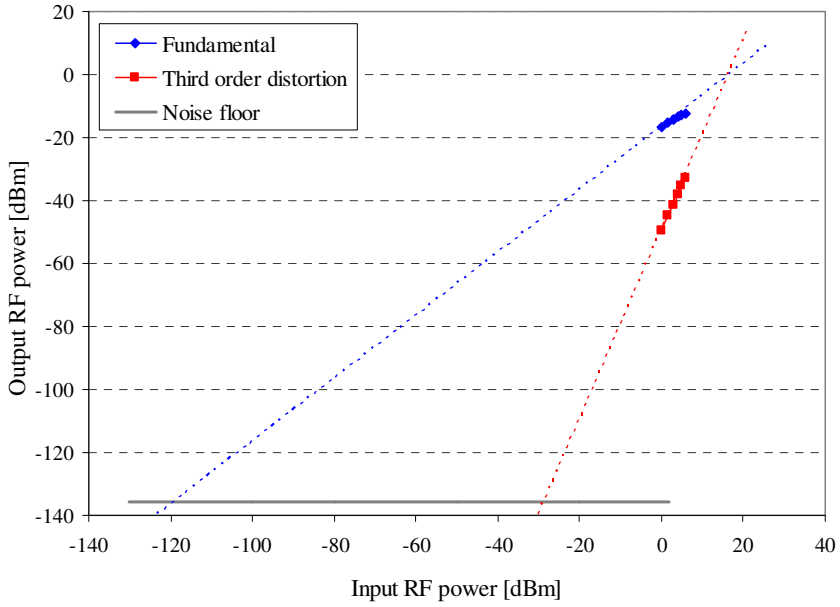

Figure 6.12 – Experimental characterization of the MZM link (Sumitomo modulator).

The experimental results of Figure 6.11 and Figure 6.12 were used to validate the simulation results obtained with the VPISystems™ modelling. Each simulation module was characterized with the values of the experimental devices, and the main simulation parameters are presented in Table 6.1. Note that the value used for link attenuation is increased to account for the losses from splices and connectors that were used in the experimental tests.

Table 6.1 Parameters used in VPISystems™ for the characterization of the MZM links.

Parameter		**SDM modulator**	**Sumitomo modulator**
CW laser	Output power	6 dBm	3 dBm
	RIN	-150 dB/Hz	-150 dB/Hz
MZM	V_π	5.5 V	5.5 V
	Extinction ratio	15 dB	35 dB
	Insertion loss	4.1 dB	5 dB
Link attenuation		3.8 dB	6.8 dB
Photodetector	Responsivity	0.75 A/W	0.75 A/W
	Transimpedance	450 Ω	450 Ω
	Equivalent input noise	1.3 µA	1.3 µA
	Noise bandwidth	8 GHz	8 GHz
	Cut-off frequency	8 GHz	8 GHz

Figure 6.13 and Figure 6.14 present the comparisons between simulation (dashed curves) and experimental (continuous curves) results. A general very good agreement was obtained for both links, especially for the link using the Sumitomo modulator, thereby validating the models. The lower values obtained for the simulated IM3 for the SDL MZM are probably due to the amplifier distortion, which is not considered in the simulations.

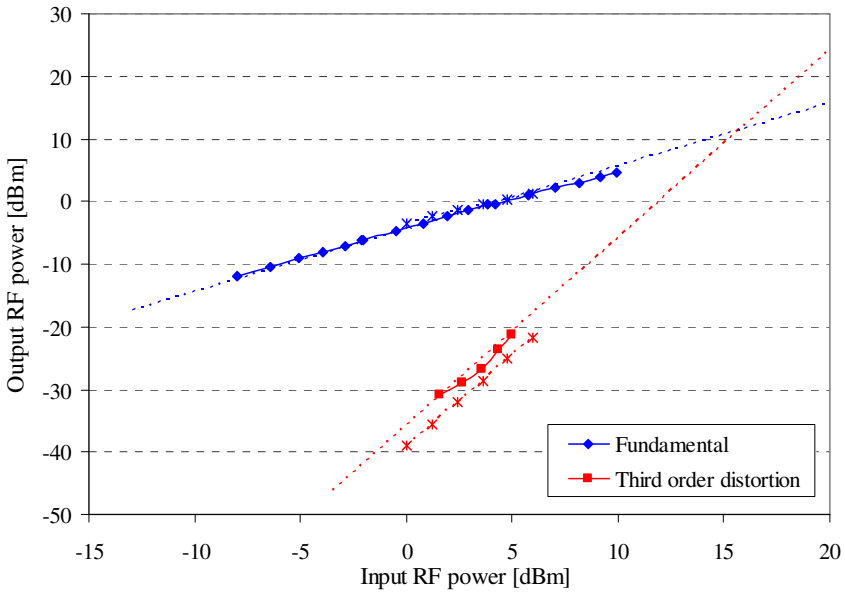

Figure 6.13 – Experimental (continuous curves) and simulated (dashed curves) characterization of the MZM link with the SDL modulator.

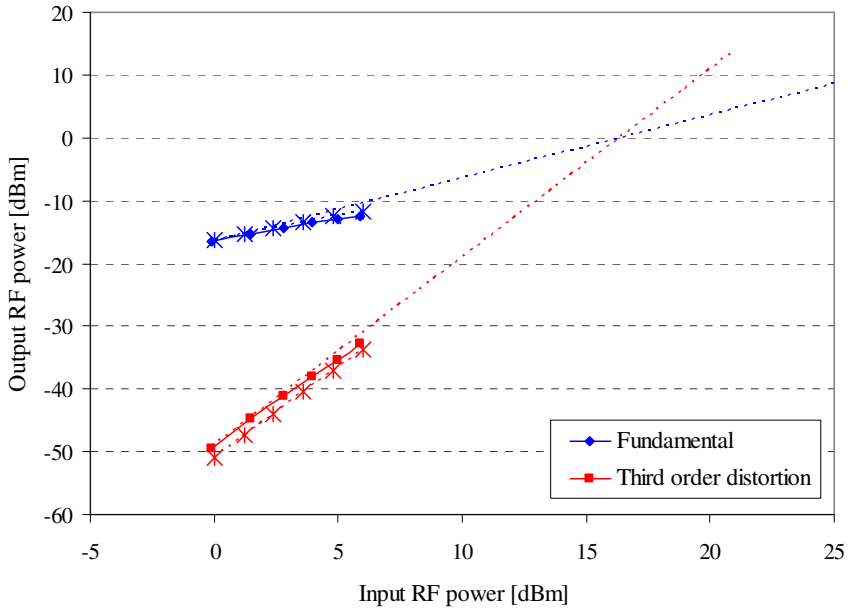

Figure 6.14 – Experimental (continuous curves) and simulated (dashed curves) characterization of the MZM link with the Sumitomo modulator.

Table 6.2 summarizes the experimental and simulation values obtained for the parameters that characterize the link, for both SDL and Sumitomo modulators, emphasizing the good match between simulation and experiment.

Table 6.2 Summary of experimental and simulation results for the MZM link.

MZM		**Gain [dB]**	**NF [dB]**	**Noise floor [dBm/Hz]**	**IIP3 [dBm]**	**SFDR [dB.Hz$^{2/3}$]**
SDL	Experimental	-4.0	12.7	-130.8	15.8	94.8
	Simulation	-4.0	13.0	-130.0	17.8	96.3
Sumitomo	Experimental	22.51	23.17	-135.35	16.34	90.31
	Simulation	22.34	23.51	-135.01	17.34	90.75

The characterization of this MZM link was also carried out in terms of Error Vector Magnitude (EVM). The EVM is a typical measure to assess the performance of wireless systems that accounts for the degradation in the signal constellations [IEEE99], [ETSI08]. For details on the EVM definition and calculation see Appendix F. The results obtained experimentally and by simulation are presented in Figure 6.15 for the SDL modulator link and in Figure 6.16 for the link with Sumitomo modulator.

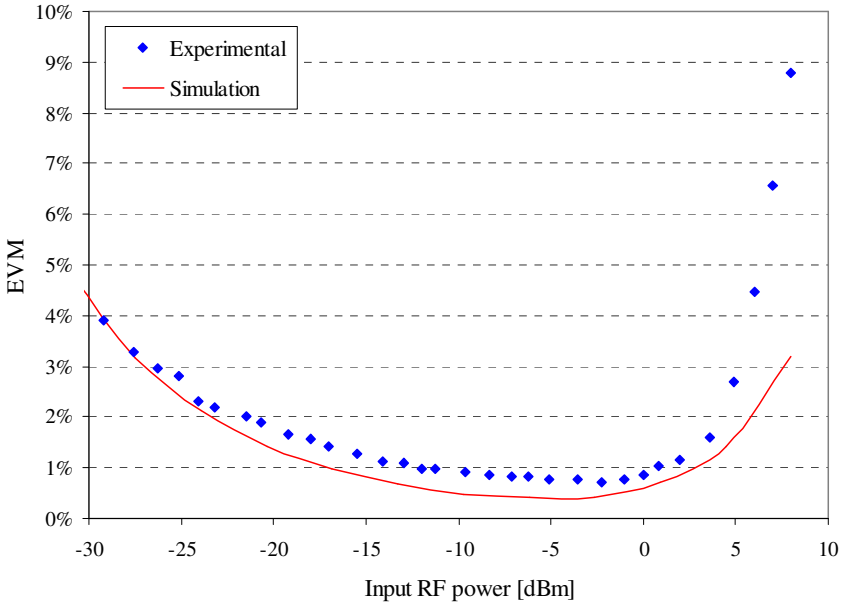

Figure 6.15 – EVM vs input power for 802.11g signal at 1 GHz (SDL modulator).

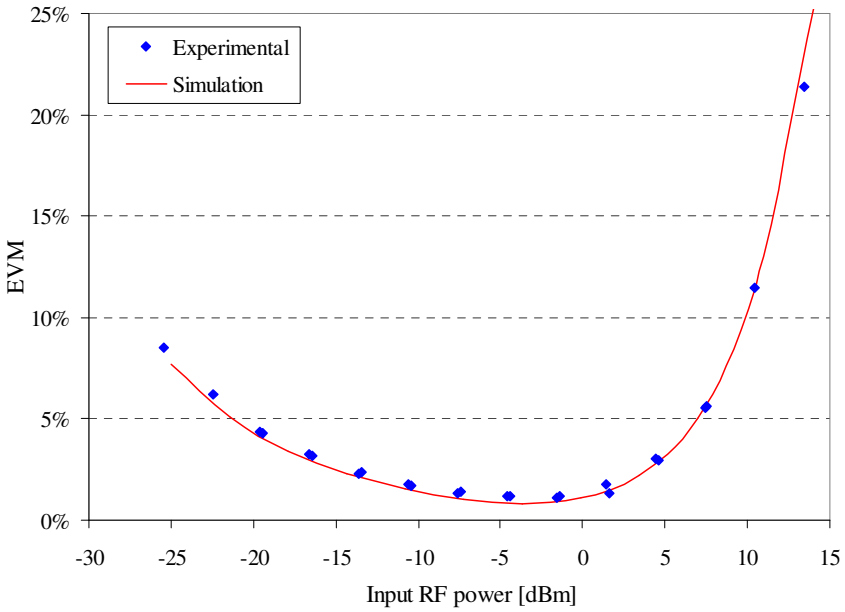

Figure 6.16 – EVM vs input power for 802.11g signal at 2 GHz (Sumitomo modulator).

The results in Figure 6.15 were obtained for a 802.11g signal at 1 GHz, and a close, although not complete, match is observed (less than 0.5% difference between experiment and simulation). Part of this difference is justified by the mismatch between the maximum amplitude of the signal and the maximum quantization level of the ADC. This mismatch has been overcome for the Sumitomo modulator. A close match between the simulated and experimental noise floors was also verified.

The EVM measurements presented in Figure 6.16 were carried out using a 802.11g signal at 2 GHz. Contrarily to the results for the SDL modulator, these results show a very close match, which validates the simulation models.

6.2.5. Predicted Performance of the FUTON System

After the modelling and corresponding validation, it is important to assess the predicted performance of the complete FUTON system, as described in sub-section 6.2.1. Therefore, simulation results were obtained using VPISystems™ for the downlink direction, considering the frequency plan defined for downlink and presented in Figure 6.7. The simulation layout is presented in Figure 6.17 and the simulation parameters are those determined in the link budget analysis and indicated in Figure 6.8.

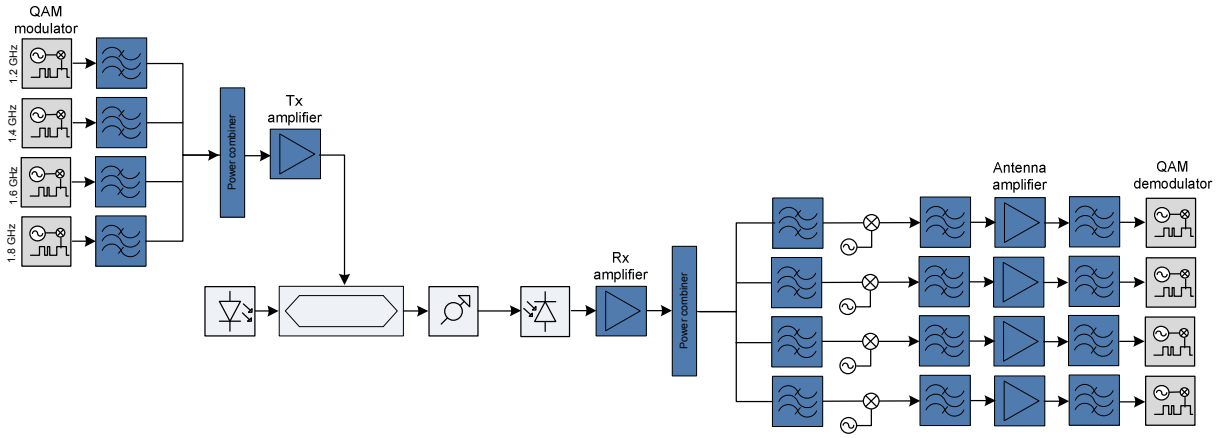

Figure 6.17 – Simulation layout for 4-channels MZM-based link transmission.

The first set of simulation results was obtained for channels with 100 MHz bandwidth, as specified for DBWS channels. A 64-QAM modulation was selected, so each channel data rate is 600 Mbit/s. Since DBWS is OFDM-based, Figure 6.18 and Figure 6.19 present the results for OFDM sizes of 64 and 512, respectively. The blue dashed curves in these figures correspond to the transmission of a single channel at 1.2 GHz, to allow for the estimation of the performance degradation when 4-channels are simultaneously transmitted. The results in Figure 6.18 and Figure 6.19 show no significant performance difference between the 4 different channels, but a clear degradation of a single channel transmission was obtained for the MZM non-linear operating region.

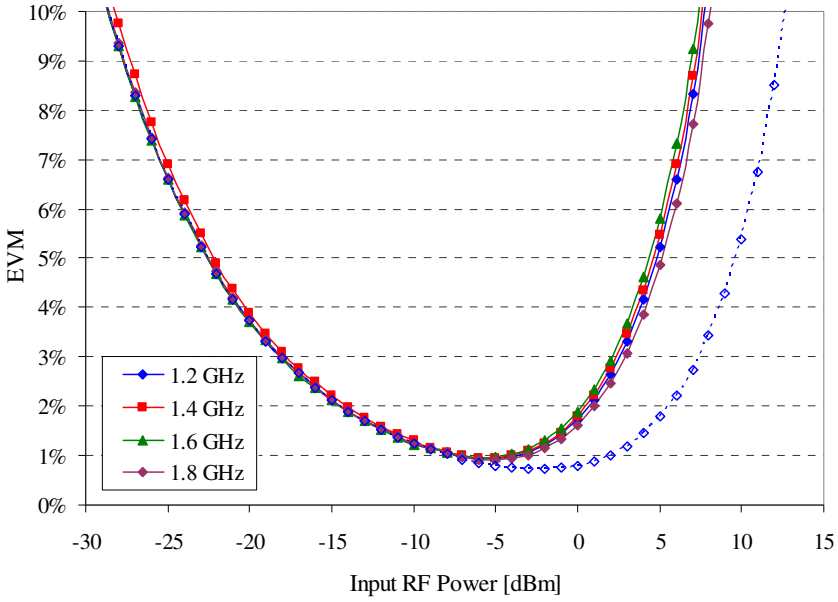

Figure 6.18 – EVM for 4-channels MZM-based downlink, each channel formatted with 64-QAM, 64 OFDM, 600 Mbit/s.

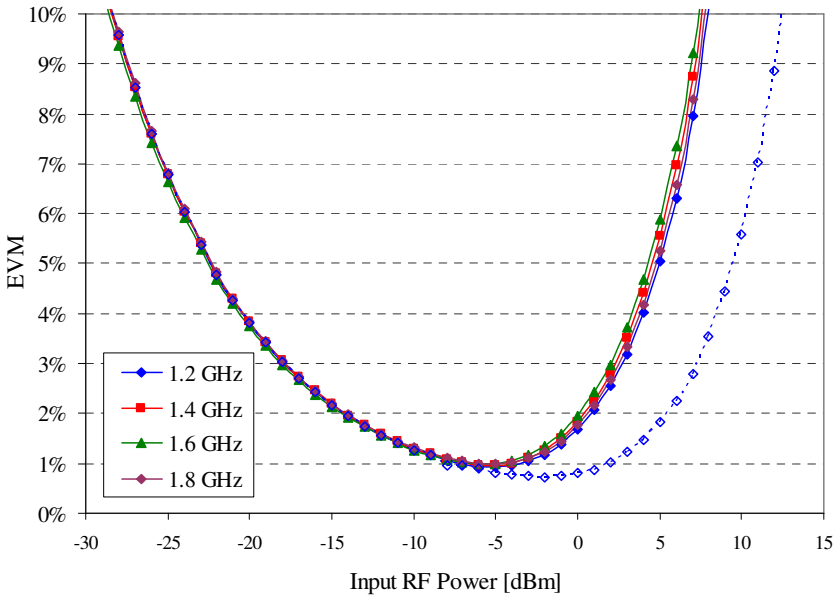

Figure 6.19 – EVM for 4-channels MZM-based downlink, each channel formatted with 64-QAM, 512 OFDM, 600 Mbit/s.

Another set of simulation results was obtained for 256-QAM modulation, therefore using 800 Mbit/s per channel. Once again, different OFDM sizes were considered. Figure 6.20 and Figure 6.21 show the results for 1024 OFDM and 2048 OFDM, respectively, and the blue dashed curve represents the transmission of a single channel at 1.2 GHz. Similarly to what was verified for 64-QAM, the results in Figure 6.20 and Figure 6.21 show

that the performance is identical for all channels being transmitted. For all the results presented, an EVM below 3% was attained for a large range of input RF powers (more than 20 dB), which is a clear indication of the viability of the system.

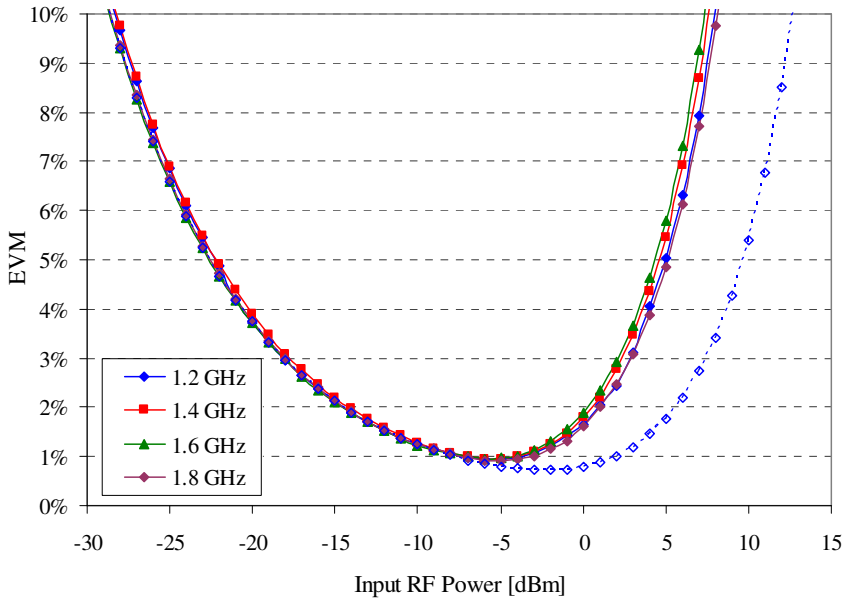

Figure 6.20 – EVM for 4-channels MZM-based downlink, each channel formatted with 256-QAM, 1024 OFDM, 800 Mbit/s.

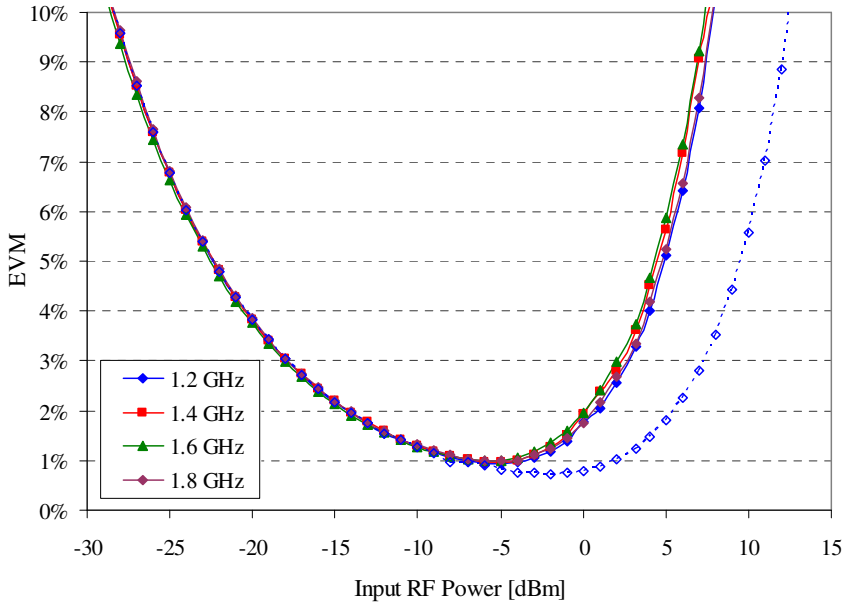

Figure 6.21 – EVM for 4-channels MZM-based downlink, each channel formatted with 256-QAM, 2048 OFDM, 800 Mbit/s.

6.3. Evaluation of Radio Channels Transmission

In the context of the FUTON project, radio channels with up to 100 MHz bandwidth were considered for next-generation systems, to provide the high data rates specified for the IMT-A systems [WDK+09]. However, a DAS network should be capable of supporting a wide range of wireless technologies, from 2G, 3G and 4G systems. Operators adopting this approach would directly benefit in terms of CAPEX, since the same physical infrastructure would be able to carry multiple technologies that differ in terms of bandwidth, data rate or modulation formats. Allocating a separate RF channel to each technology/radio signal, using a SCM scheme, is the most profitable approach.

In the following, the use of a RoF/DAS system for carrying different wireless technologies is assessed. The simulated network scenario is based on the typical RoF link depicted in Figure 6.3. The optical fibre infrastructure is assumed to have passive WDM equipment, such as multiplexers and demultiplexers. As described in Chapter 5, a good balance between the required network capacity and cost may be achieved with a DWDM architecture, suitable for the transport of multiple technologies (see sub-section 6.2.5). The power loss of the optical network was assumed to be 8 dB, excluding fibre losses. For the 1500 nm transmission window, with a fibre attenuation of around 0.2 dB/km, an average distance of 20 km was considered between the CU and the antenna sites.

The performance evaluation considered the downstream direction, from the CU towards the remote sites. A MZM-based transmitter was assumed as the optical source. The MZM, biased in quadrature and driven by the wireless signal in a push-pull configuration, is used to modulate a CW beam emitted by a laser source (see the diagram of Figure 6.10 for the schematics of the link modules). The electrical signal driving the MZM was generated using a PRBS of 2^7 - 1 modulated according to the wireless system to be transmitted in that channel. At the receiver side, after photodetection and amplification required to drive the antenna, the signal was demodulated and analyzed to estimate the performance measurements. Since no frequency up-conversion was considered, the SCM channels are simply demultiplexed using RF filters before amplification. The CW laser was characterized by an output power of 9 dBm and a linewidth of 100 kHz, for an emission frequency of 193.1 THz and a RIN of -150 dBm/Hz. The MZM was parameterized with a V_π of 5.5 V, an extinction ratio of 15 dB and an insertion loss of 4.1 dB. For the receiver, a PIN photodiode was selected, with a

responsivity of 0.8 A/W. A transimpedance of 500 Ω, an equivalent input noise current of 1.3 μA, a noise bandwidth of 8.5 GHz and a cut-off frequency of 8 GHz were considered.

6.3.1. Transmission of High-Bandwidth Channels

The most relevant technology for 4G systems is LTE, which is being developed as an upgrade of the UMTS, with the first base stations being tested nowadays. Similar to FUTON DBWS signals, LTE also uses OFDM, which enables to encode data concurrently on multiple RF carriers, allowing for increased amounts of data throughput and increased robustness, thereby guaranteeing the most efficient use of the available bandwidth.

Given the importance of OFDM in future generations, this multiplexing format is considered in the following analysis. Therefore, the transmitted signals are simulated using QAM and multiplexed using OFDM. These signals are considered to have a data rate of 40 Mbit/s, and are modulated using the 64-QAM format, with a Root-Raised Cosine (RRC) pulse shape (RRC roll-off 0.18 [ETSI08]). The multiplexing method is OFDM with 256 sub-carriers (256 OFDM). Different simulations were performed considering just a single channel at 2.5 GHz, or 3 channels at 2.25 GHz, 2.5 GHz and 2.75 GHz (frequency band typically allocated for LTE systems [ETSI08]).

The system performance was evaluated using the EVM [IEEE99], [ETSI08] to assess the signal degradation, which is affected mainly by fibre link losses, photodiode noise and MZM intrinsic nonlinearity. For QAM/OFDM signals, the LTE standard [ETSI08] specifies a maximum of 8% EVM at the end of the air link. The EVM values presented in the following results were obtained at the end of the RoF link, i.e. for signals at the input of the antenna. Therefore, a margin should be considered in the simulation for signal degradation over the air link, and thus a maximum allowed EVM of 5% was assumed. Moreover, the RF amplifier located before the antenna is usually operated near saturation, thereby producing signal distortion. A lower EVM threshold of 3% was therefore considered to provide an additional margin to account for possible distortion caused by the RF amplifiers.

Figure 6.22 presents the EVM as a function of the RF power at the input of the MZM, for different fibre lengths. The dashed lines correspond to the average EVM for the transmission of 3 channels, whereas the continuous lines correspond to the EVM for a single channel at 2.5 GHz. As shown in Figure 6.22, from lower to higher RF input powers, the EVM decreases towards a minimum, before increasing again. For low power levels, the

degradation of the signal constellation, evidenced by the high EVM values, is due mainly to fibre link losses and to the noise introduced by the photodiode. The same performance is obtained for single channel and three channel operation, as shown by the overlap between the dashed and continuous curves, for each fibre length. However, as the input power increases, the nonlinearity of the MZM becomes significant, and the signal is distorted by the in-band interfering signals, showing an EVM increase. For higher power levels, an overlap between the dashed and continuous curves for all fibre lengths is shown in Figure 6.22. This overlap confirms that the MZM non-linearity is the main source of distortion. In the single channel case, a smaller degradation is observed when compared to the 3 channels case, as the input power increases and the MZM enters the nonlinear operating region. In the 3 channels case, the EVM starts increasing for a lower RF input power than in the single channel case, -5 dBm and -1 dBm, respectively. This was expectable since a higher degradation occurs in the 3 channels case due to the beating between channels, which generates additional intermodulation products within the signal band [Cox04].

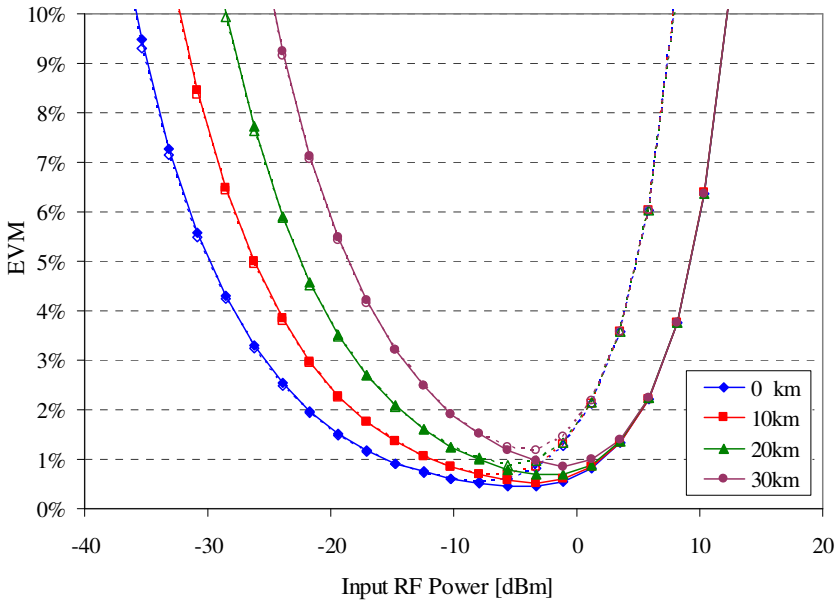

Figure 6.22 – EVM for QAM/OFDM signals transmission through different fibre lengths: single channel (continuous) and three channels (dashed).

Table 6.3 presents the EVM power margin, which is comparable to the total power range definition as presented in [ETSI00], [ETSI01], and [ETSI08], and is calculated as the RF input power range that guarantees an EVM below a specified maximum. The maximum reach that guarantees transmission with a specified maximum EVM value, for the optimum

RF input power, is also presented in Table 6.3. It can be seen that the considered average reach of 20 km may be surpassed in all considered scenarios. For the most restrictive case (fibre length of 30 km and an EVM limit of 3%), a power margin of 17 dB is obtained for the simultaneous transmission of 3 QAM/OFDM channels. This clearly indicates that RoF is suitable for transmission of next generation wireless signals, since the results comply with [ETSI08], which specifies that the total power dynamic range for LTE should be between 8 dB and 20 dB, depending on the signal bandwidth.

Table 6.3 Power margins and maximum reach for QAM/OFDM transmission.

EVM limit		**3%**		**5%**		**8%**	
		1 ch.	**3 ch.**	**1 ch.**	**3 ch.**	**1 ch.**	**3 ch.**
Power margin [dB]	0 km	33	28	39	35	45	41
	10 km	29	25	35	32	42	38
	20 km	25	21	32	28	38	34
	30 km	21	17	28	24	34	30
Maximum reach [km]		62	52	74	65	84	75

6.3.2. Transmission of 2G, 3G and 4G Radio Channels

As previously mentioned, the support of legacy systems by the next generation architectures may be proven to be of critical importance, in order to optimize investments and resources. Therefore, the performance assessment of the analogue DAS network is presented in the following, for a scenario where 4G-like signals are transmitted simultaneously with 2G- and 3G-like signals. The support of legacy systems was evaluated for modulation formats representing the GSM, for 2G, and UMTS for 3G. The GSM-like signals were modelled using Gaussian Minimum Shift Keying (GMSK), with BT of 0.5 [ETSI00], and multiplexed using FDM (GMSK/FDM), with a bit rate of 0.25 Mbit/s. For UMTS-like signals Quadrature Phase Shift Keying (QPSK) modulation was used, with RRC roll-off of 0.22, and Code Division Multiple Access (CDMA) [ETSI01] was used as multiplexing scheme (QPSK/CDMA). Carrier frequencies of 900 MHz and 2.12 GHz were selected for GMSK/FDM and QPSK/CDMA signals, respectively. The signals representative of 4G were characterized as described in sub-section 6.3.1, for a carrier frequency of 2.5 GHz.

Figure 6.23 depicts the EVM as a function of the RF input power for QPSK/CDMA (3G) and QAM/OFDM (4G) signals, considering a fibre length of 20 km. The dashed lines

correspond to the transmission of a single QPSK/CDMA or QAM/OFDM channel, and the continuous lines represent the EVM for QPSK/CDMA or QAM/OFDM signals, when GMSK/FDM, QPSK/CDMA and QAM/OFDM signals are simultaneously transmitted using SCM. The EVM curve for the transmission of 3 QAM/OFDM channels, as presented in Figure 6.22, is reproduced here in red for comparison. The results obtained for QPSK/CDMA always show a lower EVM degradation than that for QAM/OFDM signals, which is justified by the different characterization of both signals, in terms of bit rate, modulation format and carrier frequency. Once again, similar performance is obtained for the low input power region, for the single channel case and for the simultaneous transmission of the three technologies. Figure 6.23 shows a lower EVM degradation in the nonlinear region for a QAM/OFDM signal transmitted simultaneously with GMSK/FDM and QPSK/CDMA (blue curve), than when 3 QAM/OFDM channels (red curve) are considered. This is justified by the unequal separation between the channels in the first case, which results in a reduced number of in-band intermodulation products. This situation differs from the one described in sub-section 6.3.1, where the channels were equally separated in frequency, resulting in a higher intermodulation distortion.

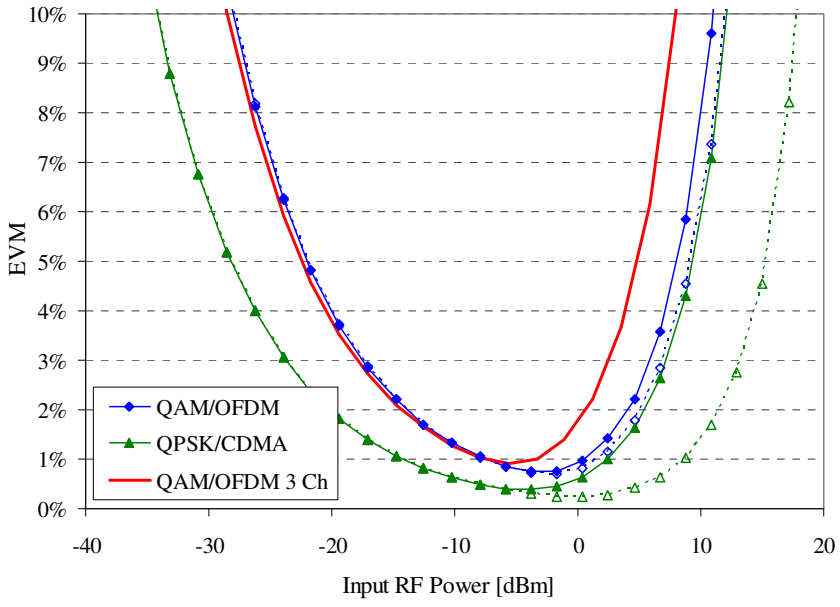

Figure 6.23 – EVM for QAM/OFDM and QPSK/CDMA transmission for a reach of 20 km: GMSK/FDM+QPSK/CDMA+QAM/OFDM (continuous) and single channel (dashed).

The performance of GMSK/FDM signals is presented in Figure 6.24, in terms of BER, for a fibre length of 20 km. The BER estimation was obtained by averaging the BER values

obtained for the in-phase and quadrature signal components. The performance of a single GMSK/FDM signal is represented by the red curve, while the blue curve corresponds to the GMSK/FDM signal transmitted together with QPSK/CDMA and QAM/OFDM channels. The results presented in Figure 6.24 show that GMSK/FDM is more resilient to the nonlinearities of the RoF link than QPSK/CDMA or QAM/OFDM, since an error free transmission is obtained for a larger power margin, both for a single GMSK/FDM signal transmission and for the simultaneous transmission of GMSK/FDM, QPSK/CDMA and QAM/OFDM signals. A BER above 10^{-12} is obtained only for RF input powers higher than 20 dBm and 15 dBm in each case, respectively, and lower than -40 dBm. This resilience of the GMSK/FDM format is due to the presence of a constant signal envelope, result of the use of GMSK, which makes these signals less vulnerable to nonlinear distortion.

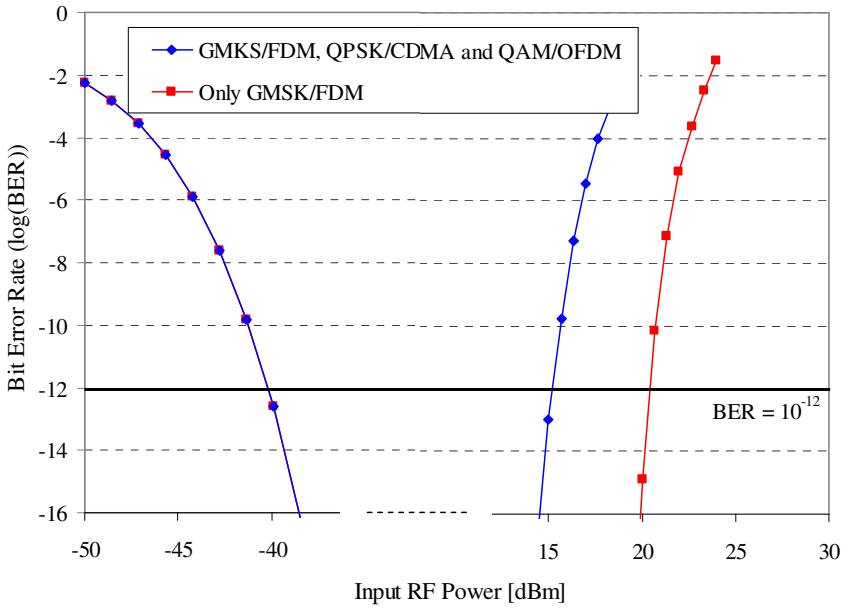

Figure 6.24 – BER for GMSK/FDM transmission for a reach of 20 km: single channel (red curve) and GMSK/FDM+QPSK/CDMA+QAM/OFDM (blue curve).

Table 6.4 shows the power margins, in dB, for GMSK/FDM, QPSK/CDMA and QAM/OFDM signals, considering the transmission of a single channel (1C) and the joint transmission of the 3 systems (3C), for different EVM and BER limits. The UMTS standard [ETSI01] specifies a maximum EVM of 17.5%. As explained in sub-section 6.3.1, for the QAM/OFDM performance evaluation lower EVM levels were assumed, to provide margins for further degradation due to transmission over the air link and amplifier nonlinearity. The power margin values presented in Table 6.4 comply with the minimum requirements specified

for GSM (30 dB) [ETSI00], UMTS (18 dB) [ETSI01] and LTE [ETSI08], thereby confirming the feasibility of RoF transmission for all wireless systems. As expected, the most critical scenario is the simultaneous transmission of 3 QAM/OFDM channels.

Table 6.4 Power margins for GSMK/FDM, QPSK/CDMA and QAM/OFDM transmission.

Power margin [dB]		**EVM**				**BER**
		17.5%	**8%**	**5%**	**3%**	**10^{-12}**
QAM/OFDM	1C	-	37	31	25	-
	3C	-	36	30	23	-
QPSK/CDMA	1C	59	50	-	-	-
	3C	54	44	-	-	-
GMSK/FDM	1C	-	-	-	-	62
	3C	-	-	-	-	55

Overall, these results show that a RoF network is suitable for the simultaneous transmission of different wireless systems, covering the legacy generations, 2G and 3G, as well as the future 4G generation.

6.4. Conclusions

The use of analogue RoF over a network architecture based on distributed antennas is emerging as a beneficial approach for supporting the demanding requirements of next generation wireless systems.

In this context, the FUTON project proposed the development of a hybrid radio-optic infrastructure, which would enable to transport transparently radio signals from/to a set of multiple remote antennas to/from a central unit. This unit is responsible for all signal processing tasks, providing means to develop new concepts and algorithms based on MIMO and inter-cell interference cancellation. The FUTON project has successfully demonstrated the feasibility of such architecture, as well as the validity of the developed algorithms for very high bandwidth radio channels that comply with the specifications imposed by IMT-A.

The enabler of the FUTON concept is its radio-optic infrastructure, which is based on simple RoF technology. Several link types were studied and modelled as possible alternatives

for this project, namely using MZMs, DMLs or RSOAs as optical sources. The MZM-based link received special attention along this chapter, where its detailed link budget modelling was presented, and the experimental validation of the simulation tests showed the reliability of the models developed. The use of these models to predict the performance of the complete link allowed assessing the system behaviour for transmitted signals with different characteristics, in terms of data rate and multi-level modulations.

Several economic and network capacity benefits are expected if DAS is considered as a possibility for the deployment of next generation wireless network architectures, especially if multiple radio systems may be carried over the same physical infrastructure. It is therefore important to assess the suitability of such scenario to support legacy and future wireless technologies. An evaluation of an analogue DAS network, using RoF, was then performed for the transmission of 4G systems, such as LTE, considering the transport of a single channel or three different channels, using SCM, showing suitable performance for both cases. Moreover, the simultaneous transport of 2G, 3G and 4G signal formats was also evaluated, and the performance assessment has shown that the RoF/DAS network is capable of transmitting simultaneously future generation and legacy systems with low degradation.

Chapter 7

CONCLUSIONS

The ever-growing bandwidth demands have been the main driver for the evolution registered in the telecommunications networks during the last decade, which has been especially remarkable in the access landscape, for both wired and wireless systems. The current progress towards next generation access networks aims to design future systems that simultaneously comply with customers and operators needs. In this context, it is of foremost importance the development of strategies to deploy cost-effective access networks, while being able to provide the necessary bandwidth demands and preventing this network segment from becoming the communications bottleneck. Generally, the present thesis was focused mainly on identifying methodologies and performance improvement approaches to help fulfilling such objective. In the following, the main conclusions of the work are highlighted and topics for future research are suggested.

7.1. Main Conclusions

The work reported in the present thesis was divided into two distinct parts, addressing in Part A relevant physical layer issues of PON systems exploiting high data rate, whereas the convergence of wired and wireless access systems, through the use of an optical infrastructure to distribute radio signals, was the focus of Part B.

Amongst the possible upgrade scenarios for EPON and GPON systems, the data rate upgrade to 10 Gbit/s has prevailed. Chapter 2 was therefore devoted to the assessment of part of the physical layer impairments characteristic of these systems. Limitations driven by the optical source, assuming that low-cost FP lasers are employed at the ONUs, were measured through the impact of MPN on the upstream system performance, showing that its influence is not negligible. The system specifications in terms of maximum allowed values for source spectral width, fibre dispersion, and network reach were identified by simulation for a target system performance, showing that for a typical transmission reach of 20 km a reduced spectral width is necessary, as well as low fibre dispersion. The effect of fibre nonlinearities in 10 Gbit/s PON systems, namely SPM, SBS and SRS, was also estimated in chapter 2, to determine the limits imposed on the power transmitted through the fibre. It was concluded that SBS is the main nonlinear impairment in these systems, limiting the power launched into the fibre to around 11.6 dBm for NRZ signals, for a typical transmission reach of 20 km. It also imposes restrictions on the network reach and/or splitting ratio, if no suppressing method is employed. The effect of SPM was considered negligible and SRS was shown to be important when an overlay analogue signal is simultaneously transmitted. Chapter 2 also addressed the issue of receiver sensitivity decrease at 10 Gbit/s, which may require the use of photodetectors with gain, mainly in scenarios with a critical power budget. In this context, the use of APD receivers was analyzed for 10 Gbit/s PONs, showing that, if operated far from an optimum value of the gain, they may instead cause performance degradation due to the added excess noise. Analytic results show that for an APD gain around 7, a compliant network performance may be attained, with penalties lower than 2 dB.

The inclusion of FEC codes to improve the performance of PON systems operating at 10 Gbit/s was evaluated in chapter 3. An overview of the fundamental concepts of the main types of correction codes was outlined, pointing out their advantages and disadvantages when applied in high data rate PON systems, which enabled to select RS codes as the most appropriate. Several performance metrics, including the NCG and the error rate, were used to identify the code parameters that should be selected for a specific network scenario. Amongst them, the correcting capability and the code overhead are the most relevant. Actually, the higher is the error burst correcting capability of the code, the higher is the overhead, and therefore a trade-off between these two parameters should be found. Moreover, for burst-mode transmission, such as for the PON upstream system, the length of the frames is also important with respect to the complexity of the encoder and decoder, which in turn may have a cost impact on the total system expenditures. The attainable performance benefits by using

FEC on the upstream 10 Gbit/s system were quantified through simulation. It was proven that the inclusion of FEC allows minimizing the penalty due to MPN in networks employing multimode laser sources, enabling less stringent specifications for critical system parameters, such as the source spectral width and fibre dispersion.

Burst-mode transmission is one of the main challenges towards the deployment of cost-effective and high performance 10 Gbit/s PON systems, and is the focus of chapter 4. The impact of this operating mode on the system performance may be reduced by introducing power equalization to minimize the near-far effect characteristic of such systems. Therefore, chapter 4 overviews available proposals to realize power equalization and, by evaluating their benefits and weaknesses when employed in access networks, concludes that the most suitable approach uses SOAs. In this context, power equalizers based on SOAs were characterized in terms of gain and recovery time and a novel 10 Gbit/s all-optical power equalization scheme based on two cascaded-SOAs was proposed to be applied in burst-mode applications. The design rules to optimize the operation of this scheme, which includes a gain stage to pre-amplify the received signal in order to saturate a SOA in the equalization stage, were devised for EPON systems, but may be easily extrapolated for other systems. The performance of the proposed equalization method was analysed for two network applications. The first, in 10 Gbit/s EPON upstream systems, showed an effective burst equalization and significant benefits regarding the dynamic range of the OLT receiver. The second application consisted on using the power equalizer at the RN of a TDM/WDM metro-access network, and benefits in terms of power gain and the overall performance of the system were obtained.

Part B of the thesis is initiated with chapter 5. This chapter, devoted to the convergence of wireless and wired access networks which is foreseen as a promising approach to provide low-cost 4G services, describes the architecture scenarios of a hybrid radio-optic infrastructure. The compatibility of radio systems with standard PON systems was evaluated to guarantee the coexistence of both technologies over the same optical infrastructure. Several possible candidate architectures for this infrastructure were addressed, and compared in terms of power budget and cost, leading to the conclusion that a CWDM approach is preferable for low cost deployments, at the expense of a reduced number of connected antenna sites, and a DWDM-based architecture should be considered if a higher user density is envisioned for the system. After defining the architecture, analogue and digital transmission modes were assessed to carry radio signals in these DAS networks, with special emphasis on digital protocols, evaluating their bandwidth capacity requirements and their use

to map radio signals over PON standardized systems. Since these digital protocols require the provisioning of a very large available bandwidth, first generation EPON and GPON systems are insufficient to support a cost-effective deployment of multiple WiMAX or LTE remote sites. For such scenarios, it is therefore necessary to rely on high data rate PONs or on the new optical access paradigms, such as NGOA. When comparing the cost of the digital approach with the analogue approach to transmit radio signals, it was found that analogue links may be more than one order of magnitude less expensive than digital links, for next generation wireless signals. This evidence results from the large data rates that are required for wideband systems, allowing to conclude that nowadays analogue transmission presents more benefits, also in terms of simplicity and lower power consumption.

In the context of hybrid radio-optical architectures based on analogue transmission, Chapter 6 is focused on the work carried out in the framework of the FUTON project. The main purpose of this project, which was successfully demonstrated, was to develop a hybrid infrastructure able to transparently carry next generation radio signals, and benefiting from MIMO and inter-cell interference cancellation mechanisms. The technology selected for FUTON was based on RoF links, using MZMs, DMLs or RSOAs as optical sources. Chapter 6 provided a detailed description of the link budget modelling based on MZMs and the experimental validation of the simulation results obtained through modelling. The predicted performance of a FUTON system based on MZM links was assessed, allowing to verify the system behaviour for radio signals with different parameterizations, proving its viability. The benefits brought by a DAS network such as FUTON include economical savings and higher network capacity, mainly if multiple radio systems may be carried over the same physical infrastructure. In this context, the suitability of such scenario was evaluated for the transport of multiple 4G systems, and also for the simultaneous transport of 2G, 3G and 4G signal formats, showing in both cases compliant performance with low degradation for the support of future and legacy systems.

7.2. Future Work

The research work carried out along the present thesis may be extended to include other relevant topics for future investigation. Maintaining the focus on upcoming systems and architectures for access networks, the data rate increase to 40 Gbit/s may be envisioned as an upgrade possibility for TDM PONs. Being able to provide an aggregated speed of 40 Gbit/s,

may allow serving each end-user with a data rate comparable to the present WDM-PON systems. Although the cost of such system is nowadays still prohibitive, some research work might be developed mainly concerning the burst-mode operation, and associated receiver, of the upstream transmission. Since this subject is already a challenge for 10 Gbit/s systems, for 40 Gbit/s very high speed electronics would be required or very efficient power equalization methods should be applied to minimize the near-far effect, thereby approaching the operation of a burst-mode receiver to that of a typical continuous receiver. This is an important investigation topic, where the use of SOAs, MZI-SOAs, EDFAs or combined electronics may be exploited to determine the most suitable and efficient method. Another important aspect that may be investigated in 40 Gbit/s systems is the type of modulation format that should be used and how is it affected by fibre dispersion and nonlinearities.

As indicated in chapter 1, the use of WDM in access systems is now envisioned as a very promising approach for next generation deployments. Although they have already been intensively studied, WDM-PONs still present some open issues that may be explored. Particularly in metro-access systems, wavelength routing and selection at the remote node and low-cost protection mechanisms should be the focus of further investigation. The RN architecture is of paramount importance in these systems, since it must provide connection towards the end-user without traffic disruption. Furthermore, the deployment of all-optical RNs may be proven to be beneficial in terms of CAPEX savings, but requires further investigation on wavelength conversion devices and amplification/regeneration characteristics.

The insight on wireless-optical convergence provided by this work combined with the recognition of NGOA as a strong candidate for future access systems enables to devise several interesting research topics. Since NGOA is based on UDWDM, with a wavelength grid of a few GHz, the support of different traffic types, of both fixed and radio services, on neighbouring channels may result in some interference that should be accounted for in the network planning. This may even become a more complex issue if SCM techniques are used to transmit the radio signals. The coexistence of baseband and RF signals should be thoroughly analyzed, evaluating the potential impact of spurious frequency interferences, which may also depend on the type of modulation device that is being utilized. In order to assess the real viability of NGOA, and taking into consideration the present high cost of tuneable lasers, an economical comparison with competing solutions should be realized, assessing its benefits in terms of capacity provided, mobile backhauling support, upgradeability and predicted lifetime.

Appendix A

SBS Theory for Optical Fibres

One of the main fibre nonlinear effects affecting optical access networks, such as PONs, is the SBS. The characterization of this effect is properly accomplished only by solving the acousto-optic equation [KKC+05], [PT06], considering that the back-reflected (Stokes) power is described by an evolutional equation where the nonlinear term is inversely proportional to the acousto-optic effective area, A^{ao}, rather than the optical effective area A_{eff}. This appendix presents the theory behind the calculation of SBS in optical fibres [KKC+05].

This analysis is based on the equation for the acousto-optic interaction, given by:

$$\frac{\partial^2 \rho}{\partial t^2} - \Gamma \nabla^2 \frac{\partial \rho}{\partial t} - \nu_l^2(r) \nabla^2 \rho = -\frac{\gamma}{2} \nabla^2 E^2 , \tag{A.1}$$

where ρ is the material density fluctuation around a mean value ρ_0, given in kg/m^3, Γ is the damping factor, given in m^2/s, and ν_l^2 is the squared longitudinal sound velocity, in m^2/s^2, that depends on the transverse radial coordinate r due to silica doping with germanium dioxide (GeO_2). This dependence creates guiding of acoustic waves in the optical fibre. The damping factor and the squared longitudinal sound velocity are given by equations (A.2) and (A.3), respectively:

$$\Gamma = \frac{\eta_{11}}{\rho_0} ; \tag{A.2}$$

$$\nu_l^2(r) = \frac{Y(r)}{\rho(r)} . \tag{A.3}$$

In equation (A.2), η_{11} is the component of the viscosity tensor, and in equation (A.3), $Y(r)$ is the Young's modulus. The γ factor in equation (A.1) represents the electrostriction constant, in F/m, and is given by:

$$\gamma = n^4 \varepsilon_0 p_{12}, \tag{A.4}$$

where n is the glass refraction index, p_{12} represents the component of the electrostriction tensor and ε_0 is the vacuum permittivity. The electric field E that is included in the right side of equation (A.1) may be represented by a superposition of forward and backward propagating electromagnetic waves, such as:

$$E(r,z,t) = \frac{f(r)}{2}\left[A_1(z,t) e^{j(\omega_1 t - \beta_1 z)} + A_2(z,t) e^{j(\omega_2 t + \beta_2 z)} \right] + c.c., \tag{A.5}$$

where $A_i(z,t)$, with $i = 1,2$, represents the slowly varying envelopes of the optical field, ω_i and β_i are the frequency and propagation constants of the optical waves, "c.c." stands for complex-conjugate, and $f(r)$ represents the fundamental optical mode profile and satisfies the following:

$$\frac{\partial^2 f(r)}{\partial r^2} - \frac{1}{r^2}\frac{\partial f(r)}{\partial r} + \left[\frac{\omega^2 n^2(r)}{c^2} - \beta_i^2 \right] f(r) = 0. \tag{A.6}$$

Looking at equation (A.1), its solution can be written as:

$$\rho(z,t,r) = \frac{1}{2}\sum_{m=1}^{M} \rho_m(z,t)\xi_m(r) e^{j(\Omega t - qz)} + c.c., \tag{A.7}$$

where $\Omega = \omega_1 - \omega_2$ is the acoustic frequency and $q = \beta_1 + \beta_2 \approx 4\pi n/\lambda$, with λ representing the wavelength of the input signal. M is the number of acoustic wave modes $\xi(r)$, which are the solutions of the unperturbed equation (A.1), and thus satisfy the eigenvalue equation:

$$\frac{\partial^2 \xi_m(r)}{\partial r^2} - \frac{1}{r^2}\frac{\partial \xi_m(r)}{\partial r} + \left[\frac{\Omega_m^2}{v_l^2(r)} - q^2 \right] \xi_m(r) = 0. \tag{A.8}$$

Here, only acoustic modes without axial variation were considered, because only these modes interact efficiently with the axially symmetric optical mode $f(r)$.

The acousto-optic interaction in optical fibres induces a nonlinear polarization, P_{NL}, which is expressed by:

$$P_{\mathrm{NL}} = \frac{\gamma \rho E}{\rho_0}. \tag{A.9}$$

By replacing expressions (A.5) and (A.7) in the equation for nonlinear polarization and following the perturbative approach for the derivation of the nonlinear pulse propagation in an optical fibre, the propagation equation for the optical powers P_1 and P_2 is obtained:

$$\frac{dP_j}{dz} \pm \alpha P_j + \frac{g_{\mathrm{B}}}{A_m^{\mathrm{ao}}} \overline{\gamma}(\nu) P_1 P_2 = 0, \tag{A.10}$$

where the plus (upper) sign applies to the forward propagating optical wave ($j = 1$) and the minus (lower) sign applies to the backward propagating (Stokes) wave ($j = 2$), α represents the fibre loss coefficient, and g_{B} is the Brillouin gain coefficient, given by:

$$g_{\mathrm{B}} = \frac{4\pi n^8 p_{12}^2}{\lambda^3 \rho_0 c w \nu_{\mathrm{B}}}, \tag{A.11}$$

where w represents the Full Width at Half Maximum (FWHM) Brillouin gain and ν_{B} represents the frequency shift.

In equation (A.10), $\overline{\gamma}(\nu)$ is the normalized Lorentzian spectral shape and A^{ao} is the acousto-optic effective area, that quantifies the peak value of the Brillouin gain, which are given by (A.12) and (A.13), respectively.

$$\overline{\gamma}(\nu) = \frac{(w/2)^2}{(\nu - \nu_1 + \nu_{\mathrm{B}})^2 + (w/2)^2}, \tag{A.12}$$

$$A_m^{\mathrm{ao}} = 2\pi \left[\frac{\int_0^{\infty} f^2(r) r dr}{\int_0^{\infty} \xi_m(r) f^2(r) r dr} \right]^2 \int_0^{\infty} \xi_m^2(r) r dr \,, \tag{A.13}$$

To evaluate the SBS threshold of one optical fibre it is necessary to solve the modal equations for acoustic (A.8) and optical (A.6) waves and calculate A^{ao} from (A.13) for several lowest-order acoustic modes.

Appendix B

All-Optical Remote Node for Metro-Access Network Convergence

The growing PON rollouts, already underway in many countries, will likely drive the development of a variety of new and even more bandwidth-intensive services. Consequently, as subscribers massively adhere to these services, the capacity requirements in the metro side can increase considerably. Traditionally, upgrading the capacity of metro networks is accomplished by installing costly Synchronous Digital Hierarchy (SDH) and WDM gear. However, a more cost-effective upgrade of the metro segment of the network can be on the horizon. More precisely, as the access and metro networks start sharing the same transmission medium, there is the potential that they will converge to use similar technologies, thus benefiting from economy of scale and lower maintenance costs, a possibility already forecasted by researchers [SPMP08] and network operators [RSG10], [SGR+11]. Actually, the expected large scale deployment of optical fibre in the access segment provides a common transmission medium to both access and metro networks, motivating the research and development of network architectures for seamless metro-access convergence, given their potential for additional cost savings.

A promising approach to realize the above mentioned convergence is to scale the PON system, although without necessarily keeping it passive end-to-end, to support with a single network infrastructure a larger number of subscribers, which were formerly partitioned into multiple access networks [SM07]. A cost-effective and scalable solution to increase the transmission capacity is to deploy WDM in the former metro part, while TDM is kept in the former access part. However, this raises important implementation challenges. Firstly, the longer transmission distances between OLT and ONU will likely require intermediate signal

amplification or regeneration. Secondly, supporting such a large number of subscribers (hundreds or even thousands) demands a very high transmission capacity. Sharing a single wavelength in the downstream/upstream among all ONUs requires increasing the channel bit rate. This may become cost-prohibitive, given the increased transmission impairments and because each ONU must be able to transmit/receive data at such high bit rates. Thirdly, the converged network will likely support a greater diversity of subscribers (for instance, residential and business customers), which can have very different requirements in terms of bandwidth, QoS, security and resilience. Finally, in the cases where the fibre-based access networks have been previously deployed and are using different protocols, bit rates or modulation formats, integrating these access networks into a single network could benefit, in some cases, from maintaining some of the deployed systems. Hence, transparency to protocol, bit rate or modulation format could increase the cost-effectiveness and flexibility of this upgrade scenario.

In the following, the challenge of deploying a converged network that can support a large number of subscribers with higher data rates than that of [SPMP08] is addressed. It intends to achieve the following goals:

- Cost-effective metro-access network;
- All-optical transmission between the central office (OLT) and the user equipment (ONU), enabling a bit-rate and protocol independent network;
- Single specification for all ONUs.

B.1. Metro-Access Proposals

The problem of implementing metro-access networks in a cost-effective way, using optical fibre as the transmission medium, has been previously addressed in several proposals. An example of such a system is given in [HKTG06]. This proposal uses a distribution WDM network connecting several RNs to a central office. Each RN drops one wavelength channel from the downstream loop with an add/drop multiplexer and subsequently uses an Optical/Electrical/Optical (O/E/O) repeater to amplify the downstream signal. Another O/E/O repeater is used to amplify the upstream signal before inserting it into the upstream loop using an add/drop multiplexer. Survivability to failures affecting the WDM distribution network is provided, through the use of two fibres (one for clockwise transmission and the other for counter-clockwise transmission) and duplicated equipment for optical transmission and

reception at the central office. The main limitation of this proposal is related to the O/E/O feature needed at the RNs. Although it ensures the desirable functionalities of amplification and wavelength conversion, the electrical processing strongly limits its applicability range, since it is neither data rate nor protocol independent. Moreover, in order to properly handle the common upstream bursty traffic, the O/E/O module used in the upstream should have burst detection and burst Clock and Data Recovery (CDR) features, making it similar to (and as expensive as) the burst-mode receiver used at the OLT.

When comparing the current standardized PON systems several differences are evident, including the number of connected ONUs, the data rate and the supported transmission protocols. Despite their advantages regarding economics and low maintenance, the currently standardized PONs present a limited capacity, in terms of the number of subscribers that may be connected, if a reasonable bandwidth must be guaranteed for each of them (even with the newest 10G EPON and XG-PON1). Additionally, they are limited to network distances typically below 20 km, which is even aggravated by optical budget problems, mainly when the number of splitter ports increases. Due to their disadvantages, these networks by themselves are not suited to serve a large number of users and/or covering a wide geographical area. Moreover, if some kind of protection is required, the fibre plant needs to be duplicated, which demands an additional investment. To obviate the limitations in legacy PONs, an alternative structure called Super-PON [MM96], [VMVQ00], [PSM+01] was introduced in the mid 90's. This network makes use of optical amplifiers to increase the available power budget. The Super-PON architecture is based on a tree-and-branch topology with a fibre length of up to 100 km and supporting up to 2048 ONUs. This network adopted the BPON specification, since it uses two separated wavelengths and ATM cell framing with line rates of 311 Mbit/s in the upstream and 2.5 Gbit/s in the downstream. Although this classical Super-PON structure has a longer reach and larger splitting ratio than a typical PON, it exhibits some disadvantages. Firstly, any failure in the fibre trunk segment (which expands up to 90 km and comprises two amplification nodes) can cause the communications break down for all the subscribers connected to the OLT. To prevent this catastrophic scenario, redundant fibre links and equipment must be deployed to assure protection. Secondly, problems might arise in the OLT reception due to the excessive accumulation of ASE noise in the upstream channel caused by the signal funnelling in the remote node. Thirdly, the bit rate assured to each of the 2048 ONUs is small and increasing it implies reducing the number of ONUs. Finally, high-cost ATM equipment in the ONU premises may cause an overly expensive network deployment. Aiming to reduce the limitations inherent to Super-PONs, a

Long-Reach EPON (LRE) has been proposed [SQPP07], [SPMP08]. This solution replaces the expensive ATM protocol technology with low cost Ethernet framing and bidirectional line rates that can range from 1 Gbit/s to 10 Gbit/s. Furthermore, instead of employing a tree-and-branch topology, it considers the use of an amplified ring-shaped feeder with individual PON segments deployed between it and the ONUs. By doing so, the OLT capacity is still shared by all users connected to the network and additional protection capabilities are provided to the feeder section. Nevertheless, using only two wavelengths is not enough to support the future bandwidth needs of the large number of subscribers expected in a metro-access network.

The WDM overlay is an obvious evolution of the standard PONs, creating the so called WDM-PONs [BPC+05]. This approach presents several advantages in terms of capacity, low latency, and service and data rate transparency. The WDM-PON system enables an optical PtP connectivity to multiple users, using a single feeder fibre, which results in a remarkably efficient use of the fibre plant. If typical long-haul and metro DWDM technology is used in WDM-PONs, each subscriber unit would be equipped with a unique transceiver tuned to its allocated WDM channel. However, even though such approach would enable a transparent metro/access network, these wavelength specific transceivers are a very expensive solution, not only due to their price, but also because they have high operational costs, regarding installation and inventory associated with managing each customer unit. For the ONUs to be identical and wavelength independent, several approaches may be employed, such as using tuneable lasers [CFA+04] or reflective schemes [SJS+06]. The first approach would be the most probable preference in a medium/long term perspective, though for now it is still cost-prohibitive. Apart from the inherent high cost, the tuneable laser approach would require a precise network control and management to define and maintain the wavelength allocation. In a WDM-PON reflective architecture, all the individual upstream wavelengths are provided by a shared network resource typically located in the OLT and the transmitter in the ONUs only requires a reflective optical modulator, such as a RSOA. However, due to the characteristics of the RSOA, this solution is limited in terms of the upstream data rate. Another strong restriction of WDM-PON is its difficulty in serving a very large number of ONUs. In the limit, and if each ONU is served by a unique wavelength, the maximum number of ONUs that may be served by a WDM-PON depends on the number of wavelengths that may be carried by the optical fibre and routed by the optical devices used in the remote nodes. Thus, with current optical technology, the number of subscribers connected with a WDM-PON is limited, which is clearly a strong handicap for designing a converged metro-access network.

More recently, intermediate WDM-PON and Super-PON solutions have been proposed [SRO+09]. These architectures use the tree-and-branch topology with support for 32 distinct wavelengths. The WDM signals are amplified at the OLT premises (in both link directions) and are transported over a 90 km feeder through two disjoint fibres, one for the upstream and the other for the downstream, each comprising 32 wavelengths. These wavelengths are then divided and routed to several PONs using a Local Exchange (LE) node comprising an AWG and EDFAs for optical power amplification. Each PON is served with two dedicated wavelengths (intended for the upstream and the downstream) with line rates of 10 Gbit/s, covering an extension of 10 km. The capacity of each wavelength can be distributed to up to 512 ONUs. These are supposed to be colourless, using tuneable lasers or RSOAs, in order to provide a generic ONU device that can be served by any wavelength of the system. This network has the main drawback of being very sensitive to failures in the LE equipment, since a fault in this node could disrupt the service to all the connected end-users. In order to avoid this scenario, redundant equipment (e.g. AWG and EDFAs) must be deployed along with protection equipment (for switching and monitoring). Since the LE architecture [SRO+09] provides each PON with an independent EDFA, the equipment duplication leads to the inclusion of, at least, 64 additional EDFAs. Furthermore, by including only one LE, the flexibility of serving users closer to the OLT is limited since the network is characterized by a long (90 km) feeder segment until the final drop section is reached.

From the discussion above, it is clear that WDM must be used to provide enough bandwidth to each subscriber, and that protection of the WDM links is a necessary feature, demanding the use of a ring topology in the former metro part. It is also evident that a pure WDM approach is still too expensive and cannot support the number of subscribers of a metro-access network. Hence, a combination of TDM and WDM seems to be the most feasible and cost-effective solution for the intended convergence. However, in the proposed architectures, this combination implies that not all ONUs transmit data using the same wavelength. Therefore, the use of the same specification for all ONUs, regardless of their location in the network, becomes challenging. In fact, among the proposals described above, only two of them can fully meet the objectives of (i) converged metro-access network, (ii) using an all-optical approach with (iii) a single specification for all ONUs. The first proposal consists of using reflective transmission schemes at the ONUs, whereas the second proposal is to have tuneable transmitters at the ONUs. A cost-based comparison between these two alternatives and the one described in the following is presented in section B.3.

B.2. Remote Node Architecture

As previously noted, a converged metro-access network will need high capacity in the links traversed by the traffic to/from all of the subscribers (the metro part). Therefore, a cost-effective and scalable solution to increase this transmission capacity, avoiding the deployment of more optical fibres or the increase of the channel bit rate, is to use WDM. However, because using a dedicated wavelength per subscriber will remain cost-prohibitive in the near future, TDM must still be used in the former access part. The use of TDM can eventually have the additional advantage of allowing backward compatibility with existing PON systems. In view of this, the combination of TDM with WDM is envisioned as one of the most feasible approaches to design a converged metro-access network [PLC+10] that supports current and future broadband services, while using mature and low-cost optical components.

Nowadays, metro and access are usually two completely distinct networks that differ in terms of technology, protocols and, in most cases, transmission medium. Maintaining these two different networks is complex and expensive and, in addition, the node interconnecting both networks must perform electronic processing of the data traversing from one network segment to the other, in order to produce compliant signals. This means that it must be able to handle the technologies and protocols employed in both networks, making these interconnection nodes rather costly. On the other side, in the envisioned metro-access network, the RN is a crucial element that provides the interface between the WDM-TDM (metro) network and the TDM (access) networks, as exemplified in Figure B.1. It is responsible for adding/dropping the upstream/downstream wavelengths carrying the traffic from/to the sub-set of subscribers that are attached to it. Given the extended reach of the envisioned metro-access network, this node must amplify/regenerate the signals. It should also be able to easily support protection mechanisms in order to provide survivability to single failures in the links carrying multiple wavelengths. In terms of backward compatibility and to cost-effectively support the needs of different types of subscribers (assuming that they are clustered in different TDM networks), the RN would benefit from being transparent to protocol, bit rate, and modulation format. Another important issue is that the ONUs should be kept simple and, equally important, they should all have the same specification, that is, the same ONU should work correctly in any end-user location without being modified for that purpose.

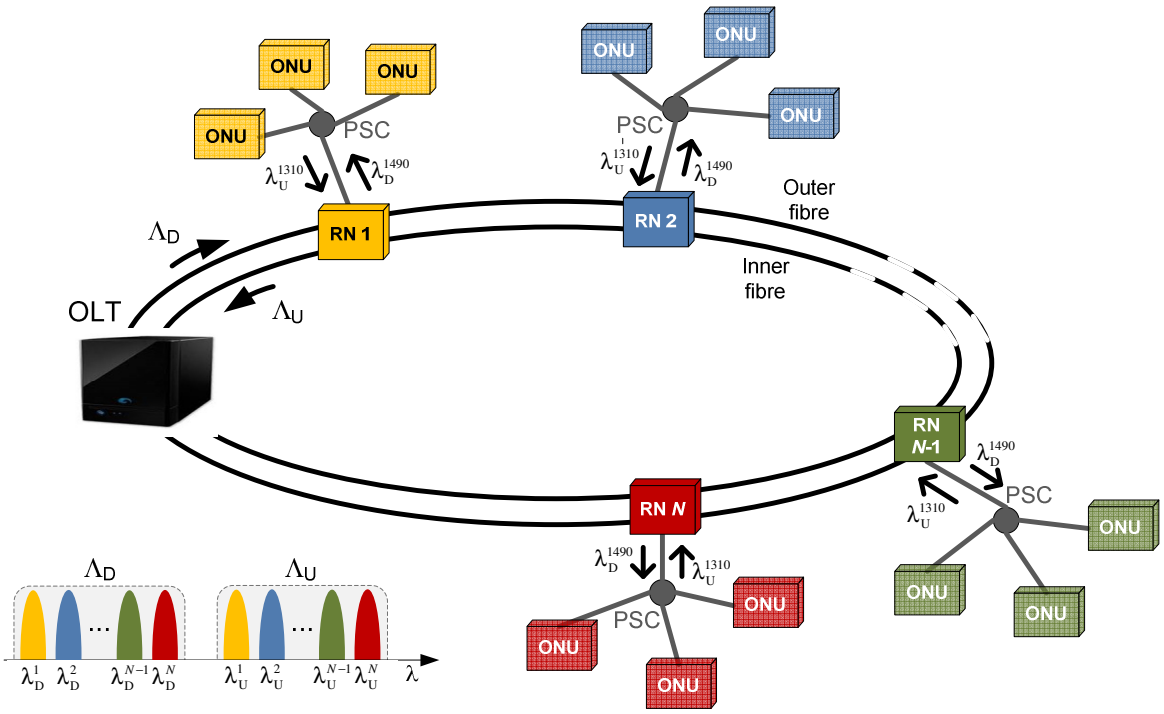

Figure B.1 – Schematic representation of the envisioned metro-access network.

In the envisioned network architecture, presented in Figure B.1, the OLT is located in a WDM ring and handles all of the ingress and egress traffic of the network. Since the aggregated traffic from all subscribers is transported over the WDM ring, this network segment is the most critical point of failure. Hence, a two-fibre ring is used to provide protection against single failures, as described in [SPMP08]. In the WDM ring, a unique wavelength pair (λ_D^i and λ_U^i) is allocated to each access segment, where the same downstream and upstream wavelengths (λ_D^{1490} and λ_U^{1310} , respectively) are time shared (TDM/TDMA) among its ONUs. This feature, which allows the use of standard-compliant ONUs and the coexistence of different xPON variants (e.g. EPON, GPON), is enabled through the use of all-optical Wavelength Converters (WCs) in each remote node, as further elaborated in the following sub-section.

B.2.1. Building Blocks of the Remote Node

The RN proposed for the envisioned metro-access network comprises a series of node elements whose functionalities are essential to successfully meet the stated objectives, namely achieving all-optical transmission between the OLT and the ONUs and guaranteeing the same specification for all ONUs. Amongst them, optical amplifier modules are included for the

upstream, and WDM splitter/couplers and wavelength converters are the remaining RN elements, for upstream and downstream.

Two RN variants are proposed. In the first one, illustrated in Figure B.2 a), the RN comprises both Downstream and Upstream Wavelength Converters (DWC and UWC), which are used to convert the wavelength in the WDM ring to/from the wavelength used in the xPON segment. In the downstream direction, the DWC shifts the wavelength extracted from the ring (λ_D^i) to the wavelength used to deliver data to the ONUs in the PON segment (λ_D^{1490}). In the opposite direction, the UWC converts the upstream wavelength from the PON (λ_U^{1310}) to that used in the ring to deliver data to the OLT (λ_U^i). The wavelength conversion is indispensable to assure that the downstream and upstream wavelengths are compliant with the xPON standards. However, in case the downstream WDM signal is within the xPON receiving band (1480 to 1500 nm), a standard-compliant ONU will be able to detect it, and thus the DWC can be spared. Hence, the second variant of the RN, which can only be used under the abovementioned condition, requires a single wavelength converter, as depicted in Figure B.2 b). The wavelength conversion can be completely performed in the optical domain, using SOA-based [LPT96] or MZI-SOA-based [LMS+07] techniques, avoiding electronic processing of the downstream and upstream signals traversing the remote node. Therefore, fully-transparent end-to-end transmission between the OLT and the ONUs is enabled.

The RN also contains one optical amplifier (OA) per fibre, to increase the available power budget and to compensate for the power losses due to fibre propagation and the other network elements located in the transmission path. For this task, any type of amplifiers, such as EDFAs or SOAs, can be used. It should be noticed that the amplifier type might influence the decision of using DWDM or CWDM in the WDM ring. Transient Control (TC) modules are also introduced as a complement to the optical amplifier, to reduce the amplifier transient effect in the time slotted upstream channel. This effect is present when bursty optical signals traverse the optical amplifiers, causing high power excursions (transients) at the amplifier output. The consequent power transients can overflow and damage the electric receivers, which could cause service disruption. In order to cope with the amplifier transients, several techniques can be employed in the TC block, such as feedback or feed-forward control mechanisms to adjust the pump laser current of the optical amplifier [FNS+08], [TCTW05].

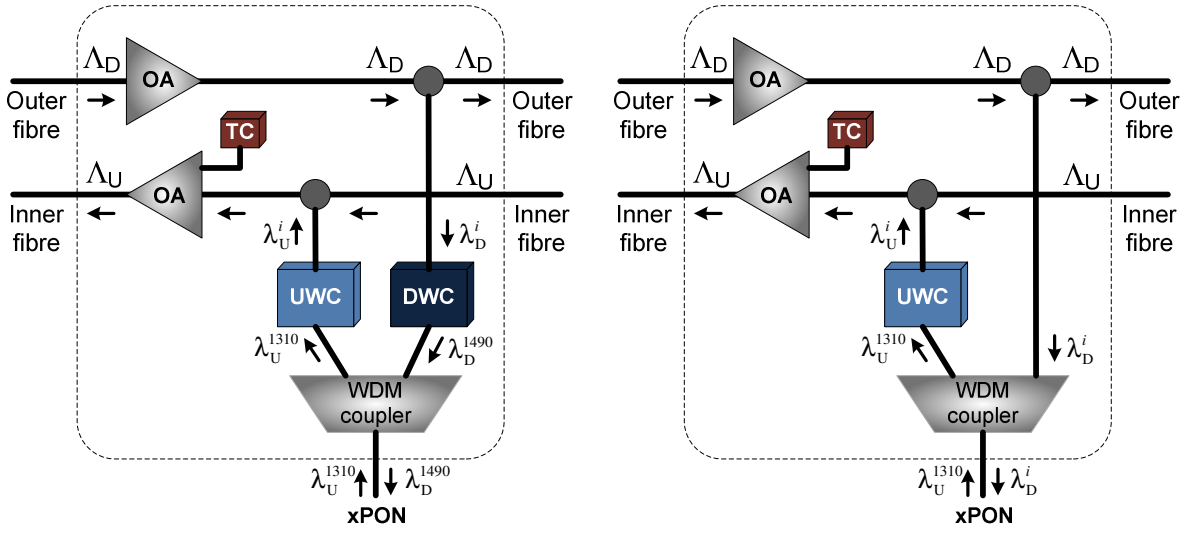

Figure B.2 – Proposed RN architecture for converged all-optical metro-access network.

The performance study presented in [SPMP08], which was made under limitative conditions because only two wavelengths were shared by the large number of subscribers, suggests the physical feasibility of the proposed network evolution, even accounting for the signal degradation introduced by the WCs.

B.2.2. Protection Switching

The proposed RN is suitable to implement high-capacity converged metro-access networks, where a transparent end-to-end connection between the OLT and the ONUs is possible relying solely on standardized xPON technology. The WDM segment is commonly supported over a physical ring topology, which can exploit path redundancy to provide highly reliable services. Moreover, in the passive segment, the service can be granted using any of the already available xPON technologies, covering a wide spectrum of FTTx solutions. Assuming the deployment of this scenario in the Internet Service Provider (ISP) network landscape, the proposed node configuration perfectly fits in the bridging function of both metro and access segments, allowing the association of low-cost network architectures with carrier-grade services.

The use of protection mechanisms is of extreme importance in metro/access networks which, given their extended reach are very susceptible to fiber cuts caused by negligent ground diggings. With this aim, the network can be designed to assure that the service is maintained to the end-users even if a fiber fault occurs in the ring [SPMP08]. In terms of data transmission, the upstream and downstream WDM signals are transmitted in both fibers, in

order to guarantee a backup path from where the bidirectional connection can be maintained. To provide this redundancy, and instead of duplicating the transceiver equipment at the OLT, a simple splitter and coupler pair can be used to connect the ring fiber ends, as exemplified by the diagram of Figure B.4.

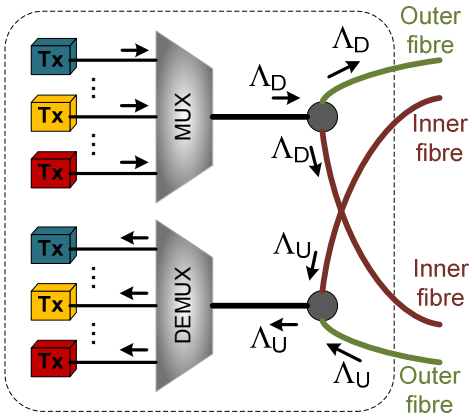

Figure B.3 – Scheme for protection switching in the OLT.

In order to comply with the protection requirements, several elements must be added to the basic remote node architecture presented in sub-section B.2.1, such as optical switches and a WDM coupler/splitter, as illustrated in Figure B.4.

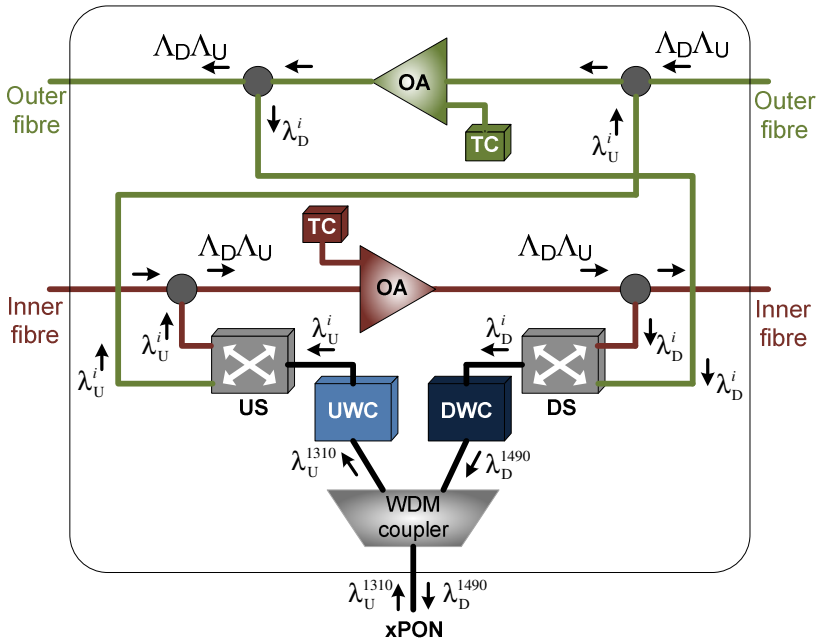

Figure B.4 – Scheme for protection switching in the RN (DWC+UWC).

By convention, assume that the outer (inner) fiber of the ring is used to transmit traffic in the clockwise (counter-clockwise) direction. During the service state, the downstream signal can be extracted from the outer fiber and the upstream can be transmitted over the inner fiber. However, in the presence of a fiber fault, all the remote nodes located after the fault will detect the absence of the downstream flow. After this detection, the state of the optical switches is changed, in order to start inserting/extracting the upstream/downstream signals on the complementary path between the OLT and the remote node. As mentioned before, all the nodes located before the fault can maintain their (service) state, since their service path was not affected by the fault. On the other hand, the nodes positioned after the fault will notice the service interruption in the downstream channel and will perform protection switching.

B.3. Comparative Economical Analysis

Besides enabling the backward compatible metro-access convergence, the proposed architecture, hereafter designated by WC-RN, should be more economical than the known alternatives that achieve the same goals, i.e. the support of an all-optical metro-access network with a single specification for all ONUs. The most straightforward approach is to use a Tunable Laser (TL) in each ONU, which will be designated by TL-ONU. Another well-known approach considers the use of a reflective device, e.g. a RSOA [SJS+06], as the ONU optical source. This approach is named R-ONU. When compared to the proposed scheme, these alternatives use simpler RNs, as they avoid WCs, but are not standard-compliant, which is a serious drawback for mass deployment. With WC-RN, the ONUs cost/complexity is reduced at the expense of increasing the RNs cost/complexity.

In the following cost-based comparison of the three solutions, it is assumed that there are no relevant differences in the OLT equipment and that all RNs have the same components, with the exception of WC-RN which, in addition, also requires one WC (UWC only) or two WCs (DWC+UWC). The WC-RN approach is assumed to use SOA-based WCs, each made with one SOA and one CW laser tuned in the desired output wavelength. The corresponding ONUs only require a typical receiver (Rx) and a typical fixed transmitter, assumed to be a CW laser coupled with an Electro-Absorption Modulator (EAM), for the sake of comparison. Alternatively, TL-ONU uses at each ONU one Rx and one tuneable transmitter, which can consist of an EAM and a TL, whereas the R-ONU uses at each ONU one Rx and one reflective device, which can consist of an EAM integrated with a SOA.

Let M denote the number of RNs in the ring and assume, without loss of generality, that each RN connects the same number N of ONUs. In this case, Table B.1 contains the number of optical devices that are required by each solution.

Table B.1 Number of optical devices as a function of M and N.

DWC+UWC	UWC only	TL-ONU	R-ONU
$2M$ SOAs	M SOAs	$N \cdot M$ TLs	$N \cdot M$ SOAs
$2M + N \cdot M$ CWs	$M + N \cdot M$ CWs	$N \cdot M$ EAMs	$N \cdot M$ EAMs
$N \cdot M$ EAMs	$N \cdot M$ EAMs	$N \cdot M$ Rxs	$N \cdot M$ Rxs

Since the same number of EAMs and Rxs is used in all solutions, the cost comparison only depends on the remaining devices. The cost thresholds that guarantee the WC-RN to be less expensive than the other alternatives are determined in the following. The conditions for WC-RN with DWC+UWC and with UWC only to be less expensive than TL-ONU are then given by expressions (B.1) and (B.2), respectively:

$$C_{SOA} < (N/2) \cdot C_{TL} - (N/2 + 1) \cdot C_{CW}; \tag{B.1}$$

$$C_{SOA} < N \cdot C_{TL} - (N + 1) \cdot C_{CW}, \tag{B.2}$$

where C_{SOA} denotes the cost of a SOA, C_{CW} the cost of a CW laser, and C_{TL} the cost of a TL. Since C_{CW} is typically much lower than C_{TL}, these conditions can be further simplified by neglecting C_{CW}, yielding the following approximations:

$$C_{SOA} < (N/2) \cdot C_{TL}; \tag{B.3}$$

$$C_{SOA} < N \cdot C_{TL.} \tag{B.4}$$

Figure B.5 depicts the cost thresholds for which WC-RN is more economical than TL-ONU, as a function of N. The plot shows that if C_{SOA} is smaller than C_{TL}, the proposed architecture is always better than the use of tunable transmitters at the ONUs (TL-ONU). In addition, it will still be better even when C_{SOA} exceeds C_{TL}, as long as the cost ratio C_{SOA}/C_{TL} is kept below $N/2$ when two WCs are used at the RN, or the same cost ratio is kept below N when a single WC is used at the RN.

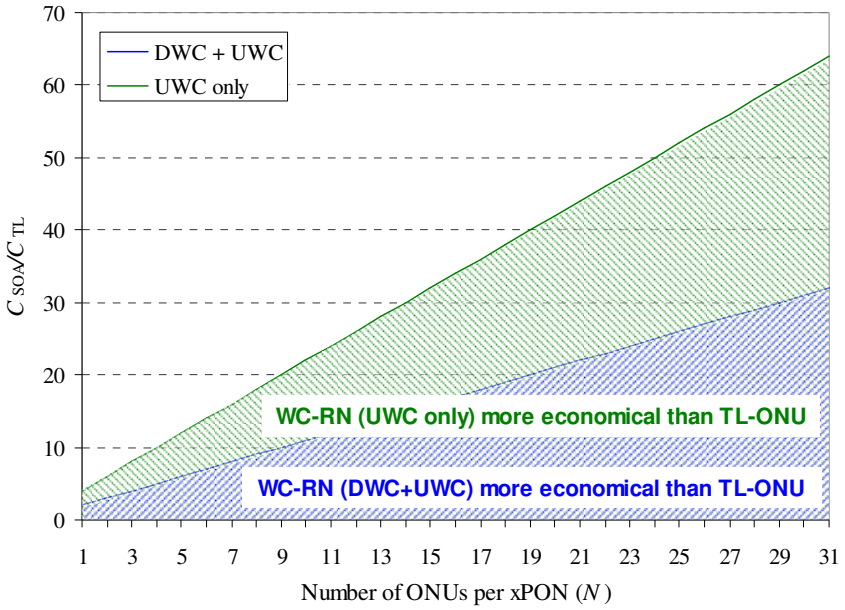

Figure B.5 – Cost thresholds between WC-RN and TL-ONU.

When comparing WC-RN with R-ONU, the conditions for DWC+UWC and UWC only to be less expensive than R-ONU are given by expressions (B.5) and (B.6), respectively.

$$C_{SOA} > [(N + 2)/(N - 2)] \cdot C_{CW}; \quad \text{(B.5)}$$

$$C_{SOA} > [(N + 1)/(N - 1)] \cdot C_{CW}. \quad \text{(B.6)}$$

Figure B.6 plots the cost thresholds above which WC-RN is less expensive than R-ONU.

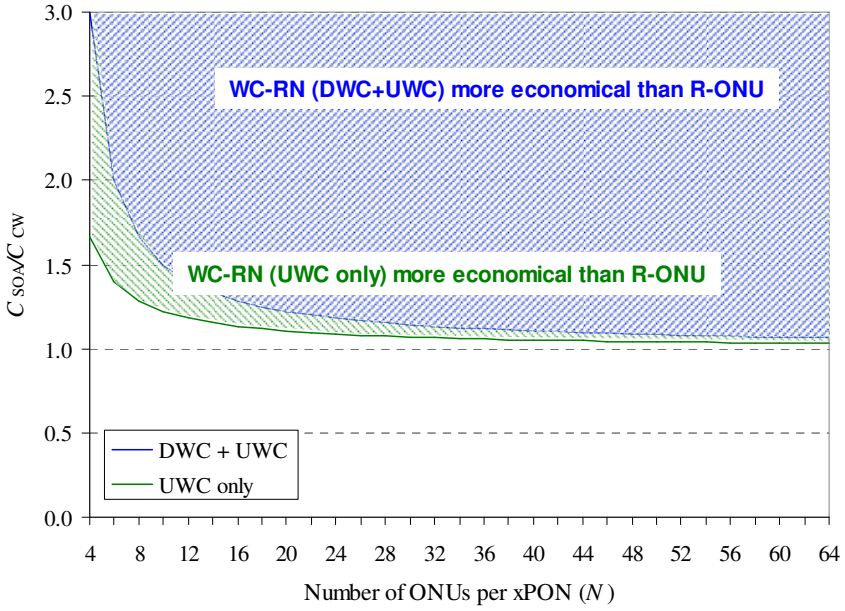

Figure B.6 – Cost thresholds between WC-RN and R-ONU.

The results presented in Figure B.6 indicated that, since C_{SOA} is several times larger than C_{CW} and it is expected to remain so, the proposed solution using either one or two WCs is always better than using R-SOAs.

The previous cost-based analysis can be complemented with a case study based on price estimates for the optical devices used in the RN and ONUs. The relative cost assessment of the solutions under consideration is based on price assumptions presented in [Tak07]. It is assumed that the fixed receiver (Rx) has a unitary cost and that the cost of all other devices is determined relatively to its cost, as indicated in Table B.2. Note that the cost of CW lasers is neglected and for the R-ONU approach the cost of an integrated device (SOA+EAM) as ONU transmitter is considered, since it represents the lower cost implementation.

Table B.2 Relative cost of the optical devices.

Optical device	**Rx**	**EAM**	**SOA**	**EAM+SOA** (integrated)	**TL**
Relative cost	1	10	20	25	40

For analysis purposes, consider a small metro-access network, with only one RN supporting 16 or 64 ONUs, and a medium-size network, with 8 RNs, each supporting 16 or 64 ONUs, in a total of up to 512 ONUs. For these topologies, Figure B.7 depicts the cost difference between the TL-ONU and R-ONU approaches relative to the cost of WC-RN, with two wavelength converters per RN (DWC+UWC). These results show that WC-RN is significantly less expensive that its competitors: the R-ONU approach is around twice the cost of approach WC-RN, whereas TL-ONU reaches almost 3.5 times the cost of WC-RN. Since the most numerous and cost-sensitive network element is the ONU, the simpler and more economical it is, the less expensive the network becomes. This is the major cause of the relative cost differences presented in Figure B.7, since WC-RN supports simple and standard-compliant ONUs, unlike the costly ONUs required by the TL-ONU and R-ONU approaches. Recalling Table B.1, the RN for R-ONU and TL-ONU does not require any extra devices, making the cost of these two approaches independent of the number of RNs, depending only on the number of ONUs connected to each RN. Moreover, for RNs supporting a larger number of connected ONUs, the relative cost of TL-ONU and R-ONU increases due to the equipment that is added per additional ONU, when compared with the WC-RN approach.

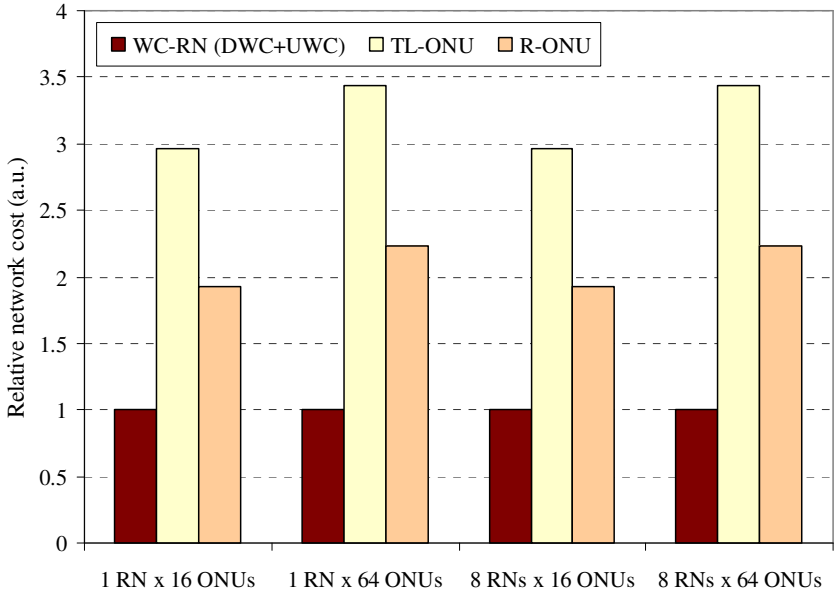

Figure B.7 – Cost of TL-ONU and R-ONU approaches relative to WC-RN (DWC+UWC).

By fixing the total number of ONUs supported by the metro-access network, Figure B.8 presents the cost difference relative to the lowest cost of the WC-RN (DWC+UWC) solution. Note that these results are valid for any total number of ONUs in the network. Once again, the TL-ONU and R-ONU approaches are shown to be over 2 times more expensive than the WC-RN approach, depending only on the number of supported ONUs. As expected, the cost of the WC-RN slightly increases with the number of RNs, since more wavelength converters are necessary to connect the same number of ONUs.

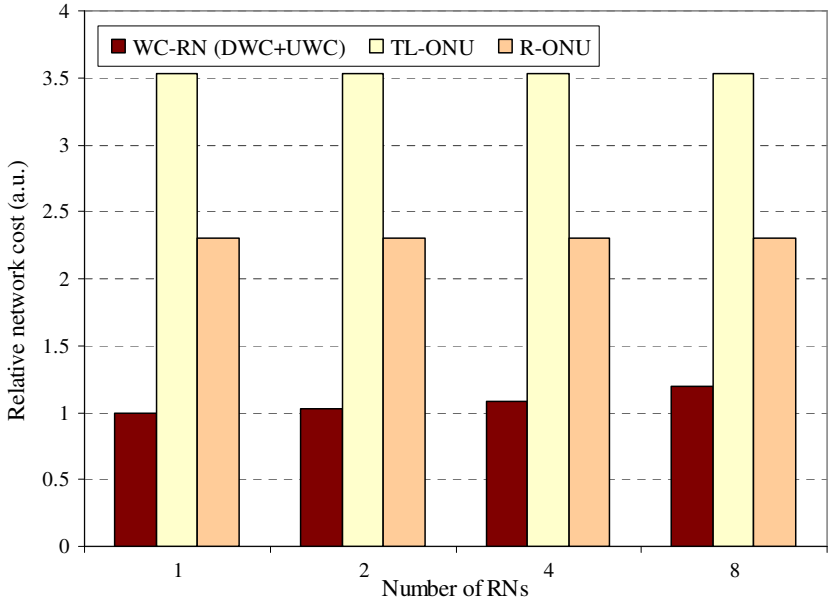

Figure B.8 – Cost of the R-ONU and TL-ONU approaches relative to WC-RN (DWC+UWC), for a fixed number of total ONUs.

The relative cost thresholds derived above clearly suggest that, for the current and expected costs of optical devices, namely CW lasers, EAMs, SOAs, and TLs, the use of WCs at the RNs of the converged metro-access network is clearly more cost-effective than the alternative solutions using complex ONUs. In the proposed approach, the complexity/cost is kept in the RNs, which are significantly smaller in number than the ONUs. Moreover, and unlike both TL-ONU and R-ONU, the WC-RN approach enables the use of standard-compliant ONUs, guaranteeing backward compatibility with already deployed access systems.

B.4. Conclusions

A novel remote node architecture using all-optical wavelength conversion was designed to enable the convergence of metro and access networks, while at the same time guaranteeing backward compatibility with standard access systems and a single specification for the subscribers terminals.

This RN scheme, besides providing an all-optical convergence of metro and access networks, has multiple advantages when compared to the known alternatives that enable the same objectives. First of all, it supports standard-compliant user terminal equipment within each xPON system, which allows including over the same network infrastructure access systems compliant with the existent standards and that were already deployed in the field. Using this RN, the support over the same infrastructure of xPON systems with different protocols and/or different bit rates is possible. Therefore, BPONs, EPONs and GPONs, as well as non standard-compliant systems or next-generation systems like 10G EPON/GPON, may coexist within the same metro-access network. Moreover, the envisioned metro-access convergence is accomplished using the described RN, in such way that a single OLT (i.e. central office enclosure) is able to serve a very large number of subscribers (well over 1024 ONUs), independently of the transmission protocol used to support the subscribers connected to each remote node.

The possibility of deploying this RN in a double-fibre ring infrastructure enables the application of path protection schemes. Since the WDM ring represents the core segment of the metro-access network, a single failure in the ring may significantly affect the operation of the entire system. Therefore, protection mechanisms are required to maintain the service in the presence one failure in the ring. Moreover, such a network has the flexibility to add xPON systems without disrupting the network service. This can be attained by temporarily activating

the protection state between the nodes adjacent to the new RN, while this node is being connected. In these circumstances, a new wavelength pair must be added to the WDM ring. These wavelengths will also undergo wavelength conversion in the new RN, in order to serve the newly added subscribers. This additional functionality can be exploited by the network owner to implement a pay-as-you-grow strategy.

A particular aspect of the proposed architecture is related to the optimization of the deployed capacity. In the case where, for instance, the capacity of a single wavelength is more than enough to serve a single xPON, the same wavelength may be used to serve another xPON connected to the ring. This can be accomplished using a drop-and-continue functionality in the first RN, where the dropped wavelength experiences power splitting to enable its propagation along the ring until it reaches the second RN. This feature improves the ability of the metro-access network to efficiently exploit the capacity installed.

As demonstrated, according to current and foreseeable prices of optical components, the envisioned system is more cost-effective than known alternatives targeting similar goals. It has been shown that those alternative approaches require more than twice the investment of the proposed one.

Overall, the metro-access convergence scenario is being foreseen as a promising approach to further reduce capital and operational expenditures in the most cost-sensitive network segment. In this context, the proposed RN architecture provides a disruptive and cost-effective solution for implementing all-optical metro-access networks, while assuring backward-compatibility with existing xPON systems.

Appendix C

CWDM-based Optical-Wireless Architecture

The convergence between wired and wireless communications is gaining momentum in the access segment of the network, enabling higher bandwidths per mobile user, while simultaneously serving a larger number of subscribers. This convergence provides a means to share the same infrastructure among fixed and mobile services, decreasing implementation, maintenance and operational expenditures.

In this context, the development of DAS networks is being addressed. In such systems a large number of dumb antennas, whose functions are limited to the transmission/reception of radio signals, are interconnected by a transparent optical fibre infrastructure that carries the radio signals to/from a central head-end, where all processing tasks take place. The hierarchical structure of a DAS network resembles that of a PON, increasing the possibilities for deploying a cost-effective converged wired-wireless system. Moreover, using one or a mixture of several multiplexing technologies, such as SCM, WDM (CWDM or DWDM), or SDM, very high capacity can be provided over the optical fibre, to each antenna site.

In future distributed wireless architectures, it is also important to guarantee the support of heterogeneous systems, eventually within the same remote antenna site, which further increases the necessary capacity. In such scenario, it is valid to assume that each RRH would require an entire wavelength capacity for uplink and another for downlink, with each wavelength supporting, through SCM, a number of radio sub-channels carrying the wireless traffic. The success of these high capacity distributed wireless architectures depends on the use of a low cost infrastructure, in terms of CAPEX and also OPEX. Thus, a passive system will be preferred, together with low cost components for the transmitters and receivers. It is therefore clear that the success of a future proof DAS network is dependent on the selection of a suitable fibre optic topology and of an advantageous multiplexing technology.

C.1. Proposed CWDM Architecture

The architecture described hereafter aims to provide a low cost infrastructure to be used in future distributed wireless systems that employ RoF technology, guaranteeing the support of a reasonably large number of RRHs per processing unit, using the least amount of optical fibre.

To guarantee a high capacity, this architecture is based on WDM and the targeted low cost is achieved by employing CWDM equipment, over an optical fibre infrastructure shared by several RRHs, as depicted in Figure C.1. The proposed configuration uses a CWDM mux/demux placed in the splitting point of a tree-like fibre-based infrastructure. The network head-end comprises a CU, where several processing units are located. Each processing unit is responsible for processing the radio signals sent/received to/from the set of RRHs to which it is connected, through the CWDM mux/demux. At the opposite side of the network, a number of RRHs is located, connected to the CWDM mux/demux using a single fibre. The RRHs are responsible for transmitting/receiving the radio signals to/from the mobile terminals, and for sending/receiving these signals through the optical fibre to/from their processing unit, located within the CU. Each RRH is served by a wavelength for uplink transmission and a different wavelength for downlink transmission, in order to guarantee the necessary capacity to support a diversity of future wireless systems.

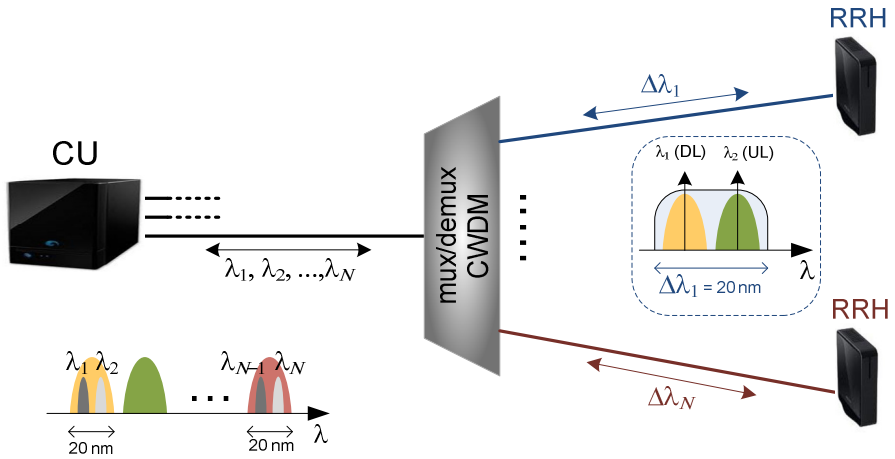

Figure C.1 – Proposed CWDM architecture for low cost and high capacity DAS.

As illustrated by the inset of Figure C.1, the differentiating factor of this architecture is the use of the 20 nm bandwidth of each CWDM mux/demux port to transport the uplink and downlink wavelengths of the same RRH. Actually, the available bandwidth per CWDM mux/demumx port is slightly less than 20 nm due to the Gaussian profile typical of these

devices. The use of the same mux/demux port for uplink and downlink wavelengths allocated to a specific RRH allows to deploy only a single fibre between the splitting point and the terminal locations, thereby decreasing the necessary amount of fibre. Furthermore, the number of RRHs that may be supported by a single processing unit, located at the CU, may be increased up to the number of CWDM mux/demux ports, which is typically 16, assuming the use of SMF and neglecting the two highly attenuated channels near the fibre water peak. When compared to a traditional CWDM system, where a single wavelength is carried by a different port of the mux/demux, this architecture enables to double the maximum number of supported RRHs.

In order to guarantee as much bandwidth as possible for the uplink channel, and to comply with possible wavelength drifts of the CWDM lasers at the RRHs, the downlink wavelength should be placed in the proximity of the limit of the CWDM mux/demux port bandwidth. This design rule enables to use low cost CWDM lasers in the RRH, typically characterized by large wavelength drifts, while the downlink lasers must be tightly controlled to avoid large wavelength drifts, thereby minimizing interference with the uplink wavelength. This tight control is affordable because these lasers are placed in the CU, where the cost is not as critical as in the remote antenna sites.

C.2. Comparison with typical DWDM/CWDM Networks

Several topologies and architectures may be envisioned for future high capacity distributed wireless networks. Amongst them, the passive tree has been proven to be the most economical topology, allowing for an optimized sharing of the fibre plant among multiple antenna sites, and the most advantageous multiplexing scheme has been realized to be WDM, which allows minimizing the amount of fibre deployed for the same supported capacity. Depending on the target cost of the system and on the number of antenna sites sharing the same processing unit, DWDM or CWDM may be selected.

If a higher equipment cost is bearable, DWDM is preferred since it provides a higher number of wavelength channels. In this scenario, the most advantageous architecture includes a DWDM mux/demux placed in a splitting point near the area comprising the set of RRHs connected to a processing unit, and the use of a reflective device in the RRHs, to remodulate a wavelength received from uplink, sending it back again (see Architecture E described in Chapter 5). The reflective devices, the necessary batteries of DWDM lasers and the DWDM

mux/demux, which must be cyclic to allow for the downlink and uplink wavelengths to be transmitted by the same port, are very expensive devices, which may be prohibitive for a successful network deployment. Despite of supporting a small number of antenna sites per processing unit, the use of CWDM enables a much lower-cost system.

Similarly to the DWDM system, in the most straightforward implementation of a CWDM system, each RRH is served by a unique uplink wavelength and a unique downlink wavelength, and a CWDM mux/demux is placed in a splitting point near the area comprising the set of RRHs connected to a processing unit. However, since no cyclic CWDM mux/demux exist, each processing unit can only support at most 8 RRHs. Moreover, in order to have a single fibre connecting the CWDM mux/demux to each RRH, an additional coupler is required for each RRH in order to join the uplink and downlink wavelengths into the same fibre, at the output of the splitting point (see Architecture A described in Chapter 5). This coupler will introduce extra power losses, which may be critical especially in the uplink, where the transmitted power is typically lower.

With the proposed configuration the drawbacks described above are minimized. Namely, a lower-cost system is achievable, and the splitting point can be connected to each RRH by a single fibre, without the need for complex and/or additional devices. In addition, an easy upgrade of a typical CWDM network, which supports only up to 8 RRHs, is enabled with the proposed configuration, by changing only the terminal equipment, and maintaining the fibre plant unchanged. This is applicable to any CWDM-PON.

Appendix D

Digital Protocols for DAS

The digital transport of radio signals to interconnect remotely located antennas with a central station is based on two vendor-driven open standards, namely the CPRI [CPR] and the OBSAI [OBS]. This open standardization has the merit of requiring lower R&D costs, a shorter time-to-market, an improved innovation, a lower pressure on pricing and a fast evolution of the technologies, in the development of a wireless infrastructure in which RRHs can be deployed in a flexible and cost-effective manner. The main purpose of these protocols is the specification of a digitized and serial interface, for 3G and 4G technologies, between a base station location, where the baseband processing functions are placed, and a RRH, that contains all the RF functions of a conventional base station.

OBSAI [OBS] was started in 2002 and defines a set of BTS modules, as well as the digital interfaces between these BTS modules, assuring the interoperability and compatibility between different vendors and manufacturers. This BTS modular structure, schematically represented in Figure D.1, allows easy scalability for small to large capacity configurations. The second industry initiative, CPRI [CPR], was initiated as a response to OBSAI, in 2003, aiming to define a publicly specification for the key internal interface of radio base stations between the REC and the RE. Unlike OBSAI, CPRI has a much narrower focus, since it does not specify mechanical or electrical interface requirements. While OBSAI defines the three major interfaces in a BTS, namely RP1 for clock and synchronization information, RP2 for exchange of user data information to/from the baseband module, and RP3 to interchange formatted air interface user and signalling data, CPRI focuses solely on the link between the RF module and baseband module in the BTS.

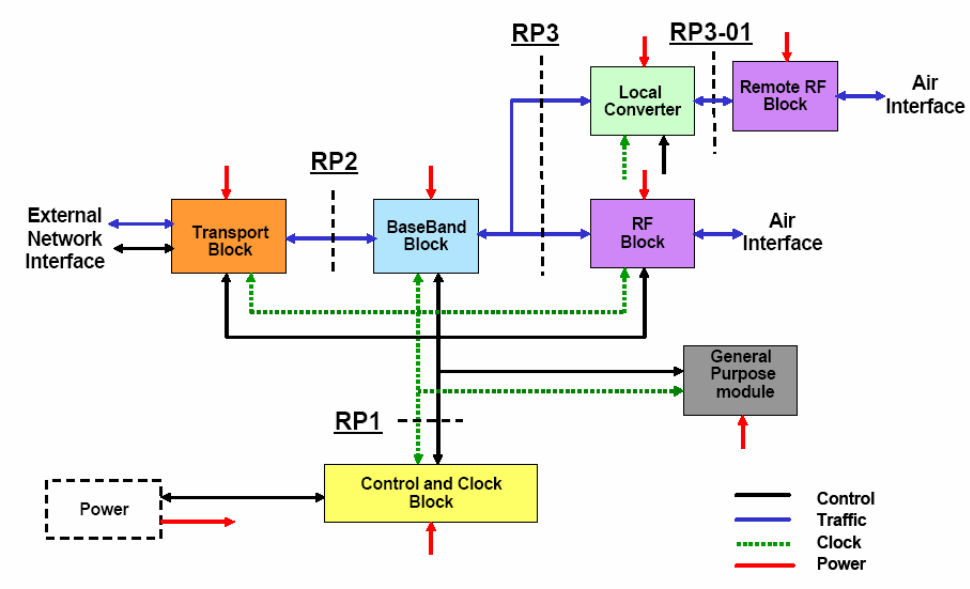

Figure D.1 – OBSAI BTS modular architecture [OBS].

Both these initiatives define digital PtP interface between the baseband module and the RF module. The use of this digital interface provides the necessary flexibility to either co-locate these two modules within a single enclosure or remotely locate the RF modules from the baseband module in a distributed topology. In order to connect and control the remotely located RF modules (RRHs), the OBSAI has defined an extension of the RP3 interface, designated by RP3-01. The protocol used by RP3-01 is in general equivalent to the RP3 protocol, but uses different physical layer technologies suitable for data transmission over longer distances. Since the remotely located RF units require control and synchronization information, the same interface used to transmit the digital baseband traffic must also be used to transmit control and synchronization data. Therefore, in OBSAI-compliant systems, RP1 data is mapped into RP3 messages, and transmitted using the RP3-01 protocol, in order to minimize the number of connections to the RRHs. Regarding CPRI, the support of remote RF units is addressed in the latter versions, extending the scope of the first standard versions.

In the following, a brief overview of both CPRI and OBSAI initiatives is presented, mainly focusing on their architectures and transmission protocols, and, for OBSAI, on the RP3-01 interface. Moreover, a feasibility study of supporting a set of RRHs using a passive distributed infrastructure, such as a PON is described. In this study it is assumed that the communication and all the control between the RRHs and the baseband module within the central location is carried out employing OBSAI, specifically using the RP3-01 interface.

D.1. CPRI Overview

The CPRI initiative resulted from the cooperation between several industry players that, by defining an interface between REC and RE modules, enables flexible and efficient product differentiation for radio base stations, while providing independent technology evolution for those modules.

The CPRI specification includes definitions for transport, connectivity and control, in the form of User Plane data, Control and Management Plane transport mechanisms and means for synchronization. The specification is limited to the link interface, defining a digitized and serial internal interface between REC and RE, as well as between two REs. This interface is responsible for multiplexing the abovementioned information flows.

D.1.1. Architecture and Topology

The CPRI architecture design is based on the fundamental aspect driving these specifications, namely the need to provide flexibility to the radio base stations. This is achieved by decomposing the radio base station into the REC and the RE, as represented in Figure D.2. The functional split between both parts is done in such a way that a generic interface based on IQ data can be defined. Two hardware dependent layers are defined: Layer 1, which supports both an electrical and an optical interface, and Layer 2, that supports the necessary flexibility and scalability.

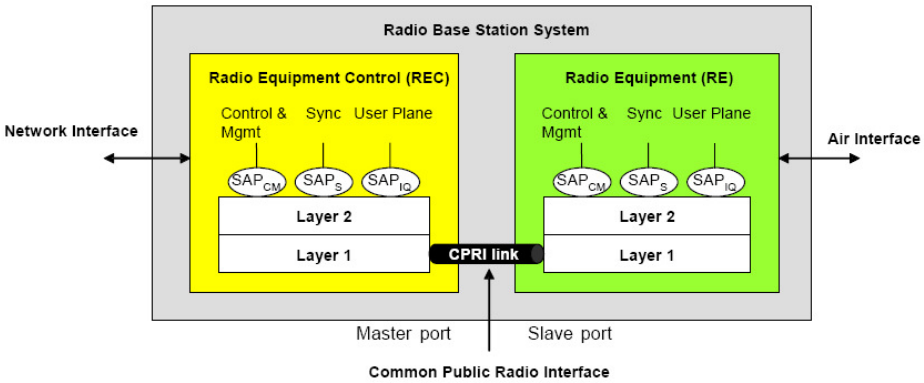

Figure D.2 – CPRI system architecture [CPR].

Both the REC and the RE modules include radio functionalities and CPRI control functionalities. REC is responsible for radio station control and management and digital

baseband processing of radio signals, being also concerned with the management of the CPRI topology. The RE provides the analogue and RF functions, such as filtering, modulation, frequency conversion and amplification, and may optionally provide interconnection functionalities between REs.

Several topologies are defined in CPRI to support a set of RRHs. In the basic configuration, one REC is connected with a simple PtP CPRI link to one RE. An extension to this basic configuration is allowed, where several parallel CPRI links are used to enhance the system capacity, which is required for large system configurations involving multiple antennas and carriers. PtMP network configurations are also specified by CPRI to support multiple REs with a single REC, as presented in Figure D.3.

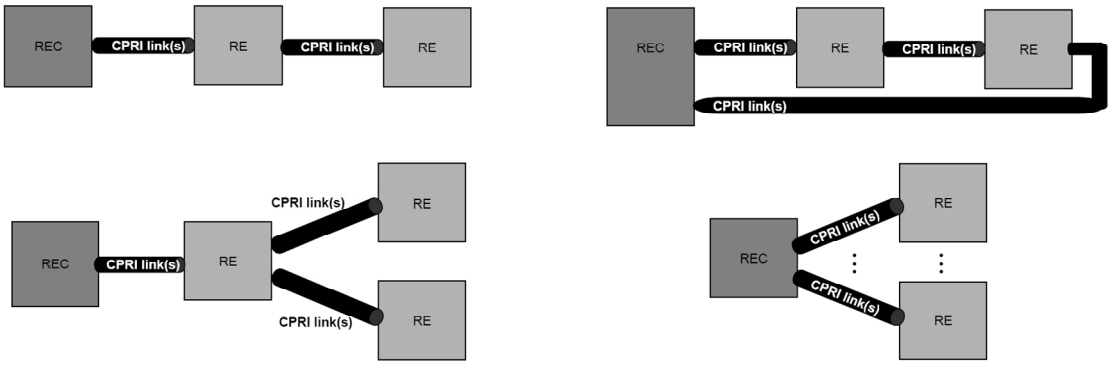

Figure D.3 – CPRI network topologies [CPR].

D.1.2. Protocol Stack

CPRI defines a protocol stack, as presented in Figure D.4, to support several information flows: the IQ data, which carries the user plane information formed by digital baseband signals; the Synchronization, carrying information for frame and time alignment; L1 Inband Protocol, which carries signalling information related to the link and directly transported by the physical layer; Control and Management data, responsible for exchanging control information between the control and management entities within the REC and the RE; Protocol Extensions field and Vendor Specific Information field, reserved for future protocol extensions and reserved for vendor particular data, respectively. The Layer 2 protocols used for Control and Management are Ethernet and High-level Data Link Control (HDLC), and additional Control and Management data may be time multiplexed with IQ data, if necessary.

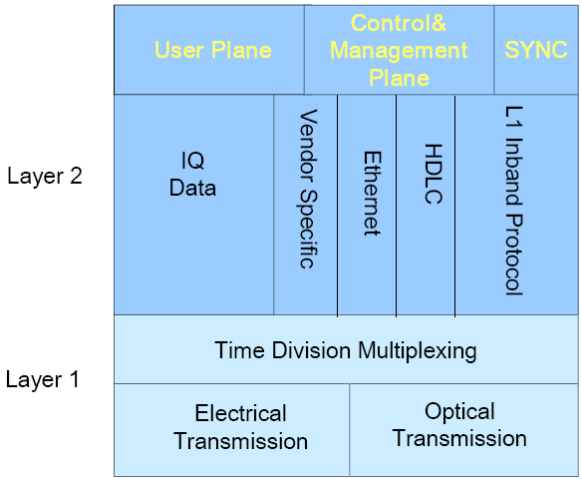

Figure D.4 – Protocol stack used by CPRI [CPR].

Layer 1 of the protocol stack defined by CPRI comprises the multiplexing process of the IQ data of different AxC, using TDM, onto an electrical or optical transmission line. CPRI line rates have been chosen in such a way that the basic UMTS chip rate of 3.84 Mbit/s can be recovered in a cost-effective way from the line bit rate taking into account the 8b/10b coding. Therefore, 614.4 Mbit/s, 1228.8 Mbit/s, 2457.6 Mbit/s, 3072 Mbit/s, 6114 Mbit/s and 9830.4 Mbit/s are supported by CPRI, and each REC and RE must guarantee at least one of these line rates.

D.1.3. Frame Structure

The basic CPRI frame is defined to have a length set through the basic UMTS chip rate, and equal to 1/3.84 MHz. It is formed by 16 words, with the first one used for control purposes. The length of each word depends on the selected CPRI line rate, as illustrated in Figure D.5 for the two lower data rates. The transmission sequence of the encoded data is defined by the 8b/10b coding, where the 10bit encoded code-groups are transmitted as a serial bit stream. The control word of one basic frame is always transmitted first.

In the CPRI frame hierarchy, a Hyperframe is defined to be embedded between the basic frame and a 10 ms CPRI frame. This Hyperframe is composed by 256 basic frames (66.67 μs) and the 10 ms CPRI frame is formed by 150 Hyperframes.

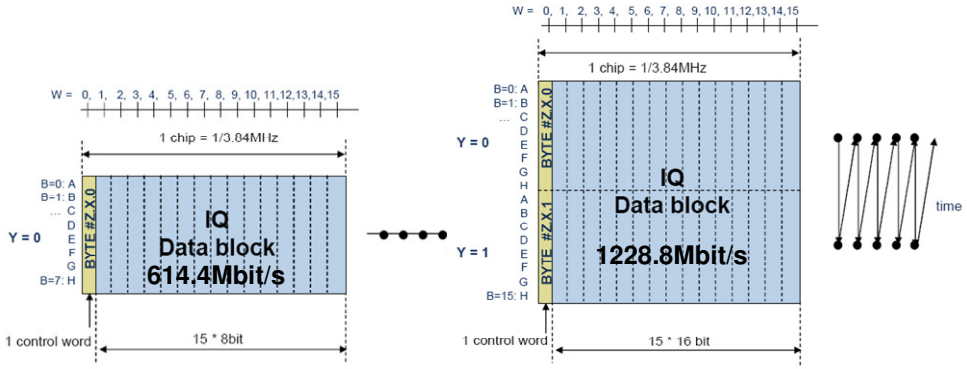

Figure D.5 – Basic CPRI frame for [CPR].

The common definition of AxC represents in CPRI a sub-part of the IQ data block of the basic frame that contains different number of IQ samples depending on the wireless protocol being supported. The IQ mapping used in CPRI is schematically represented in Figure D.6. I and Q samples in an AxC container must be interleaved and sent consecutively and in chronological order, and each AxC container is sent as a block, with no overlap allowed for AxC containers. Note that several mapping methods are defined for WiMAX protocol, namely IQ sample based, WiMAX symbol based, and backward compatible.

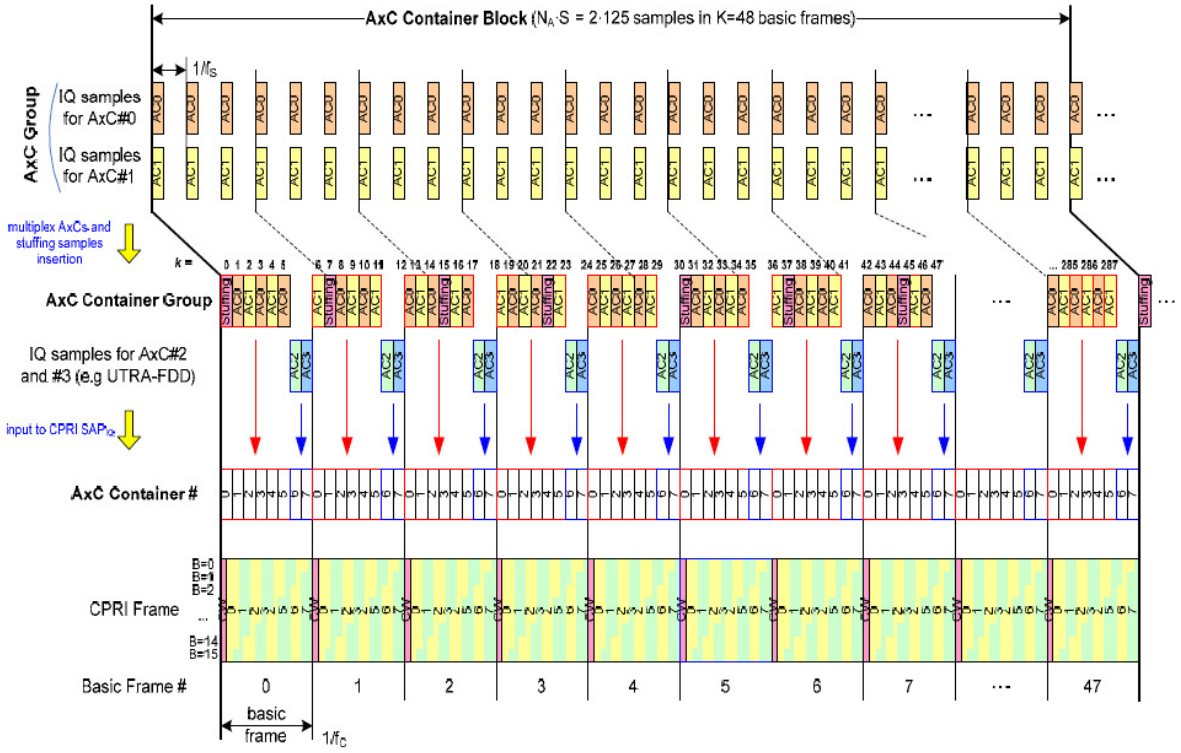

Figure D.6 – Mapping of IQ data in CPRI [CPR].

D.2. OBSAI RP3-01 Overview

Initially, OBSAI specification focused on defining the characteristics and features of the main BTS functional modules, as well as the interfaces between these modules, considering a single physical enclosure for all modules. This traditional base station model evolved to a distributed model, where the RF modules are detached from the remaining BTS modules, enabling less-expensive, simpler, and more flexible base station architectures.

In order to address this distributed system, OBSAI defined an extension for the RP3 interface [OBS3], responsible for the interconnection and data transfer between the baseband module in the BTS and the RF modules. This extension, designated as RP3-01, is therefore responsible for data transfer using the RP3 protocol, operating at line rates compatible to OBSAI specifications. Due to the number of supported line rates, an auto-negotiation process must be performed between the RRHs and the corresponding baseband module. OBSAI specification defines the use of Ethernet transmission between each pair of RP3-01 nodes. Moreover, due to the lack of a physical link for the transport of synchronization, clock and control data (RP1 interface) to the RRH, this information must be mapped into the existing RP3-01 link, using RP3 framing. The OBSAI specifications for the data link layer include delay measurements and synchronization between the baseband and the RRHs, and the multiplexing of data in the RP3-01 link. The most relevant aspects of the RP3-01 specification are addressed in the following sub-section.

D.2.1. Protocol Stack

The protocol stack used by RP3-01 is equal to the one specified for RP3, with the exception of the transport at the physical layer. This protocol stack, depicted in Figure D.7, comprises four main layers. The upper layer, named application layer, is responsible for providing the mapping of the different types of control and data packets into the payload, and for the insertion of the header to each message, including the address, the type and the timestamp fields. From bus protocol point of view, the application layer is divided in air interface applications and bus functions, with the first isolated from the second by the “Bus Interface” part. This “Bus Interface” is responsible for all functions that prepare data for transmission over the bus, including transmission and reception of messages.

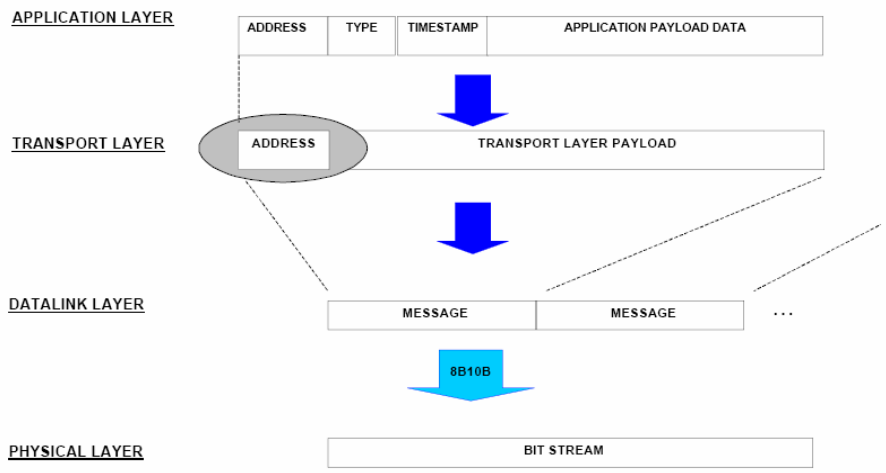

Figure D.7 – Protocol stack used by RP3-01 interface [OBS3].

The transport layer is responsible for end-to-end delivery of messages, including functions such as message routing, multiplexing/demultiplexing and summing units. The routing of messages performed at the transport layer is based on the address of each message, which occupies the first 13 bits of the message. The remaining message fields pass transparently through the transport layer. Local routing is employed at the transport layer, where each bus node knows only its output port(s) into which a message is addressed. Therefore, bus nodes do not have visibility of the entire message paths, which instead are defined by a bus control entity (Bus manager) when booting up the bus.

The data link layer is responsible for message framing and synchronization of the messages (links). The RP3 protocol defines the support of master frames, composed by consecutive message groups, which in turn are composed by several fixed length messages, together with idle information. The transmission and reception timings for maintaining link synchronization are also defined by the data link layer.

The physical layer is responsible for coding, using the 8b/10b line coding which is applied to all data transmitted over the RP3 bus, for serialization of messages, and for the data transmission. This layer is frequency and phase locked to the centralized BTS system clock.

D.2.2. Message and Framing

The RP3-01 interface adopted the message format and framing defined for RP3 protocol, which is depicted in Figure D.8. Messages used by RP3-01 are 19 bytes fixed length messages divided into the address field with 13 bits, the type field with 5 bits (to identify the wireless

protocol that is carried by that message), the timestamp field with 6 bits (to identify the limits of the message), and the payload field with 128 bits. Each byte of a message is first 8b/10b encoded (physical layer function) and then transmitted to a link. The left most byte of the address field is first transmitted to the link while the rightmost byte of the payload is the last to be sent to the link.

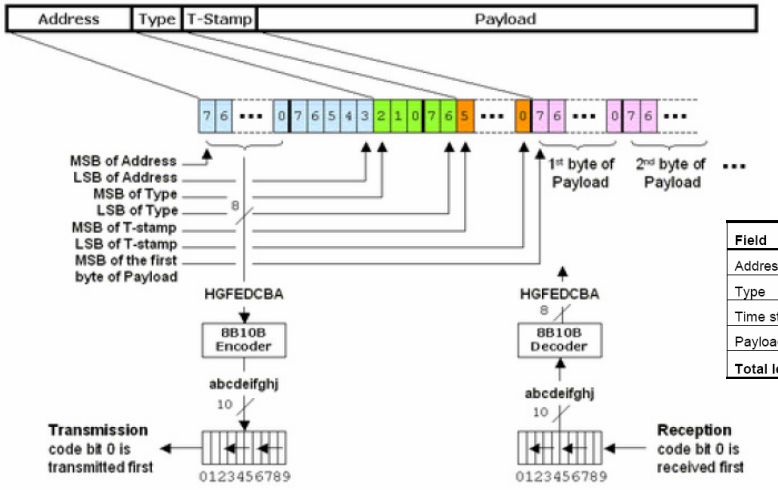

Field	Length (bits)
Address	13
Type	5
Time stamp (T-Stamp)	6
Payload	128
Total length	152 bits (=19 bytes)

Figure D.8 – Message format of RP3 protocol [OBS3].

In the RP3-01, information is transmitted using Master Frames (MFs) with a fixed duration of 10 ms, each comprising several Message Groups (MGs). A MG is a block of data consisting of multiple messages together with idle bytes. The message slots of the MGs are divided into data and control slots, and different parameter sets are specified for each wireless protocol, concerning the number of supported MGs and idle information, which will also depend on the data rate that is being used for a specific transmission channel.

The RP3 interface specifies four line rates, which are multiples of a given basic rate. These line rates are i*768 Mbit/s, with $i \in \{1,2,4,8\}$. As a result, line rates of 768 Mbit/s, 1536 Mbit/s, 3072 Mbit/s, and 6144 Mbit/s may be selected to support the system operation.

D.2.3. Architecture

The RP3-01 interface supports several topologies to interconnect a set of RRHs. The simplest topology is the PtP, where only one RRH is supported by the BTS. Other topologies, depicted in Figure D.9, include chain, ring and tree-and-branch. In these topologies, the RRHs operate as network elements, including functions such as message routing. Each RRH has only one

slave port, connected toward the BTS either directly or through other RRHs, and one or several master ports (optionally), connected to RRHs that are the next ones in the chain. The definition of the slave and master ports is carried out dynamically at the BTS startup, in such way that the RRH RP3-01 receiver/transmitter first detecting transmission from the BTS are defined as the slave port while other RRH ports are defined as master ports.

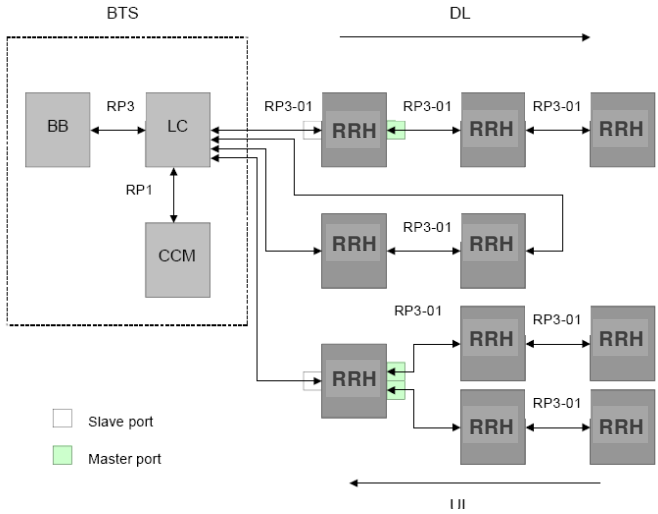

Figure D.9 – RP3-01 example architectures [OBS3].

As depicted in Figure D.9, an additional element, called Local Converter (LC) is necessary to map the RP3 and RP1 data into RP3-01 messages, and vice versa. The LC may exist as a separate module or it may be integrated with other modules, such as the baseband module. Figure D.10 provides an overview of the RP3-01 protocol functionalities, whether the LC is located in the BTS (LC-BTS), for the downstream transmission and upstream reception, or the LC is located in the RRH (LC-RRH), for the opposite operation.

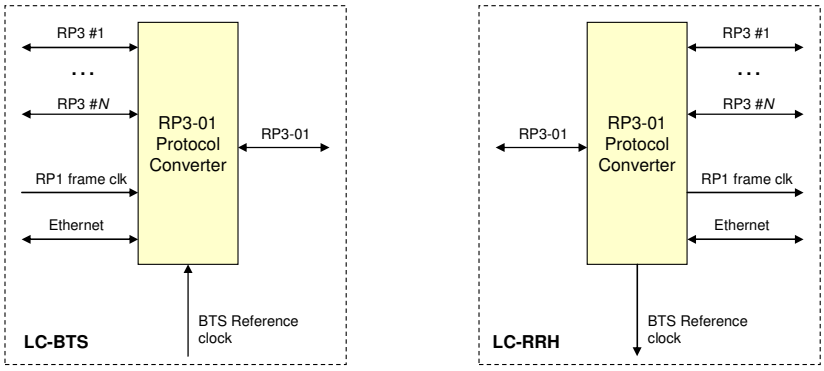

Figure D.10 – LC block diagram for BTS (LC-BTS) and for RRH (LC-RRH) [OBS3].

D.3. RP3-01 Deployment Scenarios

The deployment of OBSAI over a passive distribution system, such as PON, requires solving a set of open questions. Firstly, some remarks related to the protocol stack used by RP3-01, should be elaborated concerning the support of RP3-01 by a standardized PON system. Therefore, considering the use of a standardized GPON or EPON, their edges will have to include RP3-01 interfaces to send and receive RP3-01 bit streams. These interfaces are necessary in order to maintain the protocol stack that is defined for RP3-01 when transmitting it over a GPON/EPON. Importantly, from the point of view of the RP3-01 interfaces located at both the BTS and RRHs, the underlying GPON/EPON system must be fully transparent. In a first approach, it can be assumed that the GPON/EPON system will have access only to the RP3-01 physical layer bit stream and not to the upper layers of the RP3-01 protocol. This would limit the additional processing required at the PON terminals, although it can eventually result in difficulties regarding the support of functionalities such as addressing and synchronization.

Secondly, and as further addressed in chapter 5, a clear potential mismatch exists between the data rates supported by RP3-01 and the rates supported by standard PON systems. Moreover, both GPON and EPON frames are not large enough to carry a single RP3-01 MF. This will require the segmentation of every MF on the transmitter side, in order to fit GPON or EPON frames, and the reassembly of the MF at the receiver side. These operations must be performed without compromising the integrity of the MF, as to enable the transport of RP3-01 over a PON system. These discrepancies, in terms of line rate and framing lengths, suggest that an adaptation layer between RP3-01 and GPON/EPON system is required. This adaptation layer would be responsible to map the RP3-01 information into GPON/EPON frames for transmitting data over the PON and to perform the inverse operation when receiving the data from the PON infrastructure.

Finally, another evident difference between the topologies supported by RP3-01 and PONs is the fact that PON systems do not include active elements within the fibre plant (all the splitting points are comprised of completely passive elements). This way, in a PON, the ONUs are not cascaded as in the tree-and-branch topology presented in Figure D.9, but they are placed at the end of each branch. Following this structure, the support of distributed base stations with PONs, would have the RRH in the ONUs locations, i.e. at the end of the PON branches. In such scenario, where RRHs cannot be cascaded using the underlying PON

system and are placed at the PON end, they would only have slave ports. Anyway, each RRH placed at the end of the PON branches may be connected to other RRHs using any topology represented in Figure D.9, and in that case, those RRHs will have master ports.

Bearing in mind the abovementioned issues, several deployment scenarios involving the transmission of RP3-01 information over an underlying PON system should be analyzed. All the deployments analyzed consider the fundamental assumption of using a passive tree-and-branch topology, similar to that commonly employed in PON systems. In each deployment scenario, two extreme alternatives are analyzed regarding the number of LC ports. The first, designated as "Aggregated", considers that the LC-BTS has a single port that is shared by multiple RRHs, as represented in Figure D.11 a). The second approach considers the existence of a single port per RRH in the LC-BTS, i.e. the LC-BTS has multiple ports, each serving a single RRH. Therefore, it is designated as "Parallel" and is depicted in Figure D.11 b).

a) Aggregated alternative b) Parallel alternative

Figure D.11 – Alternative options regarding the number of LC-BTS ports.

Three different RP3-01 deployment scenarios are analyzed in the following. Firstly the transport of RP3-01 using a passive distributed fibre plant is addressed. Next, the use of GPON and EPON systems is considered to support the RP3-01 transmission. Finally, in the third scenario, RP3-01 data is assumed to be multiplexed together with fixed access traffic and transported over the same PON infrastructure.

D.3.1. Native RP3-01 over Passive Fibre Plant

The transport of native RP3-01 traffic over a passive distributed fibre plant is represented in Figure D.12. This situation assumes that RP3-01 is the only transmission protocol that is used in the system, i.e. no underlying protocol is employed to manage the transmission within the PON infrastructure.

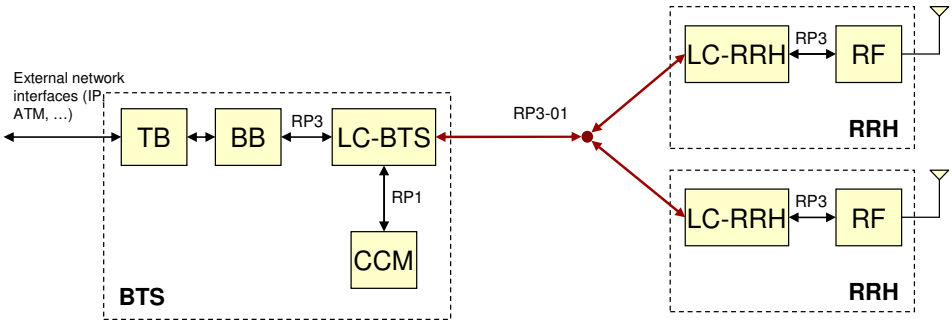

Figure D.12 – Native RP3-01 over passive fibre plant.

Considering the aggregated approach and recalling that at startup the BTS assumes that the existence of only PtP connections, either between BTS and RRHs or between RRHs, the BTS startup may not perform correctly in the presence of PtMP connections, which is exactly the case illustrated in Figure D.12. Moreover, in the upstream (from the RRHs to the BTS), this topology cannot be supported because RRHs cannot share the same upstream MF, as defined in the specifications of RP3-01.

The parallel alternative is clearly not supported in view of the absence of multiplexing after the LC-BTS. Since each RRH is served by a specific port in the LC-BTS, multiple bit streams, and possibly multiple line rates, exist at the output of the LC-BTS. Since the physical medium is directly connected to the LC-BTS without any intermediate device responsible for multiplexing the multiple channels (in the time domain, wavelength domain, etc), the transmission of these channels is impossible.

The above considerations show that the support of native RP3-01 is not possible using a distributed passive optical infrastructure, without additional multiplexing devices and/or transmission protocol.

D.3.2. RP3-01 Encapsulated on GPON/EPON Frames

A different situation considers the support of RP3-01 protocol over one of the protocols specified for PON systems, namely GPON and EPON. In this scenario, represented in Figure D.13, the underlying GPON or EPON system, comprising the OLT and a set of ONUs, transports the RP3-01 traffic generated in the BTS towards the RRHs and vice-versa. The BTS is connected to the OLT through an adaptation layer, responsible for encapsulating the RP3-01 data received from the LC-BTS output into GPON or EPON frames, depending on

the protocol that is being considered. Also, the same adaptation layer is responsible for the extraction of RP3-01 data from the GPON/EPON frames. On the opposite side of the network, each ONU is connected to an RRH module also through another adaptation layer, which has similar features to the OLT adaptation layer. In the downstream direction, the ONU receives the GPON/EPON frames and its adaptation layer must de-encapsulate RP3-01 traffic, delivering it to the corresponding LC-RRH. In the upstream, the opposite operation is performed by the adaptation layer.

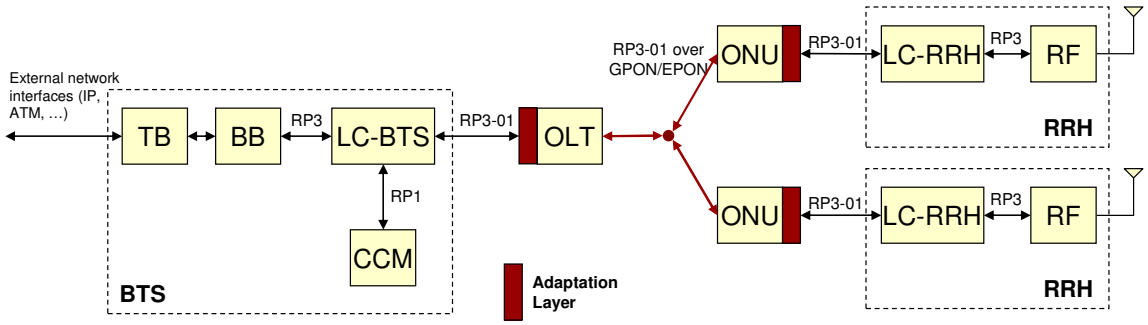

Figure D.13 – RP3-01 encapsulated on GPON/EPON frames.

In this deployment scenario, after transmission over the GPON/EPON system, the integrity of the RP3-01 bit stream has to be preserved, in order to guarantee a correct reception. Therefore, the adaptation layer must be able to segment the RP3-01 MF at the ingress side and reassemble the MF from these segments at the egress side. Furthermore, the total delay introduced by the GPON/EPON system, in both directions, must be deterministic, as to keep the MF synchronization. In this scenario, it is also necessary to assure that the GPON/EPON network elements (OLT and ONUs) are RP3-01 aware, in order to correctly deal with this traffic.

Firstly, consider the aggregated approach for this deployment scenario. In the downstream direction, the OLT adaptation layer segments the RP3-01 MF received from the LC-BTS and the adaptation layer of all ONUs reassembles it. In the upstream direction, this simple segmentation and reassembly scheme cannot be used, because each ONU receives from the LC-RRH a different MF. Therefore, each ONU receives data at RP3-01 line rate, which would result in an aggregated rate equal to the RP3-01 line rate times the number of RRHs (ONUs). This would result in an aggregated rate probably superior to that supported by both GPON and EPON systems. Alternatively, and since each MF from a RRH is only partly filled, the adaptation layer of the ONUs could process the incoming RP3-01 MF and only

transmit the client data generated by the RRH. This has the drawback of requiring going through several layers of the RP3-01 protocol stack at both ONU and OLT adaptation layers, which demands the design of a more costly adaptation layer.

The parallel approach, which uses different LC-BTS output ports for each RRH, requires associating each RRH (ONU) with a specific RP3-01 interface on the LC-BTS. The bandwidth required by this scheme equals the RP3-01 line rates times the number of RRHs that are being supported. In the downstream direction, the OLT adaptation layer segments the RP3-01 MFs from the different RP3-01 interfaces in the LC-BTS, but each ONU adaptation layer will only reassemble the MF that is addressed to the attached RRH. In the upstream direction, each ONU adaptation layer segments the RP3-01 MF and transmits it towards the OLT, where the MF from all ONUs (RRHs) are reassembled and delivered to the respective RP3-01 interfaces. The comparison of the aggregated and the parallel approach, regarding their advantages and disadvantages, is presented in Table D.1.

Table D.1 Comparison of aggregated and parallel approaches.

	Advantages	**Disadvantages**
Aggregated	More bandwidth efficient, because different RRHs can share the same MF	Complex to implement in the upstream direction, since it requires a large amount of processing at both the ONUs and the OLT
Parallel	The use of different MFs for different RRHs facilitates the upstream processing	Less flexible, because adding a new RRH requires a new port at the LC-BTS and increases the bandwidth needs by a multiple of the RP3-01 line rate

In view of these issues, it is necessary to determine the major features required by both OLT and ONUs adaptation layers, considering the use of aggregated or parallel approaches. As referred above, these adaptation layers must be able to deal with the RP3-01 traffic, mapping it according to GPON or EPON specifications. Moreover, it must also be able to properly manage the RP3-01 bit streams to guarantee that enough bandwidth is available in the PON system to support the required channels.

D.3.3. RP3-01 Multiplexed together with Fixed Access Traffic

This last deployment scenario is probably the most interesting, as it promotes the convergence between wired and wireless access systems. This scenario, represented in Figure D.14, offers

the possibility of reusing already deployed PON systems to transmit wireless traffic, consequently minimizing the implementation and management costs. It comprises typical fixed access ONUs that send/receive traffic to/from the PON system, using the transmission protocol specified for that system, GPON or EPON. Besides the typical ONUs, ONUs with an adaptation layer to convert the GPON/EPON traffic to/from RP3-01 traffic will also exist in this network. These ONUs are responsible to manage the RP3-01 traffic addressed to the antennas connected to the corresponding RRHs, as depicted in Figure D.14.

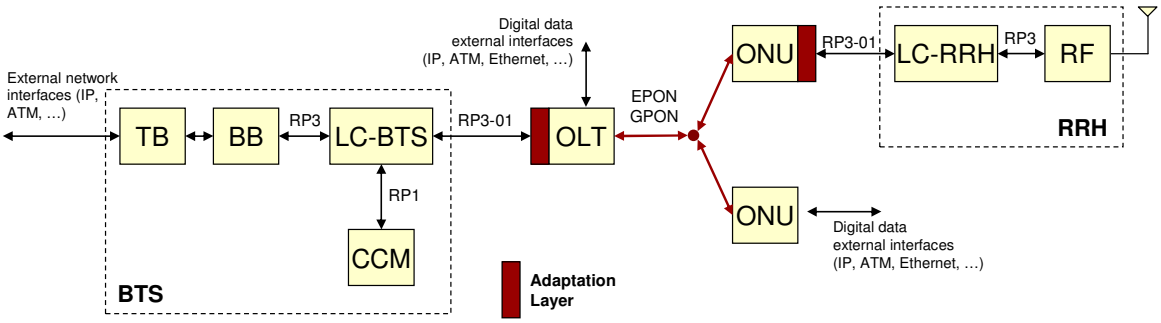

Figure D.14 – RP3-01 encapsulated on GPON/EPON frames and multiplexed together with fixed access traffic.

For this scenario, where fixed and wireless traffic are supported by the same PON system, both the aggregated and the parallel approaches suffer from the same limitations described in the previous deployment scenario, where only RP3-01 traffic is supported in the PON. In addition to those limitations, in this scenario, the OLT may have to enforce different bandwidth allocation schemes to handle the RP3-01 and the fixed access traffic, since the former has more stringent requirements, namely to preserve the RP3-01 data link layer synchronization. Therefore, if the limitations of supporting RP3-01 encapsulated in GPON/EPON frames are overcome, this system is likely to be deployed, and a good performance may be achieved by guaranteeing the use of suitable bandwidth allocation schemes. Nevertheless, the PON system has to have enough capacity to support the traffic of both fixed access clients and the RP3-01 assembled data.

D.3.4. Final Remarks

After the discussion in the previous sub-sections, it is clear that the support of RP3-01 over a PON system requires the definition of an adaptation layer, addressing several issues:

- Segmentation / reassembly of Master Frames
- Encapsulation / extraction of RP3-01 traffic into/from GPON or EPON frames
- Bandwidth management of the RP3-01 line rates
- Synchronization between the BTS and the RRHs and also between RRHs
- Stringent control of the delays
- Dynamic bandwidth allocation schemes, critical to support both fixed access traffic and RP3-01 data

The use of WDM-PON systems will eventually facilitate the support of RP3-01 in the "parallel" alternative. In this case, each RP3-01 bit stream, carrying information to/from a single RRH, would use a unique wavelength in the PON system. This solution has several benefits. Firstly, the data rate mismatch is no longer a significant problem, since each wavelength in the PON system can be operated at a sufficiently large data rate to support a given RP3-01 bit stream. Secondly, by avoiding TDM and the need for contention resolution in the upstream direction, the adaptation layer required at both the OLT and ONUs could eventually be simplified, since some of the major aspects that hamper the use of traditional PONs to support RP3-01, such as synchronization and master frame segmentation, are no longer relevant.

Appendix E

Additional Results for the Design of OBSAI and CPRI Systems

This appendix presents additional results obtained for the number of unidirectional OBSAI and CPRI links necessary to serve a RRH with multiple antennas. These results were obtained considering a channel bandwidth of 5 MHz, shown in Figure E.1 and Figure E.2 for WiMAX and LTE systems, respectively, and a channel bandwidth of 10 MHz, presented in Figure E.3 and Figure E.4 for WiMAX and LTE systems, respectively.

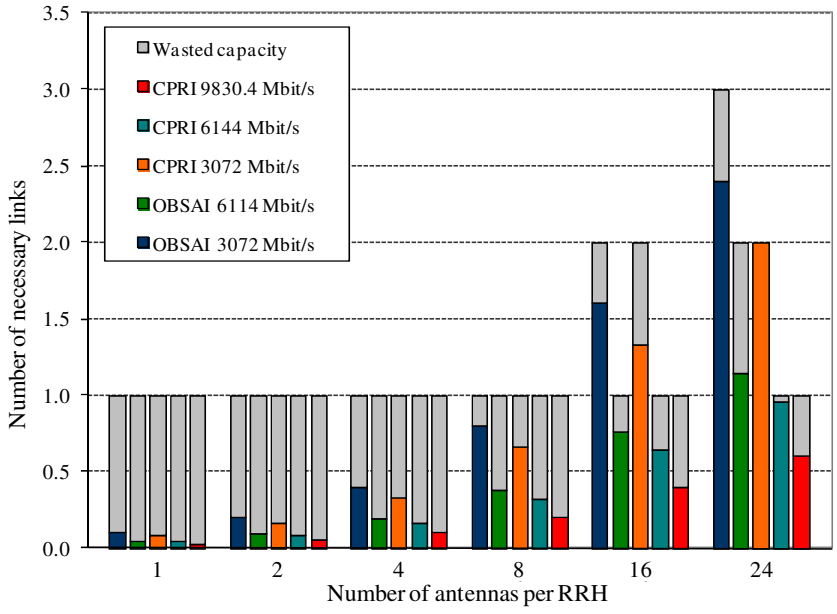

Figure E.1 – Number of necessary OBSAI and CPRI links to support multiple antennas per RRH, for a WiMAX system with channel bandwidth of 5 MHz.

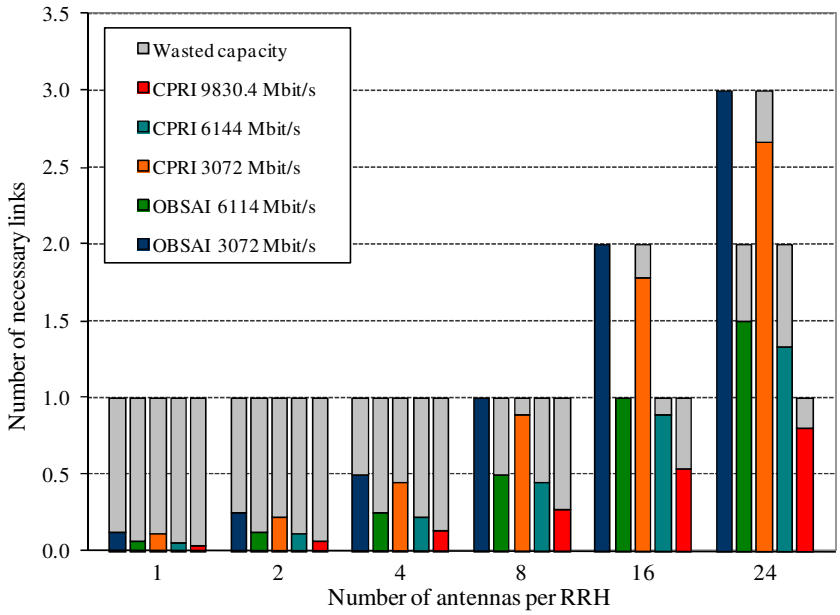

Figure E.2 – Number of necessary OBSAI and CPRI links to support multiple antennas per RRH, for a LTE system with channel bandwidth of 5 MHz.

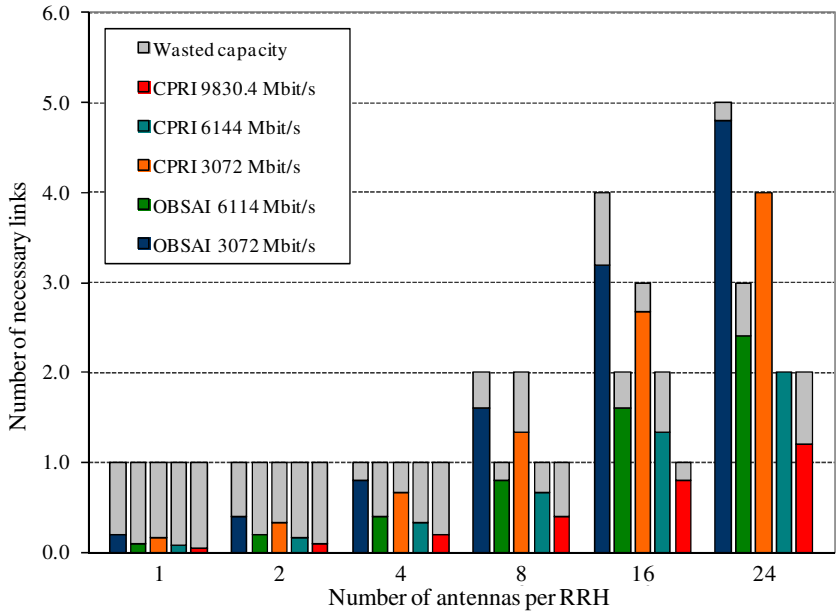

Figure E.3 – Number of necessary OBSAI and CPRI links to support multiple antennas per RRH, for a WiMAX system with channel bandwidth of 10 MHz.

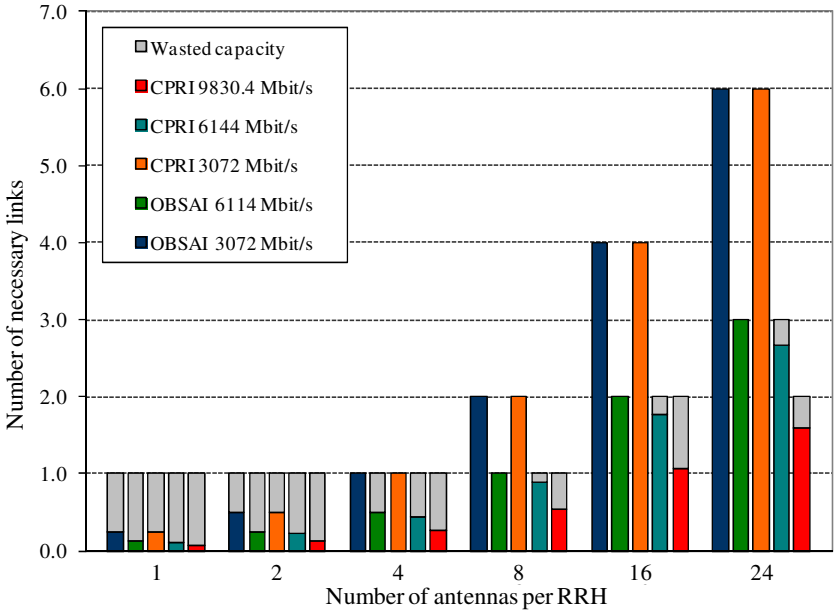

Figure E.4 – Number of necessary OBSAI and CPRI links to support multiple antennas per RRH, for a LTE system with channel bandwidth of 10 MHz.

Appendix F

Error Vector Magnitude

The most commonly adopted measure to evaluate the performance of a radio system is the EVM. Conceptually, this measure represents the degradation experienced by a multi-level signal constellation during its transmission, due to imperfections in the transmitter, transmission medium or receiver. When compared to the BER, the EVM provides additional information about both amplitude and phase errors, which allow for a more complete assessment of the channel distortion, being more closely related to the physics of the system.

In order to determine the EVM, the received (measured) symbol location is compared against the ideal symbol location, in the signal space. As presented in Figure F.1, the resulting error vector is a vector in the I-Q plane, given by the difference between the positional vectors of the measured symbol and the ideal symbol constellation points. The EVM is then defined by the magnitude of the error vector, representing the distortion level by including both magnitude and phase errors.

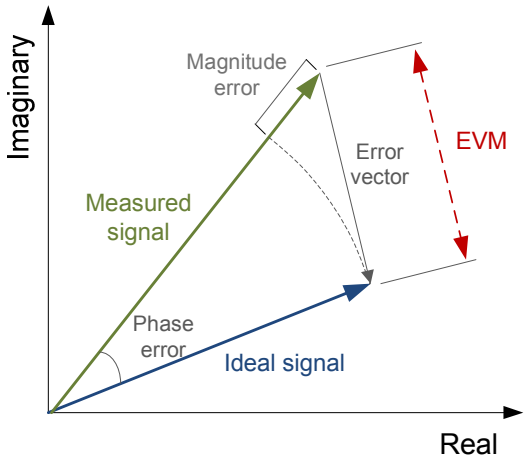

Figure F.1 – Concept of EVM.

Several modulation formats, such as QPSK, 16-QAM, 64-QAM, etc., are specified for the existing or proposed wireless protocols, which motivates the use of an effective normalization to calculate EVM, in order to enable an accurate comparison of EVM measurements between modulation types, for a given average power level.

This normalization is achieved by assuming a uniform distribution of the transmitted constellation symbols. Moreover, it is assumed that, before the normalization, the received symbols are de-rotated, so that they are aligned in the constellation [MRM+04]. This de-rotation process is based on frequency offsets, which are estimated between the sampling frequency and that of a given sub-carrier. This is a common procedure implemented in most OFDM receivers. The normalization is derived in such a way that the mean-square amplitude of all possible symbols in the constellation of any modulation scheme is one. After the symbols are normalized, the EVM is defined as the RMS value of the difference between a series of measured symbols and ideal symbols, averaged over a large number of symbols, and typically presented as a percentage of the average power per symbol of the constellation. According to [FBQ+04], the EVM is given by:

$$EVM_{\mathrm{RMS}} = \sqrt{\frac{\frac{1}{N}\sum_{k=1}^{N}\left|S_{k,\mathrm{ideal}} - S_{k,\mathrm{real}}\right|^2}{\frac{1}{N}\sum_{k=1}^{N}\left|S_{k,\mathrm{ideal}}\right|^2}}, \tag{F.1}$$

where $S_{k,\mathrm{ideal}}$ represents the ideal normalized constellation symbol associated to the k^{th} symbol, $S_{k,\mathrm{real}}$ represents the measured normalized k^{th} symbol, and N is number of symbols in the constellation. As referred above, to determine the EVM it is necessary to compare the ideal symbol values from the ideal constellation diagram with the measured voltage values. This is achieved by normalizing both ideal and measured symbols. According to [MRM+04], and after some manipulation of equation (F.1), the EVM can be represented as:

$$\begin{aligned} EVM_{\mathrm{RMS}} &= \left[\frac{1}{P_{\mathrm{S,avg}}\cdot T}\sum_{r=1}^{T}\left(\left|\left(V_{\mathrm{I},k,\mathrm{real}}\right)\cdot\left|A_{\mathrm{real}}\right| - \left(C_{\mathrm{I},k,\mathrm{ideal}}\right)\cdot\left|A_{\mathrm{ideal}}\right|\right|^2 + \right.\right. \\ &\quad \left.\left. + \left|\left(V_{\mathrm{Q},k,\mathrm{real}}\right)\cdot\left|A_{\mathrm{real}}\right| - \left(C_{\mathrm{Q},k,\mathrm{ideal}}\right)\cdot\left|A_{\mathrm{ideal}}\right|\right|^2\right)\right]^{1/2} \\ &= \left[\frac{1}{P_{\mathrm{S,avg}}\cdot T}\sum_{r=1}^{T}\left(\left|I_r - I_{0,r}\right|^2 + \left|Q_r - Q_{0,r}\right|^2\right)\right]^{1/2} \end{aligned} \quad . \tag{F.2}$$

Here, $P_{S,avg}$ is the normalized mean-square amplitude of the symbols in the constellation, always equal to one. $V_{I\text{ or }Q,k,real}$ and $C_{I\text{ or }Q,k,ideal}$ are the unnormalized voltages and integer values, respectively, of the k^{th} symbol for the measured and ideal I and Q components. A_{real} and A_{ideal} represent normalization factors for the measured and ideal constellations, respectively. The limit T ($T >> N$) includes all measured symbols.

The EVM expression presented in [IEEE99], and used along the EVM calculation in this thesis, is derived from expression (F.2) and includes some of the specific characteristics of the different modulation formats, such as the number of sub-carriers (total of 52, considering signals specified according to [IEEE99]), the length of the packets, i.e. the number of symbols in a packet, L_P, and the number of received frames, N_f. It is given by [MRM+04], [IEEE09]:

$$EVM_{RMS} = \frac{\sum_{i=1}^{N_f}\left[\frac{\sum_{j=1}^{L_P}\sum_{k=1}^{52}\left(\left|I(i,j,k)-I_0(i,j,k)\right|^2+\left|Q(i,j,k)-Q_0(i,j,k)\right|^2\right)}{52\cdot L_P\cdot P_{S,avg}}\right]^{1/2}}{N_f}. \quad \text{(F.3)}$$

By using this formulation, and considering the normalization described above, it is possible to accurately compare the EVM values across different sub-carriers, packets and frames for signals with different modulation formats, as long as the average power per symbol and the centre frequency of the signal are constant.

References

[AAS88] G. Agrawal, P. Anthony, and T. Shen, "Dispersion penalty for 1.3-μm lightwave systems with multimode semiconductor lasers", *IEEE/OSA Journal of Lightwave Technology*, vol. 6, no. 5, pp. 620-625, May 1988.

[ABB+08] E. Ackerman, W. Burns, G. Betts, J. Chen, J. Prince, M. Regan, H. Roussell, and C. Cox III, "RF-Over-Fiber Links With Very Low Noise Figure", *IEEE/OSA Journal of Lightwave Technology*, vol. 26, no. 15, pp. 2441-2448, August 2008.

[Agr01] G. Agrawal, *Applications of Nonlinear Fiber Optics*, 3rd Edition, Academic Press, San Diego, USA, 2001.

[Agr02] G. Agrawal, *Fiber-Optic Communication Systems*, 3rd Edition, John Wiley & Sons, Inc., New York, USA, 2002.

[AHK+02] K. Azadet, E. Haratsch, H. Kim, F. Saibi, J. Saunders, M. Shaffer, L. Song, and M. Yu, "Equalization and FEC techniques for optical transceivers", *IEEE Journal of Solid-State Circuits*, vol. 37, no. 3, pp. 317-327, March 2002.

[AMB01] A. Amat, G. Montorsi, and S. Benedetto, "A new approach to the construction of high-rate convolutional codes", *IEEE Communications Letters*, vol. 5, no. 11, pp. 453-455, November 2001.

[ATM88] Y. Aoki, K. Tajima, and I. Mito, "Input power limits of single-mode optical fibers due to stimulated Brillouin scattering in optical communications systems", *IEEE/OSA Journal of Lightwave Technology*, vol. 6, no. 5, pp. 710-719, May 1988.

[BDZ+04] T. Buerner, R. Dohmen, A. Zottman, M. Saeger, and A. Van Wijngaarden, "On a high-speed Reed-Solomon codec architecture for 43 Gb/s optical transmission systems", in *Proc. of International Conference on Microelectronics* (*MIEL*) *2004*, Serbia and Montenegro, May 2004, vol. 2, pp. 743-746.

[BGH+11] D. Breuer, F. Geilhardt, R. Hülsermann, M. Kind, C. Lange, T. Monath, and E. Weis, "Opportunities for next generation optical access", *IEEE Communications Magazine*, vol. 49, no. 2, pp. s16-s24, February 2011.

[Bil10] D. Bilajbegovic, "New Generation of Optical Access Networks", in *Proc. of International Convention on Information and Communication Technology, Electronics and Microelectronics (MIPRO)*, Opatija/Abbazia, Croatia, May 2010.

[Bil99] R. Billington, “Measurement methods for stimulated Raman and Brillouin scattering in optical fibres”, NPL Report COEM 31, National Physical Laboratory, Teddington, Middlesex, UK, June 1999.

[Bol04] M. Bolig, “Systemic Considerations of Forward Error Correction Codes in an Optical Transport Network”, Vitesse Semiconductor Corporation, white paper, February 2004.

[BPC+05] A. Banerjee, Y. Park, F. Clarke, H. Song, S. Yang, G. Kramer, K. Kim, and B. Mukherjee, “Wavelength-Division-Multiplexed Passive Optical Network (WDM-PON) technologies for broadband access: a review”, *OSA Journal of Optical Networking*, vol. 4, no. 11, pp. 737-758, November 2005.

[BPG+07] G. Battail, A. Poli, A. Glavieux, S. Vaton, E. Biglieri, C. Berrou, C. Douillard, M. Jézéquel, A. Piccart, R. Pyndiah, and P. Adde, *Channel Coding in Communication Networks: From Theory to Turbocodes*, ISTE Ltd, London, UK, 2007.

[BR90] P. Bayvel, and P. Radmore, “Solutions of the SBS equations in single mode optical fibres and implications for fibre transmission systems”, *Electronics Letters*, vol. 26, no. 7, pp. 434-436, March 1990.

[BRH90] J. Balance, P. Rogers, and M. Halls, “ATM access through a Passive Optical Network”, *Electronic Letters*, vol. 26, no. 9, pp. 558-560, April 1990.

[Bur01] A. Burr, “Turbo-codes: the ultimate error control codes?”, *IEE Electronics & Communication Engineering Journal*, vol. 13, no. 4, pp. 155-165, August 2001.

[BZ04] R. Baxley, and G. Zhou, “Power savings analysis of peak-to-average power ratio reduction in OFDM”, *IEEE Transactions on Consumer Electronics*, vol. 50, no. 3, pp. 792-798, August 2004.

[CABP06] C. Cox III, E. Ackerman, G. Betts, and J. Prince, "Limits on the performance of RF-over-fiber links and their impact on device design," IEEE Transactions on Microwave Theory and Techniques, vol. 54, no. 2, pp. 906-920, February 2006.

[Cae04] T. Caenegem, “B-PON, G-PON and EPON: A Guided Tour”, *FTTH Conference*, white paper, 2004.

[CAY05] W. Choi, J. Andrews, and C. Yi, “The capacity of multicellular distributed antenna networks”, in *Proc. of International Conference on Wireless Networks, Communications and Mobile Computing 2005*, Maui, USA, June 2005, pp. 1337-1342.

[CBJ90] C. Cox III, G. Betts, and L Johnson, “An Analytic and Experimental Comparison of Direct and External Modulation in Analog Fiber-Op tic Links”, *IEEE*

Transactions on Microwave Theory and Techniques, vol. 38, no. 5, pp. 501-509, May 1990.

[CFA+04] L. Coldren, G. Fish, Y. Akulova, J. Barton, L. Johansson, and C. Coldren, "Tunable semiconductor lasers: a tutorial", *IEEE/OSA Journal of Lightwave Technology*, vol. 22, no. 1, pp. 193-202, January 2004.

[CG91] T. Chu, and M. Gans, "Fibre-optic microcellular radio", in *Proc. of Vehicular Technology Conference (VTC) 1991*, Maryland Heights, USA, May 1991, pp. 339-344.

[Chr90] A. Chraplyvy, "Limitations on lightwave communications imposed by optical-fiber nonlinearities", *IEEE/OSA Journal of Lightwave Technology*, vol. 8, no. 10, pp. 1548-1557, October 1990.

[CLU+07] B. Charbonnier, H. Le Bras, P. Urvoas, Q. N'Guyen, M. Huchard, and A. Pizzinat, "Upcoming perspectives and future challenges for ROF", in *Proc. of IEEE International Topical Meeting on Microwave Photonics 2007*, Vitoria, Canada, October 2007, pp. 21-23.

[Coo91] A. Cooper, "Fibre-Radio: a new technique for delivering cordless access services", in *Proc. of Global telecommunications Conference (GLOBECOM) 1991*, Phoenix, USA, December 1991, pp. 999-1005.

[Cor] Corning® SMF-28e® Optical Fiber Specifications, August 2004. Available: www.corning.com/docs/opticalfiber/co9562.pdf

[Cox04] C. Cox III, *Analog Optical Links: Theory and Practice*, Cambridge University Press, Cambridge, UK, 2004.

[CP06] F. Coppinger, and D. Pichler, "RF video overlay in an Ethernet passive optical networks", in *Proc. of Optical Fiber Communication* (*OFC*) *Conference 2006*, Anaheim, USA, March 2006, paper OThK7.

[CPR] CPRI Specification, available at www.cpri.info.

[CS97] J. Cartledge, and R. Srinivasan, "Extraction of DFB laser rate equation parameters for system simulation purposes", *IEEE/OSA Journal of Lightwave Technology*, vol. 15, no. 5, pp. 852-860, May 1997.

[CSM00] D. Cassioli, S. Scotti, and A. Mecozzi, "A time-domain computer simulator of the nonlinear response of semiconductor optical amplifiers", *IEEE Journal of Quantum Electronics*, vol. 36, no. 9, pp. 1072-1080, September 2000.

[CSZE01] D. Chiaroni, N. Sauze, T. Zami, J. Emery, "Semiconductor Optical Amplifiers: a key technology to control the packet power variation", in *Proc. of European Conference on Optical Communication* (*ECOC*) *2001*, Amsterdam, The Netherlands, September/October 2001, paper We.B.2.6.

[CYC+09] N. Cheng, S. Yen, J. Cho, Z. Xu, T. Yang, Y. Tang, L. Kasovsky, "Long Reach Passive Optical Networks with Adaptive Power Equalization Using Semiconductor Optical Amplifiers", in *Proc. of Asia Communications and Photonics (ACP) Conference and Exhibition 2009,* Shanghai, China, November 2009, paper FS4.

[DB94] M. Van Deventer, and A. Boot, "Polarization properties of stimulated Brillouin scattering in single-mode fibers", *IEEE/OSA Journal of Lightwave Technology*, vol. 12, no. 4, pp. 585-590, April 1994.

[DED+09] F. van Dijk, A. Enard, G. H. Duan, A. Accard, F. Lelarge, O. Parillaud, A. Akrout, G. Valicourt, S. Ginestar, A. Ramdane, "Laser diodes for microwave and millimeter wave photonics", *in Proc. of Mediterranean Microwaves Symposium (MMS) 2009,* Tangiers, Morocco, November 2009.

[DHS+98] S. Danielsen, P. Hansen, K. Stubkjaer, M. Schilling, K. Wünstel, W. Idler, P. Doussiere, F. Pommerau, "All Optical Wavelength Conversion Schemes for Increased Input Power Dynamic Range", *IEEE Photonics Technology Letters*, vol. 10, no. 1, pp. 60-62, January 1998.

[DK95] E. Dawson, and A. Khodkar, "Burst-error correcting algorithm for Reed-Solomon codes", *Electronics Letters*, vol. 31, no. 11, pp. 848-849, May 1995.

[DMF10] F. Diehm, P. Marsch, and G. Fettweis, "The FUTON prototype: proof of concept for coordinated multi-point in conjunction with a novel integrated wireless/optical architecture", in *Proc. of IEEE Wireless Communications and Networking Conference* (*WCNC*) *2010 – Workshop on Integrated Optical-Wireless Networks*, Sydney, Australia, April 2010.

[DNG+06] A. Das, A. Nkansah, N. Gomes, I. Garcia, J. Batchelor, and D. Wake, "Design of low-cost multimode fiber fed indoor wireless networks", *IEEE Transactions on Microwave Theory and Techniques*, vol. 54, no. 8, pp. 3426-3432, August 2006.

[EFM] Ethernet in the First Mile website: www.ethernetinthefirstmile.com.

[EKM10] F. Effenberger, J. Kani, and Y. Maeda, "Standardization trends and prospective views on the next generation of broadband optical access", IEEE Journal of Selected Areas in Communications, vol. 28, no. 6, pp. 773-780, August 2010.

[ETSI00] ETSI EN 300 910 V8.5.1, "Digital cellular telecommunications system (Phase 2+); Radio transmission and reception (GSM 05.05 version 8.5.1 Release 1999)", November 2000.

[ETSI01] ETSI TS 125 104 V4.3.0, "Universal Mobile Telecommunications System (UMTS); UTRA (BS) FDD; Radio transmission and reception (3GPP TS 25.104 version 4.3.0 Release 4)", December 2001.

[ETSI08] ETSI TS 136 104 V8.3.0, "LTE; Evolved Universal Terrestrial Radio Access (E-UTRA); Base Station (BS) radio transmission and reception (3GPP TS 36.104 version 8.3.0 Release 8)", November 2008.

[ETSI97] ETSI EN 300 744 V1.1.2, "Digital Video Broadcasting (DVB); Framing structure, channel coding and modulation for digital terrestrial television", August 1997.

[EW96] R. Esman, and K. Williams, "Brillouin scattering: beyond threshold", in *Proc. of Optical Fiber Communication* (*OFC*) *Conference 1996*, San Jose, USA, February/March 1996, paper ThF5.

[FBQ+04] S. Forestier, P. Bouysse, R. Quere, A. Mallet, J. Nebus, and L. Lapierre, "Joint optimization of the power-added efficiency and the error-vector measurement of 20-GHz pHEMT amplifier through a new dynamic bias-control method", *IEEE Transactions on Microwave Theory and Techniques*, vol. 52, no. 4, pp. 1132-1141, April 2004.

[FGW+03] M. Fischer, G. Gupta, L. Wang, K. Kojima, O. Mizuhara, and V. Swaminathan, "FEC performance under optical power transient conditions", *IEEE Photonics Technology Letters*, vol. 15, no. 11, pp. 1654-1656, November 2003.

[FHJ+98] R. Feldman, E. Harstead, S. Jiang, T. Wood, and M. Zirngibl, "An Evaluation of Architectures Incorporating Wavelength Division Multiplexing for Broad-Band Fiber Access", *IEEE/OSA Journal of Lightwave Technology*, vol. 16, no. 9, pp. 1546-1559, September 1998.

[FN93] D. Fishman, and J. Nagel, "Degradations due to stimulated Brillouin scattering in multigigabit intensity-modulated fiber-optic systems", *IEEE/OSA Journal of Lightwave Technology*, vol. 11, no. 11, pp. 1721-1728, November 1993.

[FNS+08] Y. Fukada, T. Nakanishi, K. Suzuki, N. Yoshimoto, and M. Tsubokawa, "Gain-Clamp Light Auto Level Control (GCL-ALC) technique for gain-controllable burst-mode PON amplifying repeater", in *Proc. of Optical Fiber Communication* (*OFC*) *Conference 2008*, San Diego, USA, February 2008, paper OThT5.

[Fos98] K. Foster, "DSL Modem Standards - Removing the Access Botleneck", *IEE Seminar The Universally-Connected Planet! Or, What Standard do I Want?*, London, UK, December 1998.

[FPSM11] F. Ferreira, S. Pato, H. Silva, and P. Monteiro, "On supporting multiple signal formats over a FUTON system", in *Proc. of International Conference on Optical Design and Modelling (ONDM) 2011*, Bologna, Italy, February 2011.

[FS02] X. Fernando, and A. Sesay, "Adaptive Asymmetric Linearization of Radio Over Fiber Links for Wireless Access", *IEEE Transactions on Vehicular Technology*, vol. 51, no. 6, pp. 1576-1586, November 2002.

[FSA] Full Service Access Network (FSAN) website: http://fsanweb.com/.

[FUT] FUTON Project website: www.ict-futon.eu.

[FZZ+99] Y. Fei, X. Zheng, H. Zhang, Y. Guo, B. Zhou, "A Novel Scheme of Power Equalization and Power Management in WDM All-Optical Networks", *IEEE Photonics Technology Letters*, vol. 11, no. 9, pp. 1189-1191, September 1999.

[GPMG09] N. Gomes, S. Pato, P. Monteiro, and A. Gameiro, "Radio over fibre for the support of 4th generation mobile/wireless communications", in *Proc. of European Workshop on Photonic Solutions for Wireless, Access, and In-House Networks 2009*, Duisburg, Germany, May 2009.

[GPNL05] B. Gopalakrishnapillai, M. Premaratne, A. Nirmalathas, C. Lim, "Power Equalization Using Polarization Rotation in Semiconductor Optical Amplifiers", *IEEE Photonics Technology Letters*, vol. 17, no. 8, pp. 1695-1697, August 2005.

[HHL84] C. Henry, P. Henry, and M. Lax, "Partition fluctuations in nearly single-longitudinal-mode lasers", *IEEE/OSA Journal of Lightwave Technology*, vol. LT-2, no. 3, pp. 209-216, June 1984.

[HKTG06] W. Huang, J. Kuo, T. Ti, and L. Gao, "System and apparatus for a carrier class WDM PON providing trunk protection with increased fiber utilization, distance and bandwidth", Patent Application Publication, no. US 2006/0083513 A1, April 2006.

[HLH+10] A. Hekkala, M. Lasanen, I. Harjula, L. Vieira, N. Gomes, A. Nkansah, S. Bittner, F. Diehm, and V. Kotzsch, "Analysis of and compensation for non-ideal RoF links in DAS", *IEEE Wireless Communications*, vol. 17, no. 3, pp. 52-59, June 2010.

[HTF+01] P. Healey, P. Townsend, C. Ford, L. Johnston, P. Townley, I. Lealman, L. Rivers, S. Perrin, and R. Moore, "Spectral slicing WDM-PON using wavelength-seeded reflective SOAs", *Electronics Letters*, vol. 37, no. 19, pp. 1181-1182, September 2001.

[IEEE04] IEEE Std. 802.3ah-2004 (Amendment to IEEE Std. 802.3-2002), "Media Access Control Parameters, Physical Layers, and Management Parameters for Subscriber Access Networks", September 2004.

[IEEE05] IEEE Std 802.3-2005, "Carrier Sense Multiple Access With Collision Detection (CSMA/CD) Access Method and Physical Layer Specifications, 2005.

[IEEE09] IEEE Std. 802.3av-2009 (Amendment to IEEE Std. 802.3-2008), "Physical Layer Specifications and Management Parameters for 10 Gb/s Passive Optical Networks", October 2009.

[IEEE99] IEEE Std. 802.11a-1999 (Supplement to IEEE Std. 802.11-1999), "High speed Physical Layer in the 5GHz Band (Adopted by the ISO/IEC and redesignated as ISO/IEC 8802-11:1999/Amd 1:2000(E))", September 1999.

[IEEEav] IEEE P802.3av Task Force [Online]. Available: www.ieee802.org/3/av

[IFR97] P. Iannone, N. Frigo, and K. Reichmann, "Wavelength-Division Multiplexed Passive Optical Networks as a Multiple Service Provider Access Platform", *Lasers and Electro-Optics Society Annual Meeting (LEOS)*, vol. 2, pp. 85-86, San Francisco, USA, November 1997.

[Inf11] Infonetics Research, "PON, FTTH, and DSL Aggregation Equipment and Subscribers: 1Q11", Analysis Report, June 2011.

[IO93] H. Ichikawa, and M. Ogasawara, "A centralized control microcell radio system with spectrum delivery switches", *IEICE Transactions on Communications*, vol. E76-B, no. 9, pp. 1115-1121, September 1993.

[ITU00] ITU-T Recommendation G.975, "Forward error correction for submarine systems", October 2000.

[ITU01] ITU-T Recommendation G.983.3, "A broadband optical access system with increased service capability by wavelength allocation", March 2001.

[ITU03] ITU-R Recommendation M.1645, "Framework and overall objectives of the future development of IMT-2000 and systems beyond IMT-2000", May 2003.

[ITU05] ITU-T Recommendation G.983.1, "Broadband optical access systems based on Passive Optical Networks (PON)", January 2005.

[ITU07a] ITU-T Recommendation G.650.2, "Definitions and test methods for statistical and non-linear related attributes of single-mode fibre and cable", July 2007.

[ITU07b] ITU-T Recommendation G.984.5, "Gigabit-capable Passive Optical Networks (G-PON): enhancement band", September 2007.

[ITU08] ITU-T Recommendation G.984.1, "Gigabit-capable Passive Optical Networks (GPON): general characteristics", March 2008.

[ITU10] ITU-T Recommendation G.987.1, "10-Gigabit-capable Passive Optical Networks (XG-PON): general requirements", January 2010.

[JK95] L. Joiner, and J. Komo, "Decoding binary BCH codes", in *Proc. of IEEE Southeastcon'95*, Raleigh, USA, March 1995, pp. 67-73.

[Kam01] N. Kamiya, "On algebraic soft-decision decoding algorithms for BCH codes", *IEEE Transactions on Information Theory*, vol. 47, no. 1, pp. 45-58, January 2001.

[Kei99] G. Keiser, *Optical Fiber Communications*, 3rd Edition, McGraw-Hill, Singapore, 1999.

[KERW05] H. Kim, M. Emmelmann, B. Rathke, and A. Wolisz, "A radio over fiber network architecture for road vehicle communication systems", in *Proc. of IEEE 61st Vehicular Technology Conference (VTC 2005-Spring)*, Stockholm, Sweden, May 2005, pp. 2920-2994.

[KKC+05] A. Kobyakov, S. Kumar, D. Chowdhury, A. Ruffin, M. Sauer, and S. Bickam, "Design concept for optical fibers with enhanced SBS threshold", *Optics Express*, vol. 13, no. 14, pp. 5338-5346, July 2005.

[KLN+08] A. Koonen, M. Larrodé, A. Ng'oma, K. Wang, H. Yang, Y. Zheng, and E. Tangdiongga, "Perspectives of radio over fiber technologies", in *Proc. of Optical Fiber Communication* (*OFC*) *Conference 2008*, San Diego, USA, February 2008, paper OThP3.

[KMV+02] A. Kobyakov, M. Mehendale, M. Vasilyev, S. Tsuda, and A. Evans, "Simulated Brillouin scattering in Raman-pumped fibers: a theoretical approach", *IEEE/OSA Journal of Lightwave Technology*, vol. 20, no. 8, pp. 1635-1643, August 2002.

[KP02] G. Kramer, and G. Pesavento, "Ethernet passive optical network (EPON): building a next-generation optical access network", *IEEE Communications Magazine*, vol. 40, no. 2, pp. 66-73, February 2002.

[KPP+07] G. Kanellos, N. Pleros, D. Petrantonakis, P. Zakynthinos, and H. Avramopoulos, "40 Gb/s 2R burst mode receiver with a single integrated SOA-MZI switch", *Optics Express*, vol. 15, no. 8, pp. 5043-5049, April 2007.

[Kra05] G. Kramer, "Ethernet Passive Optical Networks", McGraw-Hill, 2005.

[KSB04] A. Kobyakov, M. Sauer, and A. Boskovic, "Raman-induced polarization-dependent power penalty in fiber-to-the-home networks", in *Proc. of European Conference on Optical Communication* (*ECOC*) *2004*, Stockholm, Sweden, September 2004, paper We4.P.086.

[KT69] T. Kasami, and N. Tokura, "Some remarks on BCH bounds and minimum weights of binary primitive BCH codes", *IEEE Transactions on Information Theory*, vol. IT-15, no. 3, pp. 408-413, May 1969.

[KY03] Y. Katayama, and T. Yamane, "Concatenation of interleaved binary/non-binary block codes for improved forward error correction", in *Proc. of Optical Fiber Communication* (*OFC*) *Conference 2003*, Atlanta, USA, March 2003, paper WN2.

[LCL+09] H. Lee, S. Cho, J. Lee, E. Jung, J. Yu, B. Kim, S. Lee, S. Lee, J. Koh, B. Sung, S. Kang, J. Kim, and K. Jeong, "First commercial service of a colorless gigabit

WDM/TDM hybrid PON system", in *Proc. of Optical Fiber Communication* (*OFC*) *Conference 2009*, San Diego, USA, March 2009, paper PDPD9.

[Lee05] H. Lee, "A high-speed low-complexity Reed-Solomon decoder for optical communications", *IEEE Transactions on Circuits and Systems – II: Express Briefs*, vol. 52, no. 8, pp. 461-465, August 2005.

[LKB+85] R. Linke, B. Kasper, C. Burrus, I. Kaminow, J. Ko, and T. Lee, "Mode power partition events in nearly single-frequency lasers", *IEEE/OSA Journal of Lightwave Technology*, vol. LT-3, no. 3, pp. 706-712, June 1985.

[LKH+08] M. Lasanen, A. Kotelba, A. Hekkala, P. Järvensivu, and A. Mämmelä, "Adaptive Predistortion Architecture for Nonideal Radio Transmitter", in *Proc. of IEEE Vehicular Technology Conference Spring 2008*, Marina Bay, Singapore, May 2008, pp. 1256-1260.

[LMS+07] V. Lal, M. Masanovic, J. Summers, G. Fish, and D. Blumenthal, "Monolithic wavelength converters for high-speed packet-switched optical networks", *IEEE Journal of Selected Topics in Quantum Electronics*, vol. 13, no. 1, pp. 49-57, January/February 2007.

[LNL+05] R. Luo, T. Ning, T. Li, L. Cai, F. Qiu, S. Jian, and J. Xu, "FTTH - A promising broadband technology", in *Proc. of the International Conference on Communications, Circuits and Systems*, Hong Kong, China, May 2005.

[LPT96] J. Lacey, G. Pendock, and R. Tucker, "All-optical 1300-nm to 1550-nm wavelength conversion using cross-phase modulation in a semiconductor optical amplifier", *IEEE Photonics Technology Letters*, vol. 8, no. 7, pp. 885-887, July 1996.

[LSK06] C. Lee, W. Sorin, and B. Kim, "Fiber to the home using a PON infrastructure", *IEEE/OSA Journal of Lightwave Technology*, vol. 24, no. 12, pp. 4568-4583, December 2006.

[LWF+07] Y. Li, C. Wu, S. Fu, P. Shum, Y. Gong, L. Zhang, "Power Equalization for SOA-Based Dual-Loop Optical Buffer by Optical Control Pulse Optimization", *IEEE Journal of Quantum Electronics*, vol. 43, no. 6, pp. 508-516, June 2007.

[Mit09] J. Mitchell, "Radio over fibre networks: advances and challenges", in *Proc. of European Conference on Optical Communication* (*ECOC*) *2009*, Vienna, Austria, September 2009, paper 2.4.5.

[Miz06] T. Mizuochi, "Recent progress in forward error correction and its interplay with transmission impairments", *IEEE Journal of Selected Topics in Quantum Electronics*, vol. 12, no. 4, pp. 544-554, July/August 2006.

[MM96] D. Mestdagh, and C. Martin, "The Super-PON concept and its technical challenges", in *Proc. of the International IFIP-IEEE Conference on Broadband Communications 1996*, Montreal, Canada, April 1996, pp. 333-345.

[MPL+10] P. Monteiro, S. Pato, E. López, D. Wake, N. Gomes, and A. Gameiro, "Fiber optic networks for distributed radio architectures: FUTON concept and operation", in *Proc. of IEEE Wireless Communications and Networking Conference* (*WCNC*) *2010 – Workshop on Integrated Optical-Wireless Networks*, Sydney, Australia, April 2010.

[MPP+09] P. Monteiro, S. Pato, J. Pedro, J. Santos, D. Wake, A. Nkansah, N. Gomes, E. López, and A. Gameiro, "Radio-over-fiber as the enabler for joint processing of spatially separated radio signals", in *Proc. of IEEE/LEOS Summer Topical Meetings* (*LEOSST*) *2009*, Newport Beach, USA, July 2009, pp. 43-44.

[MRM+04] M. McKinley, K. Remley, M. Myslinski, J. Kenney, D. Schreurs, and B. Nauwelaers, "EVM Calculation for Broadband Modulated Signals", in *Proc. of the 64th ARTFG Microwave Measurement Conference*, Orlando, USA, December 2004.

[MSL+09] J. Mietzner, R. Schober, L. Lampe, W. Gerstacker, and P. Hoeher, "Multiple-Antenna Techniques for Wireless Communications – A Comprehensive Literature Survey", *IEEE Communications Surveys & Tutorials*, vol. 11, no. 2, pp. 87-105, Second Quarter 2009.

[NKL+99] J. Nilsson, J. Kim, Y. Lee, S. Hwang, S. Yoon, S. Kim, " Multi-channel power-equalizing reflective erbium-doped fiber amplifier", in *Proc. of IEEE Conference on Lasers & Electro-Optics (CLEO) & The Pacific Rim 1999*, Seul, Korea, August/September 1999, paper ThH5.

[OBS] OBSAI Specification, available at www.obsai.org.

[OBS3] OBSAI, Reference Point 3 Specification, Version 4.0. Available: http://www.obsai.org.

[Oga82] K. Ogawa, "Analysis of mode partition noise in laser transmission systems", *IEEE Journal of Quantum Electronics*, vol. QE-18, no. 5, pp. 849-855, May 1982.

[Pat06] S. Pato, *Analysis and Evaluation of Proposals for Implementation of 10 Gbit/s Ethernet Passive Optical Networks*, M.Sc. thesis, Universidade de Coimbra, June 2006.

[PCA+02] D. Penninckx, E. Caro, O. Audouin, M. Khan, and O. Aït-Sab, "Forward-error correction for time-slotted optical packets", in *Proc. of Optical Fiber Communication* (*OFC*) *Conference 2002*, Anaheim, USA, March 2002, paper WO5.

[PCB06] F. Payoux, P. Chanclou, and R. Brenot, "WDM PON with a single SLED seeding colorless RSOA-based OLT and ONUs," in *Proc. of European Conference on Optical Communication* (*ECOC*) *2006*, Cannes, France, September 2006, paper Tu4.5.1.

[PFMS10] S. Pato, F. Ferreira, P. Monteiro, and H. Silva, "On supporting multiple radio channels over a SCM-based distributed antenna system: a feasibility assessment", in *Proc. of IEEE ICTON 2010 – 12th International Conference on Transparent Optical Networks*, Munich, Germany, June/July 2010, paper We.A3.5.

[PJS+07] S. Park, D. Jung, D. Shin, H. Shin, I. Yun, J. Lee, Y. Oh, and Y. Oh, "Colorless Operation of WDM-PON Employing Uncooled Spectrum-Sliced Reflective Semiconductor Optical Amplifiers", *IEEE Photonics Technology Letters*, vol. 19, no. 4, pp. 248-150, February 2007.

[PLC+10] J. Prat, J. Lazaro, P. Chanclou, R. Soila, A. Gallardo, A. Teixeira, G. TosiBeleffi, I. Tomkos, "Results from EU project SARDANA on 10G extended reach WDM PONs", in *Proc. of Optical Fiber Communication* (*OFC*) *Conference 2010*, San Diego, USA, March 2010, paper OThG5.

[PLJ+04] S. Park, C. Lee, K. Jeong, H. Park, J. Ahn, and K. Song, "Fiber-to-the-Home Services Based on Wavelength-Division-Multiplexing Passive Optical Network", *IEEE/OSA Journal of Lightwave Technology*, vol. 22, no. 11, pp. 2582-2591, November 2004.

[PLJ04] Y. Park, C. Lim, I. Jung, "ONU Power Equalization of Ethernet PON Systems", *IEEE Photonics Technology Letters*, vol. 16, no. 8, pp. 1984-1986, August 2004.

[PLMS07] S. Pato, R. Luis, P. Monteiro, and H. Silva, "On the impact of nonlinear effects in 10 Gbit/s Ethernet passive optical networks", in *Proc. of ConfTele 2007 – 6th Conference on Telecommunications*, Peniche, Portugal, May 2007, pp. 577-580.

[PMF+08] S. Pato, R. Meleiro, D. Fonseca, P. André, P. Monteiro, and H. Silva, "All-optical burst-mode power equalizer based on cascaded SOAs for 10-Gb/s EPONs", *IEEE Photonics Technology Letters*, vol. 20, no. 24, pp. 2078-2080, December 2008.

[PMG+09] S. Pato, P. Monteiro, N. Gomes, A. Gameiro, and T. Kawanishi, "Next-generation distributed and heterogeneous radio architectures: the FUTON project", in *Proc. of IEEE Asia-Pacific Microwave Photonics* (*APMP*) *Conference 2009*, Beijing, China, April 2009.

[PMS06] S. Pato, P. Monteiro, and H. Silva, "Performance evaluation of the physical layer for 10 Gbit/s Ethernet passive optical networks", in *Proc. of AccessNets 2006 – 1st International Conference on Access Networks*, Athens, Greece, September 2006.

[PMS07a] S. Pato, P. Monteiro, and H. Silva, "Analysis of the optimum APD gain for 10 Gbit/s Ethernet passive optical networks", in *Proc. of Symposium on Enabling Optical Networks* (*SEON*) *2007*, Aveiro, Portugal, June 2007.

[PMS07b] S. Pato, P. Monteiro, and H. Silva, "Impact of mode-partition noise in the performance of 10 Gbit/s Ethernet passive optical networks", *Proc. of IEEE ICTON 2007 – 9th International Conference on Transparent Optical Networks*, Rome, Italy, July 2007, paper Mo.P.18.

[PMS09] S. Pato, P. Monteiro, and H. Silva, "On using all-optical burst-mode power equalization in converged metro-access networks", in *Proc. of IEEE ICTON 2009 – 11th International Conference on Transparent Optical Networks*, Ponta Delgada, Portugal, June/July 2009, paper We.B2.1.

[PP12] S. Pato and J. Pedro, "Optical Network Architectures for the support of future wireless systems", chapter in "Next generation wireless communications using radio over fibre (The FUTON project)", *John* Wiley *& Sons*, 2012, to be published.

[PPM09] S. Pato, J. Pedro, and P. Monteiro, "Comparative evaluation of fibre-optic architectures for next-generation distributed antenna systems", in *Proc. of IEEE ICTON 2009 – 11th International Conference on Transparent Optical Networks*, Ponta Delgada, Portugal, June/July 2009, paper We.P.5.

[PPMS11] S. Pato, J. Pedro, P. Monteiro, and H. Silva, "Prospects of supporting distributed antenna systems over next-generation optical access and metro-access networks", in *Proc. of IEEE ICTON 2011 – 13th International Conference on Transparent Optical Networks*, Stockholm, Sweden, June 2011, paper Th.A6.2.

[PPS+08] S. Pato, J. Pedro, J. Santos, P. Monteiro, and A. Gameiro, "Fibre optic networks for distributed radio architectures: topology overview", in *Proc. of Symposium on Enabling Optical Networks* (*SEON*) *2008*, Porto, Portugal, June 2008.

[PPS+09a] S. Pato, J. Pedro, J. Santos, H. Silva, J. Pires, and P. Monteiro, "All-optical remote node for cost-effective metro-access convergence", in *Proc. of ConfTele 2009 – 7th Conference on Telecommunications*, Santa Maria da Feira, Portugal, May 2009.

[PPS+09b] S. Pato, J. Pedro, J. Santos, A. Arsénio, P. Inácio, and P. Monteiro, "On building a distributed antenna system with joint signal processing for next-generation wireless access networks: the FUTON approach", in *Proc. of ConfTele 2009 – 7th Conference on Telecommunications*, Santa Maria da Feira, Portugal, May 2009.

[PSM+01] A. Phillips, J. Senior, R. Mercinelli, M. Valvo, P. Vetter, C. Martin, M. Van Deventer, P. Vaes, and X. Qiu, "Redundancy strategies for a high splitting

optically amplified passive optical network", *IEEE/OSA Journal of Lightwave Technology*, vol. 19, no. 2, pp. 137-149, February 2001.

[PSM09] S. Pato, H. Silva, and P. Monteiro, "Forward error correction in 10 Gbits/s Ethernet passive optical networks", *OSA Journal of Optical Networking*, vol. 8, no.1, pp. 84-94, January 2009.

[PSP+08] S. Pato, J. Santos, J. Pedro, P. Monteiro, and H. Silva, "On supporting radio over fiber and passive optical network systems with a common fiber plant: compatibility aspects", in *Proc. of IEEE ICTON 2008 – 10th International Conference on Transparent Optical Networks*, Athens, Greece, June 2008, paper Th.PD.1.

[PT06] S. Pato, and S. Ten, "Effect of nonlinearities in a 10 Gbit/s EPON system", presented at *Plenary Meeting of IEEE P802.3av 10GEPON Task Force*, Dallas, USA, November 2006. Available: www.ieee802.org/3/av/public/2006_11/3av_0611_pato_ten_1.pdf

[Rap02] T. Rappaport, *Wireless Communication: Principles & Practices*, 2nd Edition, Prentice-Hall, New Jersey, USA, 2002.

[RC01] J. Rebola, and A. Cartaxo, "Gaussian approach for performance evaluation of optically preamplified receivers with arbitrary optical and electrical filters", *IEE Proceedings – Optoelectronics*, vol. 148, no. 3, pp. 135-142, June 2001.

[RS02] R. Ramaswami, and K. Sivarajan, *Optical Networks: A Practical Perspective*, 2nd Edition, Morgan Kaufmann, San Francisco, USA, 2002.

[RSG10] H. Rohde, S. Smolorz, and E. Gottwald, "Next generation ultra-high capacity PONs", in *Proc. of IEEE Annual Meeting of the Photonics Society*, Denver, USA, November 2010.

[SA00] M. Sadiku, and C. Aduba, "Cable modem technology", *IEEE Potentials*, vol. 19, no. 4, pp. 26-27, October-November 2000.

[SCC97] C. Su, L. Chen, and K. Cheung, "Theory of burst-mode receiver and its applications in optical multiaccess networks", *IEEE/OSA Journal of Lightwave Technology*, vol. 15, no. 4, pp. 590-606, April 1997.

[SGR+11] S. Smolorz, E. Gottwald, H. Rohde, D. Smith, A. Poustie, "Demonstration of a Coherent UDWDM-PON with a Real-Time Processing", in *Proc. of Optical Fiber Communication (OFC) Conference 2011*, Los Angeles, USA, March 2011, paper PDPD4.

[Shi05] H. Shinohara, "Broadband access in Japan: rapidly growing FTTH market", *IEEE Communications Magazine*, vol. 43, no. 9, pp. 72-78, September 2005.

[SHP+88] J. Stern, C. Hoppitt, D. Payne, M. Reeve, and K. Oakley, "TPON - A Passive Optical Network for Telephony", in *Proc. of European Conference on Optical Communication* (*ECOC*) *1988*, Brighton, UK, September 1988.

[SHTT90] M. Stern, J. Heritage, R. Thurston, and S. Tu, "Self-phase modulation and dispersion in high data rate fiber-optic transmission systems", *IEEE/OSA Journal of Lightwave Technology*, vol. 8, no. 7, pp. 1009-1016, July 1990.

[SIS+05] R. Sato, T. Ito, Y. Shibata, A. Ohki, Y. Akatsu, "40-Gb/s burst-mode optical 2R regenerator", *IEEE Photonics Technology Letters*, vol. 17, no. 10, pp. 2194-2196, October 2005.

[SJ03] R. Sadhwani, and B. Jalali, "Adaptive CMOS Predistortion Linearizer for Fiber-Optic Links", *IEEE/OSA Journal of Lihtwave Technology*, vol. 21, no. 12, pp. 3180-3193, December 2003.

[SJS+06] H. Shin, D. Jung, D. Shin, S. Park, J. Lee, I. Yun, S. Kim, Y. Oh, and C. Shim, "16 x 1.25 Gbit/s WDM-PON based on ASE-injected R-SOAs in 60 ºC temperature range", in *Proc. of Optical Fiber Communication* (*OFC*) *Conference 2006*, Anaheim, USA, March 2006, paper OTuC5.

[SM07] D. Shea, and J. Mitchell, "A 10-Gb/s 1024-way-split 100-km long-reach optical-access network", *IEEE/OSA Journal of Lightwave Technology*, vol. 25, no. 3, pp. 685-693, March 2007.

[Smi72] R. Smith, "Optical power handling capacity of low loss optical fibers as determined by stimulated Raman and Brillouin scattering", *Applied Optics*, vol. 11, no. 11, pp. 2489-2494, November 1972.

[Soe00] S. Soerensen, "Optical Beat Noise Suppression and Power Equalization in Subcarrier Multiple Access Passive Optical Networks by Downstream Feedback", ", *IEEE/OSA Journal of Lightwave Technology*, vol. 18, no. 10, pp. 1337-1347, October 2000.

[SPMP08] J. Santos, J. Pedro, P. Monteiro, and J. Pires, "Long-reach 10 Gbps Ethernet passive optical network based on a protected ring architecture", in *Proc. of Optical Fiber Communication* (*OFC*) *Conference 2008*, San Diego, USA, February 2008, paper OTuI2.

[SQPP07] J. Santos, O. Quadros, J. Pedro, and J. Pires, "Design and performance evaluation of protected Super-PON access networks using a dedicated protection ring architecture", in *Proc. of DRCN 2007 – 6th International Workshop on Design and Reliable Communication Networks*, La Rochelle, France, October 2007.

[SRO+06] S. Smolorz, H. Rohde, P. Ossieur, C. Antony, P. Townsend, T. Ridder, B. Baekelandt, X. Qiu, S. Appathurai, H. Krimmel, D. Smith, A. Poustie, "Next

generation access networks: PIEMAN and beyond", in *Proc. of International Conference on Photonics in Switching 2009*, Tirrenia, Italy, September 2009.

[SSG+10] E. Sá, C. Silva, A. Gomes, "CRRM for RAT selection in the UMTS and WiMAX optimisation", in *Proc. of Future Network & Mobile Summit 2010, Florence*, Italy, June 2010.

[SZNA04] Y. Shi, X. Zhang, Z. Ni, and N. Ansari, "Interleaving for combating bursts of errors", *IEEE Circuits and Systems Magazine*, vol. 4, no. 1, pp. 29-42, First Quarter 2004.

[Tak07] M. Takizawa, "Progress and issues concerning the power budget discussions in the power budget Ad Hoc", presented at *Plenary Meeting of IEEE P802.3av 10GEPON Task Force*, Orlando, USA, March 2007. Available: http://www.ieee802.org/3/av/public/2007_03/3av_0703_takizawa_1.pdf

[TCT05] A. Tran, C. Chae, and R. Tucker, "Optical packet power equalization with large dynamic range using controlled gain-clamped SOA", in *Proc. of Optical Fiber Communication* (*OFC*) *Conference 2005*, Anaheim, USA, March 2005, paper OME46.

[TCTW05] A. Tran, C. Chae, R. Tucker, and Y. Wen, "EDFA transient control based on envelope detection for optical burst switched networks", *IEEE Photonics Technology Letters*, vol. 17, no. 1, pp. 226-228, January 2005.

[TF02] O. Tonguz, F. Flood, "EDFA-based DWDM lightwave transmission systems with end-to-end power and SNR equalization", *IEEE Transactions on Communications*, vol. 50, no.8, pp. 1282-1292, August 2002.

[TKT06] A. Tychopoulos, O. Koufopavlou, and I. Tomkos, "FEC in optical communications – A tutorial overview on the evolution of architectures and the future prospects of outband and inband FEC for optical communications", *IEEE Circuits & Devices Magazine*, vol. 22, no. 6, pp. 79-86, November/December 2006.

[Tom03] W. Tomlinson, "Technologies for dynamic gain and channel power equalization", in *Proc. of Optical Fiber Communication* (*OFC*) *Conference 2003*, Atlanta, USA, March 2003, paper TuM1.

[Tor84] D. Torrieri, "The information-bit error rate for block codes", *IEEE Transactions on Communications*, vol. COM-32, no. 4, pp. 474-476, April 1984.

[URK+06] V. Urick, M. Rogge, P. Knapp, L. Swingen, F. Bucholtz, "Wide-band predistortion linearization for externally modulated long-haul analog fiber-optic links", *IEEE Transactions on Microwave Theory and Techniques*, vol. 54, no. 4, pp. 1458-1463, April 2006.

[Vit71] A. Viterbi, "Convolutional codes and their performance in communication systems", *IEEE Transactions on Communications Technology*, vol. COM-19, no. 5, pp. 751-772, October 1971.

[VMVQ00] I. Van de Voorde, C. Martin, J. Vandewege, and X. Qiu, "The SuperPON demonstrator: an exploration of possible evolution paths for optical access networks", *IEEE Communications Magazine*, vol. 38, no. 2, pp. 74-82, February 2000.

[VPP+10] G. Valicourt, F. Pommereau, F. Poingt, M. Lamponi, G. Duan, P. Chanclou, M. Violas, and R. Brenot, "Chirp Reduction in Directly Modulated Multi-Electrode RSOA Devices in Passive Optical Networks", *IEEE Photonics Technology Letters*, vol. 22, no. 19, pp. 1425-1427, October 2010.

[WDK+09] C: Wijting, K. Doppler, K. KallioJarvi, T. Svensson, M. Sternad, G. Auer, N. Johansson, J. Nystrom, M. Olsson, A. Osseiran, M. Dottling, J. Luo, T. Lestable, S. Pfletschinger, "Key technologies for IMT-Advanced mobile communication systems", *IEEE Wireless Communications*, vol. 16, no. 3, pp. 76-85, June 2009.

[WiM08] WiMAX System Evaluation Methodology, version 2.1, WiMAX Forum, July 2008.

[WIRF98] S. Woodward, P. Iannone, K. Reichmann, and N. Frigo, "A Spectrally Sliced PON Employing Fabry-Perot Lasers", *IEEE Photonics Technology Letters*, vol. 10, no. 9, pp. 1337-1339, September 1998.

[WNA+10] D. Wake, A. Nkansah, P. Assimakopolous, N. Gomes, M. Violas, Z. Liu, S. Pato, F. Ferreira, G. De Valicourt, R. Brenot, and F. Van Dijk, "Design and performance of radio over fibre links for next generation wireless systems using distributed antennas", in *Proc. of Future Network & Mobile Summit 2010, Florence*, Italy, June 2010.

[WNA+11] D. Wake, A. Nkansah, P. Assimakopolous, N. Gomes, M. Violas, Z. Liu, S. Pato, F. Ferreira, G. De Valicourt, R. Brenot, and F. Van Dijk, "Rádio sobre Fibra", *RTI – Redes, Telecom e Instalações*, November 2011, to be published.

[WNG+10] D. Wake, A. Nkansah, N. Gomes, G. De Valicourt, R. Brenot, M. Violas, Z. Liu, F. Ferreira, and S. Pato, "A comparison of radio over fiber link types for the support of wideband radio channels", *IEEE/OSA Journal of Lightwave Technology*, vol. 28, no. 16, pp. 2416-2422, August 2010.

[WNG09] D. Wake, A. Nkansah, and N. Gomes, "Optical transmission link design for a distributed broadband wireless system", in *Proc. of European Workshop on Photonic Solutions for Wireless, Access, and In-House Networks 2009*, Duisburg, Germany, May 2009.

[WPP+09] D. Wake, S. Pato, J. Pedro, E. López, N. Gomes, and P. Monteiro, "Comparison of remote radio head optical transmission technologies for next generation wireless systems", in *Proc. of IEEE Lasers and Electro-Optics Society* (*LEOS*) *Annual Meeting 2009*, Belek-Antalya, Turkey, October 2009, pp. 442-443.

[WSL+04] H. Wessing, B. Sorensen, B. Lavigne, E. Balmefrezol, and O. Leclerc, "Combining control electronics with SOA to equalize packet-to-packet power variations for optical 3R regeneration in optical networks at 10 Gbit/s", in *Proc. of Optical Fiber Communication* (*OFC*) *Conference 2004*, Los Angeles, USA, February 2004, paper WD2.

[Yam96] I. Yamashita, "The latest FTTH technologies for full service access networks", in *Proc. of IEEE Asia Pacific Conference on Circuits and Systems (APCCAS)*, Seoul, Korea, November 1996.

[YB97] G. Yabre, and J. Bihan, "Reduction of nonlinear distortion in directly modulated semiconductor lasers by coherent light injection", *IEEE Journal of Quantum Electronics*, vol. 33, no. 7, pp. 1132–1140, July 1997.

[YLLW02] L. Yin, J. Lu, K. Letaief, and Y. Wu, "Burst-error-correcting algorithm for Reed-Solomon codes and its performance over a bursty channel", in *Proc. of IEEE International Conference on Communications, Circuits and Systems and West Sino Exposition 2002*, Chengdu, China, June/July 2002, vol. 1, pp. 77-81.

[ZA10] J. Zhang, and N. Ansari, "Design of WDM PON with tunable lasers: the upstream scenario", *IEEE/OSA Journal of Lightwave Technology*, vol. 28, no. 2, pp. 228-236, January 2010.

[ZBEG10] I. Zuazola, J. Batchelor, J. Elmirghani, and N. Gomes, "UWB PIFA for simplified transceivers", *Electronics Letters*, vol. 46, no. 2, pp. 116-117, January 2010.

[Zir92] M. Zirngibl, "An optical power equalizer based on one Er-doped fiber amplifier", *IEEE Photonics Technology Letters*, vol. 4, no. 4, pp. 357-359, April 1992.